

Plant protein gel formation mechanisms and their applications as delivery systems of bioactive compounds

by

Chen Yang

A thesis submitted in partial fulfillment of the requirements for the degree of

Doctor of Philosophy

in

Food Science and Technology

Department of Agricultural, Food and Nutritional Science
University of Alberta

© Chen Yang, 2016

Abstract

The objective of this research was to understand the gel formation mechanisms of plant proteins by both heat- and cold-induced methods, and use the knowledge gained to design plant protein gels with improved mechanical properties for food applications and as nutraceutical delivery systems. In the first study, the formation mechanisms and properties of heat-induced canola protein gels were investigated. At low pH and temperature, the gels exhibited randomly aggregated particulate fractal network structures, while at high pH and temperature, the macro-porous dense wall network structures were established. The protein conformational study and gel dissociation test suggested that the higher heating temperature and pH induced more unfolded structures through splitting inter- and intra-chain disulfide bridges so as to facilitate the establishment of molecular interactions. Remarkably, the macro-porous dense wall structure exhibited much stronger gel strength than the gel with particulate fractal structure.

In the second study, cold-set oat protein gels possessing a percolating network structure were prepared using glucono- δ -lactone (GDL) as an acidification agent. The polymer-like percolating structures were established by active oat protein monomers as small building block units through abundant cross-linking points. By increasing the GDL concentration, more intra-floc linkages and greater particle volume fractions were created at the supramolecular level, resulting in a dense rough gel wall with superior mechanical properties. In particular, gel formed with 10% GDL that exhibited compact network structure with small pores and a thick wall had an

excellent water-holding capacity (90%) and comparable mechanical strength to egg white gel. Moreover, the cold gelation has provided the opportunity for oat protein gels to be used as delivery systems of heat labile active compounds, as the gels can be formed at ambient temperature.

Accordingly, in the third study, novel core-shell beads were developed from oat protein in combination with shellac via a cold-gelation method at ambient temperature. The optimized sample showed a homogeneous, smooth and integrated shell structure stabilized by hydrophobic interactions between oat protein and shellac. *In vitro* tests in the simulated gastro-intestinal tract indicated that the beads could effectively prevent premature diffusion of the contained riboflavin, and protect *L. acidophilus* and amylase in the harsh environment of gastric fluids at low pH with pepsin. When transferred into the simulated intestinal tract, riboflavin and *L.acidophilus* were sustainably released to exert health benefits.

Finally, oat protein-shellac nanoparticles with controllable sizes ranging from ~ 90 to 300 nm were fabricated by the cold gelation method for delivery of resveratrol. These nanoparticles exhibited regular spherical shapes, good colloidal stability and high encapsulation efficiencies of up to 90%. *In vitro* tests showed that the resveratrol uptake and transport could be increased 7.2 and 12.9 times, respectively, compared to free resveratrol. *In vivo* test in rat models demonstrated that the nanoparticles could significantly improve the oral bioavailability of resveratrol and prevent the CCl₄-induced hepatotoxicity by reducing oxidative stress of the tissue.

This research has advanced fundamental understanding of canola and oat protein gelling mechanisms in controlling gel microstructures and mechanical properties, which has laid a good foundation for applying this knowledge in developing novel gelling ingredients of plant origin. The novel beads and nanoparticles based on oat protein were fabricated at ambient temperature without using organic solvents; thus they have good potential to be developed into delivery systems of bioactive molecules to create functional food ingredients for improvement of public health.

Preface

Chapter 3 of this thesis has been published as Chen Yang, Yixiang Wang, Thava Vasanthan, Lingyun Chen, Impacts of pH and heating temperature on formation mechanisms and properties of thermally induced canola protein gels, *Food Hydrocolloids*, Volume 40, March 2014, Pages 225-236. In this chapter, my responsibility was to collect and analyze all the data as well as to write the manuscript. Assistance was received from Dr. Yixiang Wang in obtaining the SEM micrographs and revising the manuscript. Dr. Thava Vasanthan was my co-supervisor. Dr. Lingyun Chen was the supervisor and corresponding author and contributed to the experimental design, data discussion, manuscript edits and submission.

Chapter 4 of this thesis has been published as Chen Yang, Yixiang Wang, Lingyun Chen, Fabrication, characterization and controlled release properties of oat protein gels with percolating structures induced by cold gelation, *Food Hydrocolloids*, Volume 62, July 2017, Pages 21-34. In this chapter, I was responsible for experimental design, collecting and analyzing all the data, as well as to write the manuscript. Assistance was received from Dr. Yixiang Wang in designing the experiment, obtaining the SEM micrographs and revising the manuscript. Dr. Lingyun Chen was the supervisor and corresponding author and contributed to the experimental design, data discussion, manuscript edits and submission.

Chapter 5 of this thesis has been submitted as Chen Yang, Yixiang Wang, Lei Lu, Larry Unsworth, Leluo Guan, Lingyun Chen, Oat protein-shellac beads: superior protection and

delivery carriers for sensitive bioactive compounds. In this chapter, my responsibility was to design the experiment, collect and analyze all the data, as well as to write the manuscript. Assistance was received from Dr. Yixiang Wang in experimental design, obtaining the SEM micrographs and DSC data, and revising the manuscript. Lei Lu and Dr. Larry Unsworth assisted in obtaining ITC results. Dr. Leluo Guan provided assistance in probiotics related test. Dr. Lingyun Chen was the supervisor and corresponding author and contributed to the experimental design, data discussion, manuscript editing and submission.

Another manuscript was generated based on the data in Chapter 6; this manuscript will soon be submitted by Chen Yang, Yixiang Wang, Guangyu Liu, Yike Xie, Yi Lu, Wei Wu, Lingyun Chen. I was responsible for the experimental design, data collection and analysis as well as the manuscript composition. Assistance was received from Dr. Yixiang Wang in experimental design, obtaining the TME micrographs and revising the manuscript. G. Liu assisted in the cell culture test. Y. Xie, Dr. Y. Lu, and Dr. W. Wu helped with the *in vivo* test. Dr. Lingyun Chen was the supervisor and corresponding author and contributed to the experimental design, data discussion, manuscript edits and submission.

Acknowledgements

I would like to thank my supervisor Dr. Lingyun Chen for her instruction and support of my research during my PhD studies. Without her continuous support and encouragement, my work could not have been completed. Many thanks to Dr. Chen for her training in designing experiments, experimental skills, academic writing, and presentation skills, which help me to become a qualified Ph.D student and mature researcher. I would like to thank Dr. Thava Vasanthan and Dr. Feral Temelli for their constructive suggestions to my research project during committee meetings. I would also like to thank Dr. Leluo Guan for her help and support on microbiology test. Many thanks to Dr. Larry Unsworth for his help in completing the ITC test. I sincerely thank Dr. Wei Wu and Dr. Yi Lu, Fudan University, China, for their help and support in the *in vivo* tests.

Many thanks go to the wonderful lab members of 3-52 and 3-30. Thank you very much for your companionship, heartwarming support and friendship. Special thanks to Dr. Yixiang Wang for his great support and help during my PhD research in terms of experimental design, conducting experiments, and academic writing. I would like to thank Mr. Zhigang Tian for his help with the HPLC and DSC tests, and other technical problems.

Finally, with all my love, I would like to thank my family for their support and love. To my beloved parents, I really appreciate their boundless support, encouragement, understanding, and care during the time of my studies. To my sweet and loving husband, Hongbo Luan, thank you very much for your infinite love, patience, encouragement, and understanding. Thanks for being my lover, my friend, and my partner. You are always the source of my strength and faith that raises me up to go forward.

Table of Contents

Abstract	ii
Preface	v
Acknowledgements	vii
Table of Contents	viii
List of Tables	xiii
List of Figures	xiv
List of Abbreviations and Symbols	xx
Chapter 1	1
Introduction and research hypotheses and objectives	1
1.1 Introduction	1
1.1.1 Canola proteins.....	3
1.1.2 Oat proteins	5
1.1.3 Protein gelling properties	8
1.1.4 Protein gels as nutraceutical delivery system.....	10
1.2 Hypotheses and objectives	12
Chapter 2	14
Literature review	14
2.1 Food protein gels	14
2.1.1 Globular protein gels.....	15
2.1.2 Gelatin gels.....	19
2.2 Development of protein gels	20
2.2.1 Hydrogen bonds	21
2.2.2 Hydrophobic interactions	22
2.2.3 Electrostatic interactions	23

2.2.4 van der Waals interactions	24
2.2.5 Disulfide bonds	25
2.3 Formation mechanism of protein gels	26
2.3.1 Thermal-induced protein gels.....	26
2.3.2 Cold-set protein gels.....	28
2.3.3 Fractal analysis for gel formation mechanism	30
2.4 Protein-polysaccharide complex gels.....	33
2.4.1 Thermodynamic compatibility (associative separation)	34
2.4.2 Thermodynamic incompatibility (segregative separation).....	35
2.4.3 Different types of protein and polysaccharide complex gels	35
2.5 Food applications of protein gels	37
2.5.1 Protein gelling property in food applications.....	37
2.5.2 Protein gel-based controlled release delivery system for nutraceuticals.....	39
2.6 Opportunities of using plant protein gels for food applications.....	52
Chapter 3.....	53
Impact of pH and heating temperature on formation mechanisms and properties of thermally induced canola protein gels.....	53
3.1 Introduction	53
3.2 Materials and methods	55
3.2.1 Materials and chemicals.....	55
3.2.2 Canola protein extraction	56
3.2.3 Zeta potential, thermal and rheological properties of canola protein suspensions.....	57
3.2.4 Preparation of heat-induced canola protein gels	58
3.2.5 Mechanical properties	58
3.2.6 Gel morphology.....	59
3.2.7 Protein structures and interactions in canola protein gels	59

3.2.8 Statistical analysis	60
3.3 Results and discussion.....	61
3.3.1 Canola protein fractionation and characterization	61
3.3.2 Gel mechanical properties	65
3.3.3 Canola protein gel formation mechanism	68
3.4 Conclusions	83
Chapter 4.....	85
Fabrication, characterization and controlled release properties of oat protein gels with percolating structure induced by cold gelation	85
4.1 Introduction	85
4.2 Materials and methods	87
4.2.1 Materials.....	87
4.2.2 Gelation process of OPI solutions with GDL addition	88
4.2.3 Cold-set OPI gel preparation.....	89
4.2.4 OPI gel properties.....	89
4.2.5 Gel morphology.....	90
4.2.6 Protein structures in OPI gels.....	90
4.2.7 Determination of fractal dimension.....	92
4.2.8 Encapsulation and protection of bioactive compounds.....	93
4.2.9 Controlled release of bioactive compounds	95
4.2.10 Statistical analysis	96
4.3 Result and discussion	96
4.3.1 Cold-set OPI gel preparation and characterization	96
4.3.2 OPI gel formation mechanism study	105
4.3.3 Encapsulation and controlled release of bioactive compounds.....	117
4.4 Conclusions	123

Chapter 5.....	125
Oat protein-shellac beads: superior protection and delivery carriers for sensitive bioactive compounds	125
5.1 Introduction	125
5.2 Materials and methods	128
5.2.1 Materials.....	128
5.2.2 Preparation of OPI, shellac solutions and their mixtures	129
5.2.3 Characterization of OPI – shellac mixtures.....	130
5.2.4 Preparation of OPI-shellac based beads (OSB).....	131
5.2.5 Characterizations of the OPI-shellac based beads.....	131
5.2.6 Loading of bioactives in the beads.....	133
5.2.7 Release profiles in the simulated gastro-intestinal environment.....	133
5.2.8 Stability of the bioactive compounds in the simulated gastro-intestinal environment.....	134
5.2.9 Statistical analysis	135
5.3 Results and discussion.....	136
5.3.1 Solution behavior and interactions of OPI and shellac mixtures	136
5.3.2 Core (OPI) – shell (OPI-shellac) bead structure characterizations	140
5.3.3 Bio-related applications.....	147
5.4 Conclusions	156
Chapter 6.....	158
Fabrication of novel protein-shellac nanoparticles for improved bioavailability of resveratrol and its antioxidant effect in vivo	158
6.1 Introduction	158
6.2 Materials and methods	160
6.2.1 Materials.....	160
6.2.2 Preparation of resveratrol-loaded OPI-shellac nanoparticles.....	161

6.2.3 Characterization of nanoparticles.....	162
6.2.4 In vitro release study	163
6.2.5 Cell culture	164
6.2.6 In vivo study.....	169
6.2.7 Statistical analyses.....	173
6.3 Results and discussion.....	174
6.3.1 Characterization of resveratrol-loaded OPI-shellac nanoparticles.....	174
6.3.2 In vitro release properties.....	177
6.3.3 In vitro cellular uptake and transport	182
6.3.4 In vitro cellular antioxidant activities.....	189
6.3.5 In vivo pharmacokinetic studies in Wistar rats	192
6.3.6 Hepatoprotective effect	196
6.4 Conclusions	200
Chapter 7.....	202
Summary, conclusions and suggestions for future research	202
7.1 Summary and conclusions.....	202
7.2 Significance of the research	206
7.3 Recommendations for future work.....	207
References	209

List of Tables

Table 3-1. Effect of different pH values on thermal properties of canola proteins (15% w/v)....	62
Table 4-1. Experimentally measured rheological data and derived microscopic structural parameters of OPI gels prepared at different GDL concentrations.	112
Table 5-1. Various ratios and components of OPI/shellac solutions.....	129
Table 6-1. Encapsulation capacity (EC), encapsulation efficiency (EE), size, polydispersity index (PDI), zeta-potential and surface hydrophobicity of resveratrol-loaded OPI-shellac NPs...	175
Table 6-2. Pharmacokinetic parameters of resveratrol (RSV) obtained after the administration of the different formulations tested at a dose of 20 mg/kg.....	194

List of Figures

- Fig. 2-1.** Scanning electron micrographs of (a) filamentous gel, (b) particulate gel, and (c) percolating gel. Adapted from Chen et al. (2006) and Czerner et al. (2013).....17
- Fig. 2-2.** Mechanisms of denaturation and aggregation of filamentous and particulate gels.....27
- Fig. 2-3.** Mechanisms of denaturation/aggregation and cold-set gelation of globular proteins induced by addition of Ca^{2+} 29
- Fig. 2-4.** Mechanisms of filamentous and particulate protein cold-set gelation induced by addition of Ca^{2+} 32
- Fig. 2-5.** Associative or segregative interactions of protein and polysaccharide mixtures33
- Fig. 2-6.** Illustration of controlled release mechanism: diffusion, swelling, and degradation.....49
- Fig. 3-1.** Temperature dependence of storage modulus (G' , ●) and loss modulus (G'' , ○) of CP1 and CP2 (15%, w/v) suspensions with a heating rate of 5 °C/min at a frequency of 1 Hz. The data are shifted along the vertical axis by 10^a with the given value to avoid overlapping....64
- Fig. 3-2.** Effects of pH and heating temperature on the mechanical properties of thermally-induced CP1 and CP2 gels (15%, w/v).68
- Fig. 3-3.** SEM images of the cross-sections of thermally-induced CP1 gels (15%, w/v) formed at different pHs and heating temperatures: (a) pH 5, 80 °C; (b) pH 7, 80 °C; (c) pH 9, 80 °C; (d) pH 11, 80 °C; (e) pH 5, 120 °C; (f) pH 7, 120 °C; (g) pH 9, 120 °C, 3min; and (h) pH 9, 120 °C. Scale bar: 5 μm69
- Fig. 3-4.** SEM images of the cross-sections of thermally-induced CP2 gels (15%, w/v) formed at different pHs and heating temperatures: (a) pH 5, 80 °C; (b) pH 7, 80 °C; (c) pH 9, 80 °C; (d)

pH 11, 80 °C; (e) pH 5 120 °C; (f) pH 7, 120 °C; (g) pH 9, 120 °C; and (h) pH 11, 120 °C. Scale bar: 5 µm.....	71
Fig. 3-5. Deconvoluted FTIR spectra of CP1 and CP2 suspensions (5% w/v in D ₂ O) at different pHs upon heating from 25 to 80 °C (a, b, c) and dried CP1 and CP2 gels formed at 120 °C (d).....	74
Fig. 3-6. Frequency dependence of storage modulus (G') of CP1 and CP2 gels (15%, w/v) formed at different pHs and 120 °C with or without soaking in dissociation reagents.....	78
Fig. 3-7. Photos of CP1 gels (15%, w/v) prepared at different pHs and 120 °C with or without soaking in dissociation reagents.....	80
Fig. 3-8. Photos of CP2 gels prepared (15%, w/v) at different pHs and 120 °C with or without soaking in dissociation reagents.....	82
Fig. 4-1. Time dependence of pH value (a, b) and storage modulus (G') (c, d) of OPI solutions with addition of different GDL concentrations. (e, f) Frequency dependence of storage modulus (G', solid) and loss modulus (G'', open) of OPI gels prepared at different GDL concentrations. a, c, and e represent gels prepared at 5% (w/v) protein concentration; b, d, and f represent gels prepared at 7% (w/v) protein concentration.....	97
Fig. 4-2. (a) Compressive stress, (b) springiness, and (c) water holding capacity of OPI gels prepared at different GDL and protein concentrations. Different letters on the top of the columns indicate the significant difference ($p < 0.05$).....	100
Fig. 4-3. SEM images of OPI gels prepared at different GDL concentrations: (a) OG5-3; (b) OG5-5; (c) OG5-10; (d) OG5-15; (e) OG7-3; (f) OG7-5; (g) OG7-10; and (h) OG7-15. Scale bar: 5 µm; scale bar of inserts: 2 µm.....	103

Fig. 4-4. Fourier-deconvoluted FTIR spectra of (a) OPI solutions (1% w/v in D₂O) upon heating and cooling; and (b) preheated OPI solutions (1% w/v in D₂O) with different GDL concentrations.....106

Fig. 4-5. (a) Size distributions of OPI in water at pH 8 before heating (BH), after heating to 115 °C (AH) and preheated OPI solution with 3% GDL. AFM images of OPI solutions: (b) BH; (c) AH to 115 °C; and (d) preheated OPI solution with 3% GDL.....108

Fig. 4-6. (a) Storage modulus - strain profiles of OPI gels prepared at different protein concentrations and 3% GDL. Double-logarithmic plots of critical strain (b) and storage modulus (c) of OPI gels prepared at different GDL contents as a function of protein concentrations.....111

Fig. 4-7. Schematic illustration of formation mechanism of cold-set OPI gels with percolating network structure induced by GDL.....115

Fig. 4-8. (a) Activity of encapsulated α -amylase after being immersed in SGF for 0.5, 1, 1.5, and 2 h. (b) Viable count and (c) survival of encapsulated *Lactobacillus acidophilus* after being immersed in SGF for 0.5, 1, 1.5, and 2 h. (d) Release profiles of riboflavin from drug-loaded OG7-10 gels at 37 °C in HCl-saline buffer (pH 1.2) for 2 h and then in PBS buffer (pH 7.4) for 15 h with or without digestive enzymes.....118

Fig. 4-9. SEM images of OG7-10 gels after being immersed in SGF for 1 h (a) and 2 h (b) at 37 °C. Scale bar: 10 μ m.....120

Fig. 5-1. Dependence of (a) storage modulus (G' , solid symbols) and loss modulus (G'' , open symbols) and (b) complex viscosity on the angular frequency for oat protein-shellac composite solutions.....137

Fig. 5-2. (a) Raw data plot of heat flow against time for titration of shellac (1 mM) into OPI (4.97 μ M) at pH 8; and (b) binding isotherm of OPI-shellac complex derived from the integrated raw data. The curve represents a modelling result obtained from fitting the data.....138

Fig. 5-3. FTIR spectra of OPI-shellac composite beads (OSB-0, OSB-1, OSB-4, and OSB-5) and the mixed dry powder of OPI and shellac (OS-mix).....141

Fig. 5-4. SEM images of surface of OPI-shellac composite beads: (a) OSB-0; (b) OSB-1; (c) OSB-3; and (d) OSB-5. Scale bar: a, b, and c-2 μ m; d-5 μ m; internal picture-20 μ m.....143

Fig. 5-5. DSC thermograms of OPI-shellac beads with OPI and shellac mixture shell at different ratios.....145

Fig. 5-6. SEM images of cross section of OPI-shellac composite beads: (a) OSB-0; (b) OSB-1; (c) OSB-3; and (d) OSB-5. Parallel lines in red indicate the shell structure of beads. Scale bar: 2 μ m.....146

Fig. 5-7. (a) Release profiles of riboflavin from OSB at pH 1.2 for 2 h and in pH 7.4 PBS for another 10 h at 37 $^{\circ}$ C. (b) Release profiles of riboflavin from OSB in simulated gastric fluid (pH 1.2 + pepsin) for 2 h and in simulated intestinal fluid (pH 7.4 + pancreatin) for 7 h at 37 $^{\circ}$ C.....149

Fig. 5-8. (a) Encapsulation efficiency of OSB with various shell materials; (b) Survival ratios of encapsulated *Lactobacillus acidophilus* after immersing in simulated gastric fluid (pH 1.2 + pepsin) for 0.5, 1, 1.5, and 2 h; (c) Release profile of encapsulated *Lactobacillus acidophilus* from OSB-1 after immersing in simulated intestinal fluid (pH 7.4 + pancreatin).....153

Fig. 5-9. Activity of encapsulated α -amylase in OSB-1 after immersing in simulated gastric fluid (pH 2 + pepsin) for 0.5, 1, 1.5, and 2 h.....156

Fig. 6-1. TEM images of resveratrol-loaded OPI-shellac nanoparticles: (a) NP-0S; (b) NP-50S; (c) NP-100S; and (d) NP-200S.....177

Fig. 6-2. Release profiles of resveratrol from fresh OPI-shellac nanoparticles: (a) pH 2; (b) pH 7.4; (c) SGF; and (d) SIF.....178

Fig. 6-3. (a) Cell viability of Caco-2 cells after incubation with OPI-shellac nanoparticles for 24h; (b) RSV uptake efficiency of nanoparticles and free-resveratrol (Free-RSV) (Significant difference between formulations was expressed as ^{a,b,c} at $p < 0.05$; significant difference between time within the same formulation was expressed as ^{A,B,C; X,Y,Z; x,y,z} at $p < 0.05$, respectively) and (c) uptake mechanism by Caco-2 cells. Difference between various inhibitor within same formulation was expressed as ^{a,b; A,B,C; x,y,z} at $p < 0.05$, respectively.....183

Fig. 6-4. CLSM images of Caco-2 cells incubated with NP-100S (0.25 mg/mL) at (a) 37 °C for 1 h; (b) 37 °C for 3 h; (c) 37 °C for 6 h; and (d) 4 °C for 6 h. Scale bar: 10 μm..... 185

Fig. 6-5. Resveratrol transport efficiency across Caco-2 cell monolayer at 37 °C for 6 h. Data represent mean ± standard deviation, n =3. Different letters indicated significant difference ($p < 0.05$).....188

Fig. 6-6. (a) Cell viability of Chang liver cells incubated with OPI-shellac NPs for 24 h; (b) Quantification of intracellular ROS in DCFH-DA-labelled Chang liver cells. Values with different letters are significantly ($p < 0.05$) difference. and (c) Increase in intracellular glutathione content in Chang liver cells treated with nanoparticless and free-resveratrol (Free-RSV). Significant difference between formulations was expressed as ^{a,b,c,d} at $p < 0.05$; significant difference between concentrations within same formulation was expressed as ^{x,y,z} at $p < 0.05$190

Fig. 6-7. Resveratrol plasma concentration versus time after a single administration at a dose of 20 mg/kg. RSV-inject: intravenous administration of resveratrol; Free-RSV: oral administration of resveratrol suspension; NP-0S and NP-100S: resveratrol-loaded OPI-shellac nanoparticles.....193

Fig. 6-8. (a) Effects of resveratrol treatment (20 mg/kg) on serum aspartate aminotransferase (AST) and alanine aminotransferase (ALT) levels in 20% CCl₄ (in olive oil 2.5 mL/kg) induced liver injury. Each column represents the mean of 6 animals, # significant difference from blank ($p < 0.01$), * significant difference from control ($p < 0.01$) and Free-resveratrol (Free-RSV). Effects of resveratrol treatment (20 mg/kg) on (b) catalase (CAT), (c) glutathione (GSH), and d) ROS levels in 20% CCl₄ (in olive oil 2.5 mL/kg) induced liver injury. Different letters indicated significant difference ($p < 0.05$) between each group.....197

Fig. 6-9. Liver histological sections of rats from (a) blank; (b) control; (c) Free-resveratrol (Free-RSV); and (d) NP-100S groups.....199

List of Abbreviations and Symbols

ΔG	Gibbs free energy
ΔH	Enthalpy of mixing
ΔS	Entropy of mixing
2-ME	2-mercaptoethanol
ALT	Alanine aminotransferase
ANOVA	Analysis of variance
AST	Aspartate aminotransferase
ATCC	American Type Culture Collection
AUC	Area under the curve
BSA	Bovine serum albumin
CAT	Catalase activity
CFU	Colony forming units
C_{max}	Peak plasma concentration
Col	Colchicine
CP1	Water-soluble canola protein isolate
CP2	Salt-soluble canola protein isolate
CPZ	Chlorpromazine hydrochloride
CSLM	Confocal laser scanning microscopy
CyD	Cytochalasin D
DAPI	4',6-diamidino-2-phenylindole
DCFH-DA	2,7-dichlorodihydro-fluorescein diacetate
D_f	Fractal dimension
DLS	Dynamic light scattering
DMEM	Dulbecco's modified eagle medium
DMSO	Dimethyl sulfoxide
DSC	Differential scanning calorimetry
DTNB	5,5-dithiobis (2-nitrobenzoic acid) (DTNB)
EC	Encapsulation capacity
EE	Encapsulation efficiency
FAO	Food and Agriculture Organization
FBS	Fetal bovine serum
FITC	Fluorescein isothiocyanate
FLI	Filipin III
F_r	Relative bioavailability
FTIR	Fourier transform infrared spectroscopy
G'	Storage modulus

G''	Loss modulus
GDL	Glucono- δ -lactone
GI	Tract Gastrointestinal tract
GRAS	Generally recognized as safe
GSH	Glutathione
HBSS	Hank's balanced salt solution
HEPES	4-(2-hydroxyethyl)-1-piperazineethanesulfonic acid
mBBr	Monobromobimane
MTT	Thiazolyl blue tetrazolium bromide
Mw	Molecular weight
Nano- ITC	Nano-Isothermal Titration Calorimeter
NEAA	Non-essential amino acids
NP	Nanoparticles
NR-NPs	Nile red-labeled nanoparticles
Ø	Concentration of the gel
OG	Oat protein gel
OPI	Oat protein isolate
OS	Oat protein isolate-shellac
OSB	Oat protein isolate-shellac bead
PBS	Phosphate-buffered saline
PDI	Polydispersity index
PQ	Partitioning quotient
RB	Rose Bengal
ROS	Reactive oxygen species
RP-HPLC	Reverse phase high performance liquid chromatography
RSV	Resveratrol
SDS	Sodium dodecyl sulfate
SDS-PAGE	Sodium dodecyl sulfate polyacrylamide gel
SEM	Scanning electron microscopy
SGF	Simulated gastric fluid
SIF	Simulated intestinal fluid
S_o	Surface hydrophobicity
T_{1/2}	Half-life in the terminal phase
t-BHP	tert-Butyl hydroperoxide
T_d	Denaturation temperature
TEER	Transepithelial electrical resistance
TEM	Transmission electron microscopy
T_g	Glass transition temperature
WHC	Water holding capacity

WHO

β

β -LG

γ_0

World Health Organization

Auxiliary parameter;

Beta-lactoglobulin

Critical strain

Chapter 1

Introduction and research hypotheses and objectives

1.1 Introduction

The global interest in the development of plant protein based products is growing because of their lower cost, sustainability, religious reasons, cultural reasons, and reduced risk of spreading disease such as bovine spongiform encephalopathy (mad cow disease) (Lai & Guo, 2011; Kim, Furuya, & Tabata, 2014; Gaowa et al., 2014). So far, soy protein is the most widely explored and consumed plant protein and plays an important role in the non-animal protein market (Agriculture & Agri-Food Canada, 2015). Soy protein has good functionalities such as gelling, emulsifying, foaming, and water and oil-holding capacity (Nishinari, Rang, Guo, & Phillips, 2014). Soy protein especially has an excellent gelling property, thus has been extensively utilized in the food industry, such as in tofu products and comminuted meats as binder (Kinsella, 1979; Poysa, 2006). However, soy protein alone is insufficient to meet the requirements from the markets and consumers for more diversified functionalities and sensory attributes. The emerging canola protein and oat protein are good sources of plant proteins. Canola meal contains up to 36-39% protein on a dry weight basis, which has been suggested as a good source of plant protein for human consumption due to its well-balanced amino acid composition and high biological value (Pastuszewska, Ochtabinska, & Morawski, 2000; Aider & Barbana, 2011). Considering the large amount of by-products produced by the oil extraction process, one clearly sees that it would be

greatly beneficial to the agricultural industry to develop techniques to use this canola protein source in value-added products. Oat has the highest protein level (12-24%) among cereals and a superior amino acid profile containing high quantities of essential amino acids, lysine and threonine (Mohamed, Biresaw, Xu, Hojilla-Evangelista, & Rayas-Duarte, 2009, Klose & Arendt, 2012). Oat protein is the by-product after β -glucan extraction and currently awaits research to develop its full value (Inglett, Lee, & Stevenson, 2008). In particular, the 12S globulin proteins in canola and oat are similar to those of 11S soy globulin protein. Therefore, proteins from canola and oat may have good potential to provide novel plant based functional ingredients for food and non-food applications.

In addition to the high nutritional values, food proteins are widely used in formulated foods because of their excellent functional properties, such as emulsification, gelation, foaming, and water-/oil-binding capacity. Among these functional properties, the gelling property is especially interesting. Since protein gels with diverse mechanical properties and three-dimensional microstructure can be formed by controlling the aggregation of protein molecular chains through covalent and non-covalent interactions, they offer the ability to produce various foods with distinct textures and the possibility to entrap molecules of interest into gel networks and protect and deliver them to the physiological targets (Chen, Remondetto, & Subirade, 2006). The good gelling properties of soy protein, as well as the soy protein gel-based nutraceutical delivery systems, have been emphasised (Maltais, Remondetto, Gonzalez, & Subirade, 2005; Maltais,

Remondetto, & Subirade, 2009). Canola protein and oat protein, which are similar to soy protein, thus possess gelling potential (Khattab, & Arntfield, 2009; Ma & Wood, 1987). However, research on canola protein and oat protein gelation properties and their applications is limited.

1.1.1 Canola proteins

Along with steadily increasing canola production, Canada produced approximately 17.2 million tons of canola in 2015, as reported by the Canola Council of Canada. The global demand for canola is mainly for its edible oil. However, a protein-rich meal is left behind after oil has been removed from the seed. This residue is mainly used as animal feed. Canola meal contains up to 36-39% protein on a dry weight basis, which has been suggested as a good source of plant protein for human consumption due to its well-balanced amino acid composition and high biological value (Pastuszewska et al., 2000; Aider & Barbana, 2011). Canola protein is made up of approximately 70% of salt soluble globulins, 20% of alcohol-soluble prolamins, and 10-15% water-soluble albumins (Salunkhe, Chavan, Adsule, & Kadam, 1992). Globulin and albumin fractions are two major storage proteins in canola seeds. Cruciferin is a neutral 12S globulin with high molecular weight of 300 kDa (Hoglund, Rodin, Larsson, & Rask, 1992). It is a hexameric protein where each subunit contains acidic/ α (30 kDa) and basic/ β (20 kDa) polypeptides linked by both disulfide bonds and non-covalent bonds to form more complex structures (Monsalve, Villalba, Lopez-Otin, & Rodriguez, 1991; Schwenke, 1994). In the secondary structure, cruciferin has a low content of α -helical structure (10%) and a high content of β -sheet

conformation (50%) (Zirwer, Gast, Welfle, Schlesier, & Schwenke, 1985). Napin is a basic 2S albumin with low molecular weight of 14 kDa (Hoglund et al., 1992). It is composed of two polypeptide chains with molecular weights of 9 kDa and 4 kDa that are held together mainly by disulfide bonds (Monsalve et al., 1991; Schwenke, 1994), while the secondary structure of napin contains a high α -helical structure (40-46%) and a low content of β -sheet conformation (12%) (Schwenke, 1994). Prolamins in rapeseed exist as oleosin, which is a structural protein associated with oil bodies (Ghodsvali, Khodaparast, Vosoughi, & Diosady, 2005), and the molecular weight is around 15-26 kDa (Huang, 1992). The amino acid composition of the canola protein is well balanced and show high glutamine, glutamic acid, arginine and leucine contents, and low amounts of sulfur-containing amino acids (Chabanon, Chevalot, Framboisier, Chenu, & Marc, 2007). These compositions may change depending on the protein extraction process.

Since soy protein gelling properties are widely used to produce various foods with distinct textures, analogous opportunities may exist for canola proteins. The gelling properties of canola proteins had been studied mostly in terms of the least gelling concentration, rheological properties or gel microstructure (Gill & Tung, 1978; Khattab & Arntfield, 2009). To improve the gelling properties, modification of protein structure, for example, by transglutaminase (TG) treatment (Pinterits & Arntfield, 2008), and the inclusion of low levels of polysaccharides such as κ -carrageenan were conducted (Uruakpa & Arntfield, 2004). Limited works reported the interactions involved in the canola gel network formation. In spite of the progress made by other

researchers, canola protein gel properties, gelation mechanism and interactions involved in gel formation, and stability prepared under different processing conditions were not fully elucidated. Gels with different network structures may have different functional properties (Remondetto, Paquin, & Subirade, 2002; Remondetto, Beyssac, & Subirade, 2004). These different structures can be induced by modulating protein conformation and interactions through controlling processing conditions such as pH, temperature, protein concentration, and salt concentration, among others. Although several studies have been carried out on the molecular profile of canola protein, there is limited literature that relates these findings to its gelling properties. Thus, a more comprehensive study on canola protein gel should be conducted to better understand the gel formation mechanism and relationship between structure and gel properties.

1.1.2 Oat proteins

Oat is an important food grain in the world and contains high amounts of valuable nutrients, such as soluble fiber, proteins, unsaturated fatty acids, vitamins, minerals, and antioxidants (Klose & Arendt, 2012). Canada is the world's largest oat exporter, accounting for 45-50% of world oat exports in 2009-2010 (Agriculture and Agri-Food Canada, 2013). Currently, oat products is mainly used for human consumption and animal feed. Specifically, the high content of soluble fiber in oat, β -glucan, has the ability to reduce blood cholesterol, regulate blood glucose level, and reduce the risk of heart disease (Zhu, Du, & Xu, 2016). Several techniques

have been developed to extract and concentrate β -glucan (Vasanthan & Temelli, 2008). The remaining major component, oat protein, is awaiting research to develop its full value.

Oat contains high amounts of protein, which can be as high as 12-24% after removing the high cellulose and low protein hull (Gulvady, Brown, & Bell, 2013). The major storage protein in oats belongs to the globulin fraction, which accounts for 70-80% of total proteins. The major oat globulin fraction is 12S that is similar to 11S legume protein (Peterson, 1978), and other minor fractions are 7S and 3S, which are believed to be vicilin-like proteins (Klose & Arendt, 2012). The 12S fraction contains two major subunits with a molecular weight of about 20-24, and 27-37 kDa, called the acid α - and basic β -subunits (Burgess, Shewry, Matlashewski, Altosaar, & Mifflin, 1983; Shotwell, Boyer, Chesnut, & Larkins, 1990). Since each subunit contains only a single conserved cysteine residue, the α - and β -subunits are disulfide bonded in the native globulin, forming a dimer with a molecular weight of 53-58 kDa (Burgess et al., 1983; Muench & Okita, 1997). Then the dimers further associate into a hexamer with a molecular weight of 322 kDa (Peterson, 1978). The 7S globulin of oats has major subunits with a molecular weight of about 55 kDa, while the 3S fraction is consistent with two major components with a molecular weight of 15 and 21 kDa (Robert, Adeli, & Altosaar, 1985). Unlike other crops such as wheat, barley, and rye that have a high percentage of prolamins as the storage protein, the prolamin content (4-15%) in oats is known to be low. Oat prolamin contains two major components with a molecular weight of 20 and 43 kDa and a minor part of 36 kDa (Ma & Harwalkar, 1984). Albumin

represents at most 10% of the oat storage proteins, while glutelins in oat are found in very low proportion (Robert, Nozzolillo, Cudjoe, & Altosaar, 1983). Oat albumin composes the major part with a molecular weight of 15 kDa and a minor component of 6 kDa. In spite of high protein content, oat protein is superior to other plant proteins also because of its higher amounts of limiting amino acid lysine and threonine (Gulvady et al, 2013; Klose & Arendt, 2012). It has been reported that seven of the eight essential amino acids (isoleucine, leucine, lysine, methionine, phenylalanine, threonine, and valine) make up approximately 32.3 and 31.2% of total amino acids for oat protein isolate and oat flour, respectively (Liu et al., 2009). The percentage of some essential amino acids fulfilled or exceeded their respective percentage stated in ideal protein; however, the slightly low level of lysine and methionine in oat protein isolate is not sufficient to supply children as recommended by the Food and Agriculture Organization of the United Nations (FAO) of United States and World Health Organization (WHO) (Liu et al., 2009).

Since the oat protein 12S fraction is pretty similar to the 11S fraction of soy (glycinin), it has a high potential to act as a gelling agent. However, studies on oat protein gelling properties are still limited. Previous works demonstrated that oat protein could only form strong gels at pH 9-10, but the gel was weak and had low water holding capacity at acidic and neutral pH (Ma & Harwalkar, 1984; Ma, Khanzada, & Harwalkar, 1988). Some modifications, such as acetylation and succinylation, were applied to improve oat protein gelling properties (Ma & Wood, 1987). However, these oat protein gels were still weak compared to those animal proteins. More recently,

Nieto-Nieto et al. (2014) prepared trypsin treated oat protein thermal-induced gels with comparable mechanical strength to egg white protein gel at pH 9, suggesting that oat protein can be used as new gelling materials in food formulations based on plant resources. The same research group also demonstrated the improved thermal gelling properties of oat protein through combination with polysaccharide, and revealed that heat-induced oat protein gels exhibited a percolating network structure (Nieto-Nieto, Wang, Ozimek, & Chen, 2014; 2015; 2016), which was similar to gelatin but different from many other globular proteins that usually formed particulate or filamentous microstructure (Lefèvre, & Subirade, 2000). Such percolating structure not only confers the gel good mechanical properties (Forte, D'Amico, Charalambides, Dini, & Williams, 2015), but is also of relevance when developing drug delivery systems (Kim, Furuya, & Tabata, 2014). This structure has opened an opportunity for oat protein to be developed as a novel gelling ingredient to improve food texture. In spite of good potential, cold induced oat protein gels have never been reported. Since gels are formed at ambient temperature, cold gelation will provide new opportunities for oat protein gels to be used as gelling ingredient in food systems where heating is unfavorable, or as delivery systems of heat labile bioactive compounds.

1.1.3 Protein gelling properties

Gel is an infinite three-dimensional water-swollen network of hydrophilic polymers that can hold a large amount of water and exhibit semi-solid morphology (Qiu & Park, 2001). Gelation, as

one of the most important functional properties of proteins, provides a structural matrix for holding water, flavor, sugar, and food ingredients in various food applications, as well as providing texture and mechanical support in foods (Jideani, 2011). For example, soy protein isolate is commonly used in comminuted meats (sausage, meat loaves) to impart firmness, palatability, and texture upon gelation following cooking and improve moisture retention and overall yields (Jideani, 2011). Factors that are known to affect protein gelation include protein concentration, pH, ionic strength, heating temperature, and the presence of non-protein components (e.g. polysaccharides and fats), which in turn impact gel microstructures (Sathe, 2002; Remondetto et al., 2002). At pH level apart from the protein isoelectric point or at low ionic strength, globular protein gel forms a filamentous microstructure that is composed of more or less flexible linear strands, while at pH near the protein isoelectric point or at high ionic strength, this gel shows a particulate microstructure that is composed of large and spherical aggregates. The gel microstructures directly determine the gel bulk properties. For example, particulate gel has less elastic behavior and lower rupture resistance and water holding capacity, while filamentous gel shows more elastic behavior and high resistance to rupture and water-holding capacity (Remondetto et al., 2002). Therefore, understanding the relationship between microstructure and sensory texture is important to develop new products with desired sensory quality.

1.1.4 Protein gels as nutraceutical delivery system

Nutraceuticals have attracted much attention recently since they have physiological benefits and/or the capacity to reduce the risk of chronic diseases (Chen et al., 2006). However, many nutraceuticals are sensitive to environmental conditions during food processing and storage (Bell, 2001), and/or have low oral bioavailability due to insufficient gastric residence time, and low permeability and/or solubility within the intestinal tract, all of which limit their potential health benefiting activities *in vivo* (Chen et al., 2006; Bell, 2001). Therefore, it is necessary to develop efficient vehicles to maintain the activities of these sensitive compounds and deliver them to the physiological target within the organism.

Recently, food protein hydrogels have attracted interest because they not only possess the ability to entrap molecules of interest within networks, and protect and transport them to the physiological target, but also have considerable nutritional value (Chen et al., 2006; Peppas et al., 2000). Moreover, gels with diverse microstructures and properties can be formed by controlling the assembly of protein molecular chains, thus offering the possibility of developing desirable carriers targeting different applications (Chen et al., 2006). Over the last decades, the most widely studied plant protein gel-based delivery vehicle was soy protein gel, which was developed in various sizes (bulk gel, micro- and nano-sized gel) to encapsulate and deliver nutraceuticals (Vilela, Cavallieri, & da Cunha, 2011; Maltais, Remondetto, & Subirade, 2009; Chen & Subirade, 2009; Zhang, Field, Vine, & Chen, 2015). Other plant proteins, such as zein, gliadin, and barley

protein, had also been extensively studied and developed as delivery systems for nutraceuticals (Lai & Guo, 2011; Yang, Zhou, & Chen, 2014). However, these vehicles were not gel-based systems. The most important advantage of gel-based delivery systems is that they have a high water-holding capacity and good biocompatibility to provide a non-reactive environment for sensitive bioactive compounds, such as enzymes, bioactive peptides, and probiotics. Since they can easily be denatured or inactivated at acidic pH, the challenge for developing delivery systems for these sensitive bioactive compounds is to protect the intact molecules in harsh stomach conditions and target delivery to small intestine. Nevertheless, soy protein gels are not sufficient to protect these sensitive bioactive compounds against low pH and pepsin digestion. Thus, plant protein-based gel with advanced properties and desired structures are required.

More recently, cold-induced soy protein gel has become an interesting matrix for delivery of bioactive compounds. This method requires a heating step during which proteins are denatured and then polymerized into soluble aggregates. This step is followed by a cooling step and then the addition of Ca^{2+} or glucono- δ -lactone (GDL), resulting in the formation of a network of soluble aggregates (Maltais et al., 2005). In this case, the gelation is achieved at ambient temperature. This approach has opened opportunities to encapsulate heat-sensitive nutraceuticals to develop novel functional foods (Chen et al., 2006). In the preliminary work, cold-set gelation of canola protein could be formed at alkaline pH (e.g. pH higher than 9), which is not suitable for encapsulation of sensitive bioactive compounds, whereas oat protein cold-set gelation could be

fabricated at neutral pH. Thus, designing cold-set oat protein gel as a delivery system for sensitive bioactive compounds will be a promising and interesting opportunity to develop functional foods.

1.2 Hypotheses and objectives

In the light of previous studies, this thesis research tested the following hypotheses:

1) Properties of thermally-induced canola protein gels can be improved by modulating gel microstructures through modification of the gel forming conditions (pH, heating temperature).

2) Cold-set gels can be formed by oat protein and the gel strength can be improved by modulating gel microstructures through modification of the gel forming conditions (pH, GDL concentration).

3) Micro- and nano-particles can be developed from cold-set oat protein based gels as novel nutraceutical delivery systems.

The objectives of this research program are to achieve the following:

I. To study the effects of gel forming conditions (pH, heating temperature, or GDL concentration) on thermally-induced canola protein and cold-set oat protein gel properties (Chapters 3 and 4).

II. To investigate the formation mechanism of thermally-induced canola protein and cold-set oat protein gels (Chapters 3 and 4).

- III. To explore the feasibility of using cold-set oat protein based gel as oral delivery vehicles for nutraceuticals to improve their bioavailability (Chapters 5 and 6).

The realization of this research will advance our fundamental knowledge of canola/oat protein gel formation mechanisms, and correlate the canola/oat protein molecular structures to the bulk gel properties such as mechanical strength, water-holding capacity, permeability and digestion. Accordingly, the gel structures can be designed at the molecular level to achieve desirable applications, which may open a new route to enhance canola and oat consumption and develop their value-added applications. Future collaboration with the food industry will lead to cooperation of new gelling ingredients as meat binder or fat replacer in food formulations to replace animal proteins or other plant proteins, or creation of new functional foods to reduce the risk of chronic disease and improve public health. Such huge opportunity will provide a new commercialization route for canola/oat protein to significantly benefit Canadian farmers.

Chapter 2

Literature review

2.1 Food protein gels

Hydrogels are hydrophilic polymer networks which have the capacity to retain large amounts of water and exhibit semi-solid status (Qiu & Park, 2001). Covalent and non-covalent bonds, including disulfide bonds, hydrogen bonding, hydrophobic interactions, van der Waals interactions, and/or physical entanglements were involved in the formation of the three-dimensional network of hydrogel (Kamath & Park, 1993). During the past decade, the synthetic polymer hydrogels have been widely used for biomedical and pharmaceutical applications such as tissue engineering (Tessmar & Gopferich, 2007), drug delivery (Nanjawade, Manvi, & Manjappa, 2007) and contact lenses (Keay, Edwards, & Stapleton, 2007). However, these synthetic polymers are not food-grade materials, which limited their application in food industry.

Biopolymers derived from food sources, such as proteins and polysaccharides, have received considerable attention from the food industry and academia due to their good biocompatibility, biodegradability and renewability (Wang, Bamdad, Song, & Chen, 2012). The gelling property is one of the most important functionalities of biopolymer. They can be used to improve food texture and sensory properties. For example, in some dairy products, carrageenan, pectin and gelatine are widely utilized to increase the viscosity and stability in dairy products. The gelling

properties of whey and soy proteins allow them to be binders for meat products. Moreover, they can be used to encapsulate flavors, nutraceutical compounds and even microorganisms (Banerjee & Bhattacharya, 2012; Jideani, 2011; Chen et al., 2006).

Among these biopolymers, food proteins are especially interesting, since they are macro-nutrient and have excellent functional properties, including water-holding capacities and emulsifying, foaming, and gelling properties (Kinsella, 1981; Walstra, 2003; Wang et al., 2012). Gelation is one of the most important and interesting functional properties of protein. By controlling the mechanism of protein molecular chains association, protein hydrogels with diverse microstructures can be formed. They exhibit different texture and mechanical properties, which allow them to be used in various food products. Also, food protein hydrogels also work as biocompatible matrices to retain water, flavour, color, bioactive components, among others. (Nieto-Nieto, 2015; Chen et al., 2006). Several food proteins have demonstrated excellent gelling properties, including gelatin, whey protein, soy protein, casein, egg protein, and pea protein. (Forte et al., 2015; Maltais et al., 2009; Chen & Subirade, 2006; Yan & Pochan, 2010). Among these proteins, gelatin, whey protein, and soy protein are most widely used for the fabrication of gels.

2.1.1 Globular protein gels

Globular proteins (soy protein, whey protein, egg protein, casein, etc) are water-soluble proteins which have a spherical shape that is folded by protein's tertiary structure with a

hydrophobic interior and a polar exterior. Gelation of globular proteins, such as whey and soy proteins, have been studied extensively for years because of their physiochemical significance (such as solubility, protein molecular structures, response to heating temperature and pH, *etc.*), their sophisticated food processing activities including the generation of microgels under shear and their potential to replace fat and change texture (Clark, Kavanagh, & Ross-Murphy, 2001).

2.1.1.1 Thermally-induced globular protein gels

Traditionally, globular protein hydrogels are achieved through heat treatment. At a temperature higher than protein denaturation temperature, protein unfold to expose the buried hydrophobic amino acid residues. Subsequently, protein molecules aggregate into a three-dimensional network through covalent and non-covalent interactions (Chen et al., 2006; Twomey, Keogh, Mehra, & O’Kennedy, 1997; Renkema & van Vliet, 2002). Depending on the preparation conditions, such as heating temperature, pH and ionic strength, protein molecular aggregate into different structure, resulting in various hydrogel network arrangements (Lefèvre & Subirade, 2000). Usually, two types of globular protein gels, particulate and filamentous gels (Figs. 2-1a and b), can be obtained by adjusting the pHs and ionic strengths during gelation. Under the condition of low ionic strength while pH around protein isoelectric point, or the condition of high ionic strength while pH being far from the isoelectric point, proteins formed particulate gels due to the reduced electrostatic interactions and enhanced turbidity (Barbut & Foegeding, 1993; Morris, 2009). These particulate gels are usually composed of large and almost

spherical aggregates (Fig. 2-1a). At pH values far from the protein isoelectric point and under low ionic strength, the repulsive forces between polypeptide chains are enhanced, which promotes the formation of filamentous gels or fine-stranded gels (Fig. 2-1b) (Lefèvre & Subirade, 2000). These kinds of gels are composed of more or less flexible linear strands making up a regular network. For example, thermal-induced bovine milk β -lactoglobulin gel prepared at 80°C exhibited an opaque particulate structure at pH 4 and 6 (near β -lactoglobulin isoelectric point), while the gel was transparent when formed at a pH above 6 and below 4 (far from β -lactoglobulin isoelectric point) and showed filamentous structure (Lefèvre & Subirade, 2000). Various gel structures determine different gel properties. The particulate gels are coarser, opaque, weak, and brittle, and they have lower water holding capacities compared to filamentous gels (Urbonaite et al., 2016).

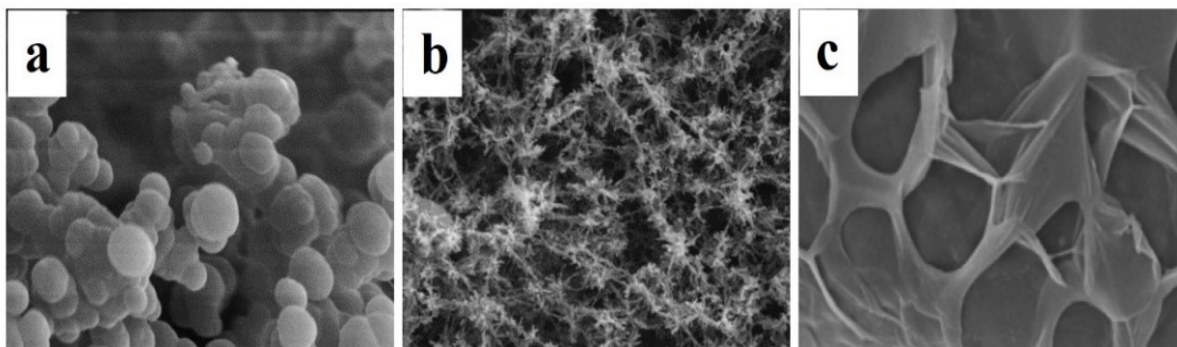


Fig. 2-1. Scanning electron micrographs of (a) filamentous gel, (b) particulate gel, and (c) percolating gel. Adapted from Chen et al. (2006) and Czerner et al. (2013).

2.1.1.2 Cold-set globular protein gels

As an alternative gelation method, cold-set gelation, has recently been developed for globular protein. This method requires a heating step during which proteins are denatured and then associated into soluble aggregates. After cooling, Ca^{2+} or glucono- δ -lactone (GDL) was added to the protein solution to form a network of soluble protein aggregates at an ambient temperature (Roff & Foegeding, 1996). Depending on the Ca^{2+} or GDL concentration, cold-gelation also generates filamentous and particulate gels (Fig. 2-1a and b) (Roff & Foegeding, 1996; Maltais et al., 2009). For example, when Ca^{2+} concentration is 20 mM, the electrostatic repulsive force among whey protein aggregates diminishes rapidly by Ca^{2+} , promoting the fast and random growth of whey protein aggregates in all directions. As a result, whey protein forms particulate gel structure in this situation. On the other hand, a lower Ca^{2+} concentration (10 mM) promotes aggregation growth preferentially along linear ways due to surface charges of protein molecules that are not totally screened, resulting in the formation of a filamentous gel (Maltais, Remeondetto, & Subirade, 2008). Ca^{2+} plays an important role for cross-linking of carboxyl groups of pre-denatured soy proteins since Ca^{2+} reduces the repulsion forces among protein molecules. The low surface repulsion forces facilitate the development of interactions such as hydrophobic interactions, hydrogen bonding, and van der Waals interactions among proteins. Similar to thermal-induced particulate and filamentous gels, these two kinds of gels formed by cold-set gelation also exhibit different gel properties. Generally, filamentous gels have higher gel

strengths with better elasticity and higher water holding capacities compared to particulate gels (Maltais et al., 2005).

2.1.2 Gelatin gels

Gelatin, a typical fibrous protein, is produced via the partial hydrolysis and denaturation of collagen (Schrieber & Gareis, 2007). There are two types of gelatin, A and B, produced from acid and alkaline pre-treatments of collagen, respectively. During heating, gelatin triple-helix structures lose their conformation and become random coiled chains. While cooling, these random coiled molecule chains rearrange into the ordered triple-helix arrangement, followed by propagating and aggregating. These conformation changes lead to the formation of the physically crosslinked hydrogel (Coppola, Djabourov, & Ferrand, 2012; Oakenfull & Scott, 2003; Forte et al., 2015; Duconseille, Astruc, Quintana, Meersman, & Sante-Lhoutellier, 2015). These physical links of gelatin gels are thermo-reversible. Chemically crosslinked gelatin gels can also be fabricated through either the addition of cross-linkers to bridge free carboxylic acid residues of glutamic and aspartic acid or amine groups of lysine and hydroxylysine of protein molecules, or the activation of carboxylic acid residues to react directly with amine groups on adjacent protein chains (Kuijpers et al., 2000; Young, Wong, Tabata, & Mikos, 2005). Aldehydes (formaldehyde, glutaraldehyde, glyceraldehyde), polyepoxides, and isocyanates are usually used to cross-link gelatin, but they may cause safety concerns (Kuijpers et al., 2000). The natural, non-toxic, and enzymatic cross-linker is an alternate approach to cross-link gelatin gels, such as genipin,

carbodiimide/N-hydroxysuccinimide, and microbial transglutaminase (Elzoghby, 2013). Gelatin gel properties, such as mechanical properties and water holding capacities, are determined by processing conditions including protein concentration, heating temperature, and cross-linker type and concentration. Importantly, unlike the globular proteins, gelatin gels exhibit polymer-like percolating network structures with high degrees of cross-linking (Fig. 2-1c) due to their triple-helix molecular chains (Coppola et al., 2012; Duconseille et al. 2015). Such structures confer on gelatin gel strong mechanical properties and excellent water holding capacities, which allow them to be extensively utilized in food industry to thicken and stabilize various products, such as yogurts, jellies, and desserts. This also makes it a good candidate for nutraceutical and drug delivery systems (Forte et al., 2015). In addition, the thermo-reversible characteristic of physically cross-linked gelatin gel is applied widely in food and pharmaceutical applications to develop temperature-triggered gel systems, which aim to “melt” the gel in the mouth or in the stomach (Hellio & Djabourov, 2006). Through controlling thermos-reversible temperature, broader applications of gelatin gel can be achieved, such as medical scaffolds, incubation of mammalian cells, and enzyme immobilization (Kerman, 2008; Sakai, Moriyama, & Kawakami, 2011; Gan, Zhang, Liu, & Wu, 2012).

2.2 Development of protein gels

The gel properties are primarily dependent on the gel three-dimensional network which is developed through cross-linking of protein molecules via covalent (disulfide bonds) and

non-covalent (hydrogen bond, hydrophobic interactions, van der Waals force, et al.) interactions (Ziegler & Foegeding, 1990). Thus, an understanding of these interactions will allow us to design desirable gel structures for different applications.

2.2.1 Hydrogen bonds

Hydrogen bonds are the short-range attractive interactions between polar groups. Hydrogen bonds occur when a hydrogen atom binds to a highly electronegative atom such as nitrogen, oxygen, fluorine, or sulfur (Schmitt, Sanchez, Desobry-Banon, & Hardy, 1998; Semenova & Dickinson, 2010). These hydrogen bonds can occur between molecules (intermolecular) or different parts of a single molecule (intramolecular). Hydrogen bonds are responsible for the secondary and tertiary structures of proteins, as they cause appreciable alignment of the participating molecules (Bryant & McClements, 1998). They are also important for protein folding and unfolding (Semenova & Dickinson, 2010). Moreover, hydrogen bonds are weakened with increasing temperatures and become stronger during cooling (Phillips, Whitehead, & Kinsella, 1994; Semenova & Dickinson, 2010), which play an important role in building gel network structures. For example, physical gelatin gels composed by ordered triple-helix segments are typical gels that are stabilized by intermolecular hydrogen bonds (Joly-Duhamel, Hellio, Ajdari, & Djabourov, 2006). Recently, gelatin gels with different stiffness were developed by modulating gelatin concentration (10-30% w/w), source (bovine/porcine), and solvent composition (0-40% w/w, glycerol/buffer mixture) (Czerner, Fasce, Martucci, Ruseckaite, &

Frontini, 2016). Stiffer gels with apparent gel strengths and swelling properties could be obtained at higher gelatin and glycerol concentrations, where higher amounts of triple helix content resulted in more hydrogen bonds. In globular protein gels, hydrogen bonding as one of the important interactions also plays a vital role in stiffening the gel network during cooling, but usually it works together with other interactions, such as hydrophobic interaction, van der Waals interaction, and disulfide bonds.

2.2.2 Hydrophobic interactions

Hydrophobic interactions occur between polymer chains that have non-polar groups when they are dispersed in aqueous solutions (Wang et al., 2012). When two or more non-polar groups are exposed in water, the extended hydrogen bonding structure of water molecules around the non-polar groups is disrupted and the entropy of the system is changed. These changes are thermodynamically unfavorable; thus the water molecules reorient around the non-polar groups and intermolecular hydrophobic interactions form to minimize the contact between water and non-polar groups and increase entropy (de Jongh, 2007; Wang et al., 2012). Hydrophobic groups behave as associated sites and have a tendency to combine with each other. In globular proteins, the hydrophobic groups are hidden inside and the hydrophilic groups are present on the surface. Since the protein molecules are expected to unfold and expose buried hydrophobic groups during heating treatment, hydrophobic interactions between non-polar segments of adjacent polypeptides tend to increase in strength when the temperature is increased (Phillips et al., 1994; McClements,

Decker, Park, & Weiss, 2009), which greatly contributes to the initial development of protein gel networks. Wang et al. (2017) reported that hydrophobic groups of wheat gluten were exposed and aggregated when heated at temperatures higher than 60°C, resulting in thermally-induced wheat gluten gels. Moreover, a regular three-dimensional network was fabricated at temperatures up to 90°C, suggesting that cross-linking had occurred among the wheat gluten molecules at higher temperatures where larger numbers of exposed hydrophobic groups contributed to the gel initial network formation. For cold-set β -lactoglobulin gels, hydrophobic interaction is the predominant force to form the gel at low iron concentrations, since the superficial charges of the protein units diminish gradually, favoring interaction among their hydrophobic regions (Remondetto & Subirade, 2003). Such a gel usually exhibits better elastic behavior compared to the gel formed at high iron concentrations.

2.2.3 Electrostatic interactions

Proteins usually contain charged side groups, so electric interactions can take place between these electrically charged molecules. The molecules with the same charges are repelled, whereas molecules with opposite charges are preferentially attracted. Depending on this, electrostatic interactions are commonly used as the driving force for protein gel formation. The net charges on protein molecules are impacted by ionic strength and pH. When the pH of the protein solution is around the isoelectric point, the net charge of the protein is zero since the number of positive and negative charges on protein molecules are equal. If the pH is below or above the isoelectric point,

the protein molecules will be either positively charged or negatively charged. Both electrostatic attraction and repulsion control the level of folding/unfolding and expansion of protein molecules and molecular flexibility (Semenova & Dickinson, 2010), which subsequently determine the gel network structure and influence the gel properties. For example, at a pH apart from β -lactoglobulin isoelectric point (pH higher than 6 or lower than 4), the protein undergoes extensive structural modification before aggregation during heating due to the existence of high electrostatic repulsive forces, which eventually promote the alignment of the polypeptide chains via hydrogen bonding and hydrophobic interactions to form a fine-strand structure (Lefèvre & Subirade, 2000).

2.2.4 van der Waals interactions

Van der Waals interactions occur between adjacent non-bonded and uncharged atoms, including forces between permanent dipoles and/or induced (temporary and fluctuating) dipoles. It is a general term to describe the universal weak long-range interactions of electrostatic origin. At very short range separations (2-3 nm), the attractive interactions are transformed into strong repulsion (Semenova & Dickinson, 2010). When polymer molecule is large enough, strong van der Waals interactions could work as attractive forces favoring aggregation of polymers to form a gel (Bryant & McClements, 1998). Van der Waals interactions exist between all groups to some extent; however, they rarely have critical or predominant influence on the net protein molecular interactions or gel formation (Semenova & Dickinson, 2010), as few changes can be observed for

this type of bond during the folding/unfolding transition. Nevertheless, in some cases, it does play an important role in protein gel formation. Cold-set β -lactoglobulin gel formed at high iron concentration (30 mM) showed particulate network structures with weak gel strength, which was essentially controlled by the van der Waals interactions due to the rapid decrease in the repulsion forces at high iron concentration (Remedetto & Subirade, 2003).

2.2.5 Disulfide bonds

Disulfide bonds are covalent bonds, which are strong chemical linkages and play an important role in the folding and stability of globular proteins. In protein structures, disulfide bonds are formed between the thiol groups of cysteine residues by the process of oxidative folding. It links two segments of the protein chain and may form the nucleus of the hydrophobic core of the folded protein, thus stabilizing the protein secondary and tertiary structures. Upon heating-/pressure-induced unfolding, protein expose internal buried disulfide bonds or sulfhydryl groups, which will subsequently undergo disulfide/sulfhydryl exchange reactions with other unfolded polypeptide chains to form a new covalent intermolecular disulfide bond (de Jongh, 2007). To stabilize the gel network structure, the role of disulfide bonds in protein gelation is to increase the length of the polypeptide chains, which can enhance molecular entanglements within the network structure, and restrict the relative thermal motions of the polypeptides (Phillips et al., 1994). In addition, heating under alkaline condition helps to split disulfide bonds used to stabilize protein secondary structure, which induces exposure of more protein molecular side chains and

develops covalent and non-covalent interactions to reinforce the gel network structure with stronger gel strength and water holding capacity. These kinds of strong covalent intermolecular disulfide bonds play an important role in the heat-/pressure-induced gelation of globular protein such as wheat gluten, soy protein, and whey protein. Keim and Hinrichs (2004) developed high-pressure-induced whey protein isolate gels at an operating pressure of 600 MPa and temperature of 30°C. As detected by means of an extraction test with different buffer systems, they identified that disulfide bonds dominated in the formed gels. The number of intermolecular disulfide bonds increased with prolonged pressure holding time, which resulted in a stronger gel with more elastic properties.

2.3 Formation mechanism of protein gels

2.3.1 Thermal-induced protein gels

The thermal-induced gelation includes three steps. Firstly, the protein unfolds during heating, which results in an exposure of hydrophobic groups; secondly, the unfolded molecules aggregate irreversibly through hydrogen bonds, hydrophobic interactions, van der Waals forces, and disulfide bonds; finally, at a sufficient protein concentration, further association of protein aggregates initiates the formation of gel (Lefèvre & Subirade, 2000; Renkema & van Vliet, 2002; Chen et al., 2006). The protein unfolding and aggregation processes directly impact the gel microstructures (particulate and filamentous structures). Taking β -lactoglobulin as an example, at a pH far from protein isoelectric point (pH > 6 or < 4), heating at 30-75°C induced dissociation of

protein dimers into monomers and denaturation of protein molecular structures (Fig. 2-2). When the heating temperature was higher than 80°C, the aggregation occurred. Thus, the extensive protein unfolding allowed a closer alignment of the polypeptide chains to form linear strand, which facilitate the formation of hydrogen bonds. Under this condition, β -lactoglobulin forms filamentous or fine-stranded structures (Lefèvre & Subirade, 2000).

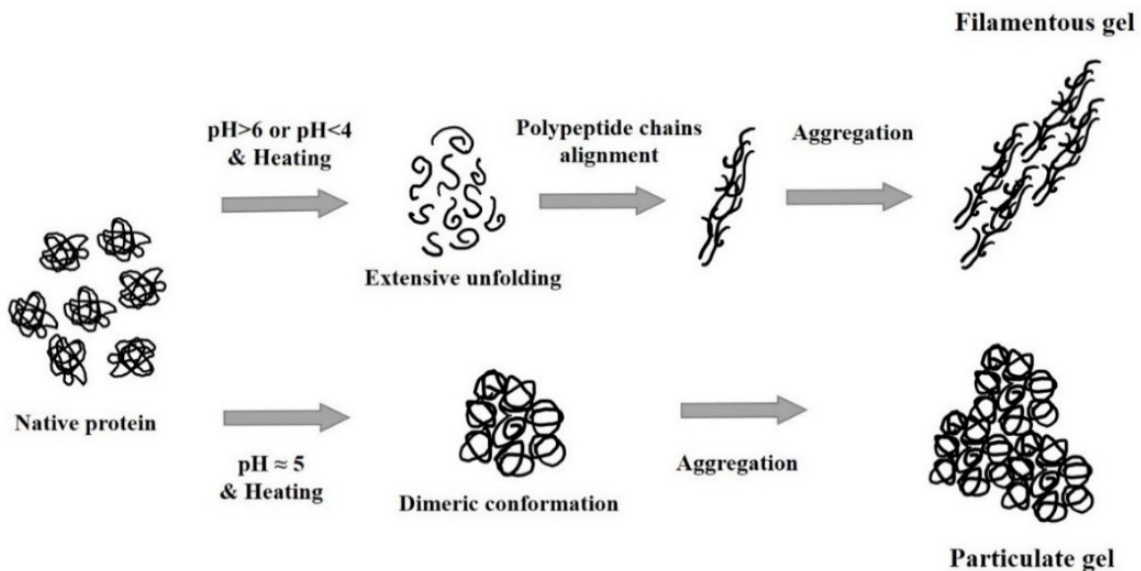


Fig. 2-2. Mechanisms of denaturation and aggregation of filamentous and particulate gels.

In contrast, at pH near protein isoelectric point, the protein structure almost preserved a native-like dimeric conformation without splitting upon reaching 75°C. Then, protein self-aggregate without changing into strand at a temperature higher than 80 °C led to the formation of particulate gel with spherical particles rather than linear strands (Fig. 2-2) (Lefèvre

& Subirade, 2000). Consequently, the differences in terms of intermolecular bonds and protein conformations are responsible for the formation of filamentous and particular gel microstructures, and eventually impact the gel's properties. In particular, the high intensity of intermolecular interactions and abundant cross-linking in filamentous gel structure can explain its better gel properties, such as strength, elasticity, and water holding capacity, compared to particulate gel.

2.3.2 Cold-set protein gels

Cold-set protein gelation includes two steps (Barbut & Foegeding, 1993; Remondetto & Subirade, 2003; Maltais et al., 2008). First, preheating above denaturation temperature causes protein molecules unfolding to expose buried hydrophobic groups and then associate into soluble aggregates that constitute the structural units responsible for the three-dimensional network of gels. To avoid the immediate aggregation of protein molecules or the formation of thermal-induced gel in this step, the protein concentration has to be below a critical value and the pH must be far from the protein isoelectric point or the ionic strength must be low enough. In the second step, salts, e.g. CaCl_2 and FeSO_4 , or acidification agents, e.g. GDL, are added to neutralize the negative charges on the structural unit surfaces to form a gel.

For salt-induced cold gelation, various salt concentrations cause different gel morphologies and formation mechanisms. At high Ca^{2+} or Fe^{2+} concentrations (30 mM) (Fig. 2-3), due to the strong and rapid decrease of repulsive forces and the disruption of energy barriers between structural units, the incipient aggregates get close enough to interact via non-covalent forces with

low potential energy, which results in a random aggregation to form clusters grown in all directions and subsequently produce particulate gel network structures. At low Ca^{2+} or Fe^{2+} concentrations (10 mM) (Fig. 2-3), the gradually diminished superficial charges of the structural units favor interactions among their hydrophobic regions, which promote the aggregate growth in a preferential linear direction and the formation of filamentous gels.

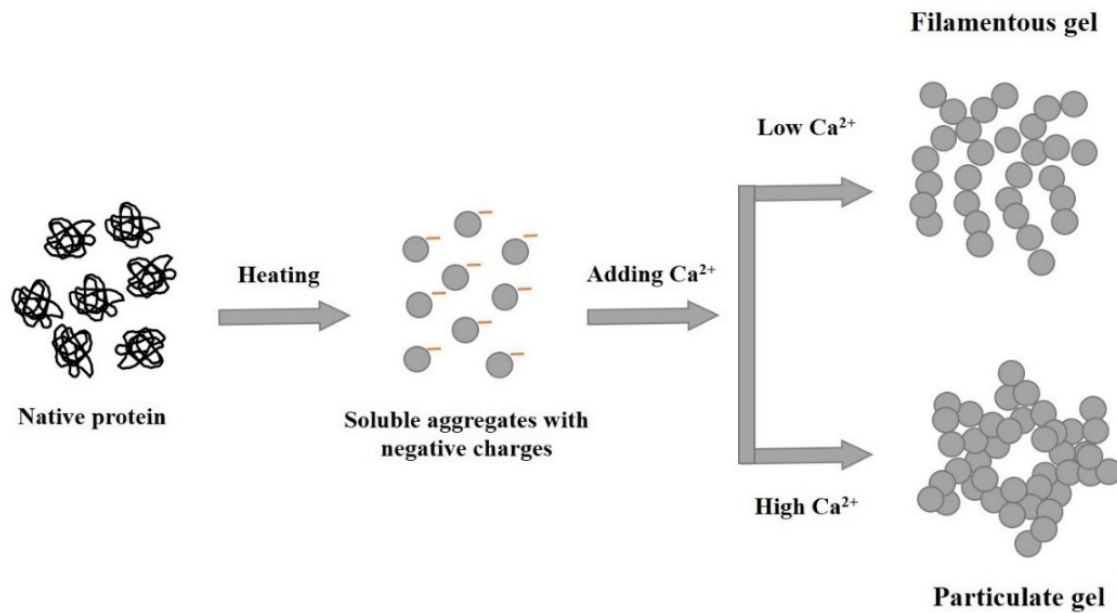


Fig. 2-3. Mechanisms of denaturation/aggregation and cold-set gelation of globular proteins induced by addition of Ca^{2+} .

GDL, as one of the acidulants usually used to produce tofu, has been used in cold-set protein gelation (Cavallieri & da Cunha, 2008; Hu et al., 2013). As with salt-induced gelation, the first step is the preheating of proteins above denaturation temperature to unfold and expose buried hydrophobic groups, followed by the association of protein molecules into soluble aggregates.

GDL can be slowly hydrolysed to gluconic acid, resulting in the reduction of pH. In the second step, GDL works by releasing protons to neutralize the negative charges of protein aggregates which are further associated to form a continuous three-dimensional network through hydrophobic interactions, hydrogen bonding, and electrostatic interactions (Tseng, Xiong, & Boatright, 2008; Tay, Xu, & Perera, 2005). Usually, GDL-induced gel formed homogenous gel network structures due to the gradual decrease of pH and the texture of gel can be modulated by protein and GDL concentration, and environmental temperature (Cavallieri & da Cunha, 2008).

2.3.3 Fractal analysis for gel formation mechanism

The protein gel structures are highly disordered, but some colloid aggregation experiments such as light scattering and transmission electro-microscopy demonstrate that the aggregate structure in certain length scales are often self-similar and can be described as a kind of fractal (Mandelbrot, 1982; Weitz, Huang, Lin, & Sung, 1985). Thus, fractal analysis as a quantitative analytical method has been utilized to explain the aggregation and gelation of proteins. It assumes that protein particles aggregate to form clusters with a fractal structure, then the subsequent association of fractal clusters in an ultimate way leads to the formation of protein gels (Wu & Morbidelli, 2001). The self-similar structure of fractals can be characterized by a non-integer dimension: the fractal dimension D_f (Mandelbrot, 1982), which is related to the packing of the aggregated particles. There are several experimental techniques available to analyze fractal structure in aggregates or gels, including rheometry, microscopy, and scattering (light, X-ray or

neutron) (Bushell, Yan, Woodfield, Raper, & Amal, 2002; Mellema, Heesakkers, van Opheusden, & van Vliet, 2000; Wu & Morbidelli, 2001). Scattering techniques are probably the most reliable method, but they are used mainly in dilute systems (volume fractions substantially smaller than 1%). Rheological measurement using a rheometer is the most suitable technique to characterize the structure of gels (Hagiwara, Kumagai, & Nakamura, 1998; Ikeda, Foegeding, & Hagiwara, 1999; Ould Eleya & Gunasekaran, 2004).

To conduct fractal analysis of protein gel using a rheological technique, a scaling model that relates the structure of gels to the rheological properties is required. Based on the studies of Brown and Ball (1985), and Shih et al. (1990), Wu and Morbidelli (2001) developed the scaling model, which assumes that the structure of gels consists of fractal clusters that aggregate with each other during gelation. In this model, there are three regimes: in the strong-link regime, the inter-floc links are stronger than the intra-floc links, and the macroscopic elasticity of the gel is provided by the intra-links; in the weak-link regime, the intra-floc links are stronger than inter-floc links, the macroscopic elasticity of the gel is given by inter-links; in transition regime, comparable inter- and intra-floc links contribute to the overall gel elasticity. According to the model, the fractal dimension that relates to cluster structures and the elastic constant that account for the elastic contribution of inter- and intra-floc links can be determined to explain the aggregation and gelation approach. For example, Maltais et al. (2008) used fractal scaling model to investigate the formation mechanism of cold-set soy protein gels (Fig. 2-4). At higher calcium

concentrations, a rapid screening of repulsive forces between structural units resulted in random aggregation with high fractal dimension values as well as high elastic constant, indicating a weak-bond regime gels (particulate gels). In contrast, at lower calcium concentrations, the comparable inter- and intra-floc interactions (low elastic constant) contributed to the growth of aggregates preferentially along linear paths to form filamentous gels.

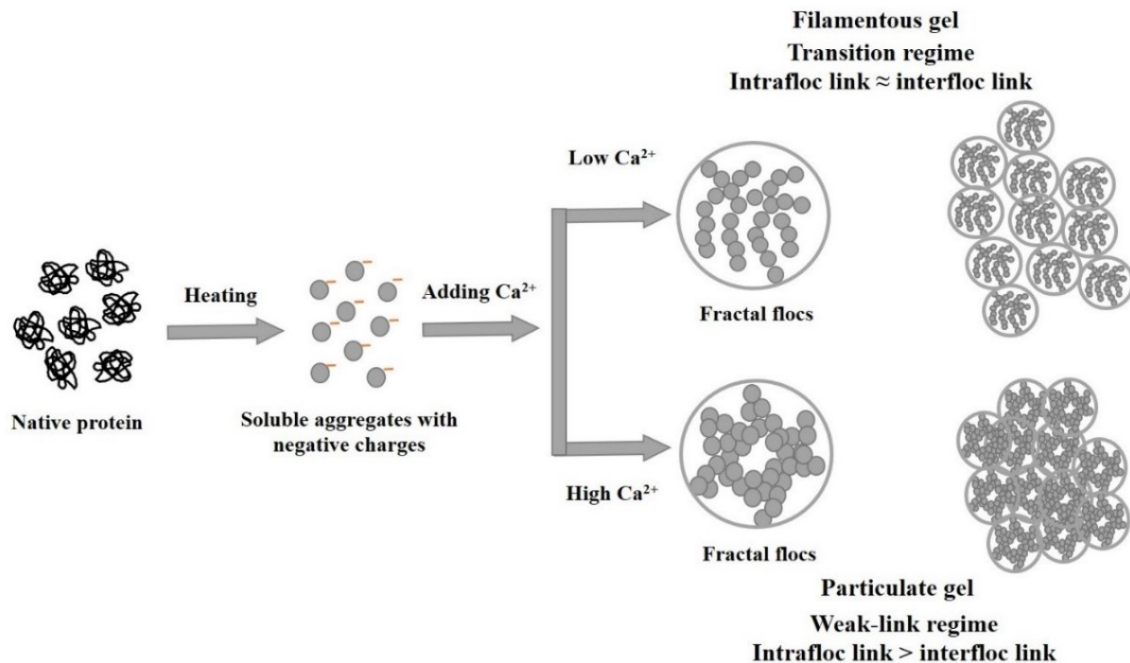


Fig. 2-4. Mechanisms of filamentous and particulate protein cold-set gelation induced by addition of Ca²⁺.

2.4 Protein-polysaccharide complex gels

In some cases, proteins are combined with polysaccharides to create hydrogels. By choosing different polysaccharides and modulating the gelling conditions, protein-polysaccharide complex gels exhibit various properties (Turgeon & Beaulieu, 2001; Le et al., 2016). As compared to the gels formed by protein or polysaccharide alone, the advantages of such composite gels include improved biocompatibility, water holding capacity, gel strength, and swelling properties (Chen, Du, & Huang, 2003; Stabenfeldt, Garcia, & Laplaca, 2006). Two different types of interactions have been found when mixing proteins and polysaccharides together: thermodynamic incompatibility and thermodynamic compatibility, depending on the electrical charges on both biopolymers (Turgeon & Laneuville, 2009).

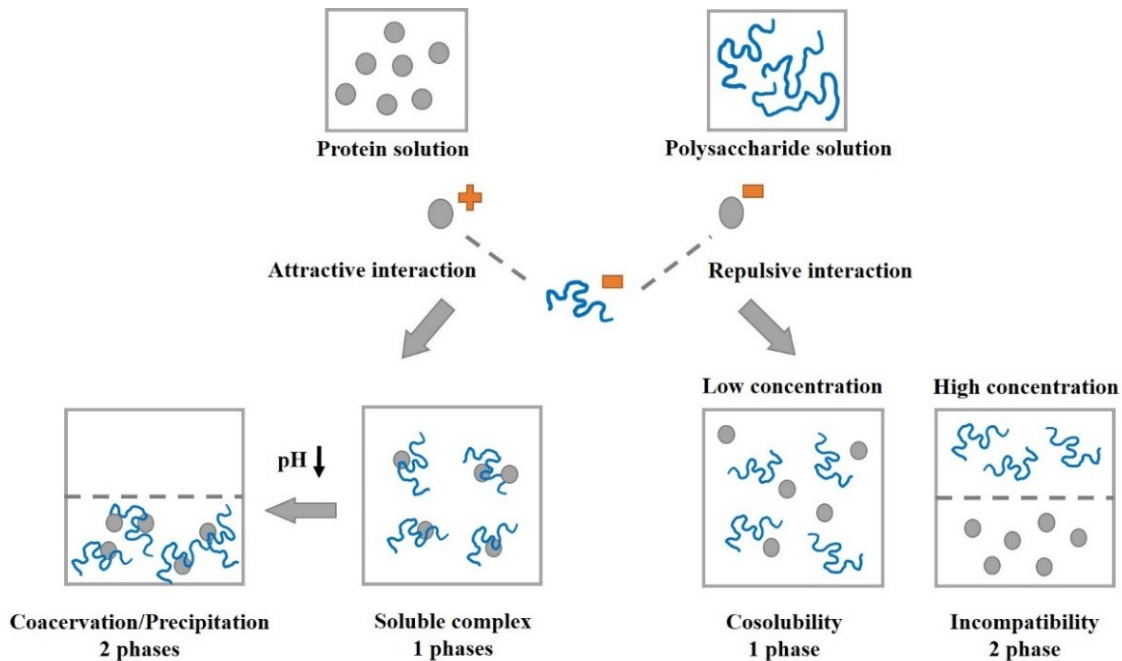


Fig. 2-5. Associative or segregative interactions of protein and polysaccharide mixtures.

2.4.1 Thermodynamic compatibility (associative separation)

For thermodynamic compatibility or associative separation, a relatively strong electrostatic attraction between two biopolymers exists and causes them to associate with each other (Fig. 2-5). Depending on several factors, mainly the protein-polysaccharide binding affinity, molecular charge density, and molecular conformation, different types of structures can be formed upon protein-polysaccharide electrostatic associative interactions (Turgeon & Laneuville, 2009), for example, complexes, coacervates, and gels.

In brief, using protein and anionic polysaccharide as an example, at pH higher than a protein isoelectric point, protein contains negative charges, thus repulsion exists between protein and polysaccharide; as pH is reduced to near the isoelectric point, localized cationic regions on the protein interact with polysaccharide leading to weak complexation (soluble complex) (Tolstoguzov, 2007; Wang et al, 2012). In the case of soluble complexes, only one phase can be observed where the complexes are uniformly distributed. Further decrease of pH induces greater electrostatic attraction between protein and polysaccharide, resulting in the formation of coacervates or inter-polymeric complexes (precipitates) which act as two distinct phases (Tolstoguzov, 2007; Wang et al, 2012). The resultant two-phase system consists of one phase that is rich in both polymers and the other phase that is depleted in both polymers (Dickinson, 2003a). Coacervates are dense spherical aggregates (vesicles), which are liquid in nature and remain in a

liquid state, while inter-polymeric complexes are protein and polysaccharide aggregates with fractal nature that phase separately as solid precipitates (Turgeon & Laneuville, 2009).

2.4.2 Thermodynamic incompatibility (segregative separation)

In the case of thermodynamic incompatibility (segregative phase separation), two polymers carry similar charges or one or both of the biopolymers are uncharged, which results in an electrostatic repulsion or no interaction between molecules and leads to the formation of two different phases (Fig. 2-5) (Turgeon & Laneuville, 2009). At sufficiently low biopolymer concentrations, they are intimately mixed and form a one-phase solution. When the protein and polysaccharide concentration increases to a certain level, two-phase separation occurs where the one phase is rich in protein and the other one is rich in polysaccharide. The molecular origin of this effect is usually the steric exclusion effect. Thermodynamic incompatibility is encouraged by low tendency of the protein and polysaccharide attractive interaction, and high molecular weight (Clark, 2006).

2.4.3 Different types of protein and polysaccharide complex gels

There are three different types of protein and polysaccharide complex gels: interpenetrating, phase-separated, and coupled gels. These gels are developed according to various protein and polysaccharide interactions.

Interpenetrating gel networks are obtained when two polymers form independent networks and at least one of which has been crosslinked in the presence of the other. The interactions between protein and polysaccharide in these kinds of gels are minimal (Morris, 1986). Protein and polysaccharide coupled gel networks can be obtained under associative conditions when two biopolymers are linked together via junction zones, which are stabilized by attractive electrostatic interactions (Oakenfull, Pearce, & Burley, 1997; Laneuville, Turgeon, Sanchez, & Paquin, 2006). Phase-separated gel network is obtained under segregative conditions where interactions between the different polymers are repulsive in nature (Turgeon & Laneuville, 2009). The microstructure formed in phase-separated gel is the result of the competition between the gelling and phase separation processes (Croguennoc, Nicolai, Durand, & Clark, 2001), which are heterogeneous when observe at the microscopic level. The balance between phase separation and gelation can be modulated by ionic strength, pH, and heating/cooling rates (Çakir & Foegeding, 2011; Çakir, Khan, & Foegeding, 2012b; Turgeon & Beaulieu, 2004). For example, compared to faster heating rate, the protein denaturation time is longer and the phase separation is enhanced when heating at a slower rate. Usually, the faster gelling biopolymer forms the continuous phase, which provides network structure for the slower gelling biopolymer to form a discontinuous phase (Almrhag et al., 2013).

Understanding protein-polysaccharide interactions as impacted by environmental conditions is important for design of gel with desired structures and properties. The mixed gels will

contribute greatly to food functionality, structural, and textures, which have tremendous potential to enlarge their utilizations in various food applications.

2.5 Food applications of protein gels

2.5.1 Protein gelling property in food applications

The gelling property of protein plays an essential role in a wide range of food products, such as jelly, desserts, meat products and tofu. As a gelling ingredient in foods, proteins provide texture and mechanical support, enhance emulsion and foam stability, thicken and gel aqueous dispersions, mimic the texture of meats, and increase water retention (Banerjee & Bhattacharya, 2012). Moreover, in food industries, protein gels are commonly used as structural matrices to hold flavor, sugar, and other food additives (Jideani, 2011).

The most common utilization of protein gels in processed foods is to impart unique sensory attributes and/or improve stability and texture of the raw materials (Dille, Draget, & Hattrem, 2015). The mechanical and rheological properties of protein gels affect the behaviour of food during processing (such as cutting, slicing, handling, *etc.*), also affect the sensory and textual properties during mastication. (van Vliet & Walstra, 1995). The mechanical properties of protein gels can be determined by small and/or large strain deformation studies. The response of a sample to a deformation is determined to show its mechanical strength. Small deformation is usually used to study the linear viscoelastic regime between stress and strain of gels, while large deformation study is often used to evaluate fracture stress (gel strength). In relation to texture, the

elastic modulus is related to firmness or hardness, while fracture stress is related to toughness or chewiness (Funami, 2011). Texture profile analysis (TPA) is widely used to measure food texture/gel mechanical properties. For the TPA test, a gel sample of a standard size and shape for biting is compressed at a fixed rate twice using a plunger attached to the universal testing machine (GF Texturometer, Instron, etc), which mimics the actions of the human jaw during mastication (Bourne, 2002; Funami, 2011). Based on TPA, some textural/mechanical parameters of protein gels can be obtained, such as hardness, compressive stress, springiness, cohesiveness, adhesiveness, and chewiness, among others (Bourne, 2002).

Gel's mechanical properties are determined by gel's microstructures as mentioned in section 2.3. For example, a particulate gel formed at pH near the protein isoelectric point has less elastic behavior and lower rupture resistance due to large particle aggregates, while a filamentous gel prepared at pH further away from the protein isoelectric point shows more elastic behavior and high resistance to rupture because of the flexible linear strands (Remondetto et al., 2002). Thus, understanding the relationship between gel microstructure and mechanical properties is important to the development of new products with desired textures. Addition of cross-linking agents or polysaccharides can also be applied to improve protein gel's mechanical properties. Donato et al. (2005) reported that pectin and BSA interpenetrate gels with homogeneous microstructures showed higher final gel strength compare to BSA gel alone. The development of

food protein gels with improved mechanical properties will strengthen their utilizations in food products by providing required food textures and sensory qualities.

2.5.2 Protein gel-based controlled release delivery system for nutraceuticals

Nutraceuticals (vitamins, probiotics, bioactive peptides, antioxidants, etc.) have received much attention due to their physiological benefits *in vivo* and/or the capacity to reduce the risk of chronic diseases (Chen et al, 2006). However, many nutraceuticals have low oral bioavailability because of insufficient gastric residency times, low permeability and/or low solubility within the intestinal tract, which limits their potential health benefit activities *in vivo* (Chen et al., 2006; Bell, 2001). In addition, many nutraceuticals are sensitive to environmental conditions, such as oxygen, pH, enzymes, and other existing compounds (Bell, 2001). For example, probiotics have been reported to have a variety of health benefits, which include providing production of nutrients and cofactors, competition with pathogens for binding site, and stimulation of host immune response (Saier & Mansour, 2005). These probiotic microorganisms must remain alive until they reach the site of action in the body to exert their beneficial effects on the host (Favaro-Trindade & Grosso, 2002). However, probiotics are sensitive to heat, moisture, oxygen, and acidic environments. Another example is resveratrol (3,5,4'-trihydroxy-trans-stilbene), a polyphenol molecule that is naturally found in a wide variety of plant species, which has demonstrated pleiotropic bioactivities including antioxidant, antiaging, anti-HIV/AIDS, and anticancer effects (Amri, Chaumeil, Sfar, & Charrueau, 2012; Singh & Pai, 2014). Despite these benefits, resveratrol has

low bioavailability due to its poor water solubility and chemical instability (Davidov-Pardo & McClements, 2014). Therefore, it is necessary to develop efficient vehicles to maintain the activities of these sensitive compounds and deliver them to the physiological target within the organism.

One of the most promising delivery vehicles is food protein hydrogel. The advantages of protein gel include: (1) they are food materials with high nutritive value (Peppas et al., 2000; Chen et al., 2006); (2) they can provide a biologically friendly environment for protecting the native structure and functional properties of the encapsulated ingredient (e.g. bioactive peptides, probiotics, etc) (Peppas et al., 2000); (3) they are well tolerated and biocompatible *in vivo*, since the high water content and soft consistency minimize mechanical irritation upon administration (Park & Park, 1996); (4) they can be designed as stimuli responsive networks that enable controlled or sustained core ingredient release corresponding to the external stimuli (e.g. pH or temperature) (Lin & Metters, 2006).

Microparticles are defined generally as particles less than about 1000 μm in size, while nanoparticles are defined as colloidal carriers with diameters ranging from 10 to 1000 nm (Allemann, Lerous, & Gurny, 1998; des Rieux, Fievez, Garinot, Schneider, & Pr at, 2006). The small size of micro-/nanoparticles allows them to be incorporated into most foods without changing their sensory qualities (Augustin, 2003). More importantly, by decreasing the matrix size from micrometers to nanometers, promising vehicles can be developed to improve the

bioavailability of nutraceuticals, especially poorly soluble substances and natural antioxidants (Chen, 2009). Due to their small sizes, nanoparticles can adhere to the intestinal mucus layer through non-specific interactions, and, thus, significantly prolong the formulation residence time by decreasing the influence of intestinal clearance mechanisms (Arbós, Arangoa, Campanero, & Irache 2002). In addition, nanoparticles can transport across the intestinal epithelium via paracellular and transcellular routes and are readily taken up by cells, which efficiently facilitate the delivery of bioactive compounds to physical targets in the body (des Rieux et al., 2006).

2.5.2.1 Formation of microparticles

A wide variety of techniques has been developed to prepare protein microparticles, including emulsifying-crosslinking, spray-drying, extrusion, and coacervation, among others. (Bruschi, Cardoso, Lucchesi, & Gremião, 2003; Ishizaka, & Koishi, 1981; Mauguet, et al., 2002).

Emulsification-gelation is a method involving a process to stabilize emulsions of oil droplets in aqueous protein solution (O/W) or aqueous protein droplets in oil phase (W/O), followed by gelation of the protein by heating, chemical or enzymatic cross linking (Cho, Shim, & Park, 2003; Gan, Cheng, & Easa, 2008). One of the advantages of this approach is the ability to produce microparticles with a wide range of diameters by controlling the emulsion size. Moreover, it is feasible for large-scale production. However, heating or chemical cross-linking in the process limit the application of this technique for encapsulation of heat-sensitive compounds. In addition to this, there are also safety concern. A recently developed method, emulsification/internal cold

gelation, opens interesting opportunities for a delivery system to encapsulate sensitive nutraceuticals (Chen & Subirade, 2006). This method is based on the release of calcium ions from an acid-soluble calcium salt in emulsified pre-denatured protein solutions to initiate the gelation of polymers to form microparticles. The microparticle size can be controlled (30-500 μm) by modulating the emulsification conditions. One disadvantage of the emulsification-gelation method is that large amounts of oil are needed during the process and washing steps are required.

Spray-drying is the most widely used technique in the food industry to encapsulate various kinds of food ingredients. It is a unit operation by which a liquid solution or suspension is passed through a small nozzle and atomized in a current of hot gas to obtain a mist of fine drops (Chen, 2009; Matalanis et al., 2011). When fabricating spray-dried microparticles, the suitable materials for encapsulation should have high solubility, low viscosity in concentrated solution, and exhibit good emulsification, film-formation and drying properties (Chen, 2009). Food proteins that contain good functional properties allow them to be viable coating materials for microencapsulation by spray-drying. The extensively used protein wall materials include soy protein, whey protein, sodium caseinate, and gelatin (Baranauskiene, Venskutonis, Dewettinck, & Verhe, 2006; Kagami et al., 2003; Keogh et al., 2001). Emulsion is the normal feeding liquid for the sprayer. Depending on the feeding materials and operating conditions, the size of microparticles is in the range of 1-50 μm (Chen, 2009). The advantage of this process includes availability of the equipment, good stability of the finished product, the possibility of large-scale

production in continuous mode, and low processing costs (Gharsallaoui, Roudaut, Chambin, Voilley, & Saurel, 2007).

Extrusion is a relatively low-temperature microencapsulation method, which involves forcing protein solution through a micro-sized nozzle into a gel, forming a solution that promotes gelation (Chen, 2009). In spite of forcing protein solution and ingredients mixture from one single nozzle, a co-axial nozzle with inner and outer nozzle can be used to prepare microgels. The core materials (protein and ingredients mixture) are forced out through the inner nozzle, while the outer nozzle is used to force coating/shell materials (protein or protein-polysaccharide mixture). When the coating material contacts the gelling agent, it forms an encapsulating matrix/coating to entrap the core materials. In this method, microparticle sizes can be controlled by adjusting the muzzle diameter; the size of smallest particles was about 1 mm in diameter. This method has often been used to form gelatin, whey protein, and soy protein microgels (Franz, Pokorova, Hampl, & Dittrich, 1998; Liu, Ding, Liu, Chen, & Zhao, 2006; Beaulieu, Savoie, Paquin, & Subirade, 2002). The advantage of extrusion is that it is less detrimental to bioactive compounds, and allows core materials to be completely surrounded by the biopolymer wall materials to provide a good barrier against oxidation and prolong the shelf life of the product (Chen, 2009; Desai & Park, 2005). One of the drawbacks of extrusion is the rather large particle size, which restricts its applications where mouth-feel is important.

Coacervation microencapsulation is the phase separation of one or many hydrocolloids from the initial solution and the subsequent deposition of the newly formed coacervate phase around the active ingredient suspended or emulsified in the same reaction medium (Gouin, 2004). Two kinds of coacervation methods, “simple” and “complex” processes, are commonly used for microencapsulation. Simple coacervation is formed through the removal of the solvent from a single colloid dispersion (Chen, 2009). This approach provides a convenient way to prepare particles and encapsulate bioactive compounds through solvent desorption. For example, gelatin and whey protein particles can be prepared using alcohol and acetone as desolvating agents (Gunasekaran et al., 2007; Weber, Coaster, Kreuter, & Langer, 2000). Complex coacervation is based on the formation of a coacervate between oppositely charged polymers, as mentioned in Section 2.4. Complexes formed with food proteins (gelatin, albumin, β -lactoglobulin, etc) and polysaccharides (gum acacia, pectin, alginate, carrageenan, etc) have been extensively developed into microparticles (de Kruif, Weinbrecka, & Vries, 2004). The sizes of complex coacervation rang from 1 to 200 μm . The advantages of coacervation microencapsulation are the high payloads and desirable release controls, while disadvantages are the complex process and using of harmful chemical cross-linking agent, such as glutaraldehyde, is needed (Gouin, 2004).

The presented microencapsulation techniques have their specific advantages and disadvantages, and the use of these techniques depends on the physicochemical properties of core and coating materials used. Accordingly, continuing improvement of microparticle preparation

methods is needed to better meet the requirements for low cost, efficiency, and safe nutraceutical delivery systems.

2.5.2.2 Formation of nanoparticles

There are two major strategies to prepare nanoparticles. The first one is the “top-down” approach, also known as the mechanical approach, in which nanoparticles are prepared by the reduction of material size through mechanical force. The other one is the “bottom-up” approach, also known as the chemical approach, in which nanoparticles are produced by self-assembly of smaller molecules in the presence of chemical reagents (Chen et al., 2006; Sanguansri & Augustin, 2006).

In the “top-down” approach, the commonly used mechanical force to break protein materials includes compressing, impacting, shearing by applying microfluidization and an emulsification mechanical process (Sanguansri & Augustin, 2006). Microfluidization and high-pressure homogenization techniques use high shear stress of liquid flow by subjecting the emulsions (W/O or O/W) through narrow nozzles under high pressure (up to 140000 kPa) to create nano-sized droplets or emulsion (Zhou, 2013). These two methods are the most widely used emulsifying techniques and the main method in the preparation of solid lipid nanoparticles which are widely developed as delivery systems for lipophilic ingredients (Solans, Izquierdo, Nolla, Azemar, & Garcia-Celma, 2005; Müller, Mäder, & Gohla, 2000). The particle size can be controlled by modulating various processing conditions (pressure and number of passes) and solution

composition (oil-to-water ratio or emulsifier-to-water ratio) (Matalanis et al., 2011). Protein nanoemulsions produced through high-pressure homogenization have demonstrated their better stability, enhanced dissolution and bioavailability comparing to conventional emulsions (McClements, 1999; Mitri, Shegokar, Gohla, Anselmi, & Müller, 2011). However, such high-energy methods may not be suitable for encapsulation of unstable bioactive compounds, such as bioactive peptides, since their functionalities may be destroyed during the high-energy and high sheering processes. Moreover, microfluidization and high-pressure homogenization produced nanoemulsion or nanoparticle systems usually need great amounts of oil, emulsifier, or organic cosolvents, which may result in potential side effects such as obesity and cardiovascular diseases caused by the high lipid content (Huang, Yu, & Ru, 2010).

In the “bottom-up” approach, protein nanoparticles are produced by self-assembly or self-organization of molecules, which include inclusion complexation, coacervation, nanoprecipitation and supercritical fluid techniques (Ezhilarasi, Karthik, Chhanwal, Anandharamakrishnan, 2013). This process can be affected by temperature, pH, concentration, ionic strength of the system, as well as the mechanical forces (pressure, shear, and ultrasound (Sanguansri & Augustin, 2006). As mentioned in the microparticle preparation section, the coacervation technique involves phase separation of a single or complex of hydrocolloids from the initial solution and subsequent deposition of the newly formed coacervate phase around the active ingredient. Inclusion complexation refers to the encapsulation of an ingredient into coating

materials through hydrogen bonding, van der Waal interactions, and/or hydrophobic interactions (Ezhilarasi et al., 2013). For example, β -lactoglobulin and pectin nanocomplexes efficiently protected DHA against degradation during accelerated shelf-life stress tests (Zimet & Livney, 2009). The nanoprecipitation technique involves the precipitation of protein from an organic solution and the diffusion of the organic solvent into the aqueous medium (Galindo-Rodriguez, Allemann, Fessi, & Doelker, 2004). Supercritical fluid techniques are also used to prepare protein nanoparticles, which can be used for the encapsulation of thermally sensitive compounds in a process similar to spray drying (Ezhilarasi et al., 2013; Reis, Neufeld, Ribeiro, & Veiga, 2006). Compared to the “top-down” approach, the nanoparticles produced using the “bottom-up” approach are usually achieved under mild conditions, which helps to preserve the stability and activities of bioactive compounds (Zhang, 2014).

Protein gel-based nutraceutical delivery systems have attracted more and more attention in the last decades, since they exhibit three dimensional networks with reliable properties and functionalities, which have great potential to incorporate bioactive compounds and provide controlled release via the oral route (Wang et al., 2012). However, the utilization of gel-based particles in the food industry is still limited due to several reasons. First, since the delivery system should not adversely affect the quality attributes of the product (e.g. appearance, texture, and flavor), a number of practical factors must be considered, including design of particle structure and size, as well as the effects on the taste, aroma, and texture. Second, protein

gel-based particles formed through physical interactions without crosslinking agents have poor mechanical strength and may be disrupted by the change of pH value or ionic strength, which impacts their encapsulation and retention efficiencies and protection abilities, and may not be suitable for robust manufacturing operations. Third, the delivery system should be prepared using food-grade ingredients; however, the stable gel particles formed using current methods usually contain toxic crosslinking agents, resulting in safety concerns (Wang et al, 2012; Davidov-Pardo & McClements, 2014). Therefore, it is necessary to explore novel non-toxic gel-based delivery systems with well-defined network through combining encapsulation techniques for nutraceuticals to achieve a greater effect on increasing their solubility, stability, and bioavailability.

2.5.2.3 Controlled release mechanisms

Controlled release is an important feature and capacity for protein gel to control the release of the encapsulated components. It is defined as a method by which one or more active ingredients are made available at a desired site and time at a specific rate (Pothakamury & Barbosa-Cánovas, 1995). The release of encapsulated ingredients present in gel is triggered by changing temperature, moisture, pH, or digestive enzymes. In general, there are three main ways in which release can occur due to the hydrophilic feature of hydrogel matrices: via diffusion, swelling followed by diffusion, or degradation (Fig. 2-6).

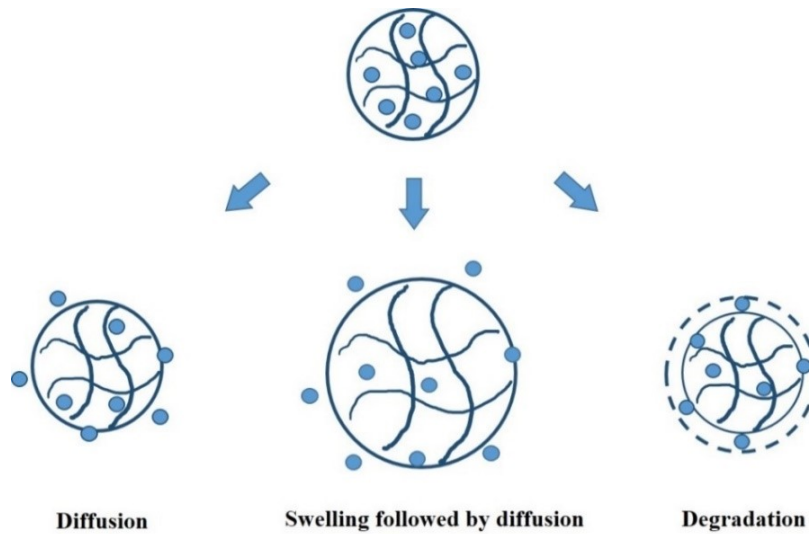


Fig. 2-6. Illustration of controlled release mechanism: diffusion, swelling, and degradation.

Diffusion controlled release system

Diffusion is considered the most common mechanism used for controlled release. It describes the diffusion of the molecules of different sizes and characteristics through random motion from the hydrogel matrix to the hydrophilic external environment during loading and storage periods (Fig. 2-6) (Garti, 2008; Wang et al., 2012). The diffusion can occur when there is concentration gradient, and the diffusion rate of active compounds from hydrogel matrix depends on several factors, such as solubility of the encapsulated compound, mesh size within the gel, type and intensity of the external stimuli, and the interactions between the gel network and the active component (Matalanis et al., 2011; Amsden, 1998; Mason, Metters, Bowman, & Anseth, 2001). The diffusion release includes three principal steps: (1) diffusion of the active agent within

the matrix; (2) dissolution or partitioning of the active agent between the matrix and surrounding fluids; and (3) diffusion away from the matrix surface (Pothakamury & Barbosa-Cánovas 1995).

Swelling followed by diffusion controlled release system

In swelling followed by diffusion controlled system, the hydrogel matrix swells due to the absorption of the fluids from medium when placed in a thermodynamically compatible medium, and the active compounds in the swollen part of the matrix transport into the external environment due to the difference in the chemical potential (Fig. 2-6) (Pothakamury & Barbosa-Cánovas 1995). The release rate of active compounds is determined by the swelling process of the matrix, where the polymer chains are more mobile and allow the compounds to diffuse out of the matrix more quickly. The critical factor that controls the swelling process or rate is the crosslinking density of the gel network. Moreover, when hydrogels contain both cationic and anionic fixed charges, the gel matrices show typical polyampholyte hydrogel characteristics, exhibiting swellability in response to the external environment (e.g. pH and ionic strength) (Chen et al., 2006). The swelling behavior of gel can be modulated by controlling the balance between cationic and anionic charges, which have been used extensively for the development of controlled release system for oral administration.

Degradation controlled release system

In the degradation controlled release system, the active component is released into the medium due to erosion or degradation process taking place at either the outer layer or throughout

the entire volume of the gel matrix (Fig. 2-6) (Matalanis et al., 2011). The erosion and degradation of the matrices are contributed by physical, chemical, or enzymatic degradation process, such as dissociation of physical bonds, hydrolysis of covalent bonds, or digestion by many different enzymes in the gastrointestinal tract. Heterogeneous or homogeneous degradation commonly happens for degradation controlled release. Heterogeneous erosion occurs as a result of degradation happening at the surface of the matrix and is commonly found in gels stabilized by hydrophobic interactions, whereas homogeneous erosion occurs when degradation happens throughout the gel matrix with a uniform rate and is commonly observed in hydrophilic gels (Pothakamury & Barbosa-Cánovas 1995). The erosion or degradation rate of the gel matrix closely relates to the rate and extent of enzyme penetration into the system, crosslinking density of the gel and/or substrate conformation, which is also important to obtain the system with desirable degradation profiles (Kamath & Park, 1993).

For most controlled delivery systems, the release of an active ingredient may be based on one or combination of release mechanisms. Development of protein based gel matrices with well-designed structures may allow variable release mechanisms of the encapsulated active compounds to achieve the timely and targeted release in the body. For example, Chen and Subirade (2009) designed soy/zein protein hydrogel (microspheres) using a cold-set gelation method, which could efficiently reduce the rapid release of riboflavin in gastro fluid, eventually delivering it to the small intestine for complete release. The diffusion mechanism played a major

role in regulating the release of riboflavin, and the microsphere with SPI/zein ratios of 5:5 and 3:7 displayed near-zero-order release kinetics in the simulated gastrointestinal fluids, which showed potential for use as delivery systems for bioactive products in functional foods (Chen & Subirade, 2009).

2.6 Opportunities of using plant protein gels for food applications

Gelatin, egg white and whey proteins are widely used as gelling ingredients in the food industry. Over the last decades, plant protein gels have attracted much interest, due to their low cost, sustainability, religious/cultural reasons, and the reduced risk of spreading disease such as bovine spongiform encephalopathy (mad cow disease) (Lai & Guo, 2011; Kim et al., 2014; Gaowa et al., 2014). Among plant protein gels, soy protein gels are popular in food applications. For example, they are used as binders or extenders to improve the texture of comminuted meats or as meat replacer (Jideani, 2011). However, soy protein alone is insufficient to meet the ever-increasing market requirements for different functionalities and sensory attributes. Thus, proteins from diverse plant sources are needed to provide new or improved nutritional and functional properties. Proteins from other crops, such as cereals and oilseeds, are potential candidates for novel food gelling ingredients. Therefore, a comprehensive understanding of plant protein gelling mechanisms and the gel properties, as well as their feasibility to encapsulate and controlled release of bioactive compounds are necessary to be established and studied.

Chapter 3

Impact of pH and heating temperature on formation mechanisms and properties of thermally induced canola protein gels

3.1 Introduction

Canola production in Canada has been steadily increasing and currently sits at approximate 9 million tons of canola seed per year. The global demand for canola is mainly for its edible oil. However, once the oil is removed from the seed, a protein-rich meal is left behind which is mainly used as animal feed. Considering the large amount of by-product produced by the extraction process, it would be greatly beneficial to the agricultural industry to develop techniques to use this canola protein source in value-added products. The major proteins in canola meal are globulin 12S groups (cruciferin) and albumin 2S groups (napin) (Bhatty, McKenzie, & Finlayson, 1968; Hoglund et al., 1992). Cruciferin is a hexameric protein where each subunit contains acidic/ α (30 kDa) and basic/ β (20 kDa) polypeptides linked by both disulfide bonds and non-covalent bonds to form more complex structures, whereas napin is composed of two polypeptide chains with molecular weights of 9 kDa and 4 kDa that are held together mainly by disulfide bonds (Dalgarrondo, Robin, & Azanza, 1986; Monsalve et al., 1991; Schwenke, 1994). Cruciferin also contains more hydrophobic amino acids, such as isoleucine, leucine and proline, and less cystine (Chabanon et al., 2007).

Food protein gelation, such as soy protein and whey protein, has been widely studied not only because of its ability to produce various foods with distinct textures, but also due to its capacity to entrap molecules of interest into gel networks and protect and deliver them to the physiological targets (Chen et al., 2006; Maltais et al., 2009; Nicolai, Britten, & Schmitt, 2011; Betz, Hörmansperger, Fuchs, & Kulozik, 2012). Analogous opportunities may exist for canola proteins as their gelling properties were demonstrated in previous studies in terms of least gelling concentration, rheological properties or gel microstructure (Gill & Tung, 1978; Khattab & Arntfield, 2009; Schwenke, Dahme, & Wolter, 1998). Modification of protein structure, for example, by transglutaminase (TG) treatment (Pinterits & Arntfield, 2008), and the inclusion of low levels of polysaccharides such as κ -carrageenan has been shown to improve gel properties in comparison to canola protein alone (Uruakpa & Arntfield, 2004). Limited works reported in terms of interactions involved in the canola gel network formation. Léger and Arntfield (1993) indicated that hydrophobic forces and electrostatic interactions were responsible for the establishment of canola gel networks, while disulfide bonding, electrostatic interactions, and hydrogen bonding corresponded to gel stabilization and strengthening. In spite of progress, this is the conclusion only based on gels formed at pH 9 at 90 °C. The canola protein gel properties, gelation mechanisms and the bonds involved in gel formation and stability prepared under different processing conditions were not fully elucidated. Gels with different network structures may have different functional properties (Remondetto et al., 2004). These different structures can be induced by modulating protein conformation and interactions through controlling processing

conditions such as pH, temperature, protein concentration and salt concentration etc. On the other hand, although numerous studies have been carried out on molecular profile of canola protein, there is limited literature that relates these findings to its gelling properties.

In our preliminary studies, pH and heating temperature were identified as critical factors to influence canola protein gel properties. Thus, the objective of this study was to prepare thermally induced canola protein gels over a broad range of pH (5–11) and temperature (80–120 °C) conditions, and investigate the impacts of pH and heating temperature on the mechanical properties and morphologies of canola protein gels. Moreover, the gel formation mechanism at molecular and supramolecular levels is explored based on an investigation of protein conformational changes and molecular interactions at different processing conditions using FTIR spectroscopy and rheometry, respectively. The relationship between canola protein structure, gel network morphology and mechanical properties is discussed.

3.2 Materials and methods

3.2.1 Materials and chemicals

Canola seeds were kindly provided by Alberta Canola Producers Commission, Edmonton, Alberta, Canada. Reagents and chemicals used in the experiments were purchased from Sigma-Aldrich (St. Louis, MO, USA) and Fisher Science (Ottawa, Ontario, Canada).

3.2.2 Canola protein extraction

Canola seeds were ground into powder using a laboratory mill with screen size of 0.5 mm (Smart grinder, Black & Decker[®], Beachwood, OH, USA). The milled canola was defatted twice using hexane with solid-to-solvent ratio of 1:6 (w/v) for 6 h at room temperature. The mixture was then centrifuged at $4,000 \times g$ (Acanti[®] J-E centrifuge, Beckman Coulter, Indianapolis, IN, USA) for 15 min, and the pellets were dried in a fume hood overnight. Canola protein fractions were extracted from the defatted canola meal according to Ismond and Welsh (1992). Briefly, the defatted canola meal was dispersed in 0.2 M NaCl solution at the solid-to-solvent ratio of 1:10 (w/v). The dispersion was stirred for 1 h at pH 8 adjusted by 1 M NaOH at room temperature, and then centrifuged at $8,000 \times g$ and for 10 min. After centrifugation, the supernatant was collected and passed through a membrane filtration system with molecular weight cut-off of 10 kDa (Centramate PE, Pall Life Sciences, Mississauga, ON, Canada). The retentate was dialyzed using cellulose membrane (molecular weight cut-off of 3 kDa) against distilled water for 72 h. The supernatant and precipitate were separated by centrifugation at $4,000 \times g$ for 15 min, and then lyophilized to obtain water-soluble and salt-soluble protein fractions, marked as CP1 and CP2, respectively. These were stored at 4 °C before use, and their protein contents were analyzed using a Leco nitrogen analyzer (Leco[®], Saint Joseph, MI, USA) with the nitrogen-protein conversion factor of 5.7. Other components in the extracted samples could be soluble starch, lipid, ash, phytic acids, and phenolic compounds, among others.

3.2.3 Zeta potential, thermal and rheological properties of canola protein suspensions

Zeta-potential values of CP1 and CP2 suspensions (0.2%, w/v) were measured at room temperature by laser Doppler velocimetry using a Zetasizer Nano-ZS (Malvern Instruments Ltd., Malvern, Worcestershire, UK) as a function of pH. The pH where zeta-potential was equal to 0 mV was considered as protein isoelectric point (IEP).

The thermal properties of CP1 and CP2 were analyzed using a DSC Q2000 apparatus (TA Instruments, New Castle, DE, USA) equipped with a refrigerated cooling system RCS90. Approximate 8 mg of 15% (w/v) canola protein slurry at different pH values (5–11) were accurately weighted in aluminum pans. The pans were then hermetically sealed and heated from 30 to 140 °C with a heating rate of 10 °C/min. A sealed empty pan was used as a reference. The peak transition temperature, known as denaturation temperature (T_d), and enthalpies of denaturation (ΔH) were computed from the endothermic peaks observed in the thermograms.

Dynamic rheology experiment was carried out on a DHR-3 rheometer (TA Instruments, New Castle, DE, USA) to study the gelation point of canola protein suspensions with different pH values. Parallel plate geometry with a gap of 1 mm was used to measure dynamic viscoelastic parameters (shear storage modulus G' and loss modulus G'') as functions of temperature (T). The value of the strain amplitude for all samples was set at 5%, which was within the linear viscoelastic regime. The dynamic temperature sweep measurements were performed from 25 to 90 °C with heating rates of 5 °C/min at an angular frequency (ω) of 1 Hz. A thin layer of

low-viscosity silicone oil was applied to prevent dehydration during the test. The temperature at which G' becomes larger than G'' is commonly used as a measure of the gelation point.

3.2.4 Preparation of heat-induced canola protein gels

Canola protein CP1 and CP2 (15%, w/v) were dispersed in distilled water and 0.5% NaCl solution at room temperature, respectively. The pH value of suspensions was adjusted to 5, 7, and 9 by adding 1 M NaOH or 1 M HCl, and then they were poured into tightly closed tubes to avoid evaporation and heated at 80, 90, 100, 110, or 120 °C for 15 min in water and/or oil bath. After cooled to room temperature, the obtained gels were washed in distilled water until neutral, and stored at 4 °C before further analysis. Some gels were also prepared at pH 11 in order to investigate the change of protein structure.

3.2.5 Mechanical properties

Mechanical properties of the obtained gels (10 mm in length and 14mm in diameter) were determined using an Instron 5967 Universal testing instrument (Instron Corp., Norwood, MA, USA) equipped with a 50 N load cell. All gel samples were compressed twice to 50% of their original height at room temperature using the constant crosshead speed of 1 mm/min, which simulated two bites of human. Two texture parameters including compressive stress and springiness were computed by software (Blue Hill 2, Instron Corp., Norwood, MA, USA). Compressive stress indicates the gel firmness calculated as the compressive force (hardness, N) over the cross-sectional area of the gel. Springiness indicates how well a gel physically springs

back after the first compression, which is measured by the distance of downstroke of the second compression (Bourne, 2002).

3.2.6 Gel morphology

The morphology observation of CP1 and CP2 gels was carried out with a Philips XL-30 scanning electron microscope (SEM) at an acceleration voltage of 6 kV. The samples were frozen in liquid nitrogen, and then freeze-dried. The surface of the gels was then sputter-coated with gold, observed and photographed.

3.2.7 Protein structures and interactions in canola protein gels

Canola protein conformational changes during the preparation of gels were characterized by FTIR. CP1 and CP2 (5%, w/v) were dispersed in D₂O and D₂O + 0.5% NaCl, respectively, and adjusted to different pH values (5, 7, 9, and 11) using 1% DCl and NaOD. The samples were then placed between two CaF₂ windows separated by a 25 µm polyethylene terephthalate film spacer for FTIR measurement. They were heated in the cell from 25 to 80 °C in 5 °C increments using a temperature controller (Peltier controller, Thermo Fisher Scientific, Pittsburgh, PA, USA), and was equilibrated for 5 min at each temperature prior to record the spectrum. To study the conformation of resultant gels, freeze dried gels were milled into powders and vacuum-dried at 40 °C for 24 h. The dried samples in KBr discs were then analyzed. The spectra of both wet and dried samples were recorded using a Nicolet 6700 spectrophotometer (Thermal Fisher Scientific Inc., Pittsburgh, PA, USA) in the range of wavenumber from 400 to 4000 cm⁻¹ during 128 scans with 2 cm⁻¹ resolution. The spectrophotometer was continuously purged with dry air from a lab

gas generator (Parker Hannifin Corp., USA). For amide I band region (1700–1600 cm^{-1}), Fourier self-deconvolution was performed using Omnic 8.1 software at a bandwidth of 24 cm^{-1} and an enhancement factor of 2.5. The established wavenumber ranges reported by Byler, and Susi (1986) were used as reference to assign the amide I band components to secondary structure motifs. The conformation proportions of α -helix, β -sheet, β -turn, and random coil for all samples were calculated directly using Omnic 8.1 software.

To evaluate the molecular interactions involved in the formation of canola protein gels, frequency sweep analysis was conducted on the CP1 and CP2 gels (15%, w/v) prepared at different pHs (5, 7, 9 and 11) and 120 °C after soaking into 2-mercaptoethanol (0.2 M), urea (2 M) and SDS (1%, w/v), which could disrupt disulfide bonds, hydrogen bonds and hydrophobic interactions, respectively. Canola protein gels with the height of 10 mm were soaked into these dissociation reagents for 48 h at room temperature. The G' value was subsequently evaluated as a function of ω from 0.1 to 100 rad s^{-1} at the 8 mm gap (compressed to 80% original height of gels) using DHR-3 rheometer.

3.2.8 Statistical analysis

All experiments were performed at least in triplicate. Results were expressed as mean \pm standard deviation. Statistical analysis was conducted using the Statistical Analysis System (SAS for windows, Release 9.0, SAS Institute Inc., Cary, NC). Analysis of variance (ANOVA) was performed to analyze the effects of pH and heating temperature on gel mechanical properties.

Tukey test was used to compare multiple means. A probability of $p < 0.05$ was considered to be statistically significant.

3.3 Results and discussion

3.3.1 Canola protein fractionation and characterization

The protein content was 88.5 and 79.3% for CP1 and CP2, respectively. According to SDS-PAGE pattern (data not shown), CP1 contained protein subunits of low molecular weight with one major band at 13–15 kDa. CP2, on the other hand, contained subunits of high molecular weight with three major bands at 50, 25–30, and 18 kDa. Previous literature indicates that napin (2S albumin) had the major band with a calculated molecular weight of 14 kDa and the minor band at 27.5 kDa, while the bands with molecular weight range of 45–50 kDa, 29–32 kDa, and 18–22 kDa represented cruciferin (12S globulin) (Wu & Muir, 2008; Krzyzaniak, Burova, & Barciszewski, 1998; Aluko & McIntosh, 2001). Thus, CP1 was mainly consisted of 2S albumin and CP2 was mainly composed of 12S globulin. The CP1 and CP2 sample exhibited isoelectric point (IEP) of around pH 8.5 and 7.0, respectively by determining zeta potential as a function of pH using a Malvern Zetasizer.

Table 3-1 shows the denaturation temperatures (T_d) and the denaturation enthalpy values (ΔH) of CP1 and CP2 at various pH values. The range of pH 5–11 was chosen for CP1 and CP2 as high pH significantly impacted their solubility according to our preliminary trials and a pH below 5 was not suitable for gel formation. One significant endothermic peak with denaturation

temperatures of 106–118 °C was observed for CP1, while CP2 had denaturation temperature between 83–93 °C.

Table 3-1. Effect of different pH values on thermal properties of canola proteins (15%, w/v).

Canola protein	pH	T _d (°C) ^A	ΔH (J/g) ^A
CP1	5	106.39 ± 0.30 a	0.1072 ± 0.02 x
	6	105.38 ± 3.20 a	0.1758 ± 0.03 x
	7	104.71 ± 1.26 a	0.2213 ± 0.04 xy
	8	109.88 ± 0.30 c	0.2104 ± 0.01 xy
	9	118.51 ± 1.50 d	1.2525 ± 0.06 z
	11	101.09 ± 1.77 b	0.6052 ± 0.15 y
CP2	5	83.93 ± 1.90 a	0.7220 ± 0.24 x
	6	88.13 ± 0.48 ab	0.8689 ± 0.14 x
	7	88.95 ± 0.25 b	1.4565 ± 0.10 yz
	8	93.05 ± 0.62 c	1.4636 ± 0.03 yz
	9	93.28 ± 0.38 c	1.8900 ± 0.11 z
	11	89.21 ± 0.08 b	0.8705 ± 0.25 x

^A Different letters following means ± standard deviations in a column for each protein indicate significant difference at $p < 0.05$.

These T_d values of CP1 and CP2 were similar to the result reported by Wu et al. (2008), who indicated that T_d values of purified napin (2S) and cruciferin (12S) were 109.9 °C and 90.7 °C, respectively. Comparing these two fractions, the denaturation temperature of CP1 was generally higher than that of CP2, since inter- and intra-chain disulfide bonds were the principle factor responsible for the high thermal stability of canola 2S protein (Monsalve et al., 1991). With raising sample pH from 5 to 9, the T_d and ΔH values of both CP1 and CP2 increased, indicating that higher temperature and more energy were required to denature canola protein at higher pH. Practically, both of covalent, such as disulfide bond, and non-covalent interactions, such as electrostatic interactions and chain entanglement, could impact protein thermal properties. It has been reported that the inter- and intra-chain disulfide bonds which stabilize the napin secondary and tertiary structures could be split at alkaline condition and high temperature, but remained stable when heated at acidic and neutral conditions, as the helix content of napin remained unchanged (Schwenke, Drescher, Zirwer, & Raab, 1988). Thus, with the increase of pH value from 5 to 7, probably only non-covalent interactions of CP1 were disrupted and the rising T_d and ΔH values were due to the approaching of IEP. At pH 8, the protein carried limited net charge and existed in its most stable conformation, thus more energy was needed to denature the structure. The breakage of inter- and intra-molecular disulfide bonds took place at pH 9 and the rupture of hydrogen bonds also increased, leading to the high T_d and ΔH values. However, the T_d and ΔH values of CP1 decreased at pH 11 where the molecular chains of CP1 were highly negatively charged. The strong repulsive force might inhibit the protein molecular interactions,

such as hydrophobic interactions and hydrogen bonding, which resulted in decreased T_d and ΔH values. Similar trend was also seen in the CP2 sample when pH was increased from 5 to 11.

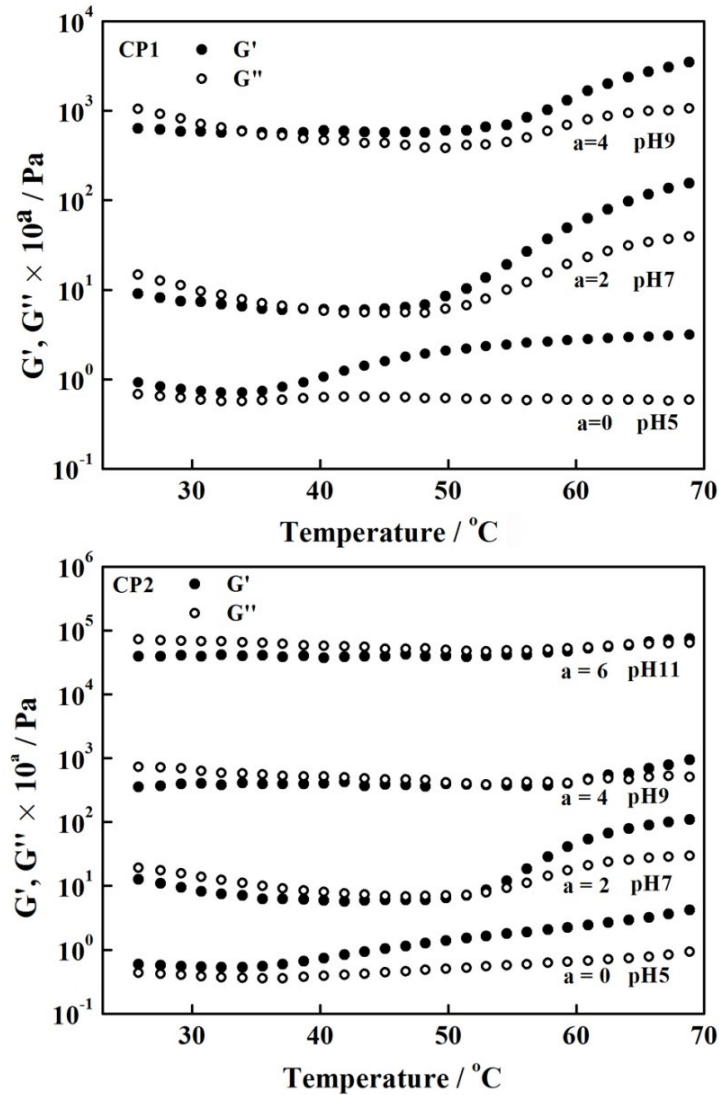


Fig. 3-1. Temperature dependence of storage modulus (G' , ●) and loss modulus (G'' , ○) of CP1 and CP2 (15%, w/v) suspensions with a heating rate of 5 $^{\circ}\text{C}/\text{min}$ at a frequency of 1 Hz. The data are shifted along the vertical axis by 10^a with the given value to avoid overlapping.

The rheological behaviors of canola protein suspensions were subsequently monitored to investigate the establishment of interactions among protein molecules under heating. Fig. 3-1 shows the temperature dependence of storage modulus (G') and loss modulus (G'') of CP1 suspensions at pH 5, 7, and 9 and CP2 suspensions at pH 5, 7, 9 and 11, respectively. The temperature at the crossover point of G' and G'' curves was characterized as an approximate value of sol-gel transition, known as gel point or gelation temperature (Cordobes, Partal, & Guerrero, 2004). At pH 5, G' value was higher than G'' value for both CP1 and CP2, even at starting temperature of 25 °C. Probably the ionization and subsequent partial unfolding of canola protein induced by the acidic environment led to the exposure of buried active sites, which promoted protein-protein interactions prior to significant thermal denaturation (Léger & Arntfield, 1993), resulted in the solid-like behavior of canola protein suspensions. At pH 7 and 9, the crossover points were observed when increasing temperature, suggesting that the transition from liquid to solid-like behaviors took place.

3.3.2 Gel mechanical properties

Fig. 3-2 shows the effects of pH and heating temperature on compressive stress and springiness of thermally induced CP1 and CP2 gels, with the former indicating the gel firmness and the latter indicating how well a gel physically springs back after the first compression. At pH 5, CP1 formed relatively weak gels regardless of heating temperature. The acidic environments induced partial unfolding of canola protein and exposed some active side chains, which might interact with each other to form small aggregates as revealed by rheological test. Nevertheless,

the disulphide bridges which used to stabilize CP1 structures were very stable at this condition, so it was hard to further unfold the protein structure even upon heating and form strong gel network. When pH value was 7, the compressive stress of CP1 gels slightly increased with increasing heating temperature, while the gel springiness was significantly improved at 120 °C. It could be understood that, the disulphide bonds in CP1 were still stable, whereas the repulsive force was reduced at the neutral condition. Thus, the aggregated protein might have more chances to combine together through non-covalent interactions at higher temperatures, which contributed to the raised springiness. The mechanical properties of CP1 gels were dramatically improved by increasing heating temperature at alkaline condition. The ones prepared at pH 9 and 120 °C showed the highest compressive stress and springiness values of 20.4 kPa and 4.8 mm (Fig. 3-2), respectively. It was deduced that the disruption of disulfide bridges between polypeptides at alkaline pH largely promoted the development of covalent and non-covalent interactions, resulting in gels with a high compressive stress and springiness.

Generally, gels formed from CP2 were stronger compared to CP1 gels. This is in accordance with previous report that cruciferin gels possessed higher gel strength than purified napin (2S albumin) gels because cruciferin contained high molecular weight component (Schwenke et al., 1998). High molecular weight could result in chain entanglement, so that there were more chances to develop non-covalent interactions. Due to the same reason as for CP1, the compressive stress of CP2 gels was not impacted by heating temperature at pH 5. At pH 7, around the CP2 IEP, the reduced repulsive forces led to more connections between protein

molecules through non-covalent interactions, thus higher compressive stress was obtained. Even stronger compressive stress values were observed at pH 9, which might be induced by more opened protein structures at alkaline condition. At pH 11, very strong gels were built, which exhibited compressive stress of 24–30 kPa, regardless the heating temperature. This suggested that complete unfolding might take place due to the breakage of disulfide bonds between polypeptides (Schwenke et al. 1988), so that the active sites could be fully exposed to develop strong interactions to reinforce the gel network. The high molecular weight, complex molecular structure and chain entanglement might cause CP2 not as flexible as CP1, resulting in moderate gel springiness.

It is worth noting that canola protein gels possessed comparable mechanical properties to those of soy protein and other legume protein gels. Lupin seed protein isolate gels, pea seed protein isolate gel, and broad bean protein isolate gels (20%, w/v) showed the compressive stress (through calculation) of approximate 8.0, 5.0 and 5.5 kPa, respectively, when compressed to 70% deformation (Makri, Papalamprou, & Doxastakis 2006). Furukawa et al. reported that 20 w/w isolated soy protein gel (30mm diameter and 15mm height) formed at 80 °C exhibited strong gel strength of approximate 7.5 N (compressive stress: 10.6 kPa) (Furukawa, Ohta, & Yamamoto, 1980). In addition, very strong and elastic CP1 and CP2 gels could be obtained when formed at alkaline pH and high temperature. The gels formed at these conditions may not to be applied to food, but these strong and elastic gels can be used for many other applications, such as scaffolds

in tissue engineering, biosensors that respond to specific molecules, and dressings for healing of wounds, among others.

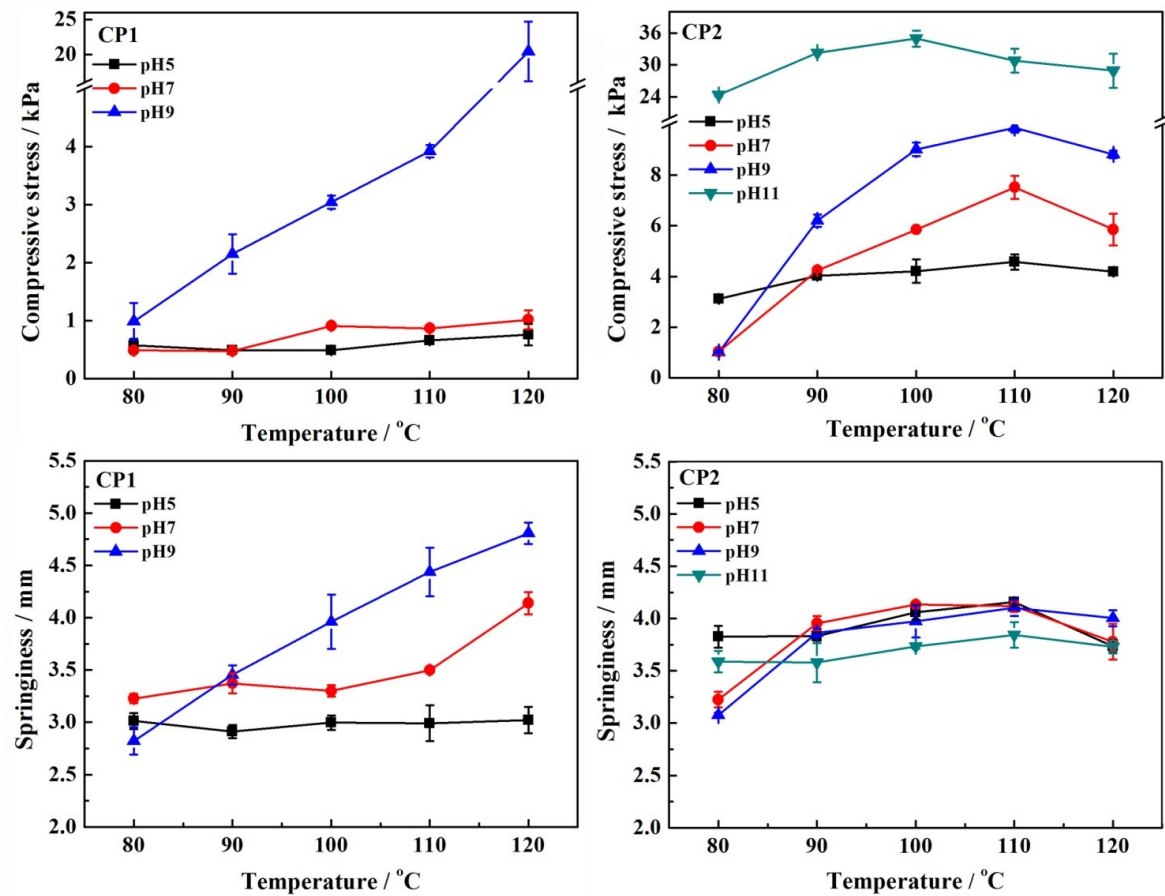


Fig. 3-2. Effects of pH and heating temperature on the mechanical properties of thermally-induced CP1 and CP2 gels (15%, w/v).

3.3.3 Canola protein gel formation mechanism

3.3.3.1 Gel morphology

Fig. 3-3 displays SEM micrographs of CP1 gels, which clearly illustrates the dependence of gel microstructure on pH and heating temperatures. A loose structure composed of small irregular

aggregates and fiber-like connections were observed in CP1 gel formed at pH 5 and 80 °C (Fig. 3-3a). With increasing pH from 5 to 7, the gel microstructures consisting of uniform larger protein aggregates became more compact and exhibited a typical particulate fractal structure. At pH 9 (Fig. 3-3c), the protein fractal aggregates seemed to be “melted” (indicated by the arrows in the Fig. 3-3c), and the gel formed at pH 11 (Fig. 3-3d) even exhibited a macro-porous wall network structure. As explained in section 3.2, at pH 7, the protein tended to form larger aggregates due to the less repulsion forces; whereas the split of disulfide bridges at pH 9 and 11 resulted in a completely different gel microstructure with dramatically improved mechanical strength.

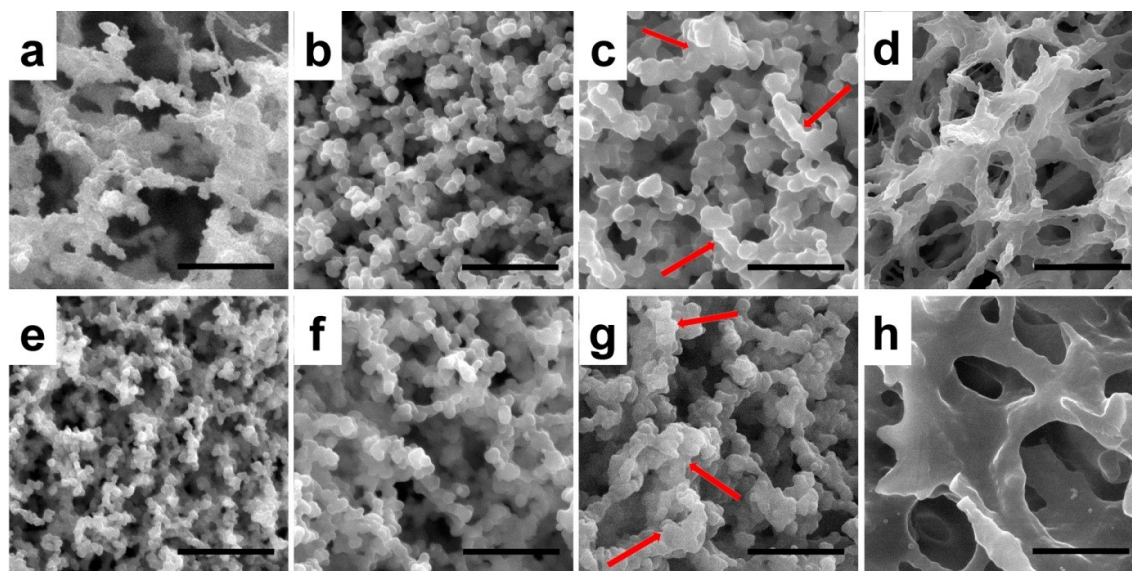


Fig. 3-3. SEM images of the cross-sections of thermally-induced CP1 gels (15%, w/v) formed at different pHs and heating temperatures: (a) pH 5, 80 °C; (b) pH 7, 80 °C; (c) pH 9, 80 °C; (d) pH 11, 80 °C; (e) pH 5, 120 °C; (f) pH 7, 120 °C; (g) pH 9, 120 °C, 3min; and (h) pH 9, 120 °C. Scale bar: 5 μ m.

Heating temperature impacted the gel microstructures as well. With increasing heating temperature from 80 to 120 °C, the gels prepared at pH 5 (Fig. 3-3e) exhibited homogeneous network structures composed of uniform small aggregates, and the fiber-like connections disappeared. At pH 7, 120 °C, more compact structures and larger aggregates with slight “melt” condition occurred, which indicated that some non-covalent interactions were developed. This slight “melt” condition might explain the similar compressive stress but improved springiness of the gels formed at pH 7 when the heating temperature was raised. Interestingly, the macro-porous and dense wall structures were also formed at 120 °C, but at a lower pH of 9. (Fig. 3-3h). Such polymer gel structure was also shown in gelatin gels (Titova, Belavtseva, Braudo, & Tolstoguzov, 1974). Gelatin possesses relatively flexible molecular chains, which allow formation of bridges between the interaction points. In the case of canola protein, the denatured protein molecular structure after split of disulfide bonds allowed formation of bridges between the interaction points as well, leading to macro-porous dense wall network structure through development of both covalent and non-covalent interactions. In order to reveal how the macro-porous and dense wall structure formed, the morphology of gel prepared at 120 °C and pH 9 by heating for 3 min (just starting to form the gel structure) was observed. As shown in Fig. 3-3g, the gel displayed a typical protein particulate fractal structure with slight “melt” condition (highlighted by the arrows in Fig. 3-3g), indicating that a further “melt” process took place during the continuous heating to establish the macro-porous and dense wall structure. As a result, gel with this kind of structure had superior mechanical properties than the gels with particulate fractal structures.

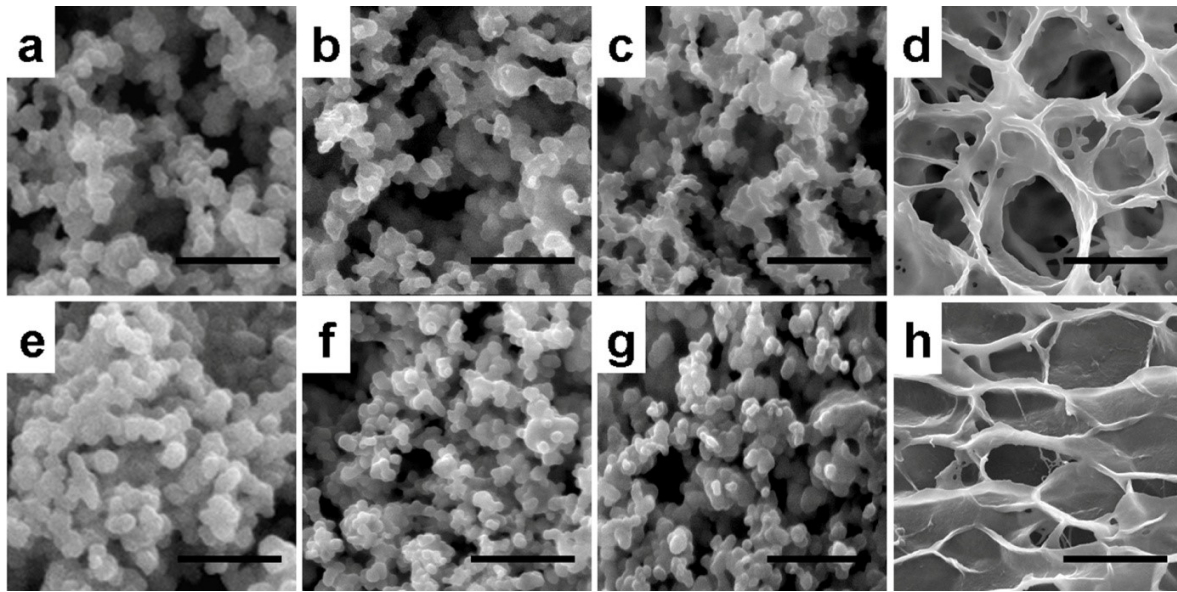


Fig. 3-4. SEM images of the cross-sections of thermally-induced CP2 gels (15%, w/v) formed at different pHs and heating temperatures: (a) pH 5, 80 °C; (b) pH 7, 80 °C; (c) pH 9, 80 °C; (d) pH 11, 80 °C; (e) pH 5 120 °C; (f) pH 7, 120 °C; (g) pH 9, 120 °C; and (h) pH 11, 120 °C. Scale bar: 5 μ m.

CP2 gels prepared at pH 5, 7, and 9 also demonstrated typical compact particulate fractal network structures (Fig. 3-4), but larger clusters within the networks were observed. The higher molecular weight of cruciferin may partially explain these larger aggregates and more compact particulate network structures with stronger mechanical properties than those of CP1 gels produced at the same conditions. With increasing processing pH, the “melt” situation and then the macro-porous wall structures were observed (Fig. 3-4d). The extremely high compressive stress observed for CP2 gels at pH 11 further proved that the protein network with polymer gel structure possessed relatively strong mechanical properties. When the heating temperature was

raised to 120 °C, the cluster density was enhanced, which explained the higher compressive stress of CP2 gels. However, unlike CP1 gel, CP2 gels formed at pH 9, 120 °C did not exhibit the macro-porous dense wall structures (Fig. 3-4g). Due to its high molecular weight and complex structures, heating at pH 9 was still insufficient to denature CP2 completely. Nevertheless, at pH 11, macro-porous structure could be formed at 80 °C (Fig. 3-4d).

Numerous studies have been conducted on whey, soya, and plasma protein fractal aggregation or gels (Renkema & van Vliet, 2002; Pouzot, Benyahia, & Nicolai, 2004; Dàvila, Parés, & Howel 2007, Maltais et al., 2008). These fractal gels were formed by random cluster-cluster aggregation. A fractal model related to the structure of colloidal gels was developed (Wu & Morbidelli, 2001) to estimate these fractal aggregations. There were three gelation regimes: strong-link, where inter-floc link stronger than intra-floc link; transition regime, where inter- and intra-floc links were equal; weak-link, where the intra-floc link were more rigid. These different gelation regimes resulted in the protein fractal gels with various microstructures and mechanical properties. As seen from SEM images, canola protein gels formed at low pH and heating temperature had similar microstructures with those fractal gels. Thus, it could be deduced that the formation mechanism of these canola protein gels followed the fractal theory and the moderate or weak inter-floc links were formed. However, the macro-porous dense wall structures were found at higher pH and heating temperature (CP1, pH 9, 120 °C and CP2 pH 11), which might be caused by different gelation mechanism rather than fractal aggregation. Therefore, a

systematic study on protein conformational changes and protein molecular interactions were conducted to understand canola protein gel formation mechanism at molecular level.

3.3.3.2 Gel conformational structures

The deconvoluted spectra in the amide I band region of 5% (w/v) CP1 and CP2 suspensions at pH 5, 7, and 9 upon heating from 25 to 80 °C (lines a–c) are shown in Fig. 3-5, as well as those of the dried CP1 and CP2 gels formed at various pHs at 120 °C (line d). CP1 and CP2 suspensions at 25 °C (line a) possessed several bands, which had been previously assigned to protein secondary structures: 1691/1689 cm^{-1} (β -sheets/turns), 1675/1670 cm^{-1} (β -sheets/turns), 1659 cm^{-1} (α -helix), 1645/1642 cm^{-1} (α -helix and random coil), 1631 and 1618 /1619 cm^{-1} (β -sheets), and 1608/1607 cm^{-1} (vibration of amino acid residues) (Byler & Susi 1986; Remondetto & Subirade, 2003; Zhang, Liang, Tian, Chen, & Subirade, 2012). The strong absorptions at 1659 and 1645 cm^{-1} indicated that α -helix and random coil dominated the secondary structure in CP1, while the absorptions at 1688, 1670, and 1631 cm^{-1} demonstrated that β -sheets was in the ascendant in CP2. This result was in accordance with previous report that napin had a high content of α -helical structure and a low content of β -sheet conformation (Schwenke et al., 1994), while cruciferin, had a low content of α -helical structure and a high amount of β -sheet conformation (Zirwer et al., 1985).

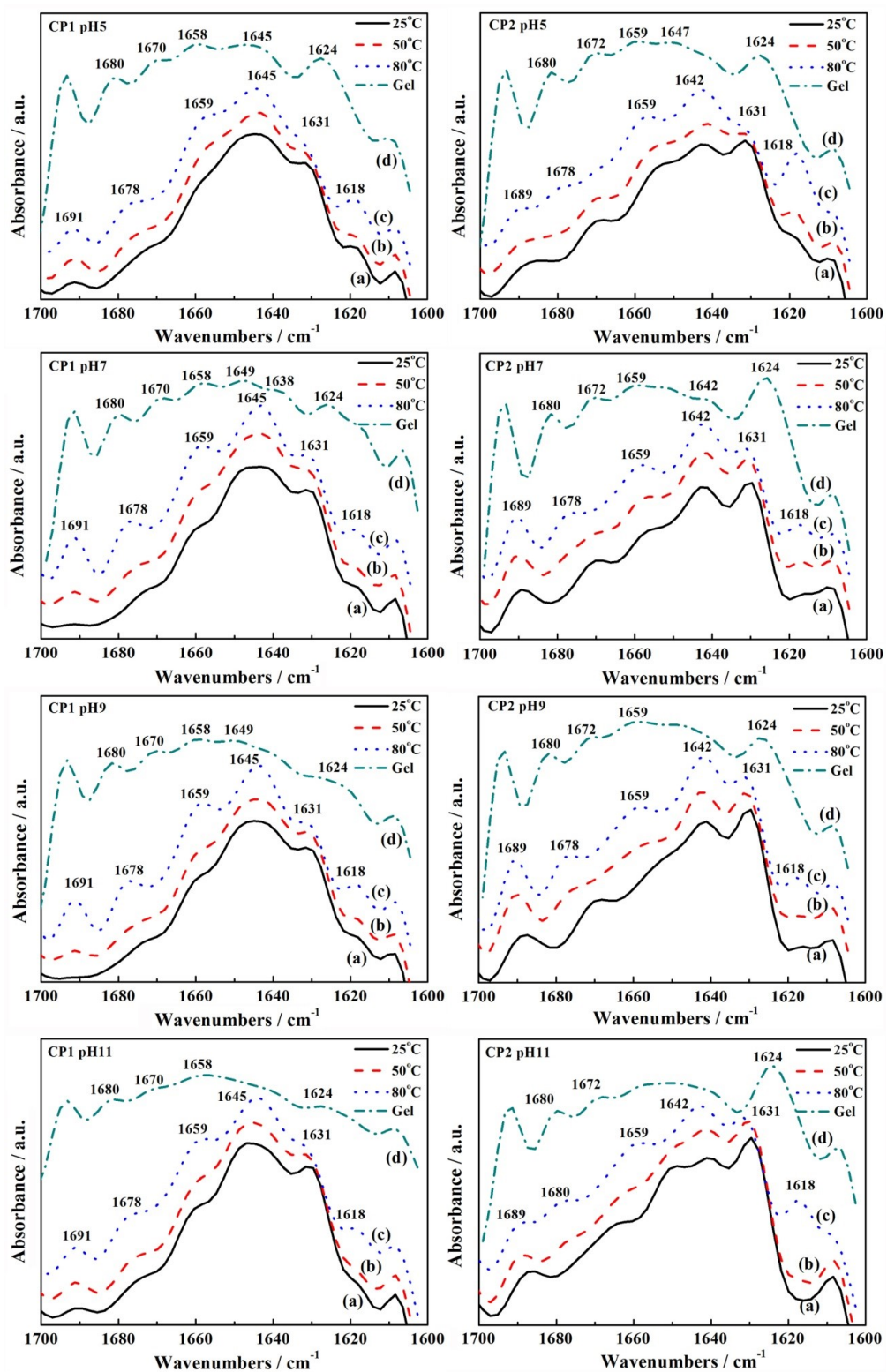


Fig. 3-5. Deconvoluted FTIR spectra of CP1 and CP2 suspensions (5% w/v in D_2O) at different pHs upon heating from 25 to 80 $^{\circ}\text{C}$ (a, b, c) and dried CP1 and CP2 gels formed at 120 $^{\circ}\text{C}$ (d).

For gels made from CP1, no discernible changes in secondary structures between different pH were observed at 25 °C, which was probably due to the stable molecular structures of CP1 fastened by disulfide bonds. With increasing the temperature from 25 to 80 °C (Fig. 3-5, CP1, line a-c), the band at 1631 cm^{-1} gradually decreased, indicating partial unfolding of CP1. Whereas the increase of band intensity at 1691, 1678, 1659 and 1618 cm^{-1} was likely to be related to the subsequent polypeptide aggregation via the exposed reactive groups. These conformational changes well explained the gelling point of CP1 at low temperature and the gradual increase of G' in the temperature sweep (Fig. 3-1, CP1). However, the position of the characteristic bands was largely retained after heating, which indicated that 80 °C was insufficient to denature CP1 molecules, but higher than 100 °C was out of the heating range of the temperature controller. Thus the dried gels formed at 120 °C at various pHs were examined (Fig. 3-5, CP1, line d) after gel formation. The amide I band was significantly altered when heating temperature increased from 80 to 120 °C. For example, at pH 11 the content of α -helix (1658 cm^{-1}) in CP1 decreased from 17.0 to 12.1% and new absorptions arose at 1680 and 1624 cm^{-1} . The band of 1624 cm^{-1} corresponded to intermolecular β -sheets caused by aggregation via hydrogen bonding, while the one at 1680 cm^{-1} indicated that β -sheets were antiparallel, especially in heat denatured proteins (Lefèvre & Subirade, 2000; Gilbert et al., 2005; Xia, Wang, & Chen, 2011, Saguer, Alvarez, Sedman, & Ismail, 2013). These changes of band intensity indicated that CP1 was unfolded and aggregated after heating at 120 °C. The greater denaturation degree of CP1 was observed at alkaline condition compared to those at pH 5 and 7, for example, when heated at 120°C, the

amount of α -helix (1658 cm^{-1}) in CP1 decreased from 17.0 to 15.6% at pH 5, whereas to 12.1% at pH 11. The decreased band of 1658 cm^{-1} at pH 9 and 11 indicated the split of disulfide bonds that used to stabilize the secondary structures of CP1.

Different from that of CP1, the secondary structure of CP2 was slightly changed at different pHs at $25\text{ }^{\circ}\text{C}$. The sample prepared at pH 5 showed stronger bands at 1618 and 1659 cm^{-1} (Fig. 3-5, CP2, line a), which indicates that the aggregation occurred even at room temperature due to partial protein unfolding in acidic pH. This observation supported the result of rheological test that G' was higher than G'' at room temperature at pH 5. When increasing heating temperature to $80\text{ }^{\circ}\text{C}$ (Fig. 3-5, CP2, lines a-c), similar to CP1, the decrease of band intensity at 1631 cm^{-1} and the increased intensity of bands at 1618 and 1659 cm^{-1} revealed the further unfolding and aggregation of protein molecules. As discussed above, CP2 had higher molecular weight, more hydrophobic amino acids and less stable structures than CP1, so it was easier for CP2 to unfold and generate interactions during the gel formation, resulting in the improved gel strength. Moreover, dramatically increased intensity of 1618 cm^{-1} of CP2 at pH 5 that corresponded to β -sheet aggregates well explained that the gel formed at pH 5 was stronger than those formed at pH 7 and 9 at $80\text{ }^{\circ}\text{C}$. The secondary structures of dried CP2 gels were also investigated, which showed similar patterns with CP1. However, the aggregation band at 1624 cm^{-1} was more obvious and less α -helix bands were found at pH 11 (Fig. 3-5, CP2, pH 11, line d). Quantitatively, when heated at 120°C β -sheet in CP2 increased from 32.1% at pH 5 to 40.9% at pH 11, while

α -helix/random coil reduced from 14.6% at pH 5 to 11.8% at pH 11. This result indicated that CP2 was further unfolded at high pH value and then reorganized under heating.

The denaturation of CP1 structures without splitting of disulfide bonds at pH 5 and 7 and CP2 at pH 5, 7 and 9 obviously impacted the aggregation of proteins to form gel network structures, which was confirmed by the particulate fractal structures of CP1 and CP2 gels in SEM figures. However, the denatured structures with splitting of disulfide bonds of CP1 at pH 9 and 11 and CP2 at pH 11 and 120 °C allowed them to develop more molecular interaction, resulting in the macro-porous and dense wall gel network structures.

3.3.3.3 Gel dissociation test

Three dissociation reagents, SDS, urea, and 2-mercaptoethanol (2-ME) were applied to disrupt hydrophobic interactions, hydrogen bonds, and disulphide bonds, respectively, so as to pursue a further understanding of the interactions involved in the canola protein gelation. Fig. 3-6 illustrates the linear viscoelastic frequency sweep response of CP1 and CP2 gels formed at 120 °C and different pHs with and without soaking into dissociation reagents.

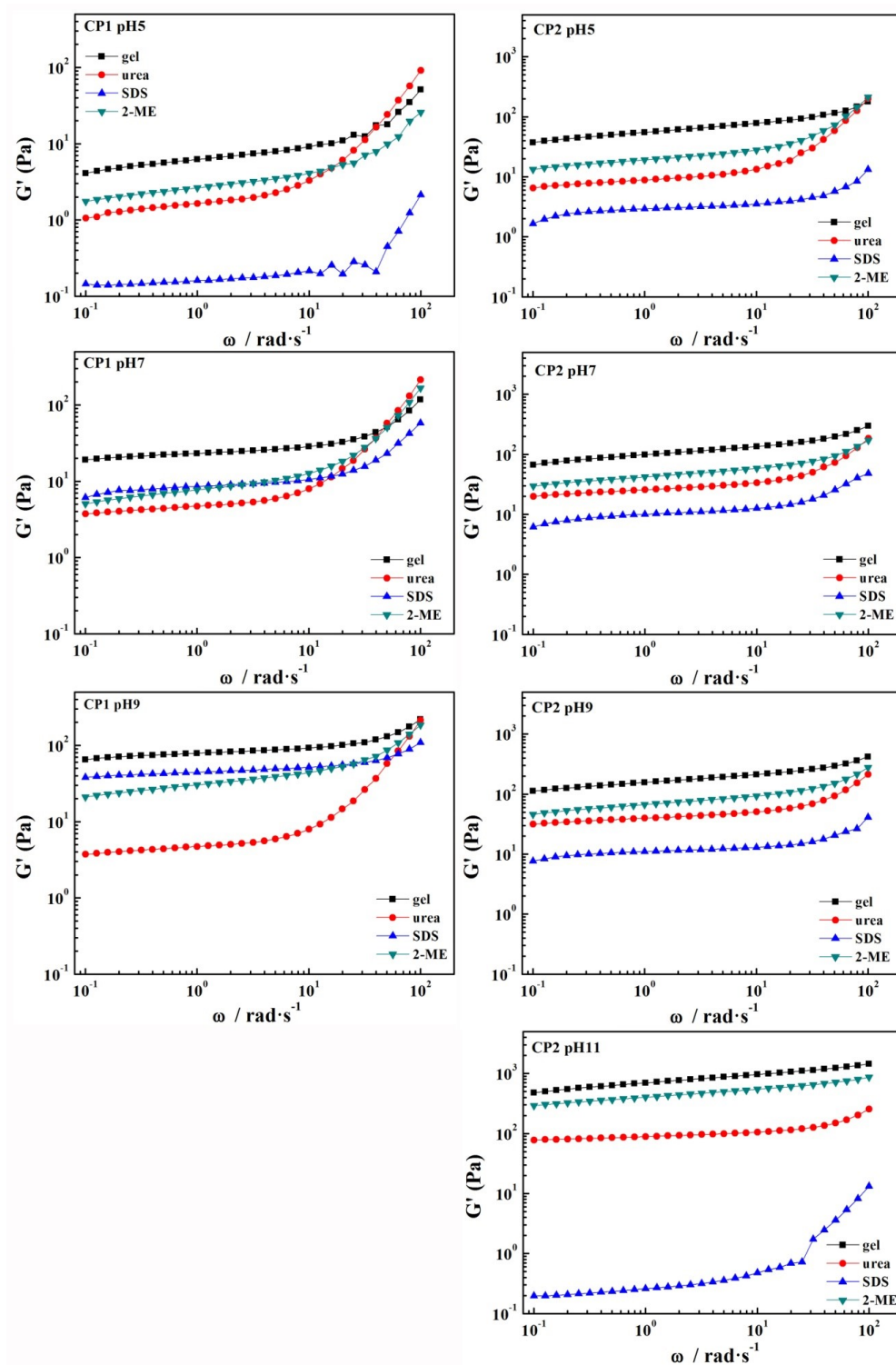


Fig. 3-6. Frequency dependence of storage modulus (G') of CP1 and CP2 gels (15%, w/v) formed at different pHs and 120 °C with or without soaking in dissociation reagents.

The storage modulus (G') curves of all gels without dissociation agents presented a linear response slightly up to high frequency, after which there was a minor deviation from the linear response. The region of the linear response increased with pH values, suggesting that the protein gel network became stronger and more elastic (Wang & Chen, 2011). After soaking into urea, SDS, and 2-ME for 48 h, CP1 and CP2 gels became weaker and lost their elasticity, as evidenced by the decrease of G' values and the region of linear response. Moreover, as shown in Fig. 3-7 and 3-8, the effects of treating with three dissociation agents on the morphology and properties of protein gels were different. Urea treated gel exhibited weak and sticky property, while soaking in 2-ME resulted in a fragile gel, but the morphology of gel did not change significantly. The diameter of gels became larger after soaking in the dissociation reagents, indicating that the swell condition occurred since some non-covalent and/or covalent interactions were broken. Most gels became semi-transparent when put them into SDS solutions, whereas the CP1 pH 5 gel seemed to be dissolved and CP2 pH 11 gel almost lost its gel morphology. The gels formed at acidic and neutral pH showed light yellow color, while the gel prepared at alkaline pH exhibited brown color. This could be attributed to the exiting of phenolic compounds, which resulted in the dark colors in canola protein gels due to enzymatic and non-enzymatic oxidation at alkaline conditions. The dark color can impact the utilization of canola proteins in food applications, therefore, an economical and efficient method should be developed to remove phenolic compound in extracted canola proteins in the future.

As shown in Fig. 3-6 CP1 pH 5, the presence of 2-ME and urea induced an obvious decrease in G' and width of linear region, suggesting that the disulfide bonds and hydrogen bonding contributed to the gel network formation. However, the stronger effect was observed in the presence of SDS, indicating that hydrophobic interactions played the most important role in CP1 gel formation at pH 5 as revealed in Fig. 3-7. Nevertheless, the main interaction changed with the gel formation pH shifted from 5 to 9, where the loss of hydrogen bonds induced the lowest G' . The different interactions observed in pH 5 and 9 could be attributed to the split of disulfide bonds at the alkaline pH, which induced exposure of more protein molecular side chains to develop hydrogen bonds to reinforce the gel network structure. It had been reported that disulfide bonds would contribute to the consolidation of β -lactoglobulin gel structures (Remondetto & Subirade, 2003). Therefore, a moderate decrease of G' value of all the CP1 gels soaked in 2-ME solution was observed, due to the disruption of inter- and intra-molecular disulfide bonds.

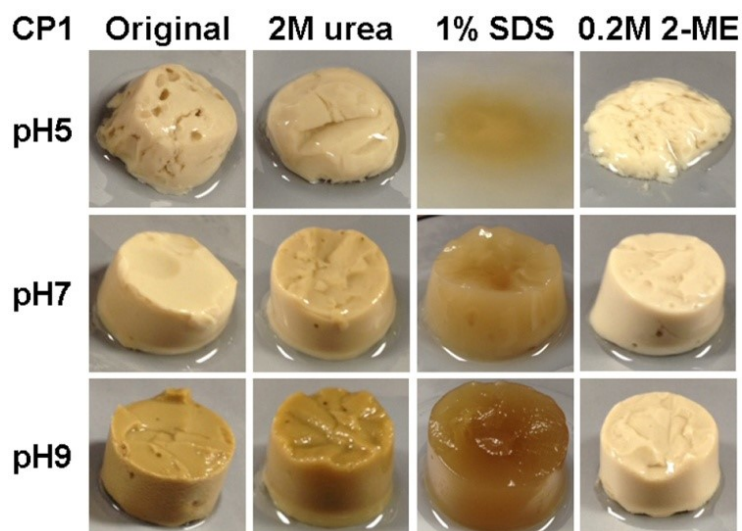


Fig. 3-7. Photos of CP1 gels (15%, w/v) prepared at different pHs and 120 °C with or without soaking in dissociation reagents.

In the case of CP2 gels, the impacts of three dissociation agents at pH 5, 7 and 9 were similar (Fig. 3-6, CP2). Although 2-ME and urea induced a significant decrease in the G' curve and width of plateau, the most striking impact was produced by SDS, suggesting the essential role of hydrophobic interactions in the CP2 gel network structures due to its high amount of hydrophobic amino acid compositions. This result was in agreement with the conclusion that hydrophobic forces and electrostatic interactions were responsible for the establishment of canola 12S globulin gel networks, while disulfide bonding, electrostatic interactions and hydrogen bonding corresponded to gel stabilization and strengthening (Léger & Arntfield, 1993). It was worth noting that soaking in SDS exhibited the most distinct effect on G' curve of CP2 gel formed at pH 11, which also reflected by the gel morphology in Fig. 3-8. It indicates that, different from the main factor of hydrogen bonding in CP1 gel, hydrophobic interactions were generated to form the macro-porous dense wall structure of CP2 gel after it was denatured. Since CP2 contained more hydrophobic amino acid than CP1 (Chabanon et al., 2007), the further exposed great amounts of hydrophobic groups in CP2 at high temperature participated in the gel establishment and stabilize the gel microstructures. Thus, other than chain entanglement and molecular weight, the more hydrophobic region of CP2 could also be one of the reasons that resulted stronger gel strength than CP1 gels even both of them were denatured. Noticeably, same as CP2 gel formed at pH 11, the hydrophobic interactions were predominant in the CP1 gel prepared at pH 5. However, the disulfide bonds of CP1 at pH 5 still exist as revealed in FTIR results. Although parts of exposed hydrophobic region of CP1 interacted to constitute the

network structure, no more interactions could be developed to strengthen this structure. In contrast, CP2 at pH 11 were unfolded with split of disulfide bonds and exposed most of hydrophobic groups. As a result, these two gels had totally opposite gel microstructures and mechanical properties.

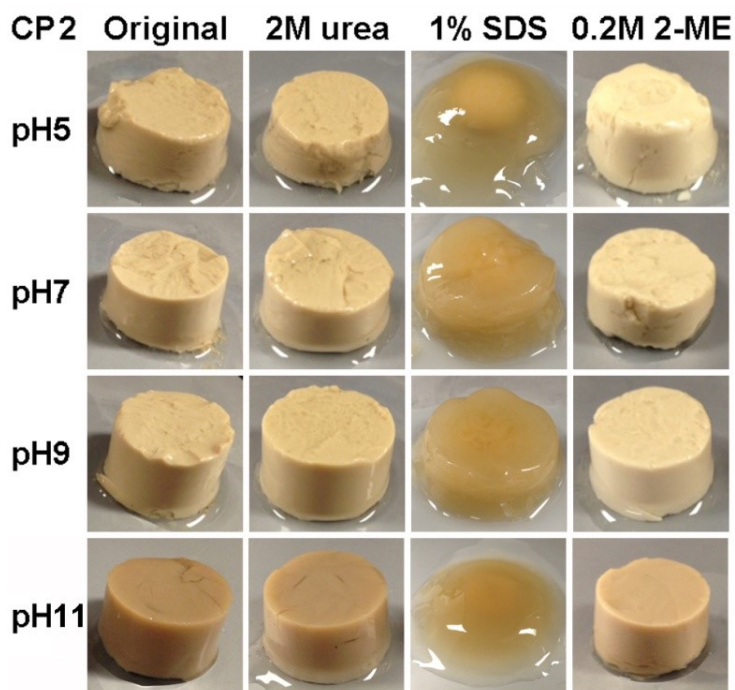


Fig. 3-8. Photos of CP2 gels prepared (15%, w/v) at different pHs and 120 °C with or without soaking in dissociation reagents.

3.3.3.4 Gel formation mechanisms

According to the above results, the thermally induced canola protein gelation mechanism could be concluded. In the case of CP1 gels, the randomly aggregated particulate fractal structures were formed mainly through hydrophobic interactions and supported by disulfide bonds and hydrogen bonds at pH 5 and 7. The protein unfolding occurred without splitting the

disulfide bonds which used to stabilize the secondary and tertiary structures of CP1 protein molecules, so it was difficult to develop more molecular interactions to reinforce the gel network structures. At pH 9 and low temperature, similar fractal aggregation structures were established firstly. With continuous heating, the unfolding of CP1 with split of disulfide bonds occurred and the active side chains were exposed to develop more interactions. Thus, the aggregated particulate fractal microstructures “melted” and the CP1 gels with macro-porous dense wall were established by the development of intermolecular hydrogen bonds.

For CP2 gels, the denaturation without split of disulfide bonds and high molecular weight induced the similar particulate fractal structures at pH 5, 7 and 9, which were mainly combined by hydrophobic interactions and supported by hydrogen bonds and disulfide bonds. Thus higher negative charge density and electrostatic repulsive forces was prerequisite for CP2 to form macro-porous wall structures. When the pH increased to 11, CP2 protein molecules were denatured with split of disulfide bonds and more interactions were thus built among their hydrophobic regions. The resultant CP2 gels were much stronger than not only CP2 particulate gels but also CP1 gels with macro-porous dense wall structures.

3.4 Conclusions

In this study, two types of gels were obtained depending on the different processing conditions. At low pH and temperature, CP1 and CP2 gels exhibited randomly aggregated particulate fractal network structures, while at high pH and temperature, the macro-porous dense

wall network structures were established. The protein conformational study and gel dissociation test suggested that the higher heating temperature and pH induced more unfolded structures through splitting inter- and intra-chain disulfide bridges so as to facilitate the establishment of molecular interactions. Remarkably, the macro-porous dense wall structure gel, as demonstrated in the result of mechanical properties test, exhibited much stronger gel strength than the gel with particulate fractal structure. Based on the results of this study, it could be concluded that the mechanical properties of canola protein gels were closely related to the different types of gel network structures, which were induced by the degree of denatured canola protein structure and the development of molecular interactions through manipulating pH value and heating temperatures. By controlling processing conditions, canola protein gels with various mechanical properties could be prepared, which were comparable to those of thermally-induced soy protein gels and legume protein gels. Therefore, the canola protein gels with clearly revealed structures have increased their potential for use in food and non-food applications.

Chapter 4

Fabrication, characterization and controlled release properties of oat protein gels with percolating structure induced by cold gelation

4.1 Introduction

Protein gels have been extensively used in biomedical and food applications due to their renewable nature, superior nutritional value, inherent biocompatibility, and biodegradability (Chen et al., 2006; Wang et al., 2012). Over the past decade, applications of animal protein based gels (collagen, gelatin, albumin, whey protein, etc.) as wound dressings, scaffolds for cell growth in tissue engineering, and nutraceutical delivery systems have been widely studied (Dobaczewski et al., 2006; Cummings, Gawlitta, Nerem, & Stegermann, 2004; Chen & Subirade, 2006; Gunasekaran et al., 2007). For globular proteins, either a particulate or filamentous gel is obtained by heating, depending on the environmental pH (Lefèvre & Subirade, 2000). Collagen and gelatin exhibit triple-helix structure (Duconseille et al., 2015), and these helices lose their conformation during heating and partially recover during cooling to form a percolating gel network with a high degree of cross-linking (Coppola et al., 2012, Oakenfull & Scott, 2003, Duconseille et al. 2015). This not only confers the gel many mechanical properties (Forte et al., 2015), but is also of relevance when developing drug delivery systems with gel scaffolds (Kim et al., 2014; Gaowa et al., 2014).

In recent years, proteins derived from plant sources are important due to health, religious and cost concerns of animal sources (Kim et al., 2014; Gaowa et al., 2014). Plant protein delivery vehicles have been developed for the controlled release of drugs, unsaturated fatty acids, vitamins, and other small bioactive compounds (Lai & Guo, 2011; Yang et al., 2014; Chen & Subirade, 2009). Although most research has focused on the formation of plant protein coacervates and particles, gels have been underrepresented despite their potential. Plant protein gels have a high water holding capacity and good biocompatibility to provide a non-reactive environment for sensitive bioactive compounds, such as enzymes and probiotics. The gelation process of soy protein has been extensively studied (Vilela et al., 2011; Maltais et al., 2005; Maltais et al., 2008), and to a lesser extent, plant proteins, such as those from pea, canola, and oat, have also demonstrated gelling properties upon heating (Sun & Arntfield, 2010; Nieto-Nieto et al., 2014).

Cold-set gelation of soybean proteins was achieved by adding Ca^{2+} ions or glucono- δ -lactone (GDL) to a preheated protein suspension (Cavallieri & da Cunha, 2008, Maltais et al., 2005; Bryant & McClements, 2000). The cold-set gels offer opportunities to prepare the means to carry and protect sensitive nutraceutical compounds and develop innovative functional food ingredients. However, cold-set gels from other plant proteins other than soy protein have seldom been reported. Oat has the highest protein level (12-24%) among cereals and a superior amino acid profile containing high quantities of essential amino acids lysine and threonine (Mohamed et al., 2009, Klose & Arendt, 2012). The major fraction of oat protein is 12S globulin, which consists of α - and β -subunits with molecular weight of about 32 and 22 kDa,

respectively. These two subunits are disulfide bonded to form a dimer, which further associates into a hexamer through non-covalent forces (Burgess et al., 1983). The previous work revealed that thermally-induced oat protein gels exhibited a percolating network structure, different from many other globular proteins but similar to gelatin (Nieto-Nieto et al., 2014). These gels had good mechanical properties and were comparable to those of egg protein. In spite of oat's potential, cold-set gelation of oat protein has never been reported. This work aimed to develop cold-set oat protein gels using GDL. The effect of various GDL levels on gel structure, mechanical properties, and water holding capacity was investigated. The gel formation mechanism is discussed by correlating the gel microscopic structure with macroscopic properties. Moreover, the ability of oat protein gels to protect enzymes and probiotics and controlled release were evaluated in a simulated human gastro-intestinal tract.

4.2 Materials and methods

4.2.1 Materials

Naked oat grain (*Avena nuda*) (crude protein 17.2%) was purchased from Wedge Farms Ltd., Arborg, Manitoba, Canada. Glucono- δ -lactone (GDL), amylase, and an amylase activity assay kit were obtained from Sigma-Aldrich Canada (Oakville, ON, Canada). *Lactobacillus acidophilus* (ATCC4536) was obtained from American Type Culture Collection (ATCC, Manassas, VA, USA). MRS broth and other chemicals (analytical grade) were purchased from Fisher Scientific (Whitby, ON, Canada). Milli-Q water was used in all experiments. Oat protein isolate (OPI) was

extracted from defatted oat flour using an alkaline and isoelectric point precipitation method according to our previous work (Nieto-Nieto et al., 2014). The protein content of OPI was $85.07 \pm 2.4\%$ determined by Leco nitrogen analyzer (FP-428, Leco Corporation, St Joseph, MI) and a nitrogen to crude protein conversion factor of 5.83 was used, while other components could be soluble fiber, starch, lipid, and ash, among others.

4.2.2 Gelation process of OPI solutions with GDL addition

A dynamic rheology experiment was carried out on a DHR-3 rheometer (TA Instruments, New Castle, DE, USA) to study the gelation process of OPI suspensions with addition of GDL. Parallel plate geometry with a gap of 1 mm was used to measure dynamic viscoelastic parameters (shear storage modulus G' and loss modulus G''). The value of the strain amplitude for all samples was set as 1%, which was within a linear viscoelastic regime. The preheated OPI (5 and 7%, w/v) solutions with different GDL contents (3, 5, 10, and 15%, w/w, based on the dry weight of protein) were placed on the plate immediately after addition of GDL and the dynamic time sweep measurements were performed at an angular frequency of 1 Hz at 25°C over a period of 1200 min. A frequency sweep was subsequently conducted as a function of angular frequency (ω) from 0.1 to 100 rad s⁻¹ at 25°C to study gel shear strength. A thin layer of low-viscosity silicone oil was applied to prevent dehydration during the test. The change of pH value during gelation was monitored simultaneously after GDL addition using a pH meter (Thermo Scientific Orion 3 Star pH Meter, Burlington, ON, USA).

4.2.3 Cold-set OPI gel preparation

OPI 5 and 7% (w/v) was dissolved in water and stirred overnight at room temperature. The suspensions were then adjusted to pH 8 using 1 M NaOH. OPI suspensions were tightly sealed in glass vial and heated at 115 °C (above denaturation temperature) in an oil bath for 15 min. Subsequently, they were cooled down to room temperature and different amounts of GDL (3, 5, 10, 15% (w/w), based on the dry weight of protein) were added to the OPI solutions. The solutions were stored at 4 °C for 1200 min to form OPI gels, and the obtained gels were coded as OG5-3, OG5-5, OG5-10, OG5-15, OG7-3, OG7-5, OG7-10, and OG7-15, corresponding to the different OPI and GDL concentrations, respectively. For example, OG5-3 gel was prepared from 5% (w/v) OPI pre-heated solution with 3% (w/w) GDL addition.

4.2.4 OPI gel properties

Mechanical properties of OPI gels were determined using an Instron 5967 Universal testing instrument (Instron Corp., Norwood, MA, USA) equipped with a 50 N load cell. The cylindrical gels had the height of about 10 mm and the diameter of around 12 mm. All the samples were compressed twice to 50% of their original height at room temperature with the constant crosshead speed of 1 mm/min. Two texture parameters including compressive stress and springiness were determined from the typical force-time curves. Compressive stress indicates the gel firmness and is calculated as the compressive force (hardness, N) over the cross-sectional area of the gel. Springiness indicates how well a gel physically springs back after the first compression, which is measured by the distance of down stroke of the second compression (Bourne, 2002).

Water holding capacity (WHC) of OPI gels was measured according to the method of Kocher and Foegeding (1993) with modifications. Gel samples (0.8-1.0 g) were placed into Vivaspin 20 centrifugal filter unit (GE Healthcare Bio-Sciences AB, Uppsala, Sweden) with 5 µm filter membrane and then centrifuged at 800 g for 5 min at room temperature. The weight of the gels was recorded before (W_t) and after (W_c) centrifugation. The centrifuged gel was dried in oven at 60°C overnight and weighted (W_d). WHC was calculated using equation (4-1).

$$\text{WHC \%} = \frac{W_c - W_d}{W_t - W_d} \times 100\% \quad (4-1)$$

4.2.5 Gel morphology

The morphology observation of OPI gels was carried out with a Philips XL-30 scanning electron microscope (SEM) at an acceleration voltage of 6 kV. The samples were frozen in liquid nitrogen and snapped immediately by tweezers to expose the inner structure, and freeze-dried before SEM observation. The cross-sections of the gels were sputter-coated with gold, observed and photographed. To test the stability in simulated gastric fluids (SGF, 0.1 M pH 2 HCl-saline with pepsin), the fresh gels were immersed in SGF for 1 and 2 h, respectively, and then were frozen, snapped, freeze-dried, and observed.

4.2.6 Protein structures in OPI gels

The protein conformation of unheated and preheated OPI solutions as well as cold-set OPI gels was characterized by FTIR. OPI (1%, w/v) was dissolved in D₂O. The solution was adjusted to pH 8 using 1% NaOD and marked as unheated OPI suspension. The same solution was heated at 115 °C for 15 min and then cooled down, which was marked as preheated OPI solution.

Different amounts of GDL (3, 5, 10, 15%, w/w) were added to preheated solutions and stored for 1200 min to prepare cold-set OPI gels. The samples were placed between two CaF₂ windows separated by 25 µm polyethylene terephthalate film spacer for FTIR measurement. D₂O with or without GDL was used as background. The spectra of samples were recorded using Nicolet 6700 spectrophotometer (Thermal Fisher Scientific Inc., Pittsburgh, PA, USA) in the range of wavenumber from 400 to 4000 cm⁻¹ during 128 scans with 2 cm⁻¹ resolution. The spectrophotometer was continuously purged with dry air from a lab gas generator (Parker Hannifin Corp., USA). For amide I band region (1700-1600 cm⁻¹), Fourier self-deconvolution was performed using Omnic 8.1 software at a bandwidth of 24 cm⁻¹ and an enhancement factor of 2.5.

Dynamic light scattering measurement was performed using a Zetasizer Nano-ZS (Malvern Instruments Ltd., UK) equipped with a 633 nm He-Ne laser to determine the size of OPI. OPI suspensions with the same concentration of gels (7%, w/v) were treated by heating at 115 °C, followed by addition of GDL. The mixtures were then rapidly diluted to 0.25 mg/mL and analyzed through three averaged sub-runs at a fixed 90° scattering angle. The size change of the untreated protein solutions (7%) were also analyzed after dilution to 0.25 mg/mL. The apparent particle size was obtained by CONTIN mode analysis.

The morphology of unheated, preheated, and GDL added OPI in solutions was determined by atomic force microscopy (AFM). OPI solutions with the same concentration of gels (7%, w/v) were treated to get unheated, preheated, and GDL added OPI solutions, then these solutions were

rapidly diluted to 0.025 mg/mL before measurement. Then, 20 μL solutions were dripped onto freshly cleaved mica and dried at room temperature. Tapping mode AFM images were collected by AFM MPF-3D (Asylum research, Oxford Instrument Company, Santa Barbara, CA, USA) and Inverted Optical Microscope Olympus 70/71 (Olympus Co., USA) under ambient conditions. The system was installed in an acoustic hood to minimize vibrational noise. A silicon-etched cantilever with a tip radius of 20-30 nm was driven at oscillation frequencies in the range of 580-600 kHz. The collected images were flattened using AS software for further analysis.

4.2.7 Determination of fractal dimension

The scaling model modified by Wu and Morbidelli (2001) was selected to determine the elastic contributions of both inter- and intra-floc links using a microscopic elastic constant of α ($0 \leq \alpha \leq 1$). The expressions of the scaling model dependence of G' and γ_0 are as follows:

$$G' \sim \phi^{\beta / (d - D_f)} \quad (4-2)$$

$$\gamma_0 \sim \phi^{(d - \beta - 1) / (d - D_f)} \quad (4-3)$$

$$\beta = (d - 2) + (2 + x)(1 - \alpha) \quad (4-4)$$

Where d is Euclidean dimension ($d=3$ in three-dimensional systems); ϕ is concentration of the gel; D_f is fractal dimension of system; β is an auxiliary parameter; x is fractal dimension of aggregate backbone of network. For colloidal gels, x is within the range of [1, 1.3].

Strain sweep measurements for cold-set OPI gels formed with various protein (5, 6, 7 and 8%, w/v) and GDL concentrations (3, 5, 10 and 15%, w/w) were carried out on DHR-3 rheometer (TA Instruments, DE, USA). The cylindrical gel with diameter of around 12 mm and height of

about 10 mm was compressed to 80% of original height using parallel plate geometry. According to our preliminary test, the compressive deformation of 20% was suitable and wouldn't affect the structure of fractal aggregates. The G' value was evaluated as a function of strain from 0.1 to 100% with an angular frequency of 1 Hz. Initial G' value, G_0 , was calculated as the average value of G' in strain range from 0.1 to 1%. Over a certain strain, G' decreased corresponding to the breakdown of gels. The critical strain (γ_0) is defined as the strain at 95% of G_0 . Based on equations (4-2) and (4-3), D_f and β can be calculated as the power-law exponents equal to the slopes of log-log plots of G' vs ϕ and log-log plots of γ_0 vs ϕ . The α value can be determined through subsequent substitution of β value to equation (4-4) with the assumed backbone fractal dimension $x=1$ and $x=1.3$, respectively.

4.2.8 Encapsulation and protection of bioactive compounds

Alpha-amylase and *Lactobacillus acidophilus* were selected as models of bioactives representing bioactive proteins/peptides and probiotics, respectively. Alpha-amylase solutions were prepared by dissolving the dry powders (7%, w/w, based on the dry weight of protein) in pre-heated oat protein solutions (7%, w/v) at room temperature, and 10% (w/v) GDL was then added to the mixtures to form gels. The nutraceutical loaded gels were cut into small pieces (5 × 5 × 5 mm) using scalpel and dried at room temperature, resulting in a dry gel of around 2 × 2 × 2 mm. For preparation of probiotics encapsulated gels, *L. acidophilus* was firstly activated on MRS agar at 37 °C for 48 h under anaerobic conditions. One colony was selected and grown in MRS broth at 37 °C for 24 h, and then sub-cultured at least three times. The culture was centrifuged at

800 g for 5 min. The precipitate was collected and dispersed in MRS broth. Subsequently, 2.5 mL suspension was added in 6 mL 10% (w/v) pre-heated OPI solution at room temperature to get the final oat protein concentration around 7% (w/v). The gels were formed by adding 10% (w/w) GDL, and then stored at 4 °C for further analysis.

The activity of encapsulated and free amylase and *L. acidophilus* was tested after immersing in simulated gastric fluid (SGF, 0.1 M, pH 2.0 HCl-saline solution with 0.1% (w/v) pepsin) for 0.5, 1, 1.5 and 2 h. The gels were taken out and washed with water. For the enzyme activity assay, the gels were immersed in Amylase activity kit buffer (500 µL) and smashed. The suspensions were centrifuged at 13,000 g for 10 min, and the supernatant was transferred into 96-well plate. The Master Reaction Mix (Amylase Assay Buffer 50 µL + Amylase Substrate Mix 50 µL) was then added and the samples were measured at 405 nm using Spectramax i3 (Molecular Devices, LLC, Sunnyvale, CA, USA) to get the initial absorbance. The absorbance was measured every 5 min at 25°C. Different concentrations of nitrophenol were used as standard. Once the most active sample was near or exceeded the end of linear range of standard curve, the measurement was stopped and the final absorbance was obtained. The amylase activity was calculated based on the equation provided by Amylase activity assay kit technical protocol (Stein, Place, Lacourse, Guglielmo, & Williams, 2015). The encapsulated enzyme without incubation in SGF was used as positive control, whereas the free enzyme incubated in SGF was used as negative control. For the probiotics stability test, sample gels were placed in MRS broth and smashed. The viability of released *L. acidophilus* was tested by plate count method through counting the number of colony

forming units (CFU) on MRS agar after incubation at 37 °C for 48 h under anaerobic conditions, and the amount of viable cells was quantified in log (CFU/mL). The survival (%) of the viable cells was the ratio of CFU numbers after and before the SGF exposure. The free cell sample incubated in SGF was used as negative control.

4.2.9 Controlled release of bioactive compounds

Riboflavin was selected as the model of bioactive compounds representing vitamins. The desired amount of riboflavin 7% (w/w), based on the dry weight of protein) was dissolved in pre-heated OPI solution (7%, w/v) at room temperature. Then 10% (w/v) GDL was added to form the gel. The nutraceutical loaded gel was cut into small pieces ($5 \times 5 \times 5$ mm) using scalpel and dried at room temperature (dry gel size: $2 \times 2 \times 2$ mm). The release profiles of riboflavin were tested in simulated gastro-intestinal tract at 37 °C. The dissolution mediums were: HCl-saline solution (pH 2.0, 0.1M); phosphate-buffered saline (PBS, pH 7.4, 0.1M); simulated gastric fluid (SGF, HCl-saline solution with 0.1% pepsin (w/v)); and simulated intestinal fluid (SIF, pH 7.4 PBS with 1.0% pancreatin (w/v)). For the release test, the riboflavin loaded gel was firstly placed in 50 mL HCl-saline solution or SGF at 37 °C and stirred at 100 rpm using a 2100C dissolution system (Distek Inc., North Brunswick Township, NJ, USA). After 2 h, the gel was transferred into 50 mL PBS or SIF for further 15 h. The riboflavin content in the release mediums was monitored with S-3100 UV-vis spectrophotometer (Scinco Co. Ltd., Gangnam, Seoul, Korea) at the wavelength of 445 nm.

4.2.10 Statistical analysis

All experiments were performed at least in triplicate. Results were expressed as mean \pm standard deviation. Statistical analysis was conducted using the Statistical Analysis System (SAS for windows, Release 9.0, SAS Institute Inc., Cary, NC, USA). Analysis of variance (ANOVA) was performed to analyze the effects of GDL concentration on gel mechanical properties. Tukey test was used to compare multiple means. A probability of $p < 0.05$ was considered to be statistically significant.

4.3 Result and discussion

4.3.1 Cold-set OPI gel preparation and characterization

4.3.1.1 OPI gel preparation

The pH change of preheated OPI solutions during acidification as a function of time is shown in Figs. 4-1a and 1b. With the addition of 3 and 5% GDL (time $t = 0$), the pH decreased rapidly in the first 100 min; while at high GDL concentrations (10 and 15%), a fast pH reduction was observed during the first 210 min. At 1200 min, most gels achieved steady-state pH values, indicating that the GDL hydrolysis reached equilibrium. However, OG7-10 and OG 7-15 had not reached equilibrium as pH slightly decreased continuously even after 1200 min likely due to the fact that longer time was required to completely hydrolyze larger amount of GDL into gluconic acid. Thus, an aging time of 1200 min was selected to prepare the gels in this study.

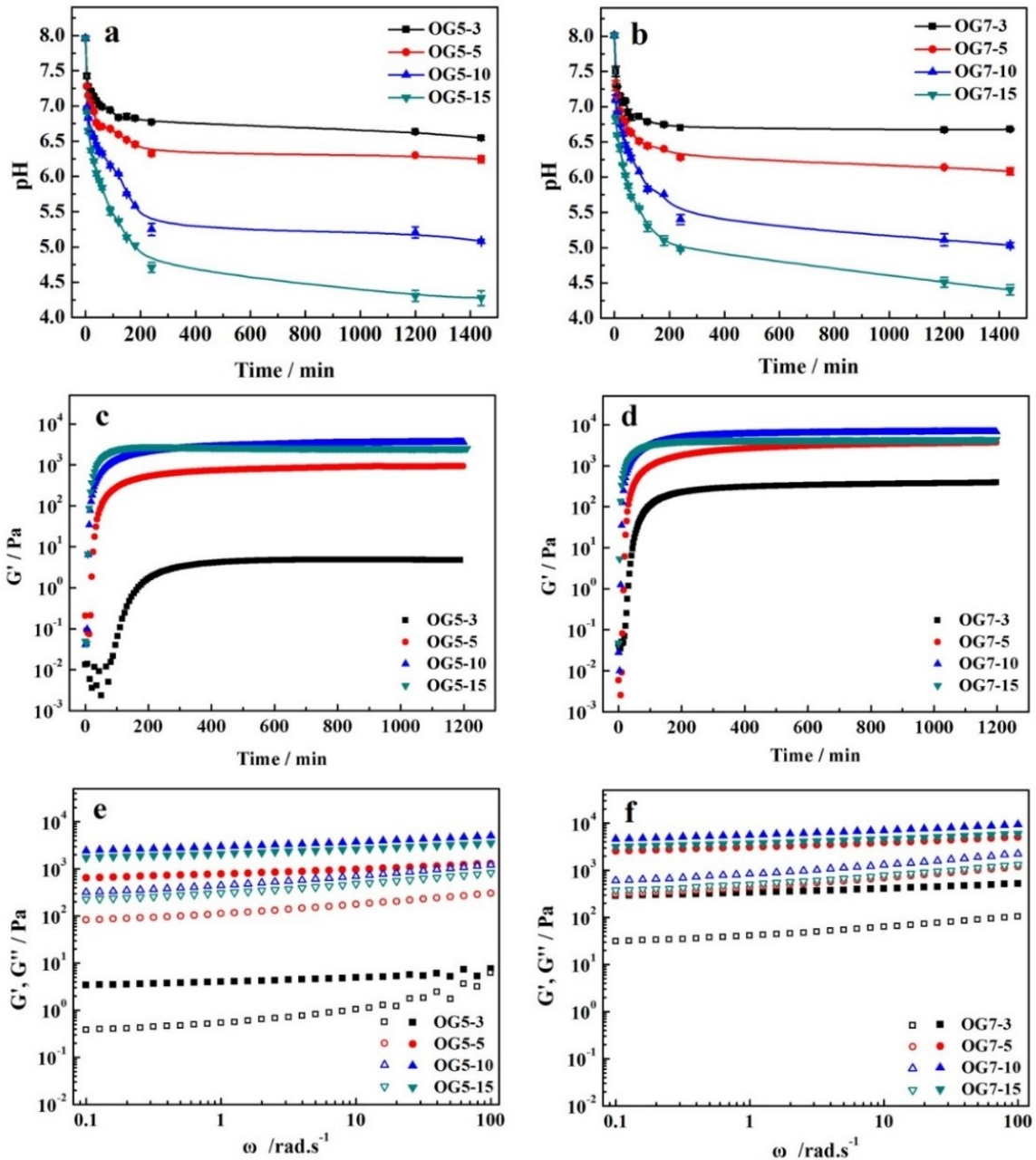


Fig. 4-1. Time dependence of pH value (a, b) and storage modulus (G') (c, d) of OPI solutions with addition of different GDL concentrations. (e, f) Frequency dependence of storage modulus (G' , solid) and loss modulus (G'' , open) of OPI gels prepared at different GDL concentrations. a, c, and e represent gels prepared at 5% (w/v) protein concentration; b, d, and f represent gels prepared at 7% (w/v) protein concentration.

Both 5 and 7% OPI solutions showed similar pH changes and final pH values. Since the GDL content determined the pH value of gel system, consequently, the gel microstructures and mechanical properties (Cavallieri & da Cunha, 2008), GDL concentrations of 3, 5, 10, and 15% (w/w) were applied to obtain gels with final pH of 6.8, 6.3 (higher than OPI isoelectric point (IEP) of 5.0), 5.2 (around IEP) and 4.4 (lower than IEP), respectively.

4.3.1.2 Rheological properties

The rheological behavior of OPI solutions with GDL addition was monitored. The initial storage modulus G' was always higher than loss modulus G'' , suggesting that the elastic modulus predominated the system (Tunick, 2010). Thus G' was chosen as the indicator to display the OPI gelation process. For Fig. 4-1c-f, the differences among the gels with different protein and GDL concentrations were significant ($p < 0.05$). Figs. 4-1c and 1d illustrate the evolution of G' values of OPI solutions with different GDL concentrations as a function of time. After GDL addition, G' rapidly increased within 200 min and then leveled off, indicating that the system transferred from fluid to viscoelastic solid (Barbut & Foegeding, 1993). The increase of G' value coincided with the decrease of pH value, and the G' reached the plateau at $\text{pH} \approx 6.8$ for all the samples. In addition, the time needed to form gel network structure was closely related to the GDL concentrations. Specifically, it took about 200 min for the OG5-3 sample with low GDL amount to reach the plateau, but only 60 min were required for the OG5-15 sample to achieve the transition. For OG5-5 and OG5-10, G' value reached the plateau after about 100 min. The

samples with 7% protein had a similar trend. This suggested that greater amounts of GDL caused the faster reduction of pH and the lower final pH values in gels, but the gel network structure formed at about pH 6.8 regardless of GDL concentration. A higher final G' value was observed with the addition of 10% GDL where the final pH value was 5.2 around the OPI IEP. Figs. 4-1e and 1f show the frequency dependence of G' and G'' of OPI gels. The G' and G'' curves of OG5-3 were frequency dependent and got very close to each other at high frequency, indicating a weak gel shear strength (Nunes, Raymundo, & Sousa, 2006. Savadkoochi & Farahnaky, 2012). All the other gels with higher GDL contents showed strong gel shear strength as their G' values were frequency independent (Zhang, Jiang, & Wang, 2007). Gels formed with a 7% protein concentration exhibited stronger shear strength than 5% OPI gels, and the greatest shear strength was observed when GDL content was 10%.

4.3.1.3 Gel mechanical properties and water holding capacity

As shown in Fig. 4-2a, GDL content significantly impacted gel compressive stress through modulation of the system pH value. When the protein concentration was 7%, the OG7-3 gel was the weakest with the final gel pH of 6.8. With increasing GDL to 10%, the final pH value decreased to 5.2 and the compressive stress dramatically rose to 28.8 kPa. A further increase of GDL to 15% led to the lower final pH value of 4.4 and compressive stress of 16.7 kPa.

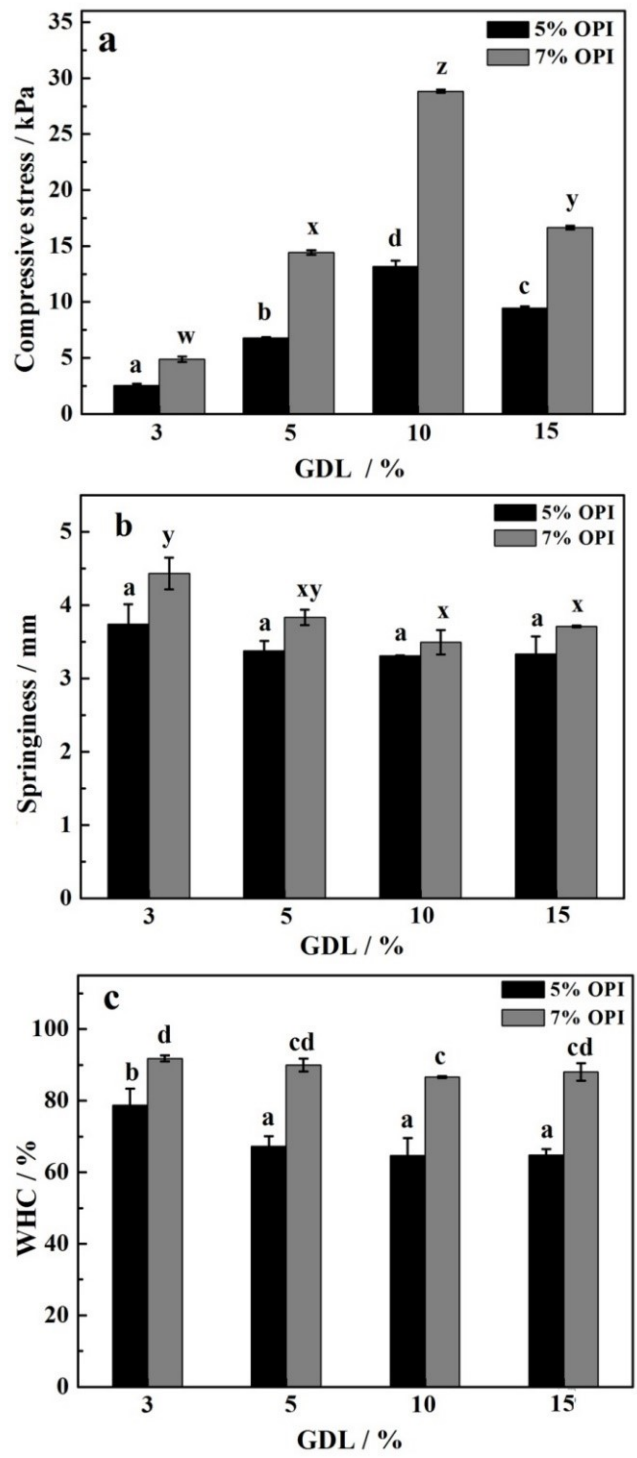


Fig. 4-2. (a) Compressive stress, (b) springiness, and (c) water holding capacity of OPI gels prepared at different GDL and protein concentrations. Different letters on the top of the columns indicate the significant difference ($p < 0.05$).

A similar trend was observed for gels prepared with 5% OPI. All the gels exhibited good springiness as they could spring back to 3.4 - 4.3 mm (68 - 86% of their original height) after the first compression, which was greater than that of particulate whey protein gels (63.7 - 68.8% of original height) (Çakır et al., 2012a). GDL content did not significantly impact the springiness of 5% OPI gels, but induced the slight decrease of springiness of 7% OPI gels (Fig. 4-2b). It is worth noting that the OG7-10 gel showed comparable compressive stress (30 kPa) to egg white gels (22-32 kPa) (Hammershøj & Larsen, 2001). This value was also larger than gels prepared from many other plant and animal proteins. For example, gels made from 20 wt% legume proteins showed the compressive stress of 5.0 - 8.0 kPa (Makri et al., 2006); the GDL-induced 7% whey protein isolate gel had the compressive stress of around 22 kPa when compressed to 80% of original height (Cavallieri & da Cunha, 2008). During mechanical property test, existence of small amount of water at the wet gel surface kept the gel surface lubricated (Fiszman, Pons, & Damásio, 1998). The preliminary test showed no significant difference between rheological properties of the gel samples with and without addition of lubrication agent such as paraffin oil. Thus no specific lubrication was used for this test. Nevertheless, it should be noted that the use of unlubricated specimen might have potentially affected the results.

Generally, gels with a large water holding capacity (WHC) are favorable for applications, since water loss can result in gel shrinkage, texture change and reduced quality (Mao, Tang, & Swanson, 2001). As shown in Fig. 4-2c, the gels prepared with 7% OPI demonstrated a large

WHC (89-92%), which were more than those of 5% OPI gels (68-80%). It was because of that more protein molecules were involved to build up the gel network and had stronger capacity to interact with water.

4.3.1.4 Gel morphology

In general, globular proteins form gels with particulate or filamentous microstructures depending on processing conditions such as pH and ionic strength. It is worth noting that a percolating network structure was observed for all cold-set OPI gels (Fig. 4-3). The same gel network structures were also observed in thermally-induced oat protein gels that were formed at a pH far away from its IEP in the previous study (Nieto-Nieto et al., 2015). However, the gel formation mechanism was different. In addition, thermally-induced oat protein gels prepared at pH 5 showed particulate structures, which are also different from the percolating structure of OG5-10 and OG7-10 gel obtained at pH of 5.2. Such percolating structure was similar to that of gelatin gels, but has seldom been reported in globulin protein gels including whey and soy. This unique percolating structure could explain the superior mechanical properties of OPI gels compared to other plant protein gels.

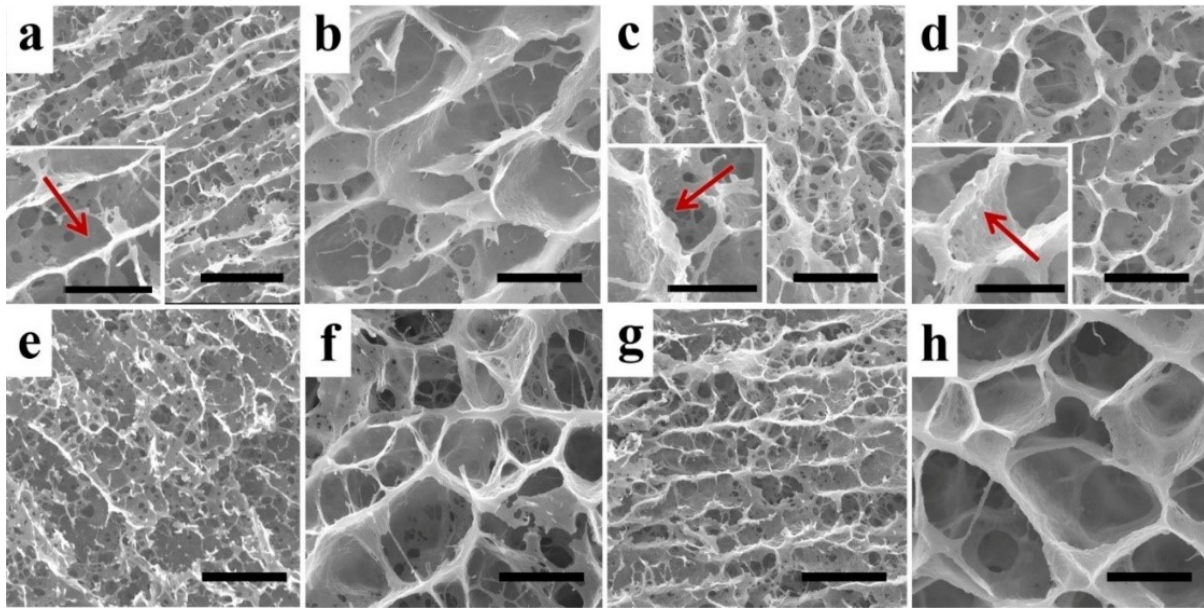


Fig. 4-3. SEM images of OPI gels prepared at different GDL concentrations: (a) OG5-3; (b) OG5-5; (c) OG5-10; (d) OG5-15; (e) OG7-3; (f) OG7-5; (g) OG7-10; and (h) OG7-15. Scale bar: 5 μm ; scale bar of inserts: 2 μm .

Various pore sizes and wall morphologies were observed depending on the final pH and pH reduction rate. Network structures with large pores (diameter: $\sim 5 \mu\text{m}$) were found when final pH values were 6.3 and 4.4 with 5 and 15% GDL addition (Figs. 4-3b, 4-3d, 4-3f, and 3h), respectively; whereas the pore size (diameter: $\sim 1 \mu\text{m}$) was much smaller when gel final pH values were 6.8 and 5.2 with 3 and 10% GDL addition (Figs. 4-3a, 4-3c, 4-3e, and 4-3g), respectively. As shown in insets of Figs. 4-3a and 4-3c, thicker walls of pores in 10% GDL gels were observed with the thickness of about 0.3-0.4 μm , while a wall thickness in 3% GDL gels was about 0.1 μm . Moreover, it could be distinguished that the walls in OG5-10 and OG5-15 consisted of aggregates. These small aggregates caused ‘rough’ walls’ morphology which was

different from the 'smooth' walls in 3% GDL gels. With addition of 10% GDL, the OPI gels exhibited the most compact structure with small pores and thick walls, resulting in the highest compressive stress. The gels prepared with 5 and 15% GDL showed mechanical properties weaker than the OPI gels with 10% GDL but stronger than the 3% GDL ones due to their larger pores. The large pore structure in Figs. 4-3h and 4-3d (OG5-15 and OG7-15) was formed when pH value was rapidly dropped to IEP. The dramatically weakened repulsive forces among protein promoted protein aggregation in a random way in all directions, thus led to rough and thick gel wall structure (inset of Fig. 4-3d). When the pH value slowly went down to lower than protein IEP with 15% GDL, the established gel network was charged again and slightly swelled, the repulsion among protein chains resulted in the enlarged pores. Thus in spite of the similar pore size, the thick and rough wall structure surrounding the pores resulted in a higher G' of 15% GDL gels than 5% GDL gels. The 3% GDL gels also contained small pores, but their walls were much thinner than 10% GDL gels, leading to the lowest compressive stress. Moreover, the changes of pore size and wall thickness in 7% OPI gels followed the same trend with the addition of different GDL amounts, which were also in accordance with their mechanical properties. The 7% OPI gels had more compact microstructures and greater compressive stress compared to 5% OPI gels, since more protein molecules were devoted to gel network formation.

4.3.2 OPI gel formation mechanism study

The unique gel structures of this study may have specific applications in a variety of food and non-food products. Further investigation was warranted to better understand the formation mechanism of OPI percolating network during cold-set gelation at molecular and supramolecular levels.

4.3.2.1 Protein conformational change

The deconvoluted FTIR spectra of OPI solutions in amide I band region are shown in Fig. 4-4a. Unheated OPI exhibited several bands which had been previously assigned to protein secondary structures: 1691 cm^{-1} (β -sheets/turns), 1670 cm^{-1} (β -turns), 1646 cm^{-1} (α -helix + random coils), 1638 cm^{-1} and 1628 cm^{-1} (β -sheets), and 1608 cm^{-1} (vibration of amino acid residues) (Byler & Susi 1986; Liu et al., 2009, Zhang et al., 2012.). When heating at 115°C (Fig. 4-4a), the spectrum significantly changed with new peaks appearing at 1682 and 1618 cm^{-1} . The band of 1618 cm^{-1} corresponded to intermolecular β -sheets caused by aggregation via hydrogen bonds (Clark, Saunderson, & Suggett, 1981), while the one at 1682 cm^{-1} indicated the antiparallel β -sheets (Bandeekar, 1992). After cooling to room temperature, the absorption intensities at 1642 and 1618 cm^{-1} increased. Anti-parallel β -sheets structures (1682 cm^{-1}) formed during heating treatment, and remained after cooling process. These results revealed that the heat treatment induced the unfolding and aggregation of OPI and the aggregation process continued during cooling. A significant amount of secondary structure including turns (1659 cm^{-1}), random

coils (1642 cm^{-1}) and β -sheet (1631 cm^{-1}) still existed in OPI after the heating and cooling treatments. It was because OPI is composed of exterior loosely arranged segments and interior tightly packed hydrophobic segments (Neito-Neito et al. 2014). These interior segments were much more stable against heat treatment than exterior loose segments, and their secondary structures remained after heating at 115°C for 15 min. Fig. 4-4b presents the deconvoluted spectra of OPI solutions after addition of GDL. The secondary structure of OPI did not significantly change in the presence of 3% GDL. A further increase of GDL led to more aggregates as the absorption at 1618 cm^{-1} was enhanced, whereas anti-parallel β -sheets structures (1682 cm^{-1}) remained almost the same. Nevertheless, comparing to the significantly increased amount of intermolecular beta sheets (1618 cm^{-1}), antiparallel beta sheet structures (1682 cm^{-1}) accounted for a small proportion.

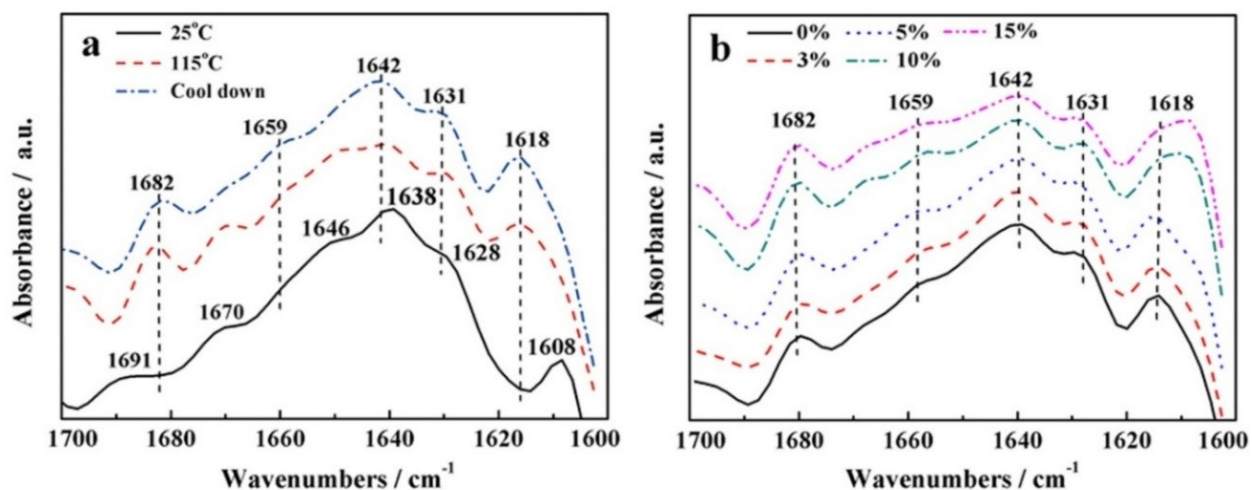


Fig. 4-4. Fourier-deconvoluted FTIR spectra of (a) OPI solutions (1% w/v in D_2O) upon heating and cooling; and (b) preheated OPI solutions (1% w/v in D_2O) with different GDL concentrations.

4.3.2.2 Protein size change

Fig. 4-5a illustrates the size distribution of native, preheated, and GDL added OPI suspensions using a dynamic light scattering (DLS) technique. The native (Fig. 4-5a, BH) OPI displayed two peaks with the approximate hydrodynamic radius of 59.6 and 620.4 nm, respectively. The large particle size of 620.4 nm could be oat protein aggregates with relatively poor solubility, while the major peak of small particles (59.6 nm) were well solublized oat protein hexamers. After heating at 115 °C for 15 min (Fig. 4-5a, AH), only one peak was observed and the hydrodynamic radius decreased to around 15.1 nm. This was in contrast to the phenomenon observed from many other globular proteins such as soy and whey where protein hydrodynamic radius dramatically increased after heating due to the considerable thermally-induced molecular aggregation (Jones, Adamcik, Handschin, Bolisetty, & Mezzenga, 2010; Maltais et al., 2008). This single peak indicated the dissociation of OPI hexamers down to monomers after heating, since the OPI monomer has a diameter of 11.8 nm and an extended conformation (Zhao, Mine, & Ma, 2004). Such monomers were only partially unfolded since significant amounts of protein secondary structure were maintained as shown in FTIR. In addition to the monomers, within the range of 30-100 nm, a small amount of large particles could be observed, which was considered as small aggregates or subunits associated by those monomers. This agreed well with the FTIR result showing the heating and cooling process promote the aggregation (Fig. 4-4a). The addition of GDL resulted in an increase of OPI

hydrodynamic radius to 43.9 nm, suggesting that the monomers with extended conformation served as active building blocks and formed the aggregates when pH value decreased. These changes were further confirmed by atomic force microscopy (AFM) observation. As shown in Fig. 4-5b, the native OPI displayed heterogeneous aggregates with disordered structures. A notable difference was observed in preheated OPI (Fig. 4-5c) where most large aggregates dissociated into small particles. The addition of GDL resulted in the appearance of large aggregates again. Although no continuous network structure was observed in Fig. 4-5d due to the dilute OPI concentration, these large aggregates could be considered as precursors of the gel network.

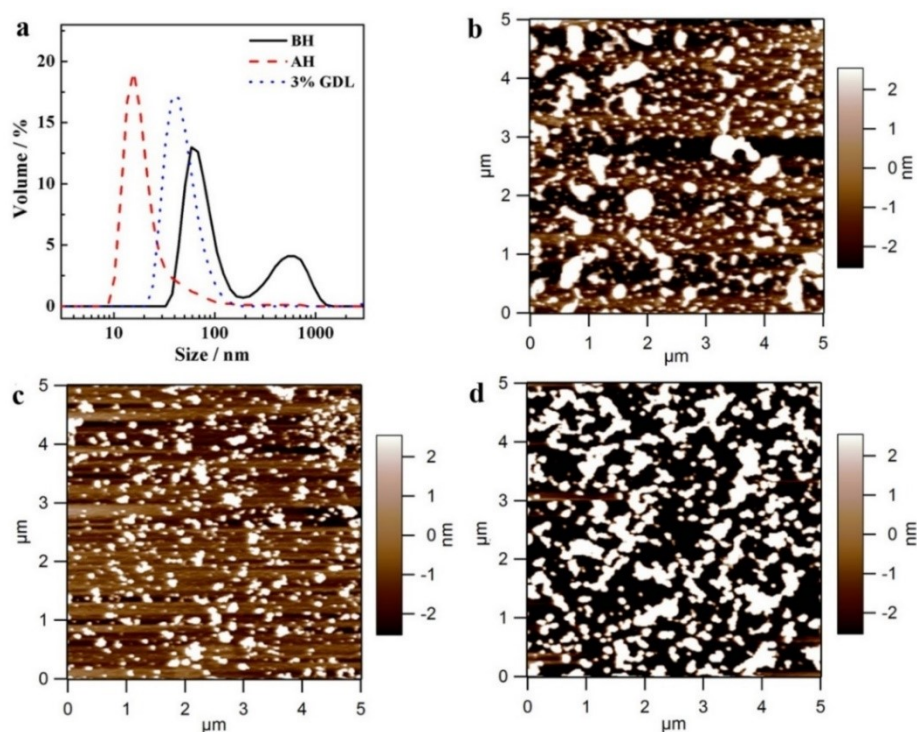


Fig. 4-5. (a) Size distributions of OPI in water at pH 8 before heating (BH), after heating to 115 °C (AH) and preheated OPI solution with 3% GDL. AFM images of OPI solutions: (b) BH; (c) AH to 115 °C; and (d) preheated OPI solution with 3% GDL.

Since the OPI monomers were small and highly reactive, they served as gel building blocks. The gel network could be developed at a near molecular level, resulting in abundant cross-linking sites to form a percolating structure. On the other hand, the initial OPI solutions were set at pH 8, where relatively strong electrostatic repulsive forces existed among OPI monomers. Thus, random protein aggregation was prevented and the bonding process was predominately linear in form due to the unscreened charges (Clark et al., 2001). It is possible that these initial building blocks formed a percolating structure following the nucleation-dependent polymerization mechanism. This mechanism was commonly reported for monomerized amyloid beta, which can be explained by two procedures. The first procedure was rate-limiting formation of an oligomeric nucleus, followed by a rapid growth phase. In the growth phase, monomers attached to the ends of the nuclei or growing fibrils (Harper & Lansbury, 1997; Lee, Culyba, Powers, & Kelly, 2011; Benseny-Cases, Klementieva, & Cladera, 2012). In this work, the first step was the initial slow nucleation phase, in which the nuclei (small aggregates) were formed by extended OPI monomers. Then the elongation stage began with the addition or condensation of monomers and/or small aggregates to form protofibrils in a linear way due to the high repulsive force. Finally, the growth and association of protofibrils led to percolating network structure.

4.3.2.3 Fractal analysis

The formation of OPI gels could also be considered as the association of disordered fractal aggregates at supramolecular level and be described in terms of fractal geometry, since the

aggregates were self-similar at a certain length scale (Hagiwara et al., 1998; Marangoni, Barbut, McGauley, Marcone, & Narine, 2000). Strain sweep measurements for cold-set OPI gels formed with various protein (5, 6, 7 and 8%, (w/v)) and GDL concentrations (3, 5, 10 and 15%, w/w) were carried out, and the scaling model modified by Wu and Morbidelli (2001) was selected to determine the elastic contributions of both inter- and intra-floc links using a microscopic elastic constant of α ($0 \leq \alpha \leq 1$). Fig. 4-6a shows the modulus-strain profile of OPI gels with 3% GDL. At all tested protein concentrations, G' values firstly remained constant as strain increased and then suddenly decreased beyond a certain strain value, which indicated the breakdown of bonds within the gel network and the transition from linear to non-linear behavior (Shih, Shih, Kim, Lin, & Aksay, 1990, Wu & Morbidelli, 2001). The strain amplitude at which G' decreased by 5% from its maximum value, as shown in the inset of Fig. 4-6a, was taken as critical strain of the gel (Shih et al., 1990). As shown in Fig. 4-6b, the gels formed with 3, 5 and 10% GDL had same transition trends where the critical strain decreased with the increase of protein concentration, whereas the gels formed with 15% GDL had an opposite transition trend. The average G' values in the linear region of strain sweep were calculated and plotted as a function of protein concentration in Fig. 4-6c. It was observed that, both critical strain vs concentration and G' vs concentration exhibited power-law relationship, and the slopes (presented as exponents in Table 4-1, A and B) were used to obtain fractal dimension (D_f) and micro-elastic parameter (α) values through equations (4-2), (4-3) and (4-4). The estimated α and D_f values of OPI gels are listed in Table 4-1.

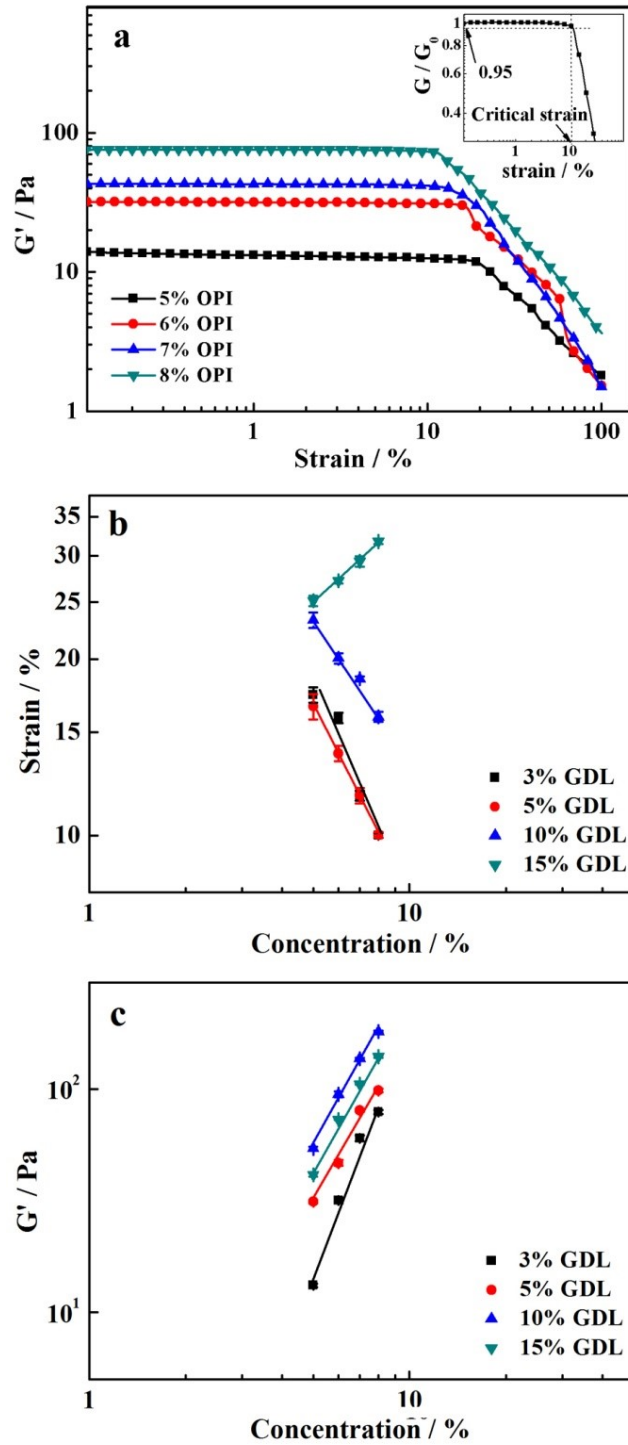


Fig. 4-6. (a) Storage modulus - strain profiles of OPI gels prepared at different protein concentrations and 3% GDL. Double-logarithmic plots of critical strain (b) and storage modulus (c) of OPI gels prepared at different GDL contents as a function of protein concentrations.

Table 4-1. Experimentally measured rheological data and derived microscopic structural parameters of OPI gels prepared at different GDL concentrations.

[GDL] % (w/w)	Power-law exponents		Model of Wu and Morbidelli (2001)				
	A ^a	B ^b	D _f ^c	β ^c	α ^c at x = 1.0	α ^c at x = 1.3	Regime
3	3.86	-1.24	2.23	2.97	0.34	0.40	Transition gel
5	2.92	-0.93	1.99	2.94	0.35	0.41	Transition gel
10	2.87	-0.77	2.04	2.73	0.42	0.47	Transition gel
15	2.28	0.65	2.31	1.56	0.81	0.83	Transition gel

^a Slope from log-log plot of G' vs Concentration.

^b Slope from log-log plot of strain vs Concentration.

^c Values of D_f, β and α based on the model of Wu and Morbidelli (2001).

The α values of 3 and 5% GDL induced gels were 0.34-0.35 (x = 1) and 0.40-0.41 (x = 1.3), and they increased slightly to 0.42 (x = 1) and 0.47 (x = 1.3) with increasing GDL concentration to 10%. It should be noted that α values rose to 0.81/0.83 with 15% GDL addition. The α value distinguishes the type of the gel and implies the relative contribution of inter- and intra-floc links in the gel network. The value of α is estimated using two x values, 1 and 1.3, which are commonly used to provide approximation of fractal dimension of the backbone of colloidal aggregates. When α = 0, it indicates strong inter-floc link gel; when α = 1, it indicates weak inter-floc link gel (strong intra-floc link); when 0 < α < 1, it suggests a transition regime with comparable contributions from inter- and intra-floc links to the gel (Ould Eleya & Gunasekaran, 2004, Wu & Morbidelli, 2001). Therefore, the gels formed with 3, 5 and 10% GDL were in the

transition regime, suggesting a comparable contributions of inter- and intra-floc bonding. However, the intra-floc link became stronger due to the reduced pH and repulsive force when GDL contents increased, and the aggregation of protein molecules in 15% GDL gels at supramolecular level was toward strong intra-floc link regime.

It was noticed that, with increasing GDL concentration from 5 to 15%, both D_f and α values significantly increased from 1.99 to 2.31 and 0.35/0.41 to 0.81/0.83, respectively. However, the gel prepared with 3% GDL also showed the high D_f value of 2.23. The D_f value is commonly used to quantify the disordered structure of aggregated particles, and indicates the relation between the number of particles in the aggregates and their typical size (Vreeker, Hoekstra, den Boer, & Agterof, 1992). The change from the strong inter-floc link type to the transition type to the strong intra-floc link type is usually associated with an increase in D_f value (Wu & Morbidelli, 2001). Whereas in current work, the high-energy barrier caused by strong electrostatic repulsive force at high final pH (3% GDL gels) resulted in protein molecules in the floc slowly approaching to each other in a linear way through strong inter-floc links. Thus it allowed the formation of a floc containing homogenous thin wall microstructure rather than a randomly aggregated one (inset of Fig. 4-3a, highlighted by the red arrow). The slow aggregation process compared to heat induced gels or cold-set gels with calcium caused the formation of clusters with different masses. Clusters with larger mass had more available bonding sites and hence grew faster, whereas a large number of small clusters resulted in a vast polydisperse cluster mass

distribution. The large electrostatic repulsive forces also caused less sticking probability, so two approaching clusters could attempt all possible mutual configurations to stick together. This increased the possibility of small clusters in the polydisperse distribution to interpenetrate into larger clusters and increase floc density (Lin et al., 1990). Since fractal dimension is related to the distribution of mass in space (Mandelbrot, 1982), this high floc density accounted for the high D_f value of 3% GDL gels. The gels formed with 3 and 5% GDL had similar α values and homogenous wall structure, but a lower D_f value of 1.99 was observed for 5% GDL gel. It was because the electrostatic repulsive forces were slightly decreased at 5% GDL due to the reduction of pH which promoted the protein interactions and led to formation of compact clusters, resulting in decreased distribution of mass in space and the reduced D_f value of 5% GDL gels. With the addition of 10% GDL, comparable inter- and intra-floc links ($\alpha = 0.42/0.47$) and particle volume fractions (D_f) of 2.04 were obtained due to a fast pH reduction rate which facilitated protein interactions and led to the network with dense and rough wall microstructure (inset of Fig. 4-3c, highlighted by the red arrow). An even faster pH reduction was generated by adding 15% GDL. It resulted in the dramatic decrease of repulsive forces and promoted protein aggregation in a random way in all directions. Thus, the possibility of strong intra-floc links (high α values) was high and the particle volume fractions increased, exhibiting a high D_f value. These high D_f and α values of 15% GDL gels were directly related to their rough and thick wall structures of pores (inset of Fig. 4-3d, highlighted by the red arrow).

4.3.2.4 Gel formation mechanism

Fig. 4-7 summarizes the formation mechanism of cold-set OPI gels. Oat protein firstly dissociated from hexamers to monomers by heating and then small parts of monomers were associated to subunits. Subsequently, the addition of GDL at ambient temperature allowed gradual pH reduction to facilitate the association of monomers and subunits. These small and highly reactive monomers and subunits acted as gel building blocks and provided abundant cross-linking sites. They formed nuclei and then protofibrils in a linear way due to the high repulsive force, and finally built up percolating network structures.

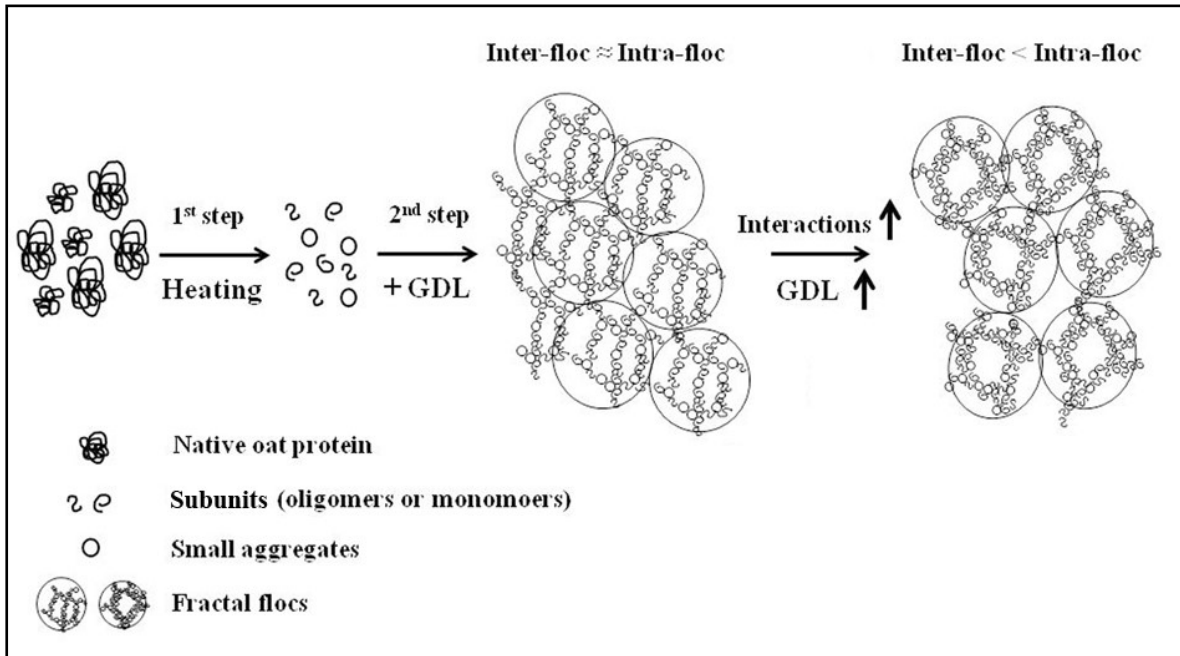


Fig. 4-7. Schematic illustration of the formation mechanism of cold-set OPI gels with percolating network structure induced by GDL.

During network formation, both final pH values and pH reduction rate played important roles in controlling aggregation behavior of oat protein molecules at the supramolecular level. This then influenced the gel network structure and strength. For 3% GDL gels with final pH of 6.8, the pH reducing rate was slow. The high electrostatic repulsive force controlled the association of OPI monomers in a linear approach through strong inter-floc interactions and induced high floc density, resulting in homogenous network with thinnest gel wall and small pores. This structure could be considered as the initial gel network. With 5% GDL addition, the final pH value decreased to 6.3. More interactions between protein molecules were developed due to the reduced electrostatic repulsive forces, which allowed a closer alignment of protein molecules based on the initial structure. However, this alteration did not change the gel volume. Thus, the pore size was enlarged to maintain the gel volume. When increasing GDL concentration to 10%, the pH reduction rate was high and the final pH was 5.2. The rapidly diminished electrostatic repulsive force facilitated the development of protein attractive interactions and more intra-floc links. Therefore, more condensation of small aggregates occurred along the wall and led to the formation of thick and rough gel wall. This final pH value was near OPI IEP. The diminished repulsive forces also resulted in the slight shrinkage of gel during formation process, thus a more compact gel structure with smaller pores (inset of Fig. 4-3c) and significantly improved strength was formed. The gels with the thickest and roughest wall microstructures (inset of Fig. 4-3d) were obtained by adding 15% GDL due to the greatest decreasing rate of pH value. However, the pore size became much larger than the 10% GDL gels

since the final pH of 4.4 was deviated from OPI IEP. Here strong repulsive forces resulted in decreased gel strength.

4.3.3 Encapsulation and controlled release of bioactive compounds

The porous gel network, large water holding capacity, and mild preparation conditions made cold-set OPI gels favorable to encapsulate and protect bioactive compounds (Chen & Subirade, 2006; Kashyap, Kumar, & Ravi Kumar, 2005; Ganguly, Chaturvedi, More, Nadagouda, & Aminabhavi, 2014). The gels prepared with 7% protein and 10% GDL (OG7-10) were selected for the following work due to their small pores, dense wall microstructure and superior mechanical strength.

4.3.3.1 Encapsulation and protection of enzyme and probiotics

Numerous studies have demonstrated health benefits of bioactive proteins/peptides, but there are still some issues about the denaturation at gastric pH level and digestion by pepsin in the stomach which resulted in reduced bioactivities. In this work, α -amylase was selected as a model to evaluate the capacity of cold-set OPI gels to stabilize a bioactive protein. The enzyme activity after encapsulation was 90%. As revealed in Fig. 4-8a, the encapsulated α -amylase remained high activity (78%) after incubation in simulated gastric fluid (SGF) for 0.5 h, whereas the activity of the enzyme without encapsulation diminished to 0. After 1 h, up to 65% of the activity remained, demonstrating the OPI gels could protect α -amylase from the harsh gastric

environment. The amylase activity decreased significantly after 2 h, although 35% activity was still remained.

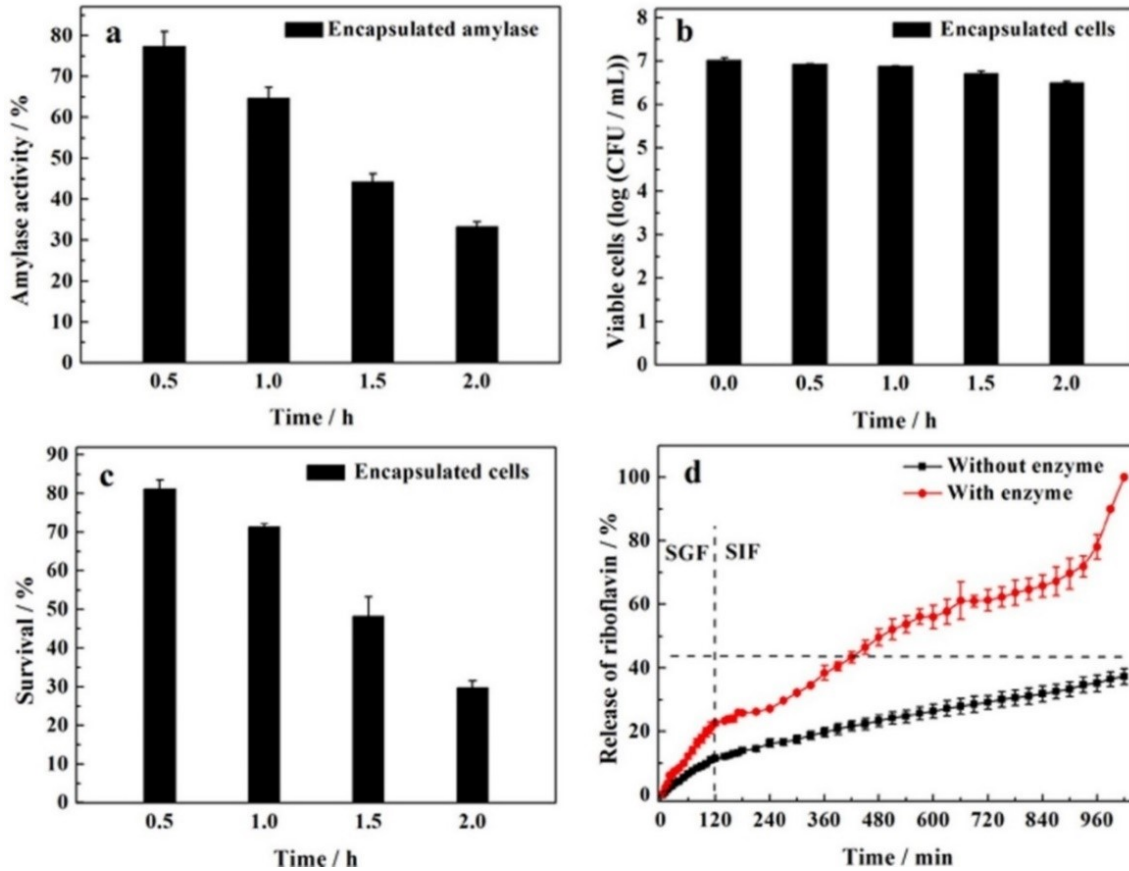


Fig. 4-8. (a) Activity of encapsulated α -amylase after being immersed in SGF for 0.5, 1, 1.5, and 2 h. (b) Viable count and (c) survival of encapsulated *Lactobacillus acidophilus* after being immersed in SGF for 0.5, 1, 1.5, and 2 h. (d) Release profiles of riboflavin from drug-loaded OG7-10 gels at 37 °C in HCl-saline buffer (pH 1.2) for 2 h and then in PBS buffer (pH 7.4) for 15 h with or without digestive enzymes.

Probiotics have many health benefits and can improve the intestinal flora, stimulate immune response, and promote nutrient absorption (Figuroa-Gonzalez, Quijano, Ramirez, & Cruz-Guerrero, 2011; Mei et al., 2014; Cheow & Hadinoto, 2013). Probiotics must be viable at high concentrations when reaching the small and large intestine in order to confer these health benefits. However, their survival in food systems is often low under the harsh conditions of low gastric acidity encountered in the gastrointestinal tract (Burgain, Gaiani, Linder, & Scher, 2011; Cook, Tzortzis, Charalampopoulos, & Khutoryanskiy, 2012; Corona-Hernandez et al., 2013). *Lactobacillus acidophilus* was selected as a model in this work. As expected, OPI gels could encapsulate and protect *L. acidophilus* in the simulated gastric environment. As shown in Figs. 4-8b and 4-8c, after 1 and 2 h incubation, the viable counts of encapsulated *L. acidophilus* were 6.9 and 6.5 log CFU/mL, with survival rates of 71.3 and 29.7%, respectively. In comparison, no viable free cells were detected after only 0.5 h incubation. Therefore, the cold-set OPI gels could protect labile bioactive compounds and organisms in the gastric environment and allow their delivery to the small intestine to exert health benefits. As shown in Fig. 4-9a, the fresh OPI gel maintained its network structure after being immersed in SGF for 1 h, suggesting it could resist pepsin digestion. After 2 h treatment in SGF (Fig. 4-9b), the OPI gel was slightly degraded but still maintained its 3D structure. This retained structure prevented the penetration of SGF and protected the encapsulated bioactive compounds.

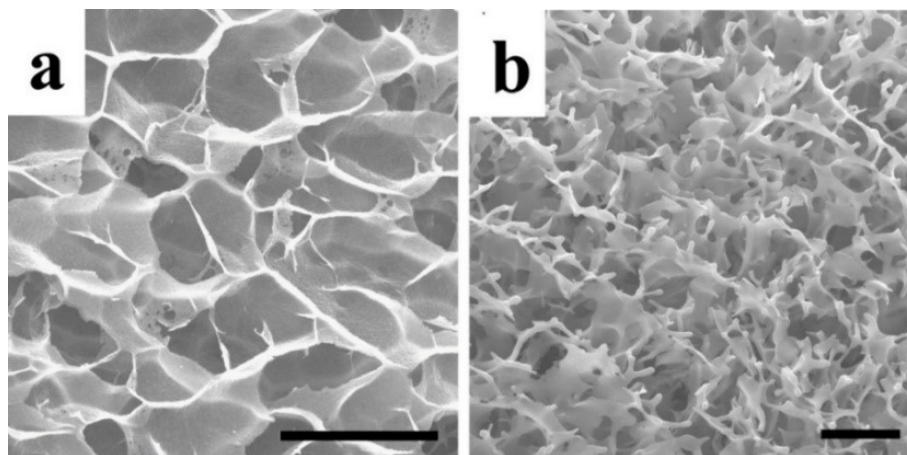


Fig. 4-9. SEM images of OG7-10 gels after being immersed in SGF for 1 h (a) and 2 h (b) at 37 °C. Scale bar: 10 μ m.

4.3.3.2 In vitro release behavior of encapsulated vitamin

For the controlled release study, riboflavin was selected as a model bioactive molecule. Riboflavin (vitamin B₂) plays a key role in the metabolism of carbohydrates, fats, and proteins. It is also important for antibody production, cell respiration and growth, and red blood cell formation (Bernardos et al., 2008). As shown in Fig. 4-8d, OPI gels released riboflavin slowly under gastric conditions (HCl-saline), with only 11.4% free riboflavin detected after 120 min. Slow release was also observed after being transferred to conditions simulating the small intestine (PBS buffer), with only 37.2% riboflavin being released even after 1020 min. In general, the mechanism of drug release from a polymer matrix can be categorized in three ways (Arifin, Lee, & Wang, 2006): (1) diffusion from the non-degraded polymer; (2) enhanced drug diffusion

due to polymer swelling; and (3) release by polymer degradation and erosion. The Korsmeyer - Peppas semi-empirical equation was applied to identify the mechanism of riboflavin release from the oat protein gel (Chen, Remondetto, Rouabhia, & Subirade, 2008):

$$M_t / M_\infty = kt^n \quad (4-5)$$

Where M_t / M_∞ is the fraction of the model molecule released after time t relative to the amount of model molecule released at infinite time, k is a constant and n is the diffusional exponent. Inferences about the release mechanism are based on the fit of this equation to the model molecule release data through 60% dissolution and comparison of the value of n to the semi-empirical values for slab geometry reported by Peppas, where $n = 0.43$ indicates Fickian diffusion, $0.45 < n < 0.89$ indicates non-Fickian transport, and $n = 0.89$ or higher indicates case II transport. The release in HCl-saline buffer (before 120 min) had n value of 0.23 ($R^2 = 0.93$), while in PBS (after 120 min) the n increased to 0.68 ($R^2 = 0.98$). This revealed that riboflavin is released by a diffusion-controlled mechanism under gastric conditions, and the enhanced riboflavin diffusion occurred due to swelling of the gel at intestinal conditions. According to our preliminary test, the swelling ratio of dry OPI gels at pH 2 and pH 7.4 was 88.9% and 104.3%, respectively. The large amount of glutamine and glutamic acid (22.4%) of oat protein (Nieto-Nieto et al., 2014) caused a greater electrostatic repulsive force at pH 7.4 and facilitated more penetration of buffer into the inter-chain spaces (Chen et al., 2008). The release behavior of riboflavin from dry OPI gel in the simulated gastro-intestinal tract with digestive enzymes was also evaluated. As shown in Fig. 4-8d, the release of riboflavin was only 22.6% after the

incubation in SGF for 120 min, and the remaining riboflavin was gradually released in SIF over 960 min as the gel matrix degraded.

The protection of enzyme and probiotics in SGF and controlled release of riboflavin in PBS or simulated gastro-intestinal fluids were attributed to the resistance to pepsin digestion and low permeability to acidic juice of OPI gel. These unique properties were closely related to OPI molecular structure and gel network structure. OPI is composed of exterior loosely arranged segments and tightly packed interior hydrophobic core (Nieto-Nieto et al., 2014). Upon heating, whey and soy proteins are completely denatured to expose hydrophobic groups (Lefèvre & Subirade, 2000; Remondetto & Subirade, 2003), whereas OPI still maintains its secondary structures and prevents the exposure of interior hydrophobic core. The subsequent addition of GDL allows the gradual decrease of solution pH value, so the protein molecules associate in an orderly way through non-covalent interactions. Pepsin preferentially attacks peptide bond involving hydrophobic aromatic amino acids (Antonov, 1977; Chen & Subirade, 2005), which explains why the OPI gel matrix with buried hydrophobic groups slowed down the protein digestion. On the other hand, according to our previous study, oat protein had large levels of leucine (8.6%), glycine (7.7%), valine (7.7%), and proline (7.3%) in spite of large glutamic acid and glutamine (22.4%) contents. The significant amount of proline also contributed to the slow digestion, since the proteins with a large proline content were generally resistant to degradation by digestive enzymes (Simpson, 2001). Collagen and gelatin gel have been shown to act as

“cage” to retain cells and biomolecules due to the structure and polyion complexation, and maintain the biological activity for a controlled release of these biomolecules during a slow digestion of the matrix (Wallace & Rosenblatt, 2003; Santoro, Tatara, & Mikos, 2014). The slow gel degradation was modulated by a high cross-linking density (Young et al., 2005). The OPI gels possess a percolating structure similar to that in collagen and gelatin gels, and may also act as a “cage” to retain biomolecules. This cage structure is developed at a near-molecular level and contains abundant cross-linking points that may contribute to the slow digestibility and low permeability of the gel. In addition, the compact and dense gel structure inhibited fast leaching of bioactive molecules (Maltais et al., 2009).

4.4 Conclusions

For the first time, cold-set oat protein gels with a percolating network structure and relatively strong mechanical properties were prepared. The gel formation mechanism study revealed that highly reactive OPI monomers and subunits served as building blocks and provided abundant cross-linking sites. With increasing GDL concentration, more intra-floc links occurred, and consequently a condensation of small aggregates formed along the wall, leading to dense rough wall microstructure. These gels could resist acidic juice and pepsin digestion, enabling them to effectively protect encapsulated enzymes and probiotics, and potentially serve as delivery systems of bioactive compounds to the small intestine. The release study demonstrated the capacity of these gels to prevent the premature release of riboflavin in simulated gastric juice, but

enabled the complete release of riboflavin in simulated intestinal juice. The simple and non-toxic procedure presented was favorable for development of industrial food and non-food applications.

Chapter 5

Oat protein-shellac beads: superior protection and delivery carriers for sensitive bioactive compounds

5.1 Introduction

Many bioactive compounds, such as bioactive peptides and probiotics, confer health benefits including antioxidant, antidiabetic, antihypertensive, antitumor, and antimicrobial effects (Sanjukta & Rai, 2016; Ambalam, Raman, Purama, & Doble, 2016). Oral administration is by far the most convenient way to deliver bioactive compounds, because of easy handling, high patient compliance, and low cost of production, especially when routine administration is necessary (Bysell, Månsson, Hansson, & Malmsten, 2011). However, the oral route is restricted for sensitive compounds due to the proteolytic activity and low pH of the stomach. These harsh conditions can inactivate probiotics, destabilize and degrade proteins, thus leading to a loss of biological activities (Vermonden, Censi, & Hennink, 2012). Natural polymer-based encapsulation materials have the potential to be used in biotechnology (cells and enzymes) and food (flavors and probiotics) due to their excellent biocompatibility and biodegradability (Langer & Peppas, 2003; de Geest et al., 2009). Food proteins are generally recognized as safe (GRAS) and biocompatible and biodegradable materials with good gelling and emulsifying capacities, which allow them to entrap both water- and lipid-soluble bioactive molecules (Dickinson, 2003b; Chen & Subirade, 2008). Oat protein is the major by-product component after β -glucan extraction and

isolation, and potential research is poised to develop its full value. The previous research using cold-set gelation methods revealed that oat protein had an excellent gelling property and exhibited percolating structure with better mechanical strength (Chapter 4). The cold-set oat protein gels provide an opportunity to carry and protect heat labile sensitive bioactive compounds. However, this protection capacity quickly decreased when it was exposed to harsh gastric conditions for more than 1 h. To improve this gel system as a carrier of bioactive compounds, an improved controlled release with a prolonged protective capacity is required.

Oat protein-shellac combination gels are proposed here as a solution to increasing resistance to gastric conditions while maintaining capacity to release bioactive compounds in the intestinal environment. Shellac is a natural and biodegradable resin of insect origin, composed of a mixture of polyhydroxy polycarboxylic esters, lactones, and anhydrides, with the main acid components of aleuritic and terpenic acids. It is insoluble in acidic to neutral aqueous media and thus acid resistant (Xue & Zhang, 2008; Bellan, Pearsall, Cropek & Langer, 2012). Shellac can interact with hydrophilic polymers, such as gelatin, based on non-covalent interactions, due to the presence of a large number of carboxylic and hydroxyl groups, and a large negative charge. In previous work, shellac was used to encapsulate silibinin (Patel, Heussen, Hazekamp, & Velikov, 2011). Due to the pH dependent solubility of shellac, encapsulated silibinin was stable in acidic solutions (pH 1.2). Encapsulation and pH-triggered release of yeast cells from shellac-based microcapsules cross-linked with Ca^{2+} have also been reported, integrating shellac with pH

sensitive polyelectrolytes (Hamad, Stoyanov, & Paunov, 2012). However, the existence of functional groups may induce polymerization that cause poor mechanical properties and instability of shellac that have limited using shellac alone in applications (Limmatvapirat, Limmatvapirat, Putipipatkachorn, Nuntanid, & Luangtana-anan, 2007). More recently, Patel et al. (2013) generated gelatin-shellac microcapsules to encapsulate epigallocatechin gallate (EGCG), silibinin, and curcumin. In this work, the gelatin-shellac mixture was precipitated in 0.1 M HCl (pH 1.0) to generate microcapsules. However, such a low pH was not suitable for the encapsulation of sensitive molecules, such as peptide, enzymes, and probiotics. It is possible to achieve oat protein-shellac gels at a neutral pH through the addition of CaCl_2 , since both of them can be cross-linked by Ca^{2+} . In addition, based on a fundamental understanding of interactions between shellac and other hydrophilic polymers, the amino groups of oat protein and the carboxyl and hydroxyl groups of shellac may interact with each other. Therefore, oat protein-shellac combination gels made at neutral or near neutral pH, show potential to better protect bioactive compound in the gastric tract for subsequent controlled intestinal release.

This research represents a proof of concept of a novel natural biopolymer delivery systems for bioactive compounds for food and biomedical applications. Specifically, this study aims to better understand the interactions between oat protein and shellac and to develop oat protein-shellac based gels at neutral pH. The capable of designed gels as delivery systems to

protect and release representative bioactive compounds, including a vitamin, an enzyme, and a probiotic is investigated.

5.2 Materials and methods

5.2.1 Materials

Naked oat grains (*Avena nuda*) (crude protein content 17.2%, w/w) were purchased from Wedge Farms Ltd., Manitoba, Canada. Oat protein isolate (OPI, M_w : 237 kDa) was extracted from defatted oat flour using alkaline solution according to previous work (Nieto-Nieto et al., 2014). The protein content of OPI was $85.07 \pm 2.4\%$ (w/w, dry weight basis) as determined by the Leco nitrogen analyzer (FP-428, Leco Corporation, St Joseph, MI, USA) and a nitrogen to crude protein conversion factor of 5.83 was used, while other components could be soluble fiber, starch, lipid, and ash, among others. Shellac (M_w : ~1000 Da), pepsin (from porcine gastric mucosa, 424 units mg^{-1}), pancreatin (from porcine pancreas, 200 USP units mg^{-1}), amylase (700 units mg^{-1}) and amylase activity kit were obtained from Sigma-Aldrich Canada (Oakville, ON, Canada). *Lactobacillus acidophilus* (ATCC4536) was obtained from American Type Culture Collection (ATCC, MD, USA). Other chemicals used in the experiment were all analytical grade and from Fisher Scientific (Whitby, ON, Canada). Milli-Q water was used in all experiments.

5.2.2 Preparation of OPI, shellac solutions and their mixtures

OPI (10%, w/v) suspension was obtained by dispersing dry protein powders into Milli-Q water and stirred overnight at 20°C. The suspension was then adjusted to pH 8 using 1 M NaOH and sealed tightly in a glass vial. The denatured OPI solution was obtained by heating the above suspension at 115 °C (above denaturation temperature) in oil bath for 15 min. Shellac (20%, w/v) was dispersed in Milli-Q water and adjusted to pH 8 using 1 M NaOH with agitation at 50°C to ensure complete dissolution. Mixtures with various OPI to shellac ratios were prepared by mixing these two neat solutions under continuous stirring at 1000 rpm and 20°C, and coded as OS-0, OS-1, OS-2, OS-3, OS-4, and OS-5, corresponding to shellac contents (based on total solid weight) of 0, 18, 46, 67, 82, and 100 w/w, respectively (Table 5-1).

Table 5-1. Various ratios and components of OPI/shellac solutions.

Samples	Solution components	
	OPI (10%, w/v) : shellac (20%, w/v)	Shellac content (based on total solid weight, %)
OS-0	10 : 0 v/v	0
OS-1	9 : 1 v/v	18
OS-2	7 : 3 v/v	46
OS-3	3 : 7 v/v	67
OS-4	1 : 9 v/v	82
OS-5	0 : 10 v/v	100

5.2.3 Characterization of OPI – shellac mixtures

The dynamic rheological behavior of the OPI-shellac mixtures was characterized by a DHR-3 rheometer (TA Instruments, New Castle, DE, USA). Parallel plate geometry with a gap of 1 mm was used to measure the dynamic viscoelastic parameters including complex viscosity, shear storage modulus G' and loss modulus G'' . The value of the strain amplitude for all samples was set as 0.5%, which was within a linear viscoelastic regime. A frequency sweep was subsequently conducted as a function of angular frequency (ω) from 0.1 to 100 rad s^{-1} at 25 °C.

The thermodynamics of the interactions of OPI with shellac was measured using a Nano-Isothermal Titration Calorimeter (Nano-ITC, TA Instruments, New Castle, DE, USA). The stock OPI (denatured) and shellac solutions prepared above were diluted to 4.97 μM and 1 mM, respectively, according to preliminary test, and degassed using a vacuum oven (Isotemp[®] Model 282A, Fisher Scientific, Ottawa, Ontario, Canada) for 5 min at 20 °C. For ITC measurement, the reference cell was filled with 10 mM phosphate buffer (pH 8). The pre-heated OPI solution in sample cell (1.442 mL) was titrated with 250 μL shellac solution. The solution in sample cell was stirred at 300 rpm throughout the experiment. The titrant solution was added through 10 successive 2 μL injections and 20 successive 10 μL injections with an interval of 180 s between consecutive injections. The first 10 successive injections with 2 μL aimed to check the initial stage of interactions, since directly using 10 μL might cause excessive shellac dropping into oat

protein solution within initial 2-3 injections. Data analysis was performed with the NanoAnalyze software (TA Instruments, DE, USA), and the independent model was applied to fit binding isotherms. Thermodynamic parameters, including binding constant (K_a), enthalpy (ΔH) and binding stoichiometry (n), were calculated by iterative curve fitting of the binding isotherms.

5.2.4 Preparation of OPI-shellac based beads (OSB)

OSB was prepared by extrusion method using a co-axial nozzle (EM-CAX, IME Technologies, Eindhoven, The Netherlands) with inner and outer nozzle diameter of 0.4 and 1.2 mm. In a brief, the preheated OPI solution (10%, w/v, pH 8, core material) was forced through the inner nozzle at the rate of 10 mL/h, and the OPI-shellac composite solutions (pH 8) with various OPI to shellac ratios (shell materials) were fed through the outer nozzle at the rate of 30 mL/h. The core-shell gel beads were fabricated by pumping both outer and inner fluids into the coagulation bath with 0.05 M CaCl₂ drop wise. The obtained beads were collected and washed 3 times using Milli-Q water. According to the composition of the shell materials (OS-0, OS-1, OS-2, OS-3, OS-4, and OS-5), the obtained beads were coded as OSB-0, OSB-1, OSB-2, OSB-3, OSB-4, and OSB-5.

5.2.5 Characterizations of the OPI-shellac based beads

The morphology observation of beads was carried out with a Philips XL-30 scanning electron microscope (SEM) at an acceleration voltage of 6 kV. The samples were frozen in liquid nitrogen, snapped immediately by tweezers to expose the inner structure, and freeze-dried for

SEM observation. The cross-section and surface of beads were sputter-coated with gold, observed and photographed.

The protein conformational changes in the bead shells were characterized by Fourier transform infrared spectroscopy (FTIR). The bead shells were prepared through dropping the OPI-shellac mixture into the coagulation bath with CaCl_2 and then dried at room temperature and milled into powders and vacuum-dried at 40 °C for 24 h. The dried powders (~ 1 mg) were mixed with KBr (~ 99 mg) to form a KBr discs. The spectra were recorded using a Nicolet 6700 spectrophotometer (Thermal Fisher Scientific Inc., Pittsburgh, PA, USA) in the range of wavenumber from 400 to 4000 cm^{-1} during 128 scans with 2 cm^{-1} resolution. The spectrophotometer was continuously purged with dry air from a lab gas generator (Parker Hannifin Corp., Milton, ON, Canada).

The thermal properties of composition of bead shells were also analyzed using a DSC Q2000 apparatus (TA Instruments, New Castle, DE, USA) equipped with a refrigerated cooling system RCS90. The dried sample powders (~6-8 mg) were weighted in aluminum pans. The pans were then hermetically sealed and subjected to a heat-cool-heat treatment from 30 to 200 °C with a heating rate of 10 °C/min. A sealed empty pan was used as a reference. The glass transition temperature (T_g) was taken as the midpoint of the specific heat increment at the glass transition.

5.2.6 Loading of bioactives in the beads

Riboflavin, *Lactobacillus acidophilus* and amylase were selected as three models of sensitive bioactives representing vitamins, probiotics and enzymes that need protection. For *L. acidophilus* suspension preparation, the frozen cells were activated on MRS agar at 37 °C for 48 h under anaerobic conditions, and then one colony was selected and grown in 20 mL MRS broth (Oxoid, Basingstoke, Hampshire, England) at 37 °C for 24 h. The cells were sub-cultured at least three times prior to prepare cell suspension. The culture was centrifuged at 2000 rpm (805g) for 5 min to collect the cells followed by dispersing cells in 5 mL MRS broth to get cell suspension. The beads loaded with bioactive compounds were prepared by dispersing riboflavin (5%, w/w, based on the dry weight basis of protein), amylase (10%, w/w, based on the dry weight of protein), and *Lactobacillus acidophilus* (1/6, v/v, based on the volume of protein solution) in denatured OPI solution (10%, w/v) at room temperature as core material.

5.2.7 Release profiles in the simulated gastro-intestinal environment

The release profiles of riboflavin loaded beads were assessed with a 2100C dissolution system (Distek Inc., North Brunswick, NJ, USA) at 37°C in four dissolution mediums stirred at 100 rpm: HCl-saline solution (pH 2, 0.1 M); phosphate-buffered saline (PBS, pH 7.4, 0.1 M); simulated gastric fluid (SGF, pH 2, 0.1 M HCl-saline with 0.1% pepsin, w/v); and simulated intestinal fluid (SIF, pH 7.4, 0.1 M PBS with 1.0% pancreatin, w/v). The riboflavin loaded beads (200 mg, dry weight basis) was placed in 50 mL HCl-saline solution or SGF. After 2 h, the beads

were gently washed with 10 mL PBS twice and transferred into 50 mL PBS or SIF for another 15 h. The riboflavin content in the release mediums was monitored with S-3100 UV-vis spectrophotometer (Scinco Co. Ltd., Gangnum-Gu, Seoul, Korea) at a wavelength of 445 nm.

The release ratio of cell loaded beads in SIF was also investigated. In a brief, cell-loaded beads were placed in 8 vials with ~1 g (fresh weight) bead in 20 mL SGF for each vial. After 1 h, the beads were washed with PBS and transferred into 20 mL SIF for another 7 h. The beads in one vial were taken out and washed with Milli-Q water 3 times every 1 h, followed by shifting into 5 mL MRS broth to provide a proper environment before measuring the number of colony forming units (CFU) and smashed to release the encapsulated cells. The viability of *L. acidophilus* was tested using plate count method through counting the number of CFU on MRS agar after incubation at 37 °C for 48 h under anaerobic conditions, and the amounts of viable cells was quantified in CFU/mL. Since the cell-loaded beads were placed in SGF for 1 h, the count of encapsulated cells after immersing in SGF for 1 h was set as the 100% cells. The release ratio (%) of cells in SIF was thus calculated as: total amounts of living cells after immersing in SGF for 1 h (L_T) minus living cells in beads after immersing in SIF (at regular time intervals) (L_N) then dividing by the total amounts of living cells (L_T)

5.2.8 Stability of the bioactive compounds in the simulated gastro-intestinal environment

To investigate the stability of the bioactive compounds in the simulated gastro-intestinal environment, beads loaded with *Lactobacillus acidophilus* (1 g, fresh weight of wet beads, *L.*

acidophilus $\approx 9 \times 10^7$ CFU/mL) and amylase (100 mg, weight of dry beads) were immersed in 20 mL simulated gastric fluid (SGF, pH 2, 0.1 M HCl-saline with 0.1% pepsin, w/v) at 37°C and shaken at 100 rpm. At regular time intervals (0.5, 1, 1.5 and 2 h), beads were removed from SGF and washed with Milli-Q water 3 times. Then the beads were broken to release the bioactive compounds. The viability of the *L. acidophilus* was tested by the plate count method through counting the number of colony forming units (CFU) on MRS agar after incubation at 37 °C for 48 h under anaerobic conditions. The free cells (9×10^7 CFU/mL) incubated in SGF and the encapsulated cells without immersing in SGF were set as the negative and positive controls, respectively. The count of encapsulated cells without immersing in SGF was set as the 100% cells. The survival (%) of the viable cells was the ratio of viable counts after and before the SGF exposure. The activity of the released amylase was measured by using the amylase kit (Sigma-aldrich, St. Louis, Mo, USA). As above, the encapsulated enzyme without immersing in SGF was set as the positive control (100%), and the free enzyme immersed in SGF was set as negative control. The amylase activity was calculated based on the equation provided by amylase activity assay kit technical protocol.

5.2.9 Statistical analysis

All experiments were performed at least in triplicate. Results were expressed as mean \pm standard deviation. Statistical analysis was conducted using the Statistical Analysis System (SAS for windows, Release 9.0, SAS Institute Inc., Cary, NC). Analysis of variance (ANOVA) was

performed to analyze the encapsulation efficiency of beads. Tukey's test was used to compare multiple means. A probability of $p < 0.05$ was considered to be statistically significant.

5.3 Results and discussion

5.3.1 Solution behavior and interactions of OPI and shellac mixtures

Preliminary trials suggested that OPI and shellac could develop interactions at pH 8 since the mixture showed a significantly increased viscosity compared to other tested pHs that qualified visually. Thus the solution behavior of OPI (denatured) and shellac mixture at various ratios in water was investigated at pH 8 by studying the dependence of elastic (G') and viscous moduli (G'') and complex viscosity on angular frequency of each solution. As shown in Fig. 5-1a, the rheological behaviors changed distinctly with different OPI to shellac ratios. For OPI (OS-0) and shellac (OS-5) alone, the viscous modulus (G'') was higher than elastic modulus (G') at low frequency. However, G' prevailed on the G'' when the frequency increased up to 30 and 3 $\omega/\text{rad}\cdot\text{s}^{-1}$ for OS-0 and OS-5, respectively, indicating a predominant elastic character at high frequencies. The behavior of changing from a viscous fluid when stressed at lower frequencies to an elastic body when stressed quickly, is typical of an entangled network (Maltese et al., 2006). With the addition of 18% (w/w) of shellac into OPI (OS-1), both G' and G'' values greatly increased. In addition, greater G' than G'' was observed in all frequency range, characteristic of a gel-like material. However, the weakening of the gel-like material happened with further increase of the shellac contents to 33 and 54% (w/w) observed by smaller G' and G'' values for OS-2 and

OS-3, respectively, than OS-1, and the difference between G' and G'' became smaller. On the other hand, a viscous solution behavior was observed for OS-4, as demonstrated by greater G'' values than G' in all frequency ranges; here shellac was the major component. The complex viscosity of each solution was also monitored, and a similar trend was observed. As shown in Fig. 5-1b, the mixture solution was thickest when 18% (w/w) of shellac was added (OS-1) in the OPI solution, whereas the viscosity decreased when shellac content increased. The maximum G' and viscosity obtained for OS-1 suggested that interactions may occur between OPI and shellac even when both of them were negatively charged at pH 8.

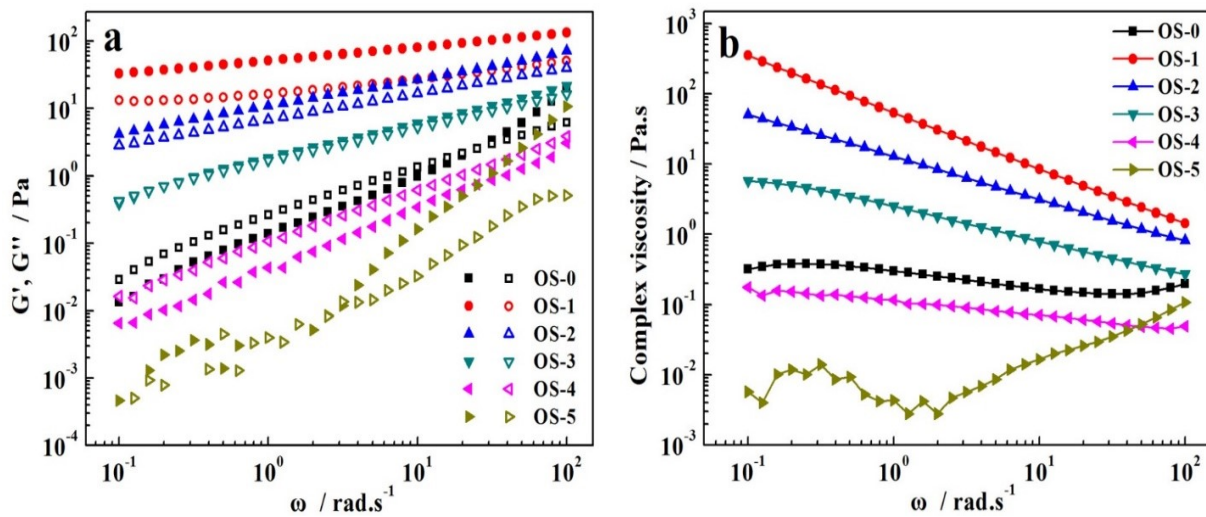


Fig. 5-1. Dependence of (a) storage modulus (G' , solid symbols) and loss modulus (G'' , open symbols) and (b) complex viscosity on the angular frequency for oat protein-shellac composite solutions.

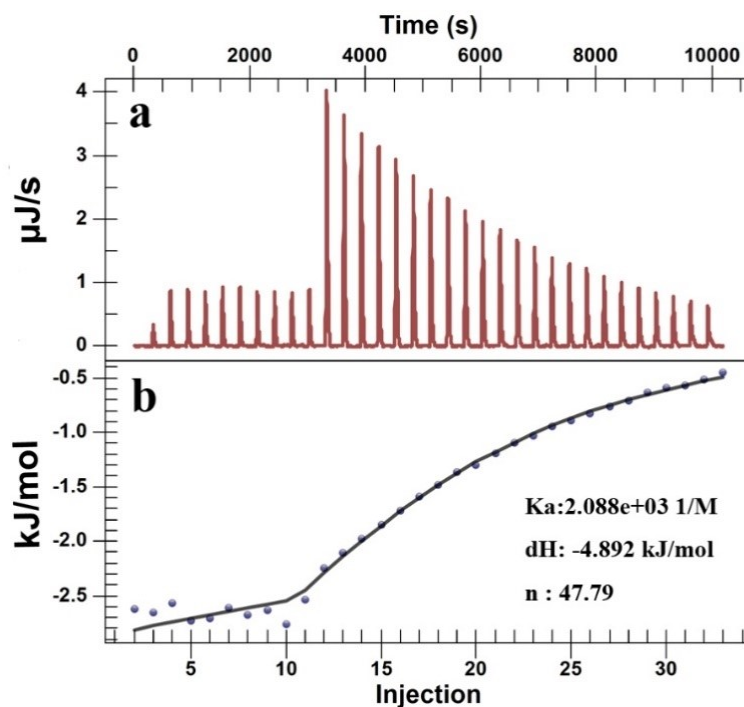


Fig. 5-2. (a) Raw data plot of heat flow against time for titration of shellac (1 mM) into OPI (4.97 μM) at pH 8; and (b) binding isotherm of OPI-shellac complex derived from the integrated raw data. The curve represents a modelling result obtained from fitting the data.

ITC was used to investigate the interactions between OPI and shellac. ITC is a powerful technique to quantify the thermodynamic parameters of biomolecular interactions since it facilitates the understanding of binding modes. In this experiment, 1 mM shellac and 4.97 μM OPI were applied; this was based on the results of the rheological property test where the addition of 18% (w/w) shellac into OPI caused a significant increase of modulus and viscosity. Fig. 5-2a shows the raw data plots of endothermic interactions and Fig. 5-2b exhibits the corresponding plots of titration isotherms derived from the integrated raw data. The energy change during

titration was fit to an independent model, and the binding number was calculated to be 47.79, indicating that approximately 48 shellac molecules were bound to one OPI aggregate. The binding constant (K_a) was calculated to be $2.088 \times 10^3 \text{ M}^{-1}$, suggesting moderate molecular interactions had occurred between these two polymers (Patel, Drost, den Adel, Hazekamp, & Velikov, 2012). The negative ΔH (-4.982 kJ/mol) and positive ΔS (47.15 J/mol.K) values suggest that hydrogen bonding and hydrophobic interactions were involved (Patel et al., 2013). The negative ΔG ($\Delta G = \Delta H - T\Delta S$) value indicates the spontaneity of the binding process. Moreover, the main effect of the ΔG value was derived from ΔS , implying significant hydrophobic interactions (Bouchemal & Mazzaferro, 2012). Thus it was likely that the hydrophobic interactions and hydrogen bonding were developed between amino acids of oat protein and carboxyl/hydroxyl and non-polar groups of shellac; these then led to the formation of cross-linking networks with a dramatically increased G' and viscosity. In the preliminary work, however, there was no significant increase of solution rheological properties when adding shellac into soy or whey protein solutions at pH 8, suggesting no or limited interactions in these mixture systems. The difference may be related to the unique property of oat globular proteins to dissociate into partially denatured monomers at pH 8 after heating treatment, whereas many other globular proteins form soluble aggregates instead during heating. The exposure of the monomer structure facilitated interactions between protein molecules and shellac. The G' and viscosity of OPI-shellac mixture solutions decreased as further increasing the shellac to 33% and further. This may be due to the interactions among oat protein molecules and the continuity of OPI network

were impacted by the larger amount of shellac. Similar results were reported for the mucus/oligosaccharide composites (Nordgård & Draget, 2011) and hordein/zein composites (Wang & Chen, 2012), where a small amount of oligosaccharide initially strengthened the polymer network and increased the solution viscosity, but larger amounts inhibited the interactions of host molecules and reduced network cross-links. When shellac was the predominant component, the shellac molecules mainly formed entanglement networks, but the interactions between shellac molecules were not strong enough to form continuous network like oat proteins. Thus, the composites with small portion of OPI could not form cross-linked networks and exhibited a solution type behavior.

5.3.2 Core (OPI) – shell (OPI-shellac) bead structure characterizations

5.3.2.1 Protein conformation in the bead shell

The protein conformation in the bead shells with various compositions was investigated using FTIR. As shown in Fig. 5-3, neat oat protein beads (OSB-1) contained several characteristic absorption bands that situated in the amide band region: 3300 cm^{-1} (amide-A) corresponding to vibration of N-H groups, 1650 cm^{-1} (amide-I) representing C=O stretching/hydrogen bonding coupled with COO^- groups, 1527 cm^{-1} (amide-II) related to the bending vibration of N-H groups and stretching vibrations of C-N groups (Kong & Yu, 2007). In the case of neat shellac beads (OSB-5), a broad hydroxyl band existed at 3450 cm^{-1} corresponding to vibration of N-H groups, 2920 and 2975 cm^{-1} representing C-H stretching, 1730 cm^{-1}

corresponding to carbonyl band and C-H stretching, and 1635 cm^{-1} related to the vinyl stretching (Derry, 2012).

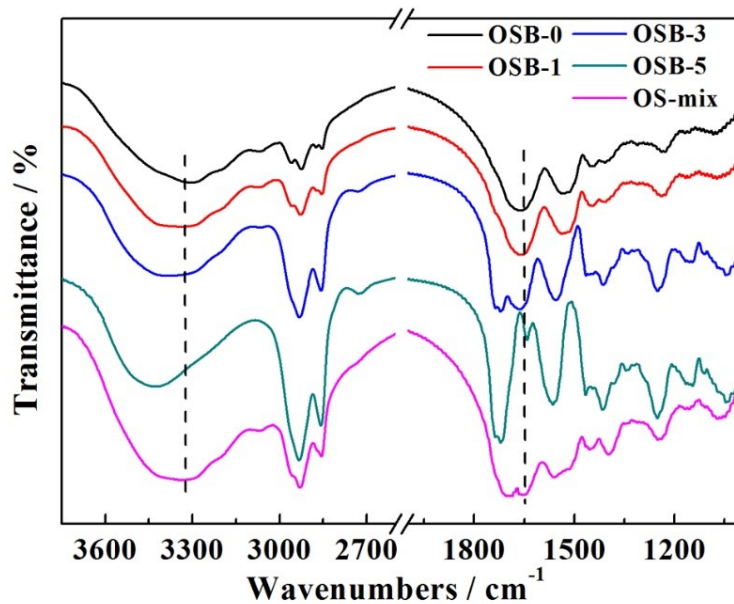


Fig. 5-3. FTIR spectra of OPI-shellac composite beads (OSB-0, OSB-1, OSB-4, and OSB-5) and the mixed dry powder of OPI and shellac (OS-mix).

When shellac content was 18% (w/w) (OSB-1) as well as 67% (w/w) (OSB-3), the intensity of the bands at 3300 , 1650 , and 1527 cm^{-1} increased compared with the bands of neat OPI (OSB-0), indicating the involvement of the amide group of oat protein in the interaction with carboxylate groups of shellac (Patel et al., 2013). Specifically, due to the large amount of glutamate and glutamine (22.4%) contained in the oats (Nieto-Nieto et al., 2014), hydrogen bonds formed more easily with shellac, while the presence of proline (7.3%), valine (7.7%), and leucine (8.6%) promoted hydrophobic interactions between OPI and shellac. When directly mixing OPI

and shellac dry powders (same ratio as OSB-1) together, two peaks at amide-I region were observed caused by OPI and shellac, respectively. This means that there was no interaction between two polymers if just blended dry. However, only one peak was observed at amide I region for OSB-1. This confirmed that shellac was well dispersed in the OPI matrix and they interacted with each other. In the spectrum of OSB-3 with large amounts of shellac (67%, w/w), a typical band of shellac at 1730 cm^{-1} was found. Comparing to the OSB-1 sample, the absorption peak of hydrogen bonded -OH group stretching vibration of OSB-3 shifted from 3300 to 3400 cm^{-1} , demonstrating weaker hydrogen bonded network. This weakened interaction in the OPI-shellac networks decreased viscosity and G' of the OS-3 solution.

5.3.2.2 Bead morphology

The diameter of fresh and dried beads was $\sim 2.1\text{ mm}$ and $\sim 1.0\text{ mm}$, respectively. The shell compositions greatly influenced the OPI-shellac bead morphology. After drying at room temperature, OSB-0, OSB-1 and OSB-2 with 0, 18, and 46% (w/w) of shellac, respectively, firm particles with smooth surfaces were created, whereas the shells of OSB-3, OSB-4 and OSB-5 with 67, 82, and 100% (w/w) of shellac, respectively, were fragile and could be easily broken. Fig. 5-4 shows the SEM images of core-shell beads surfaces. The neat oat protein (OSB-0) formed a compact structure without pores (Fig. 5-4a). Since the calcium ions quickly screened the surface charge of protein when OPI solution was added in the coagulation bath with CaCl_2 , this likely resulted in a close and tight association of oat protein molecules in all directions,

creating the compact surface of the beads (Maltais et al., 2008). With addition of 18% (w/w) shellac (Fig. 5-4b, OSB-1), the bead surface became smoother compared to that of OSB-0. The negatively charged shellac interacted with oat protein molecules and prevented the rapid aggregation of protein molecules upon addition of calcium. The slower aggregation likely promoted the orderly packing of molecules, one by one, to form a smooth surface structure. In addition, it was difficult to distinguish shellac or protein aggregates on the surface of OSB-1, indicating that shellac was well dispersed in OPI networks and these two materials were compatible to each other.

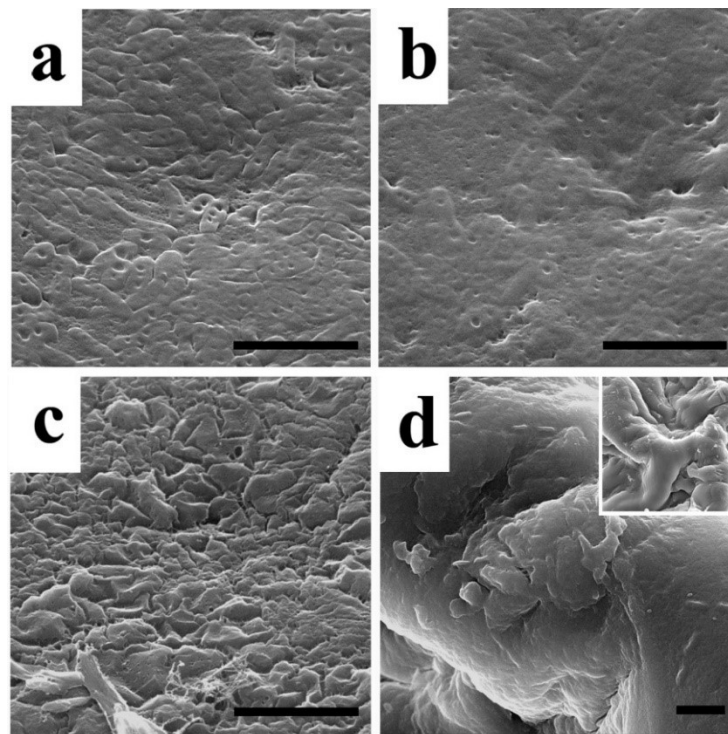


Fig. 5-4. SEM images of surface of OPI-shellac composite beads: (a) OSB-0; (b) OSB-1; (c) OSB-3; and (d) OSB-5. Scale bar: a, b, and c -- 2 μm ; d -- 5 μm ; internal picture -- 20 μm .

The compatibility of shellac and OPI was confirmed by confocal microscopy images (data not shown) in which no phase separation was observed for the microstructure of OSB-1 beads. This was further supported by the DSC results in Fig. 5-5. Only one T_g value was found for OSB-1 at 120.63°C, where the neat OPI (OSB-0) and shellac (OSB-5) exhibited T_g value at 129.4 and 98.9 °C, respectively. The only one endothermic peak and T_g value that located between the T_g s of neat OPI and shellac directly demonstrated the homogenous structure of the OPI and shellac composites with good miscibility of these two materials, likely be attributed to the interactions of oat protein molecules and shellac, as revealed by the ITC and FTIR results. For OSB-3 (Fig. 5-4c), where shellac was the predominant material, bulk aggregates were observed at the lumpy surface of the bead. Only one endothermic peak and T_g value (Fig. 5-5) of 104.9 was found for OSB-3 according to DSC results, explaining the lumpy surface with bulk aggregates forming with the homogenous OPI and shellac mixture. Nevertheless, as suggested by the rheology test, the interactions between shellac and OPI became weakened when shellac was the predominant material (67%, w/w) compared to OSB-1, where the shellac amount was only 18% (wt). Neat shellac film has been reported to exhibit poor elongation properties, brittleness, and less flexibility (Luangtana-anan, Nunthanid, & Limmatvapirat, 2010). Thus, the bulk aggregates could be related to the less flexible nature of shellac, which formed a more rigid and less viscoelastic structure. This was confirmed by the neat shellac surface structure, as shown in Fig. 5-4d, with an irregular, rough and lumpy surface due to the aggregation of shellac in the presence of calcium ions.

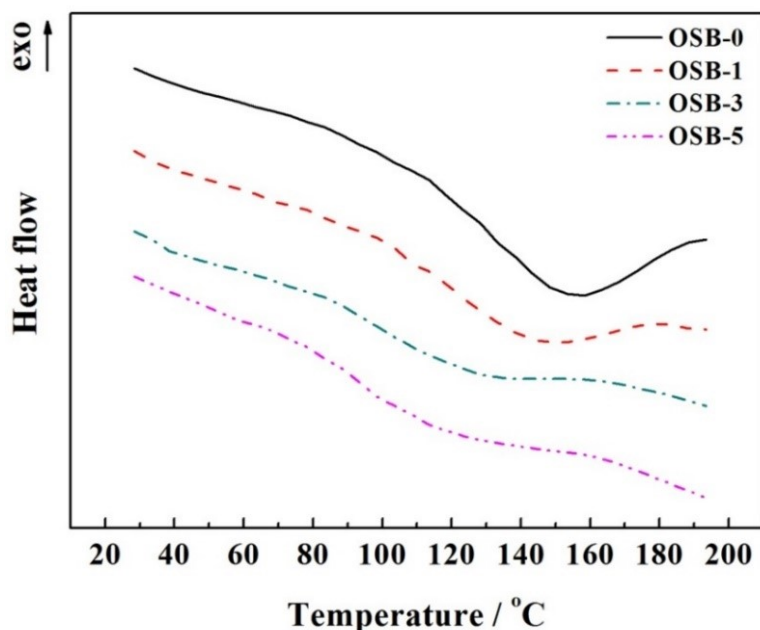


Fig. 5-5. DSC thermograms of OPI-shellac beads with OPI and shellac mixture shell at different ratios.

Fig. 5-6 shows the cross section of the beads with various shell compositions. For OSB-0 and OSB-1 (Fig. 5-6a and 5-6b), no obvious shell structure could be observed, further confirming a good compatibility between the shell and core materials that resulted in dry beads with compact and integrated structure. In contrast, obvious loose and thick shell structure (as shown within the parallel red lines) was observed in the cases of OSB-3 and OSB-5 (Fig. 5-6c and 5-6d) due to the large amount of shellac, especially for OSB-5, where some small pores could be observed on the shell structure. This could be the reason that fresh, dried OSB-3 and OSB-5 beads had a shell that could be easily separated. Such a coarse shell structure with a large amount of shellac may lead to

surface leakage of the incorporated core ingredients, or penetration of stomach juice with enzymes, resulting in a quick degradation of the bead matrix. In contrast, the shell structure with a larger amount of oat protein and smaller amount of shellac (OSB-1) exhibited a smooth and compact shell structure. In this case, the addition of oat protein could not only well cover the shortage of shellac, but maintained its functionalities.

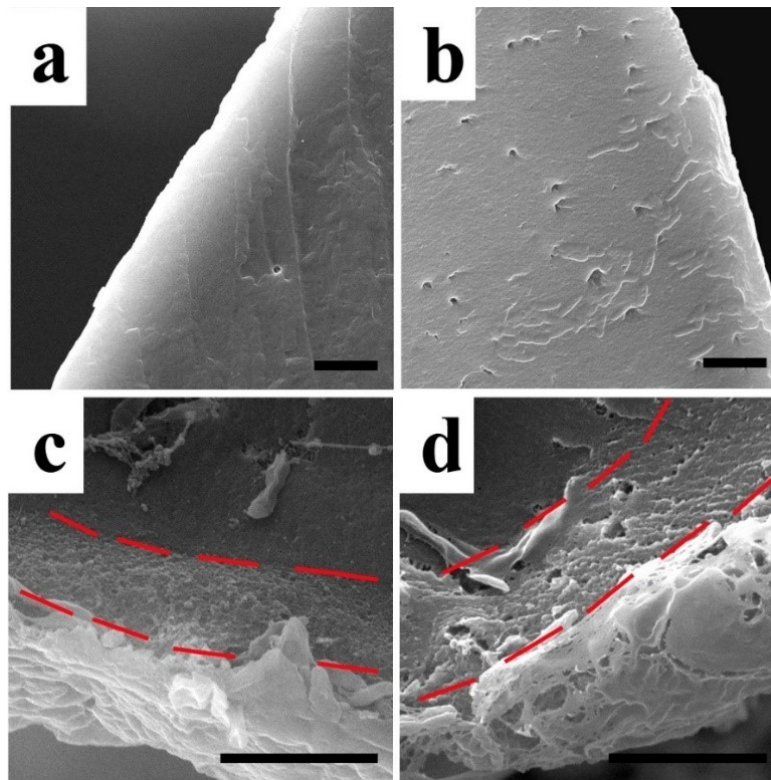


Fig. 5-6. SEM images of the cross section of OPI-shellac composite beads: (a) OSB-0; (b) OSB-1; (c) OSB-3; and (d) OSB-5. Parallel lines in red indicate the shell structure of beads. Scale bar: 2 μm .

5.3.3 Bio-related applications

5.3.3.1 *In vitro* release behavior of encapsulated vitamin

The release behavior of OSB was investigated in simulated gastric fluids (SGF) and simulated intestinal fluids (SIF) with and without digestive enzymes. Riboflavin (vitamin B₂) not only plays a key role in the metabolism of carbohydrates, fats, and proteins, but is also important for antibody production, cell respiration and growth, and red blood cell formation (Bernardos et al., 2008). However, riboflavin is sensitive to UV light and high temperatures which negatively impacting its bioactivities and limit its utilization. Thus, riboflavin was applied as a model bioactive molecule in this study. Fig. 5-7a shows the riboflavin release profiles from OSB with various OPI-shellac shells in pH 1.2 and pH 7.4 buffers without digestive enzymes. The bead with neat OPI shell (OSB-0) exhibited rapid release rate at pH 1.2, where approximately 31.4% of riboflavin was leached out after 2 h, whereas there was a relatively slower release rate at pH 7.4, where approximately 65.5% riboflavin was detected at the end of the test. In contrast, the release of riboflavin from the beads with neat shellac shell (OSB-5) at pH 1.2 was much slower, and only 11.1% of the riboflavin was released after 2 h due to the acid resistance of shellac. The fastest release rate was observed when the beads were transferred into pH 7.4 buffer; where 83.3% riboflavin was released after 12 h. The beads with various OPI-shellac composite shells exhibited different release profiles. When shellac amount was 18% (w/w) (OSB-1), the release rate was significantly less compared to OSB-0; approximately 16.6% of riboflavin was released after 2 h

at pH 1.2. At pH 7.4, OSB-1 exhibited a sustained release profile with the lowest release rate; 42.9% riboflavin was detected in the release medium after 10 h of the test. The well-established homogenous and integrated shell structure stabilized by oat protein and shellac interactions contributed to the desirable controlled release properties of OSB-1. When the ratio of shellac and OPI was near 1.0 (OSB-2), the release rate in pH 1.2 was fast and similar to OSB-0; whereas more moderate release rates in pH 1.2 and pH 7.4 were observed for OSB-3. When the concentration of oat protein was slightly lower than or comparable to shellac, the SEM images revealed these mixtures formed rigid, brittle shell structures. This impacted the integrity of the shell surface, and led to the accelerated release of riboflavin at pH 1.2. However, with a continuous increase of the shellac concentration to 82% (w/w) (OSB-4), the riboflavin release rate was slowed again to a rate similar to that of the neat shellac sample alone. The release rate of riboflavin from OSB-4 at pH 7.4 was still slower than OSB-5, a result attributed to the incorporation of oat protein, where the interactions between oat protein and shellac slowed down the collapse of the shell structure.

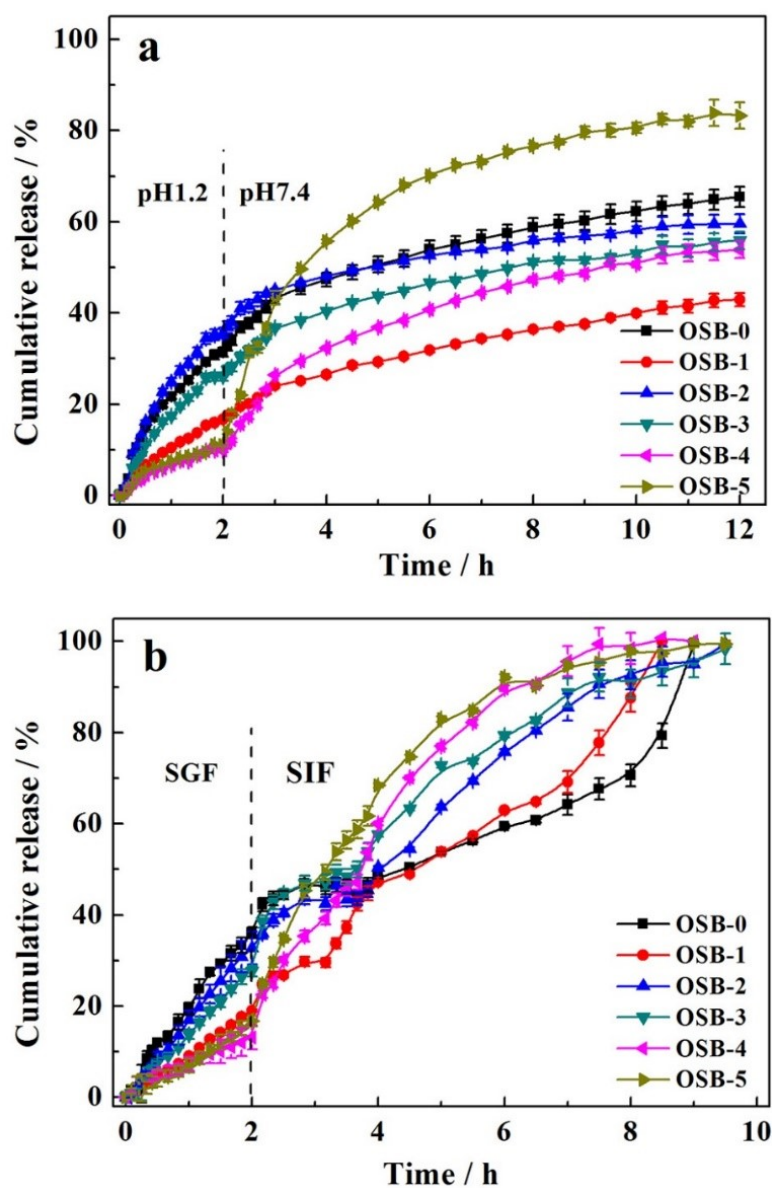


Fig. 5-7. (a) Release profiles of riboflavin from OSB at pH 1.2 for 2 h and in pH 7.4 PBS for another 10 h at 37 °C. (b) Release profiles of riboflavin from OSB in simulated gastric fluid (pH 1.2 + pepsin) for 2 h and in simulated intestinal fluid (pH 7.4 + pancreatin) for 7 h at 37 °C.

Understanding of the release mechanisms is important for the design of an efficient nutraceutical delivery system. In general, the mechanisms of drug and nutraceutical release from

a polymer matrix can be categorized in three ways (Arifin et al., 2006): (1) a diffusion-controlled system where the drug diffuses from the non-degraded polymer; (2) a swelling-controlled system, where drug diffusion is enhanced due to polymer swelling; and (3) an erosion-controlled system, where drug release is facilitated by polymer degradation and erosion. The Korsmeyer - Peppas semi-empirical equation was applied to identify the mechanism of riboflavin release from OPI-shellac based core-shell beads (Wang & Chen, 2014):

$$M_t / M_\infty = kt^n \quad (5-1)$$

where M_t / M_∞ is the fraction of the model molecule released after time t relative to the amount of model molecule released at infinite time, k is a constant and n is the diffusional exponent. Inferences about the release mechanism are based on the fit of this equation to the model molecule release data through 60% dissolution and comparison of the value of n to the semi-empirical values for slab geometry reported by Korsmeyer (1983), where $n \leq 0.50$ indicates Fickian diffusion, $0.50 < n < 1$ indicates non-Fickian transport, and $n = 1$ or greater indicates case II transport (Pandey et al., 2011). Riboflavin released from all samples possessed n values within the range of 0.59-0.75 ($R^2 = 0.98-0.99$) during 2 h at pH 1.2, indicating that the release of riboflavin occurred due to either the swelling of beads or due to the brittleness of the bead shell. In sample OSB-1, the 18% (w/w) of shellac played an important role and interacted with protein to restrict the network swelling, thus effectively prevented premature release of riboflavin in the gastric buffer. In pH 7.4 PBS buffer, riboflavin release from OSB-0, OSB-1, OSB-2, and OSB-3

displayed a typical sigmoid profile with n values in the range of 0.53-0.73 ($R^2=0.95-0.98$) in first 2 h and then 0.30-0.48 ($R^2=0.97-0.99$) in the remaining time. This indicates a two-stage release from the beads with protein dominated shells. In the first 2 h at pH 7.4, swelling of the beads enhanced riboflavin diffusion. Shellac could be dissolved when the pH was higher than 7, leading to swelling of oat protein networks when pH was far from the protein isoelectric point. When the system reached a swelling equilibrium, the release followed a diffusion-controlled mechanism. The rapid release of riboflavin from OSB-4 and OSB-5 was observed which followed an exponential pattern in pH 7.4 PBS buffer. The beads apparently underwent what is called a first-order degradation. The first-order degradation constants were calculated from the plot of log cumulative percentage of riboflavin remaining versus time which yielded a straight line with a slope of $-K/2.303$:

$$\text{Log } C = \log C_0 - Kt/2.303 \quad (5-2)$$

Where C_0 is the initial concentration of riboflavin, K is the first order rate constant, and t is the time. The K values were 0.85 ($R^2 = 0.99$) and 2.07 ($R^2 = 0.99$) for OSB-4 and OSB-5, respectively. This data indicated that the release of riboflavin from OSB-4 and OSB-5 due to the degradation, which could be attributed to the pH dependent solubility of shellac.

The release behavior of riboflavin from beads in the simulated gastro-intestinal tract in the presence of digestive enzymes was also evaluated. As shown in Fig. 5-7b, the release of riboflavin in SGF was faster than that in pH 1.2, but the release from beads with OPI-shellac

composite shells was still less than 40% after 2 h. Specifically, the release ratios from OSB-1, OSB-4 and OSB-5 were only 19.0, 13.1 and 16.7%, respectively, demonstrating a good barrier property of these composite shells against pepsin permeation. When transferred to SIF, the remaining riboflavin in OSB-4 and OSB-5 was released quickly; approximately 80% of riboflavin was released after 3-4 h. In contrast, a more sustainable release was observed for OSB-1, which is desirable for oral administration of bioactive compounds.

5.3.3.2 Encapsulation and protection of probiotics

Probiotics have many health benefits and can improve the intestinal flora, stimulate immune response, and promote nutrient absorption (Cheow & Hadinoto, 2013). Probiotics must be viable at large concentrations when reaching the small and large intestines in order to confer these health benefits. However, their survival ratio in food systems is often low under the harsh conditions of acidity encountered at the stomach (Corona-Hernandez et al., 2013). Fig. 5-8a shows the encapsulation efficiency of OSB-0, OSB-1, OSB-2, and OSB-5. For the beads with neat oat protein shell (OSB-0), an encapsulation efficiency of 70.8% was observed, a finding related to the dense network structure of neat protein shell to prevent the release of cells. Moreover, the good water holding capacity of the OPI gel core maintained the nutritive cell culture medium to keep cell alive.

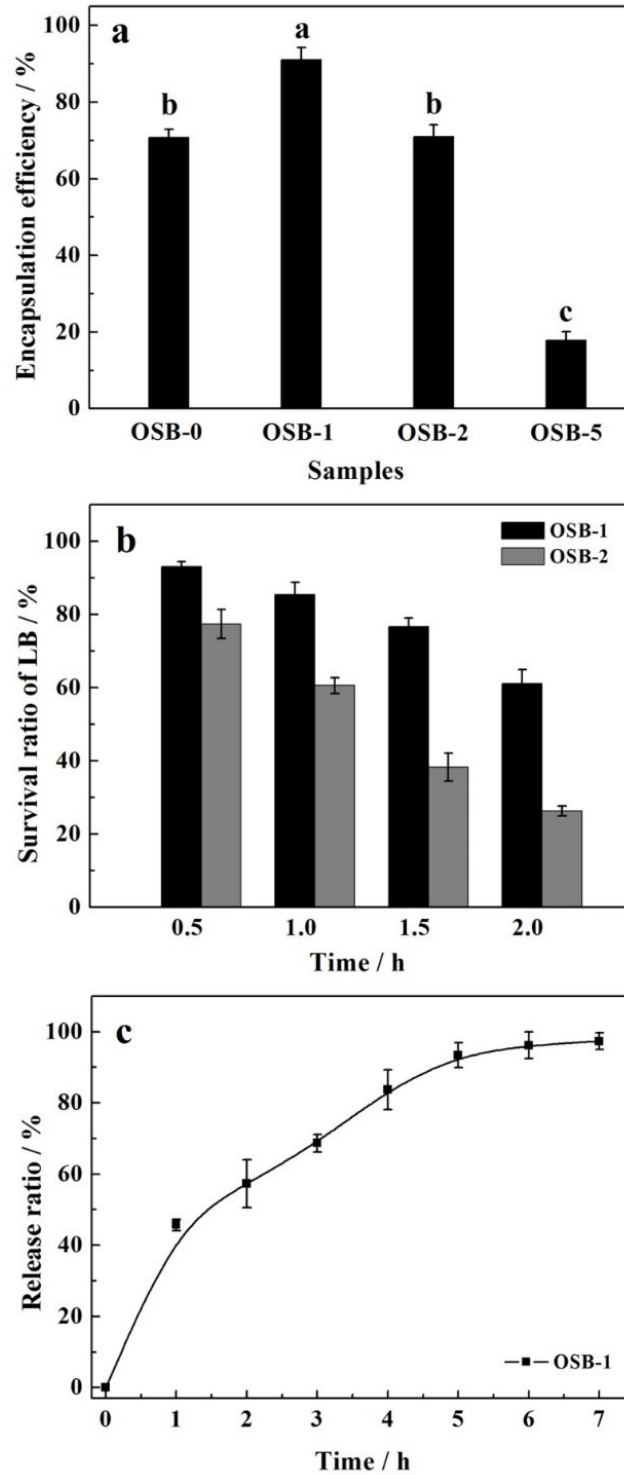


Fig. 5-8. (a) Encapsulation efficiency of OSB with various shell materials; (b) Survival ratios of encapsulated *Lactobacillus acidophilus* after immersing in simulated gastric fluid (pH 1.2 + pepsin) for 0.5, 1, 1.5, and 2 h; (c) Release profile of encapsulated *Lactobacillus acidophilus* from OSB-1 after immersing in simulated intestinal fluid (pH 7.4 + pancreatin).

When adding 18% (w/w) of shellac into shell material (OSB-1), the encapsulation efficiency significantly increased to 91.1%. Such a good encapsulation capacity can be attributed to the homogenous and integrated shell structure which was stabilized by polymer chain entanglement and non-covalent interactions. With a further increase in the shellac concentration (OSB-2), the encapsulation efficiency decreased to 71.1% which was similar to OSB-0. For the beads with neat shellac shell, the encapsulation efficiency even dropped to very low value of 17.9%, likely due to the rigid, rough and brittle shell structure with small pores, as shown in the SEM images.

According to the initial encapsulation efficiency results, OSB-1 and OSB-2 beads were then selected to further test their protection ability in SGF. Fig. 5-8b shows the survival ratios of encapsulated *L. acidophilus* after being immersed in SGF for 2 h. Interestingly, the survival ratios of cells encapsulated in OSB-1 beads were significantly greater than in OSB-2 beads. After incubating in SGF for 1 and 2 h, the survival of the encapsulated *L. acidophilus* in OSB-1 was 85.5 and 61.1%, respectively, while the survival ratios of cells in OSB-2 were 60.5 and 26.3%, respectively. For free *L. acidophilus*, after being immersed in SGF even for 0.5 h, no viable cells persisted any more (data not shown). Obviously, OSB-1 offered excellent protection to *L. acidophilus*. As mentioned above, the homogeneous and dense shell structure conferred this good cell protection functionality. The release profile of OSB-1 in SIF was further investigated by calculating the remained viable cells in beads. Fig. 5-8c shows the release ratios of *L. acidophilus* from OSB-1 after immersing in SIF for 7 h. The beads were exposed first to SGF for 1 h and then

transferred to SIF to mimic the process of passage through the GI tract. A sustainable release of cells from OSB-1 beads in SIF could be observed, and approximately 80% of cells were released after 4 h. Such a sustained release profile would enable the continuous discharge of viable probiotics into the small intestine during a normal digestive cycle.

5.3.3.3 Encapsulation and protection of enzyme

The enzyme encapsulation of OSB-1 was investigated using α -amylase as an enzyme model. α -amylase is a major enzyme used for replacement of pancreatic for systemic therapy. Moreover, it is widely applied for animal feed to improve the digestibility of carbohydrates to increase the amount of energy. However, this enzyme is unstable if exposed to high temperatures or extremes in pH conditions, and can be easily inactivated by gastric fluid. After encapsulation, the activity of encapsulated α -amylase in OSB-1 was largely retained (~96% of the load). The OPI gel core had an ability to hold a large amount of water (Chapter 4) and a homogeneous and integral shell of OSB-1 was immediately formed during preparation, thus effectively preventing the release of encapsulated amylase. The stability of encapsulated α -amylase in SGF is documented in Fig. 5-9. After incubating in SGF for 0.5 and 1 h, the activity of the enzyme remained high at relatively large values of 88% and 80%, respectively, while the activity of enzyme without encapsulation was diminished after only 0.5 h. After 2 h in SGF, 56% of the enzyme activity still remained. The gastro-protection ability of OSB-1 for amylase was better than either carboxymethyl high amylase starch and succinate high amylase starch matrices, which maintained the

encapsulated-amylase activity only to around 40% after incubating in SGF for 2 h (Massicotte, Baille, & Mateescu, 2008).

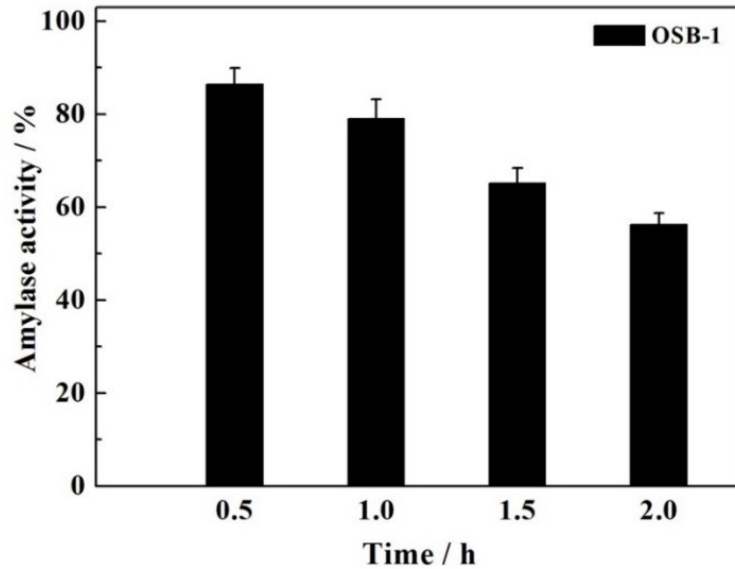


Fig. 5-9. Activity of encapsulated α -amylase in OSB-1 after immersing in simulated gastric fluid (pH 2 + pepsin) for 0.5, 1, 1.5, and 2 h.

5.4 Conclusions

For the first time, beads with oat protein core and various oat protein-shellac shells were fabricated at near neutral pH. Specifically, in the OSB-1 sample when shellac accounted for 18% (w/w) of the total dry weight at pH 8, shellac and OPI together formed strong networks mainly via hydrophobic interaction and hydrogen bonding. This amount of shellac was critical to create solid beads with a homogeneous structure and smooth bead shell in a mainly oat protein substrate. Also, 18% (w/w) of shellac played an important role to restrict network swelling by its particular way of interacting with oat protein, thus effectively preventing premature release of the riboflavin

bioactive model into the gastric fluid. The OSB-1 encapsulated riboflavin was then capable of being completely released into the simulated intestinal tract in a sustainable way that would promote its absorption in a living system. The OSB-1 beads also demonstrated a good ability to resist gastric juice and pepsin digestion, and protective capacity to encapsulated probiotics and enzymes under harsh stomach conditions. From a practical perspective, the beads were prepared using a simple extrusion method at near neutral pH and ambient temperature, suggesting that this effective delivery system may be commercially viable since it can easily be adapted and scaled up. Further, the OSB-1 is made from natural sources that are generally recognized as safe, indicating that this system has excellent potential as a future delivery system for sensitive bioactive compounds for food and biomedical applications.

Chapter 6

Fabrication of novel protein-shellac nanoparticles for improved bioavailability of resveratrol and its antioxidant effect *in vivo*

6.1 Introduction

Bioactive compounds such as therapeutic protein, peptides, and polyphenols are of great interest as substances possessing a high spectrum of biological activities that have the potential to reduce the risk of chronic diseases and improve public health. However, many of these compounds exhibit low bioavailability due to instability in the harsh gastric tract, and insufficient residency time or low solubility within the small intestine, which limits their potential activity *in vivo* (Chen et al., 2006). For example, resveratrol (3,5,4'-trihydroxy-trans-stilbene), one of the polyphenol molecules that are naturally found in a wide variety of plant species, has demonstrated pleiotropic bioactivities including antioxidant, antiaging, anti-HIV/AIDS, and anticancer effects (Amri et al., 2012; Singh & Pai, 2014). Despite these, resveratrol has low bioavailability due to its poor water solubility and chemical instability (Davidov-Pardo & McClements, 2014). After oral administration, the metabolism of resveratrol leads to the formation of glucuronide and sulfate conjugates and only trace amounts of unchanged resveratrol can be detected in plasma (Patel, Scott, Brown, Gescher, Steward, & Brown, 2011).

Nanoparticles are promising delivery systems to improve bioavailability of bioactive compounds. Due to their small size, nanoparticles can adhere to the intestinal mucosal layer

through non-specific interactions, thus significantly prolonging the formulation residence time by decreasing the influence of intestinal clearance mechanisms (Arbós et al., 2002). In addition, nanoparticles can transport across the intestinal epithelium via paracellular and transcellular routes and are readily taken up by cells, which efficiently facilitate the delivery of bioactive compounds to a specific physical target in the body (des Rieux et al., 2006). Food proteins are generally regarded as safe materials with excellent biocompatibility and biodegradability. Moreover, the good emulsifying and gelling properties of food proteins offer a capacity to incorporate both hydrophilic and lipophilic bioactive compounds. However, the preparation processes of food protein nanoparticles such as emulsification-solvent evaporation, chemical or heat-induced crosslinking, and coacervation methods usually demand the heating and high pressure homogenization treatment, and organic solvents or surfactant, which are not suitable for sensitive bioactive compounds and may cause toxicity (Acosta, 2009). Development of food protein nanoparticles that can effectively protect sensitive bioactive compounds against low pH and pepsin digestion in the gastric tract also remains a challenge due to the premature degradation of the protein networks at submicron size.

An excellent gelling property of oat protein prepared through cold-set gelation methods has been identified in Chapter 4. Formation of cold-set protein gels allows encapsulation of heat labile bioactive compounds. Furthermore, when mixing oat protein with 18% (w/w) of shellac, a natural and biodegradable resin, gel networks resistant to harsh gastric environment were formed

via hydrophobic interaction and hydrogen bonds (Chapter 5). This gel network has provided opportunity to target delivery of bioactive compounds into the small intestine where most of the bioactive compounds are absorbed to exert health benefits.

In this study, it is hypothesized that novel nanoparticles could be designed based on the oat protein-shellac networks to improve bioavailability of bioactive compounds. The objective of this study is to develop oat protein-based nanoparticles and investigate *in vitro* release, cellular uptake and transport, and *in vivo* oral bioavailability using resveratrol as the model bioactive compound, as well as the antioxidant activities of the encapsulated resveratrol through cell and rat models.

6.2 Materials and methods

6.2.1 Materials

Oat protein isolate (OPI) was extracted from defatted oat flour using an alkaline and isoelectric point precipitation method according to our previous work (Nieto-Nieto et al., 2014). The protein content was $85.07\% \pm 2.4$ (w/w, dry status) as determined by the Leco nitrogen analyzer (FP-428, Leco Corporation, St Joseph, MI, USA) and a using a nitrogen to crude protein conversion factor of 5.83, while other components could be soluble fiber, starch, lipid, and ash, among others. Shellac (M_w : ~ 1000 Da), resveratrol, pepsin (from porcine gastric mucosa, 424 units mg⁻¹), pancreatin (from porcine pancreas, 200 USP units mg⁻¹), formaldehyde, glutathione, 2,7-dichlorodihydro-fluorescein diacetate (DCFH-DA), tert-butyl hydroperoxide (t-BHP), monobromobimane (mBBr), 3-(4,5-dimethylthiazol-2-yl)-2,5-diphenyltetrazolium bromide

(MTT), dimethyl sulfoxide (DMSO), filipin III (FLI), chlorpromazine hydrochloride (CPZ) and cytochalasin D (CyD) were obtained from Sigma-Aldrich Canada (Oakville, ON, Canada). Alexa Fluor dyes and 4',6-diamidino-2-phenylindole (DAPI) were purchased from life technologies (Burlington, ON, Canada). Caco-2 cell and Chang liver (CCI-13) cell lines were obtained from American Type Culture Collection (Manassas, VA, USA). Cell culture reagents including Dulbecco's Modified Eagle's Medium (DMEM), fetal bovine serum (FBS), non-essential amino acids (NEAA), HEPES solution, trypsin-EDTA, and Hanks balanced salt solution (HBSS) were purchased from GIBCO (Burlington, ON, Canada). Other chemicals used in the experiment were all analytical grade and obtained from commercial sources.

6.2.2 Preparation of resveratrol-loaded OPI-shellac nanoparticles

OPI (4%, (w/v)) was suspended in Milli-Q water and then sealed tightly in a glass vial and heated at 115 °C (above protein denaturation temperature) in an oil bath for 15 min, followed by cooling down to room temperature. Shellac (1.25, 2.5, and 5%, (w/v)) was dissolved in Milli-Q water at pH 8 adjusted using 1 M NaOH. Resveratrol (20 mg/mL in 1 mL 70% ethanol) was mixed with 8 mL cooled OPI solutions (4%, w/v) at room temperature, and then the mixture was dispersed in a 4 mL shellac solution with various concentrations, followed by the addition of 2 mL 12.5 mM CaCl₂ solution. The obtained NPs were coded as NP-0S, NP-50S, NP-100S, and NP-200S, respectively, corresponding to the shellac concentration of 0, 1.25, 2.5, and 5% w/v, and stored at 4 °C for further analysis.

6.2.3 Characterization of nanoparticles

The size, size distribution as reflected by polydispersity index (PDI) value, and zeta potential of NPs were determined by dynamic light scattering (DLS) and laser Doppler velocimetry using a Zetasizer Nano S (Malvern Instruments Ltd, Malvern, UK) at 23°C. The samples were diluted to an appropriate concentration in Milli Q water before analysis. The morphology of NPs was observed by transmission electrical microscopy (TEM, Morgagni 268, Philips-FEI, Hillsboro, Oregon, USA) at an accelerating voltage of 80 kV (Yang et al., 2014).

Surface hydrophobicity (S_o) of NP was evaluated by the Rose Bengal method (Lukowski, Müller, Müller, & Dittgen, 1992). Briefly, Rose Bengal (RB, 20µg/mL) was added to NP suspensions with a range of increasing concentrations (0.0625, 0.125, 0.25, 0.5 mg/mL) and the mixtures were incubated for 3h. NPs were then separated by ultra-centrifugation at 50000 rpm (~70000g). The concentration of free RB in supernatant was determined by UV-Vis spectroscopy at 542.7 nm. The partitioning quotient (PQ) was calculated according to the following equation:
$$PQ = (\text{amount of RB bound on the surface of nanoparticles}) / (\text{amount of RB in dispersion medium}).$$
 The profiles were constructed for PQ as a function of the total particle surface area (SA), and SA was calculated by assuming that the NPs suspensions were mono-disperse, with diameter equal to the hydrodynamic diameter measured using DLS. The plots obtained were linear and the corresponding slopes for all concentrations tested were taken as a measure of S_o value.

For measurement of encapsulation efficiency (EE%) and encapsulation capacity (EC%), 0.5 mM CaCl₂ (determined by preliminary test) was added to fresh NPs (1:1 v/v) and centrifuged at 8000 rpm (~10000g) for 5 min to precipitate NPs and remove free resveratrol. The precipitates were treated with 70% acetonitrile, followed by ultrasonication for 30 min to extract encapsulated resveratrol (Coradini, et al., 2014). After filtration through 0.45µm filter, the extracted resveratrol solution was analyzed by a reverse-phase high performance liquid chromatography (RP-HPLC) using a 1200 Series Binary HPLC system (Agilent Technologies, Waldbronn, Germany) equipped with an Eclipse XDB-C18 column (4.6 × 150 mm), and a UV detector. Solvent A was water : trifluoroacetic acid (TFA) (99.9 : 0.1 v/v) and solvent B was acetonitrile : TFA : water (95:0.07:4.93, v/v/v). The gradient elution program was as follows: 0-5 min 20% B linear increased to 50% B; 5-7 min 50% B; 7-9 min linear decreased to 20% B; 10 min 20 % B. Resveratrol standard was prepared ranging from 0.125 to 50 µg/mL (R² = 0.99) in 70% acetonitrile and measured at 306 nm with flow rate of 0.8 mL/min. The EE and EC were calculated by the following equations, respectively:

$$EE (\%) = \frac{\text{resveratrol } (\mu\text{g}) \text{ in nanoparticles}}{\text{resveratrol } (\mu\text{g}) \text{ added}} \times 100\% \quad (6-1)$$

$$EC (\%) = \frac{\text{resveratrol } (\mu\text{g}) \text{ in nanoparticles}}{\text{nanoparticles } (\mu\text{g})} \times 100\% \quad (6-2)$$

6.2.4 *In vitro* release study

For the *in vitro* release study, 1 mL resveratrol loaded NPs was suspended in 10 mL of four dissolution mediums at 37 °C: HCl-saline solution (pH 2, 0.1 M); phosphate-buffered saline (PBS,

pH 7.4, 0.1 M); simulated gastric fluid (SGF, pH 2, 0.1 M HCl-saline with 0.1% pepsin, w/v); and simulated intestinal fluid (SIF, pH 7.4, 0.1 M PBS with 1.0% pancreatin, w/v). Samples were taken at predetermined time intervals, and the NPs were precipitated and resveratrol released by the same way as mentioned in section 6.2.3. Then the supernatant was diluted 2 times using 70% acetonitrile and analyzed by RP-HPLC system to determine the amount of released resveratrol.

6.2.5 Cell culture

Two cell lines (Caco-2 and Chang liver cells) were used in this work. A monolayer of Caco-2 cells was applied to simulate the intestinal epithelia cells where orally administered nutrients are absorbed, metabolized, or trans-located across cells (Zhang et al., 2015). Chang live cells have a cellular morphology similar to that of liver parenchymal cells which are applied to simulate the liver cell reaction to tested compounds (Senevirathne et al., 2012).

6.2.5.1 Cell viability assay

Cell viability was examined by MTT assay. Cell lines (Caco-2 and Chang liver cells) were seeded in 96-well plates at density of 8000 cells per well in 100 μ L culture medium. The cells were grown for 24 h to allow attachment before the experiment. NPs were added into each well to reach a final concentration of 0.025, 0.05, and 0.25 mg/mL, respectively, and incubated with the cells for 24h. The medium without NPs was used as a control. Then 10 μ L MTT solution (5 mg/mL in PBS) was added to each well and incubated for a further 4 h at 37 $^{\circ}$ C, followed by removal of the medium from each well and addition of 100 μ L DMSO. The absorbance was

measured at 570 nm using a microplate reader (SpectraMax, Molecular Devices, Sunnyvale, CA, USA). The cell viability was expressed as percent of living cells compared to the control wells.

6.2.5.2 NPs cell uptake efficiency and mechanism study

Confocal laser scanning microscopy (CLSM) was used to observe the uptake of fluorescence-labeled NPs in Caco-2 cells. Briefly, 0.025% (w/v) Nile red was dissolved in 70% ethanol followed by centrifugation at 12000 rpm for 10 min, and the supernatant was used to replace resveratrol for nanoparticles preparation. Caco-2 cells (1×10^5 cells/well) were seeded on the glass bottom micro-well dishes (P35G-1.5-14-C, MatTek Corp., Ashland, MA, USA) and cultured for 5-7 days until 100% confluence was reached. On the day of the experiment, the cells were equilibrated with HBSS (without phenol red) at 37°C for 30 min. The buffer was then replaced with 2 mL NP suspensions (0.25 mg/mL in HBSS) and incubated for 1, 3, and 6 h at 37°C or 4°C. At each end point, the cells were gently washed 3 times using HBSS and fixed with 4% paraformaldehyde (w/v in PBS pH 7.2) for 15 min. WGA-Alexa Fluor 488 conjugate and DAPI were then used to stain cell membrane and nuclei, respectively. The cells were examined using CLSM 510 Meta (Carl Zeiss Microscopy, Jena, Germany) and an oil immersion objective (40×) was used to visualize the samples. Images were processed with ZEN 2009 LE software (Carl Zeiss Micro Imaging GmbH, Oberkochen, Germany).

For cell uptake efficiency evaluation, Caco-2 cells (1×10^5 cells/well) were seeded in 6-well plates and cultured for 5-7 days. When reaching confluence, the cells were incubated with HBSS

(without phenol red) at 37 °C for 30 min. The medium was then replaced by 2 mL resveratrol-loaded NP suspensions (0.25 mg/mL in HBSS) or Free-resveratrol (concentration equal to resveratrol loaded in 0.25 mg/mL NPs), and incubated for 1, 3, and 6 h at 37 °C. To understand the uptake pathways of NPs, the cells were incubated with inhibitors, including 10 µg/mL cytochalasin D (CyD), 5 µg/mL chlorpromazine hydrochloride (CPZ), and 5 µg/mL filipin III (FLI) at 37 °C for 30 min. After being washed with HBSS, the medium was replaced by 2 mL resveratrol-loaded NP suspensions (0.25 mg/mL in HBSS) and incubated for 6 h at 37 °C. The cells were then gently washed 3 times using HBSS and lysed in RIPA buffer (500 µL) while kept on ice for 30 min. Cell lysates were mixed with ethanol (1:1 v/v) to extract resveratrol through ultrasonication for 30 min. The mixtures were centrifuged at 12000 rpm (15294g) for 10 min followed by evaporation using Vacufuge® vacuum concentrator (Eppendorf AG, Barkhausenweg, Hamburg, Germany). The residue was dissolved in 0.1mL 70% acetonitrile and analyzed by RP-HPLC.

6.5.2.3 Transport efficiency of resveratrol-loaded NPs

Caco-2 cells (2.6×10^5 cells/cm²) were seeded onto 6-well polyester Transwell® (pore size 3 µm) (Corning Costar, Cambridge, UK). The culture medium in apical and basolateral compartments was changed every other day for at least 21 days to allow the cells to differentiate and form a confluent monolayer. The integrity of the cell monolayer was monitored by measuring the transepithelial electrical resistance (TEER) using an epithelial tissue voltohmmeter (EVOM2,

World Precision Instruments, Sarasota, FL, USA). The TEER was calculated according to the following equation:

$$\text{TEER } (\Omega\text{cm}^2) = (R_{\text{total}} - R_{\text{filter}}) * A \quad (6-3)$$

where R_{total} and R_{filter} are the resistance values (Ω) of the filter with and without cells respectively, and A is the surface area of the Transwell® insert (cm^2). Monolayers with TEER values higher than $500 \Omega\text{cm}^2$ were used for transport study. TEER was also measured after the transport experiments to monitor the monolayer integrity. For evaluation of TEER reversibility, the nanoparticles were incubated with Caco-2 cell monolayers for 6h, and then replaced by culture medium. The cells were further incubated for 24 h, and the TEER value was monitored.

Caco-2 cell monolayers were gently washed 3 times with HBSS and equilibrated at $37 \text{ }^\circ\text{C}$ for 30 min. Resveratrol-loaded NP suspensions or Free-resveratrol solution (1.5 mL, 0.25 mg/mL NPs, equal to $3\mu\text{g/mL}$ resveratrol) were added to the apical chamber and 2.5 mL HBSS was applied to the basolateral chamber. After 6 h incubation at $37 \text{ }^\circ\text{C}$, solution in the basolateral chamber was collected and ethanol was added (1:1 v/v) to extract resveratrol. Then the mixture was concentrated at $30 \text{ }^\circ\text{C}$ until dry using a Vacufuge® vacuum concentrator. The residue was re-dissolved in 200 μL 70% acetonitrile, and the amount of resveratrol was measured using RP-HPLC.

6.2.5.4 Antioxidant activity

DCFH-DA, oxidation sensitive dye, was used to evaluate the intracellular formation of reactive oxygen species (ROS) (Senevirathne et al., 2012). Chang liver cells were seeded on black 96-well microplates at a density of 8000 cells per well in 100 μ L culture medium and cultured for at least 24 h for attachment. Then the cells were labeled with DCFH-DA (20 μ M, diluted in HBSS) for 30 min in the dark, followed by washing with HBSS (3 \times) and replacing the medium with different concentrations of resveratrol-loaded NPs (0.125 and 0.25 mg/mL) or Free-resveratrol (equal to the amounts of resveratrol loaded in 0.125 and 0.25 mg/mL NPs). After 6 h incubation, cells were washed with HBSS (3 \times) and 150 μ L 1000 μ M H₂O₂ (diluted in HBSS) were added. The amount of H₂O₂ was determined through a preliminary MTT test. The fluorescence of dichlorofluorescein (DCF) induced by the oxidation of DCFH in the presence of ROS was monitored (excitation at 485 and emission at 528 nm). The cells grown without nanoparticles and H₂O₂ treatment were blank, and the cells only treated by H₂O₂ were the control.

Cellular glutathione (GSH) content was determined using mBBR as a thiol staining reagent (Je, Cho, Gong, & Udenigwe, 2015). Chang liver cells were seeded on black 96-well microplates at a density of 8000 cells per well in 100 μ L culture medium and cultured for at least 24 h for attachment. The cells were then treated with different concentrations of resveratrol-loaded NPs (0.025, 0.125, and 0.25 mg/mL) or free-resveratrol (equal to the amounts of resveratrol loaded in 0.025, 0.125 and 0.25 mg/mL NPs). After 6 h incubation, cells were washed with the HBSS (3 \times)

and labeled with 40 μ M mBBr for 4h at 37 °C in the dark, followed by measuring the fluorescence intensity of mBBr-GSH (excitation at 360 and emission at 465 nm). The increase in fluorescence intensity indicates the higher content of cellular GSH expressed as % increase compared to control (cells without NP treatment).

6.2.6 *In vivo* study

6.2.6.1 *In vivo* pharmacokinetic studies

Pharmacokinetic studies were performed to test the oral bioavailability of encapsulated resveratrol in male Wistar rats (200-250g, Experimental Animal Center of Fudan University, China). The rats were fasted overnight to avoid interference with absorption before oral administration of the formulations, but were allowed free access to water. They were randomly distributed into four groups (n = 6/group): (i) resveratrol suspension (Free-resveratrol); (ii) and (iii) resveratrol-loaded NPs (NP-0S & NP-100S) for oral gavage; and (iv) positive control, a group of rats treated intravenously with the resveratrol dissolved in ethanol/Kolliphor® EL (1:1 v/v). Each animal received the equivalent amount of resveratrol at a dose of 20 mg/kg body weight either by oral gavage or intravenously via the tail vein. Blood samples were collected in the heparinized tubes from each rat at 0, 5, 30, 60 min and 1.5, 2, 3, 4, 5, 6, 7, 8, 9, 10, 12, 24 h following administration of oral gavage, and at 0, 5, 10, 15, 30, 45, 60, 90, 120, 240, 360 min following administration of intravenous injection. Blood samples were centrifuged at 3000 rpm

(~4000 g) for 10 min immediately after collection, and plasma aliquots were kept frozen at -80°C until HPLC analysis.

For analysis, 200 μ L aliquot of plasma were mixed with 100 μ L internal standard (IS, 1 μ g/mL naproxen) and 4mL of ether followed by vortex for 10 min to extract all the resveratrol. The mixture was centrifuged at 5000 rpm (~7000 g) for 10 min to separate ether phase from the mixture. The extracted resveratrol and IS were dried by nitrogen and re-dissolved in the 100 μ L mobile phase. The amount of resveratrol in plasma was analyzed using RP-HPLC. The resveratrol standard was prepared ranging from 0.023 – 1.5 μ g/mL ($R^2 \geq 0.99$). Linearity, accuracy, and precision values on the same day and between days at low, medium, and high concentration of resveratrol were within the acceptable limits ($R^2 \geq 0.99$). The resveratrol recovery from plasma was around 90%.

The resveratrol plasma concentration was plotted against time. The pharmacokinetic analysis was performed using the DAS software. The following parameters were estimated: the peak plasma concentration (C_{max}), the area under the curve (AUC), and the half-life in the terminal phase ($t_{1/2}$). The relative bioavailability (Fr, %) of resveratrol was estimated by the following equation:

$$Fr (\%) = AUC_{oral} / AUC_{iv} \times 100 \quad (6-4)$$

where AUC_{oral} and AUC_{iv} were the area under the curve of the oral administration and intravenous injection, respectively.

6.2.6.2 Determination of *in vivo* hepato-protective activity

- ***Experimental design***

For the hepatotoxicity study, CCl₄ was used to induce acute liver damage according to the method of Ikeda et al. with some modifications (Ikeda, et al., 2008). Wistar rats (300 - 350 g) were randomly divided into four groups (n=6 /group): (i) & (ii) rats were given by gavage with distilled water for three days; (iii) & (iv) rats were given by gavage with Free-resveratrol (resveratrol-suspension, 20 mg/kg resveratrol dissolved in water) or NP-100S (equal to 20 mg/kg resveratrol) for 3 days (3 times/day). On day 4, group (i) was treated with olive oil (2.5 mL/kg), and all other groups were treated with a single dose of 20% CCl₄ in olive oil (2.5 mL/kg) by intraperitoneal injection. All rats were sacrificed after 24 h to collect blood and liver tissue for observation. Blood samples were centrifuged at 3000 rpm for 10 min to separate the plasma. Liver tissues were weighted and homogenized with 0.9% saline solution in the proportion of 1:1 (w/v) liver/saline.

- ***Biochemical analysis***

The enzymatic activities of serum aspartate aminotransferase (AST) and alanine aminotransferase (ALT) were determined using a commercial kit (Biosino, Bio-technology and Science Inc., Beijing, China).

- ***Catalase activity***

The homogenized liver samples were centrifuged at 5000 rpm for 10 min at 4°C, and the supernatant was diluted 2 times and applied for determination of catalase activity (CAT). In a brief, 50 µL of samples were mixed with 650 µL 50 mM PBS (pH 7.0) and then added to a quartz cuvette. Hydrogen peroxide (0.3 mL, 20 mM) was used as substrate and added in the cuvette, followed by measuring absorbance immediately using spectrophotometer at 240 nm. Enzymatic activity was expressed as U/min/mg protein according to the method described by Aebi with some modifications (Aebi, 1984).

- ***Determination of reduced glutathione***

The homogenized liver samples were centrifuged at 5000 rpm for 10 min at 4°C, and the supernatant was diluted two times and applied for determination of hepatic glutathione content (GSH). GSH was determined by using 5,5-dithiobis (2-nitrobenzoic acid) (DTNB) (Shim et al., 2010). In a brief, 0.5 mL of 4% sulfosalicylic acid was mixed with 0.5 mL sample supernatant followed by centrifugation at 3000 rpm (~4000 g) for 10 min. Then 2 mL of 0.1M PBS were mixed with 0.5 mL supernatant, and 10 µL of 0.01M DTNB were added in the mixture. After 15 min, the absorbance of the mixture was measured at 412 nm. GSH content was determined through a standard curve (commercial reduced glutathione) and expressed as micromoles/g of protein.

- ***Determination of antioxidant activities***

The homogenized liver samples were centrifuged at 5000 rpm for 10 min at 4°C, and the supernatant was applied for determination of content of reactive oxygen species (ROS) in liver tissue according to the method of Llacuna with modifications (Llacuna et al., 2009). In a brief, 100 µL supernatant of liver homogenate were added to 900 µL 50 mM PBS (pH 7.0). Then 50 µL of 100 µM H₂DCF-DA were added to 950 µL of this solution. The mixture (150 µL) was transferred to black 96-well microplate and incubated for 4 h at room temperature in dark. The absorbance was measured by a fluorescence reader at an excitation of 485 nm and an emission of 530 nm.

- ***Pathological histology***

Liver tissues were fixed with 4% formaldehyde followed by embedding in paraffin. Then the samples were stained with hematoxylin and eosin (Shanghai Rui Yu Biological Technology Co. Ltd., Shanghai, China) and examined with a DMI4000D microscope (Leica Microsystems, Wetzlar, Germany).

6.2.7 Statistical analyses

All experiments were performed at least in triplicate. Results were expressed as mean ± standard deviation. Statistical analysis by means of one-way analysis of variance (ANOVA) were performed, followed by the Tukey test. A probability of $p < 0.05$ was considered to be statistically significant.

6.3 Results and discussion

6.3.1 Characterization of resveratrol-loaded OPI-shellac nanoparticles

The OPI molecules were dissociated from hexamers to monomers and the active side chains were exposed during the oat protein pre-heating treatment. These active side chains allowed conjugation of OPI with resveratrol to form OPI-resveratrol complex granules via either primary amino groups or sulfhydryl groups through non-covalent interactions (Weyermann, Lochmann, Georgensa, & Zimmer, 2005; Acharya, Sanguansri, & Augustin, 2013). In the previous work, it was found that moderate interactions between OPI and shellac were driven by hydrophobic interactions and hydrogen bonding at pH 8 as revealed by ITC and FTIR results (Chapter 4). Thus in this work, the resveratrol-loaded OPI-shellac network structure was formed by introducing the resveratrol-OPI complex into the shellac solution at pH 8. This formation was followed by the addition of CaCl_2 to further reinforce the network when both OPI and shellac were crosslinked by calcium.

As shown in Fig. 6-1, well dispersed spherical nanoparticles were successfully prepared, which showed relatively narrow size distribution as reflected by a PDI value of 0.41-0.47, except for the sample NP-0S without shellac showing a PDI value of 0.62. Since the high PDI indicates that nanoparticles had low homogeneity in size distribution (Dragicevic-Curic, Gräfe, Gitter, Winter, & Fahr, 2010), the decreasing of PDI of NP-50S, NP-100S and NP-200S suggested that the particle size distribution became more homogenous as the shellac concentration increased.

Table 6-1. Encapsulation capacity (EC), encapsulation efficiency (EE), size, polydispersity index (PDI), zeta-potential and surface hydrophobicity of resveratrol-loaded OPI-shellac NPs.

Sample	EC%	EE%	Size (nm)	PDI	Zeta-potential (mV)	Surface hydrophobicity
NP-0S	1.62±0.1c	59.99±3.87d	322.73±18.45a	0.620±0.034a	-35.45±0.37d	0.036±0.003a
NP-50S	1.79±0.06b	75.63±2.82c	176.53±15.81b	0.473±0.019b	-39.33±0.10c	0.017±0.001b
NP-100S	1.81±0.05a	85.12±1.93b	106.96±10.06c	0.410±0.014c	-43.45±1.07b	0.008±0.0004c
NP-200S	1.79±0.04b	90.57±2.42a	88.64±5.84d	0.405±0.008c	-48.08±0.77a	0.004±0.0001d

a-d Different letters following the means ± standard deviation indicate significant difference ($p < 0.05$).

As depicted in Table 6-1, particles without shellac (NP-0S) possessed a diameter of 323 nm and zeta potential of -35 mV. With the addition of shellac, the particle size significantly decreased to 176.5, 107.0, and 88.6 nm for NP-50S, NP-100S, and NP-200S, and the surface charge increased to -39.3, -43.5, and -48.1 mV, respectively. Shellac was negatively charged due to the abundance of carboxyl groups at pH 8, so the NPs surface charge increased when negatively charged shellac was introduced in the system. The strong surface charge prevented extra aggregation of OPI-shellac particles, resulting in NPs of smaller size and relatively uniform distribution. The Rose Bengal partitioning experiment was conducted to study the surface hydrophobicity of the resveratrol-loaded OPI-shellac NPs. For NP-0S, a highest surface

hydrophobicity (0.036) was observed. With the increasing shellac amount from 1.25 to 5% (w/v), the surface hydrophobicity significantly decreased from 0.017 to 0.004. This decrease further suggested development of hydrophobic interactions between OPI and shellac involving non-polar groups of protein chains (Chapter 5). Thus less non-polar groups were exposed outside. Meanwhile, the protection role of the network formed by shellac and OPI efficiently inhibited the diffusion of resveratrol into the aqueous medium during nanoparticle preparation, thus improving the encapsulation efficiency (EE) of NPs from 60.0 to 90.6% by increasing shellac amount from 0 to 5% (w/v). The encapsulation efficiency (EC) of NPs was in the range of 1.6-1.8%. Current daily intake of resveratrol is recommended as around 4 mg/day (Vang et al., 2011), while increasing this level may lead to improvement in human health (Davidov-Pardo & McClements, 2014). However, 2.5-6g doses per day of resveratrol can cause mild to moderate gastrointestinal symptoms (Brown et al., 2010). Based on the EC value, approximately 0.2-28 g OPI-shellac NPs will be required to provide around 4 mg – 1 g resveratrol per day, which is appropriate for oral applications.

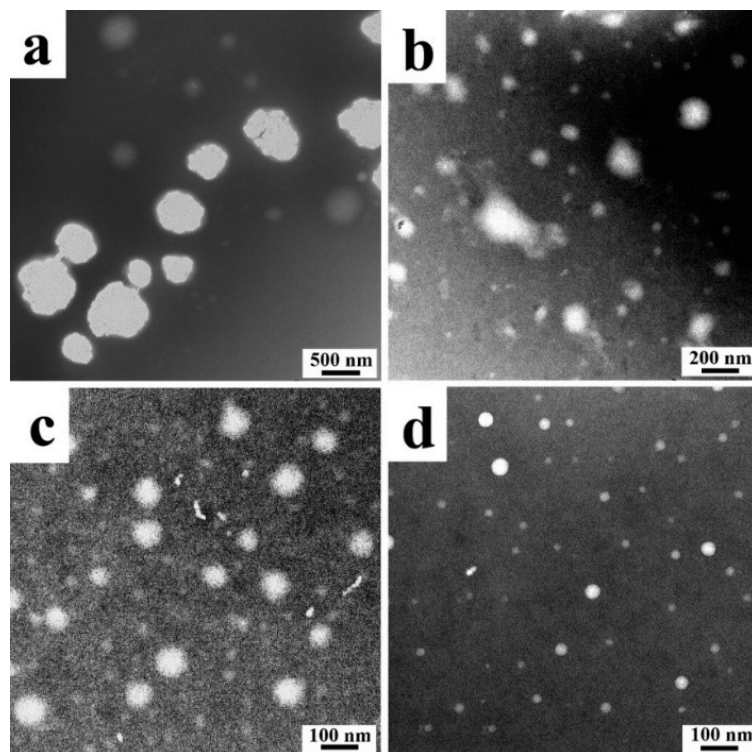


Fig. 6-1. TEM images of resveratrol-loaded OPI-shellac nanoparticles: (a) NP-0S; (b) NP-50S; (c) NP-100S; and (d) NP-200S.

6.3.2 *In vitro* release properties

The cumulative release profiles of resveratrol-loaded OPI-shellac NPs in the simulated gastro-intestinal pH without digestive enzymes are shown in Fig. 6-2a and 6-2b. Release in pH 2 buffer (Fig. 6-2a) was noticeably faster from NP-0S than other particles, where more than 30% of resveratrol was released during the first 2 h. With the addition of shellac, the moderate release of resveratrol was observed for NP-50S, the release of resveratrol decreased to less than 30% within 2 h. The NP-100S and NP-200S nanoparticles exhibited the lowest release rates. Around 12% of resveratrol was gradually released from NP-100S and NP-200S within the initial 2 h. In pH 7.4 buffer, the release rate of resveratrol was slower than in pH 2, and reduced release rate with

higher shellac concentration was observed (Fig. 6-2b). Although NP-0S showed the fastest release rate, less than 20% of resveratrol was released during the first hour and around 40% after eight hours. Steady release of resveratrol was observed for all the samples with approximately 30.88, 24.13, and 22.82% of resveratrol detected for NP-50S, NP-100S, and NP-200S, respectively, at the end of test after 8 h.

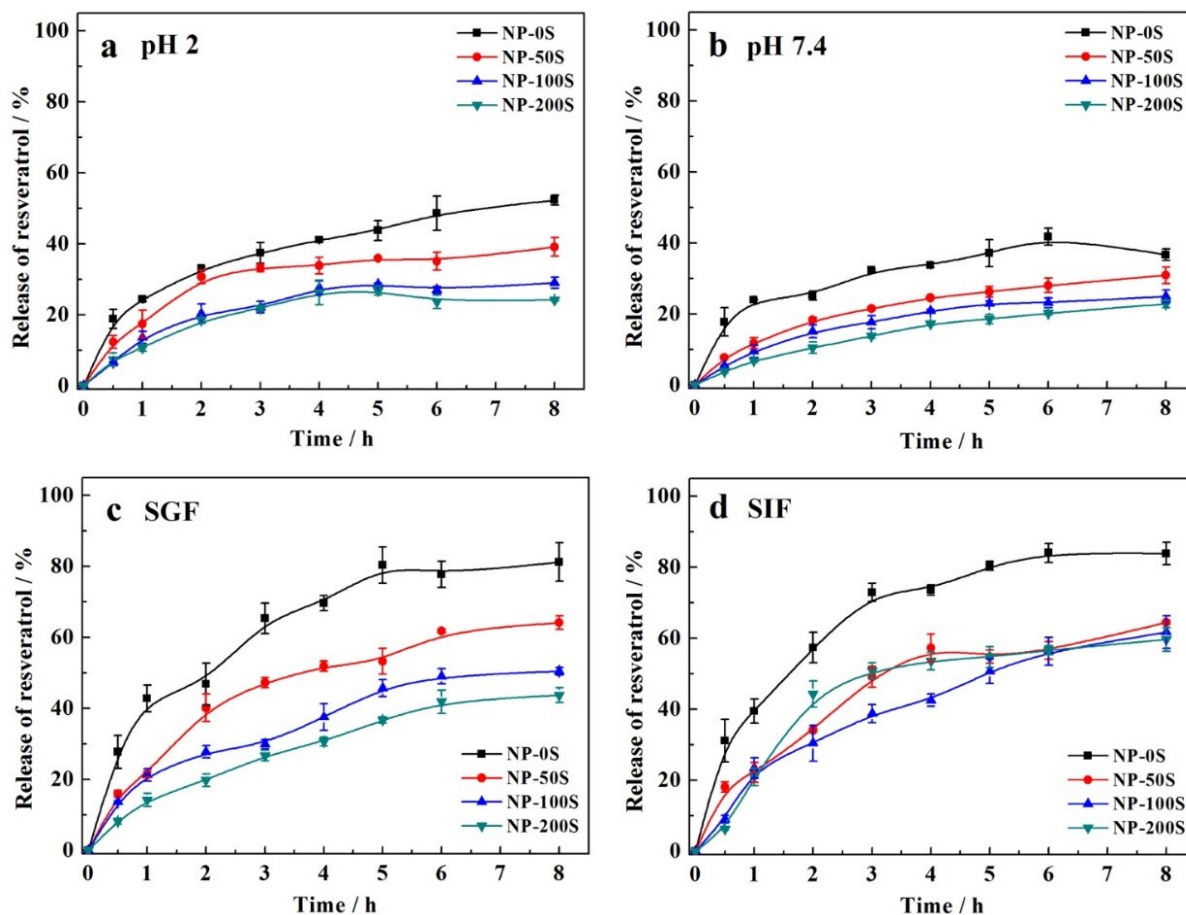


Fig. 6-2. Release profiles of resveratrol from fresh OPI-shellac nanoparticles in: (a) pH 2; (b) pH 7.4; (c) SGF; and d) SIF.

In general, the mechanism of drug release from a polymer matrix can be categorized in three ways, including diffusion from the non-degraded matrix, enhanced diffusion due to polymer matrix swelling, and release due to matrix degradation and erosion. The Korsmeyer-Peppas semi-empirical equation was applied to identify the mechanism of resveratrol release from OPI-shellac nanoparticles (Wang & Chen, 2014):

$$M_t / M_\infty = kt^n \quad (6-5)$$

where M_t / M_∞ is the fraction of the model molecule released after time t relative to the amount of model molecule released at infinite time, k is a constant, and n is the diffusional exponent. Inferences about the release mechanism are based on the fit of this equation to the model molecule release data through 60% dissolution and comparison of the value of n to the semi-empirical values for slab geometry reported by Peppas (1983), where $n \leq 0.50$ indicates Fickian diffusion, $0.50 < n < 1$ indicates non-Fickian transport, and $n = 1$ or higher indicates case II transport (Pandey et al., 2011). In pH 2 buffer (Fig. 6-2a), resveratrol release from NP-0S and NP-50S had n values within the ranges of 0.61-0.81 ($R^2 = 0.97-0.98$) during the first two hours, and then decreased to 0.32-0.48 ($R^2 = 0.96-0.98$) in the remaining time. This result indicates a two-stage release from NP-0s and NP-50S. At the beginning, more rapid resveratrol diffusion occurred due to the pH induced swelling of protein in the pH 2 buffer (Chen & Subirade, 2009). When the delivery systems reached equilibrium, the release followed a diffusion-controlled mechanism with a slow release rate. For NP-100S and NP-200S, resveratrol release had n values within the range of 0.45-0.46 ($R^2 = 0.97-0.98$) during 8 h in pH 2 buffer, which suggests a

diffusion-controlled release mechanism. The slow release at pH 2 during the first two hours was favorable which is the expected time for food product to pass from the stomach into the intestine. In such way, most of the payload could reach the small intestine. This slow release at pH 2 was expected because OPI-shellac interactions in networks played an important role to restrict the nanoparticle swelling at the gastric pH (Chapter 5), which limited the diffusion of resveratrol from NPs. In pH 7.4 buffer (Fig. 6-2b), resveratrol release from all the samples had n values within the range of 0.26-0.46 (0.96-0.99), indicating a diffusion-controlled release mechanism. At pH 7.4 most of the $-\text{COO}^-$ groups were involved in electrostatic interactions with Ca^{2+} (Chen & Subirade, 2009), thus the net negative charge in the NP networks was relatively weaker, thus restricted permeation of the buffer into the networks, resulting in slower release rates. The sustainable release in pH 7.4 could facilitate absorption of the encapsulated resveratrol in the small intestine.

The release behaviors of resveratrol from OPI-shellac NPs in the simulated gastro-intestinal fluids in the presence of the digestive enzymes were also evaluated. As shown in Figs. 6-2c and 6-2d, the release rates of resveratrol in SGF and SIF were faster than those in pH 2 and pH 7.4 buffers due to the enzyme induced degradation of the particle matrix. In SGF (Fig. 6-2c), NP-OS also showed the fastest release rate, where the burst release of resveratrol was observed in the initial two hours with 46% resveratrol detected in the release medium due to the protein network degradation by pepsin. With the addition of shellac, the burst release was efficiently controlled

and less than 20% of resveratrol was detected within two hours for NP-100S and NP-200S. This result indicated that the structure of the OPI-shellac nanoparticles, especially with the appropriate shellac concentration (NP-100S and NP-200S), had the ability to retard the resveratrol release in a simulated gastric environment in the presence of pepsin. This structure has provided opportunity to preserve most of the loaded resveratrol in the nanoparticle matrix for delivery to the intestinal tract. In SIF (Fig. 6-2d), at least 70% of resveratrol was released from NP-0S in the first three hours due to the protein network degradation by the enzymes in the pancreatin. The burst release phenomenon was also observed in the NP-50S and NP-200S samples with 50% resveratrol detected in the release medium after initial 3 h. In contrast, for NP-100S, the burst release was efficiently inhibited, and only 38.71% resveratrol was released after 3 h. Then the resveratrol was gradually released up to 61.67% in the following 5 h. The burst release in the initial 3 h in NP-50S and NP-200S could be due to the structure of OPI-shellac coating that was impacted by shellac amount. The lower amount of shellac (NP-50S, 1.25%, w/v) probably was not enough to form strong interactions with OPI. Therefore, the fabricated OPI-shellac coating could not efficiently resist digestion by digestive enzymes, which resulted in accelerated release. Too much shellac (NP-200S, 5%, w/v) could disrupt the integrity of OPI network and form a coarse coating structure, as revealed by the previous work (Chapter 5), leading to the penetration of digestive enzymes and increasing of the release rate of resveratrol. The purpose to designing OPI-shellac NPs was not only to protect the bioactive compound in harsh stomach conditions and deliver them into the small intestine, but also to allow them to be absorbed by the small intestine

and released in the physical target to improve the bioavailability and health benefits eventually. This process requires a slow and steady release of the loaded bioactive compounds from the nanoparticles, thus the nanoparticles and encapsulated resveratrol can be uptaken together by the small intestine.

6.3.3 *In vitro* cellular uptake and transport

The cell uptake of resveratrol-loaded OPI-shellac NPs was evaluated, since the efficient cellular uptake within cells is essential to develop effective delivery systems (Win & Feng, 2005). The confluent Caco-2 cell monolayer can form tight junction complexes and possess similar morphological, functional, and electrical properties to human small intestinal cells (Hidalgo, Raub, & Borchardt, 1989). Thus, Caco-2 cells have been widely used as an *in vitro* model to evaluate the uptake and transportation of nanoparticles across the small intestinal epithelium for drug delivery (He, Hu, Yin, Tang, & Yin, 2010). The toxicity of NPs was firstly measured by MTT assay. As shown in Fig. 6-3a, the cell viability was higher than 90% for all the nanoparticles at all the concentrations tested. This result indicates a good biocompatibility of OPI-shellac NPs even at a relatively high concentration of 0.25 mg/mL.

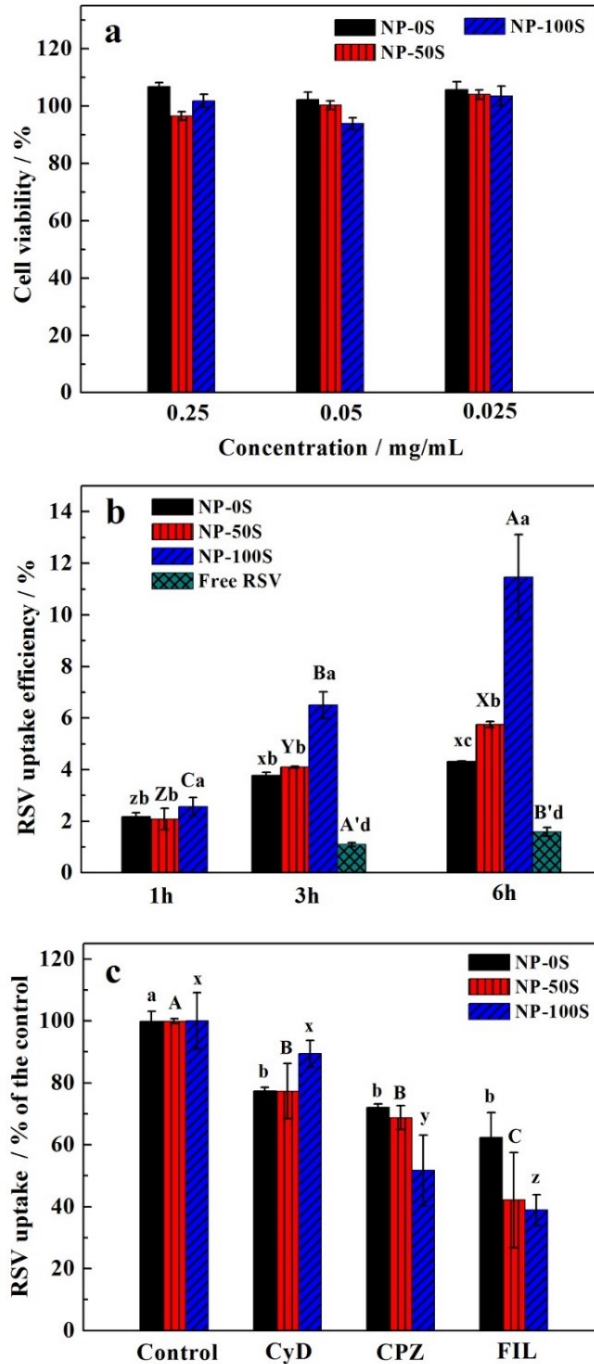


Fig. 6-3. (a) Cell viability of Caco-2 cells after incubation with OPI-shellac nanoparticles for 24h; (b) RSV uptake efficiency of nanoparticles and free-resveratrol (Free-RSV) (Significant difference between formulations was expressed as ^{a,b,c} at $p < 0.05$; significant difference between time within the same formulation was expressed as ^{A,B,C; X,Y,Z; x,y,z} at $p < 0.05$, respectively) and (c) uptake mechanism by Caco-2 cells. Difference between various inhibitor within same formulation was expressed as ^{a,b; A,B,C; x,y,z} at $p < 0.05$, respectively.

The quantitative data of cell uptake of resveratrol-loaded NPs analyzed by measuring the amount of resveratrol detected in cytoplasm are shown in Fig. 6-3b. Only 1.6% free resveratrol was detected in cells even after 6h of incubation. In contrast, the uptake of resveratrol encapsulated in NP-0S, NP-50S, and NP-100S increased by 2.7, 3.6, and 7.2 times, respectively, after 6 h of incubation. The uptake efficiency of nanoparticles was in the order of NP-100S > NP-50S > NP-0S where both the particle size and surface charge became larger. NP-200S was not included in the test as a burst release was observed for this sample in GIF. NP-100S was selected as a delivery system for further study due to the highest uptake efficiency. It was expected that nanoparticles with a smaller size had a higher uptake efficiency, since the larger size needs a stronger driving force and additional energy in the cellular internalization process (He et al., 2010). Usually nanoparticles with stronger negative charges have lower uptake efficiency due to the repulsion forces between the particles and the negatively charged apical membranes of Caco-2 cells. The effective uptake of the NPs with negative charge could be related to their surface carboxyl groups. Once the NPs had reached the cell membrane, carboxyl groups on the NP surface could overcome the repulsion and facilitate binding to membrane-bound receptors (e.g. clathrin-mediated uptake receptors) to activate the endocytosis machinery (Jiang et al., 2011; Shang et al., 2014). NP-100S showed the highest uptake partially due to the smallest size. Moreover, NP-100S contained more shellac with a higher amount of carboxyl groups that facilitated their uptake.

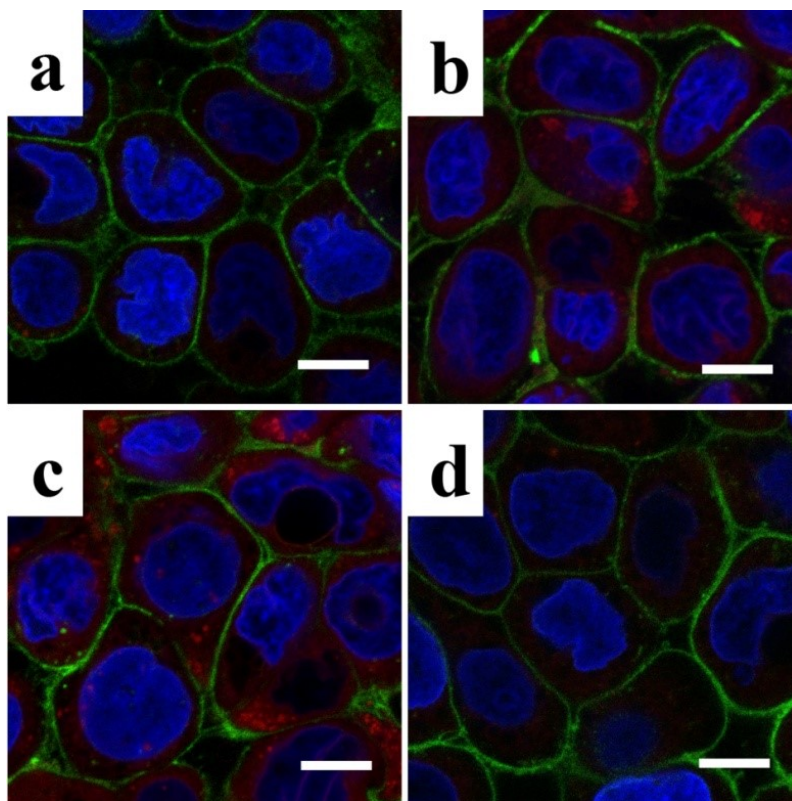


Fig. 6-4. CLSM images of Caco-2 cells incubated with NP-100S (0.25 mg/mL) at (a) 37 °C for 1 h; (b) 37 °C for 3 h; (c) 37 °C for 6 h; and (d) 4 °C for 6 h. Scale bar: 10 μm.

Fig. 6-4 shows confocal microscopic images of Caco-2 cells after incubation with NR-NP-100S at various incubation times and temperatures. It was reported that free Nile Red (NR) cannot be taken up by cells (Roger, Lagarce, Garcion, & Benoit, 2009), thus the intracellular fluorescence detected by CLSM was only due to the internalized NR-NPs rather than free NR or potential NR released from NPs. At the fixed NP concentration (0.25mg/mL) and temperature (37 °C), cells incubated with NR-NPs for 6h distinctly exhibited more intracellular fluorescence signal (Fig. 6-4c) compared to those for 1h (Fig. 6-4a) and 3h (Fig. 6-4b), which

was in agreement with the quantitative data that measured by RP-HPLC. Apart from time, the uptake of NR-NPs was also impacted by temperature. When incubation was performed at 4 °C for 6 h (Fig. 6-4d), the intracellular fluorescence signal was much lower than that at 37 °C (Fig. 6-4c). The low uptake degree at low temperature could be explained by the lower metabolic activity of the cells and the decreased fluidity of the cell membrane, which led to a possible restriction in the energy-dependent transcellular processes (He et al., 2010). Accordingly, the uptake mechanisms of OPI-shellac NPs by Caco-2 cells could be mainly energy-dependent endocytosis.

There are four different mechanisms involved in energy-dependent endocytosis: phagocytosis, clathrin-mediated endocytosis, caveolae-mediated endocytosis, and macropinocytosis (Conner & Schmid, 2003; Hillaireau & Couvreur, 2009). In order to further understand the type of energy-dependent endocytosis, uptake experiments were performed with the presence of different inhibitors (Fig. 6-3c). Cytochalasin D (CyD) is an inhibitor for macropinocytosis / phagocytosis through blocking the F-actin polymerization and membrane ruffling (Harley, Dance, Drasar, & Tovey, 1997). It has been reported that the Caco-2 cell line was considered to be non-phagocytic cells (Luo, Teng, Wang, & Wang, 2013), thus only macropinocytosis would be reflected using Caco-2 cell models. Chlorpromazine hydrochloride (CPZ) inhibits clathrin-mediated endocytosis by a mechanism that made clathrin unavailable for assembly at the cell surface, where adaptor complex (AP2) and clathrin are redistributed away from the plasma membrane (Jiang et al., 2012). Filipin III (FLI) blocks the caveolae-mediated

endocytosis pathway through forming filipin-sterol complex to disassemble the caveolae-1 coat (Jiang et al., 2012). The treatment of CyD led to around a 20% reduction in the resveratrol uptake for NP-0S and NP-50S, whereas only a 10% decrease of resveratrol uptake was observed for NP-100S. The presence of CPZ caused a significant decrease (~ 50%) in the cellular uptake of resveratrol-NP-100S, while around a 20-30% decrease of resveratrol was observed for NP-0S and NP-50S. The addition of FLI induced a remarkable decrease in resveratrol uptake in the NP-50S and NP-100S with around 60% reduction compared to the control, while approximately a 30% reduction of resveratrol was observed for NP-0S. In summary, the endocytosis of NP-50S and NP-100S appeared to be primarily regulated by caveolae-mediated endocytosis and clathrin-mediated endocytosis pathway, and the macropinocytosis route was involved as well. For NP-0S, there was no remarkable difference among each endocytosis pathway, suggesting that all three pathways played roles in cellular uptake. It has been reported that clathrin-mediated endocytosis leads to an intracellular pathway for particles around 90-150 nm where endosomes fuse with lysosomes to degrade their loaded contents. Caveolae-mediated endocytosis is the most promising pathway for the transport of vulnerable compounds into the enterocytes, as this route avoids the lysosomal degradation and is generally for particulates smaller than 60 nm. Macropinocytosis is typically exploited for the uptake of larger particulate materials but smaller than 5 μm , where the filling of the pocket occurs in a non-specific manner induced by electrostatic interactions, hydrophobic interactions, hydrogen bonding, among others. (des Rieux et al., 2006; Bareford & Swaan, 2007). The multiple endocytosis pathways for OPI-shellac

nanoparticles resulted in the high cellular uptake efficiency, thus may improve the overall intestinal transport of resveratrol. One of the primary pathways, caveolae-mediated endocytosis, for NP-50S and NP-100S, was especially suitable to protect sensitive bioactive compounds that avoided the lysosomal degradation.

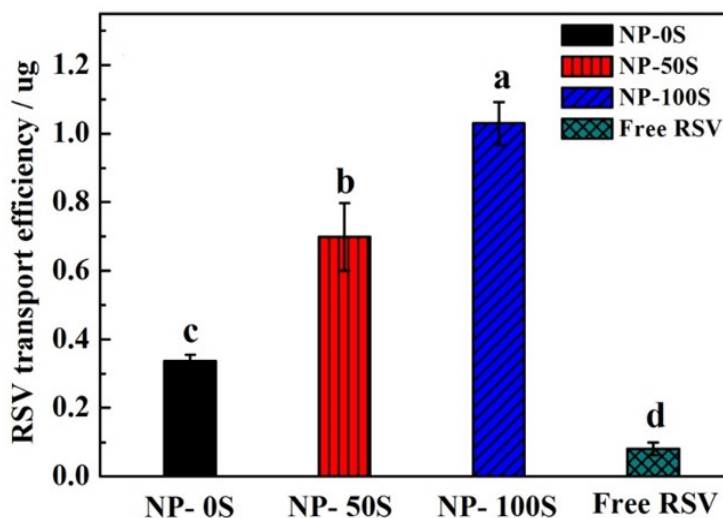


Fig. 6-5. Resveratrol transport efficiency across Caco-2 cell monolayer at 37 °C for 6 h. Data represent mean \pm standard deviation, $n = 3$. Different letters indicated significant difference ($p < 0.05$).

The transport efficiency of resveratrol-loaded OPI-shellac NPs to move across the Caco-2 cell monolayer from the apical chamber to the basolateral chamber was also investigated, where free resveratrol was applied as a control. As shown in Fig. 6-5, only 0.1 µg of free resveratrol was transported after six hours of incubation. When loaded with nanoparticles, the amounts of resveratrol that were detected in the basolateral chamber increased to 0.3, 0.7, and 1.0 µg for NP-0S, NP-50S, and NP-100S, respectively, which was 4.3, 8.8, and 12.9 times higher than free

resveratrol. The increase of transport efficiency of resveratrol could be attributed to the particle size and surface property, where NP-100S exhibited the highest transport efficiency. The high transport efficiency of OPI-shellac NPs allowed them to transport across the epithelial cells into the blood stream to release resveratrol to improve its bioavailability and health benefits.

6.3.4 *In vitro* cellular antioxidant activities

An imbalance between the production of reactive oxygen species (ROS) and the antioxidant defense mechanisms in human beings leads to critical damage to living organisms, such as neurodegenerative disease, diabetes, cardiovascular disease, and inflammatory disorders (Dixon & Stockwell, 2014). It has been reported that resveratrol had antioxidant activity that could strengthen endogenous cellular antioxidant mechanism, scavenge ROS directly, and prevent cells from exogenous-induced oxidative stress and increase extracellular GSH content (Quincozes-Santos et al., 2013). Resveratrol-loaded OPI-shellac NPs have demonstrated their ability to pass the Caco-2 cell monolayer that simulate the intestinal epithelial cells. Thus, they may enter the portal venous circulation and pass through the liver for hepatic metabolism. Chang liver cells exhibits cellular morphology similar to that of liver parenchymal cells, thus are usually used to simulate the liver cell reaction to the tested compounds (Senevirathne et al., 2012). The cytotoxicity of resveratrol-loaded NPs on Chang liver cells was tested by MTT assay and the cell viability was higher than 85% for all three NPs samples in the concentration range of 0.025-0.25 mg/ml (Fig. 6-6a), suggesting a good biocompatibility of OPI-shellac NPs with Chang liver cells.

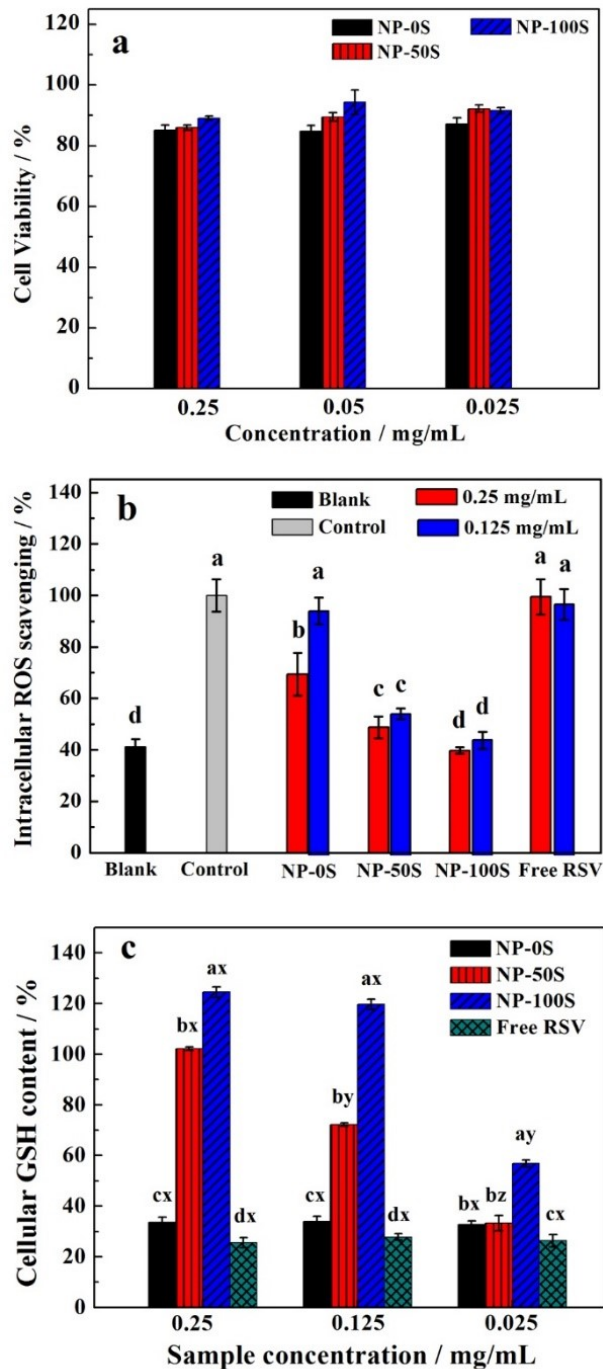


Fig. 6-6. (a) Cell viability of Chang liver cells incubated with OPI-shellac NPs for 24 h; (b) Quantification of intracellular ROS in DCFH-DA-labelled Chang liver cells. Values with different letters are significantly ($p < 0.05$) difference. and (c) Increase in intracellular glutathione content in Chang liver cells treated with nanoparticles and free-resveratrol (Free-RSV). Significant difference between formulations was expressed as ^{a,b,c,d} at $p < 0.05$; significant difference between concentrations within same formulation was expressed as ^{x,y,z} at $p < 0.05$.

The decomposition of H₂O₂ to hydroxyl radical in the presence of metal ions can disrupt the balance between production and removal of ROS in the exposed cells (Circu & Aw, 2010), so H₂O₂ was used to induce harmful cellular oxidative stress. Fig.6-6b shows the changes of the ROS content of Chang liver cells after incubation with resveratrol-loaded NPs at a concentration of 0.125 and 0.25 mg/mL and free-resveratrol (concentration equals to resveratrol in 0.125 and 0.25 mg/mL NPs). The cell group treated only with H₂O₂ was set as control and the ROS content was set as 100%, while the group without treatment of H₂O₂ and NPs was set as blank and the ROS content was measured as 40%. The cells treated with free-resveratrol exhibited a high ROS content that was similar to the control. This high ROS content could be related to its low uptake efficiency as revealed in cell uptake test. When the cells were incubated with 0.25 mg/mL NP-0S, the ROS content decreased to 69.4%. For NP-50S and NP-100S, the ROS content was remarkably reduced to 54.8 and 44.5% even at the nanoparticle concentration of 0.125 mg/mL. This result indicated that NP-50S and NP-100S were efficiently taken in Chang liver cells and the released resveratrol maintained its functionality to scavenge the hydroxyl radicals.

Intracellular glutathione (GSH), a major antioxidant molecule in cells, is closely related to oxidative stress. A decrease in GSH content causes increasing vulnerability to oxidative stress. Resveratrol can activate Nrf2, a transcription factor that regulates the heme oxygenase 1 (HO1), which modulates several detoxification genes that encode antioxidant proteins, such as GSH (Escartin et al., 2011). Therefore, the higher resveratrol delivered to the cells could result in more GSH biosynthesis. Fig. 6-6c shows the increase in GSH content of Chang liver cells after

incubation with resveratrol-loaded NPs at three different concentrations ranging from 0.025 to 0.25 mg/mL and free-resveratrol (concentration equals to resveratrol in 0.025, 0.125, and 0.25 mg/mL NPs). The cell group without treatment of NPs was set as control and the results were calculated as the percent increase in GSH content compared to the control. The free- resveratrol exhibited minimum GSH value of around 25%, and there was no significant difference among free-resveratrol sample with different concentrations. The cellular GSH contents treated with resveratrol-loaded NP-0S were slightly higher than those of free-resveratrol and increasing NP-0S concentrations did not significantly improve the cellular GSH contents, which might be also attributed to the low cellular uptake of NP-0S. It was worth noting that, for NP-50S and NP-100S, the GSH contents were remarkably raised with the increase of nanoparticle concentration, and reached 124.5% when treated with 0.25 mg/mL NP-100S. This further indicates the efficiency of NP-100S to improve bioactivities of resveratrol. Therefore, NP-100S was chosen for the *in vivo* tests.

6.3.5 *In vivo* pharmacokinetic studies in Wistar rats

Due to the desirable release profile in the simulated gastro-intestinal fluids, high uptake and transport efficiency, and strong antioxidant activities in cellular model, NP-100S was chosen as the optimum formulation to encapsulate and deliver resveratrol for *in vivo* test. Pharmacokinetic studies were performed to evaluate the improvement of resveratrol oral absorption by NP-100S, and NP-0S was employed for comparison. Fig. 6-7 shows the plasma concentration-time profiles

of resveratrol after intravenous or oral administration to rats at a single dose of 20 mg/kg. The main pharmacokinetic parameters are summarized in Table 6-2.

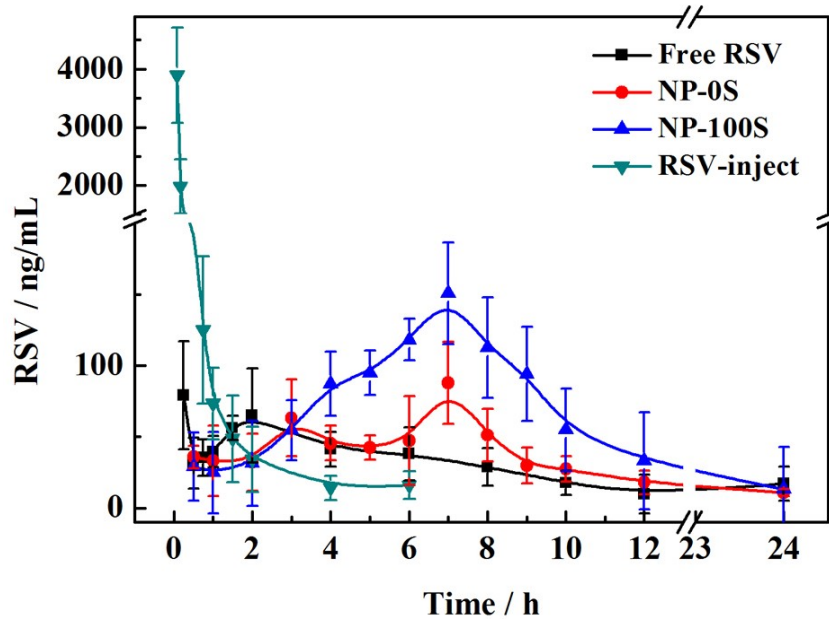


Fig. 6-7. Resveratrol plasma concentration versus time after a single administration at a dose of 20 mg/kg. RSV-inject: intravenous administration of resveratrol; Free-RSV: oral administration of resveratrol suspension; NP-0S and NP-100S: resveratrol-loaded OPI-shellac NPs.

Table 6-2. Pharmacokinetic parameters of resveratrol (RSV) obtained after the administration of the different formulations tested at a dose of 20 mg/kg.

	Route	AUC (ug/L*h)	C _{max} (ug/L)	t _{1/2} (h)	Fr (%)
RSV-inject	iv	1275.8 ± 215.1 a	3697.2 ± 448.6 a	1.5 ± 0.5 d	100.00
Free-RSV	oral	334.2 ± 67.6 d	90.9 ± 28.0 c	4.1 ± 1.9 c	26.19
NP-0S	oral	648.1 ± 108.2 c	92.7 ± 42.3 c	5.7 ± 1.9 b	50.80
NP-100S	oral	923.4 ± 182.0 b	136.2 ± 21.1b	6.3 ± 1.7 a	72.38

RSV-inject: intravenous administration of resveratrol; Free-RSV: oral administration of resveratrol suspension; NP-0S and NP-100S: resveratrol encapsulated in OPI-shellac NPs; AUC: area under the curve; C_{max}: peak plasma concentration; t_{1/2}: half-life of the terminal phase; and Fr: relative oral bioavailability. Different letters following means ± standard deviations indicate significant difference (*p* < 0.05).

The intravenous administration of resveratrol solution in ethanol/Kolliphor® EL (1:1, v/v) (resveratrol-inject) was set as positive control, while the oral administration of resveratrol suspension (free-resveratrol) was used as negative control. For the intravenous administration, the resveratrol concentration in plasma decreased rapidly during the first two hours. The peak plasma concentration (C_{max}) of resveratrol was 3697.2 µg/L, while the area under the curve (AUC) and half-life of the terminal phase (t_{1/2}) were 1275.8 µg/L*h and 1.46 h, respectively. After oral administration of resveratrol suspension, the resveratrol plasma concentration reached a maximum value of 90.9 µg/L after 15 min, and a second peak was observed after 2 h. The plasma levels of resveratrol decreased gradually within 24 h post-administration. Although the t_{1/2} was prolonged to 4.1, the AUC decreased to 334.2 µg/L*h compared to resveratrol-inject. Such a

decrease was directly related to the extensive metabolism of resveratrol (Wenzel & Somoza, 2005) to generate glucuronide and sulfate derivatives, which decreased the circulating level of free resveratrol and facilitated the excretion of metabolite by the kidneys via the urine (Walle, Hsieh, Delege, Oatis, & Walle, 2004). When resveratrol was loaded in NP-0S, the C_{max} slightly increased to 92.7 $\mu\text{g/L}$, and the AUC and $t_{1/2}$ rose remarkably to 648.1 $\mu\text{g/L}\cdot\text{h}$ and 5.7 h, respectively, compared to free-resveratrol. Through modification of nanoparticles with shellac (NP-100S), the amount of resveratrol in the plasma increased during the first 7 h until reaching a maximum, and then decreased gradually in the following 17 h. The AUC, C_{max} , $t_{1/2}$ and relative oral bioavailability (Fr%) of resveratrol delivered by NP-100S were significantly higher than that reached by the free-resveratrol and NP-0S. Notably, the $t_{1/2}$ of resveratrol in NP-100S was 4.3 times higher than the intravenous administration of resveratrol solution, which ensured the prolonged drug residence and longer absorption time in the gastro-intestinal (GI) tract. The improved bioavailability of resveratrol delivered by NP-100S was attributed to its small size and surface carboxyl group that allowed efficient internalization by cells and transportation from intestinal epithelium into circulation. The sustainable release of resveratrol from NP-100S in the intestinal environment also contributed to the improved oral bioavailability. Many strategies have been proposed to improve resveratrol absorption. For example, resveratrol loaded in methylcellulose and Tween 80 nanoparticles showed oral bioavailability of close to 30% after the administration of a single dose of 50 mg/kg in rats (Kapetanovic, Muzzio, Huang, Thompson, & McCormick, 2011). More recently, the oral bioavailability of resveratrol loaded in either Eudragit

or chitosan/lecithin nanoparticles was 39 and 61%, respectively, after the administration of a dose of 50 mg/kg (Oganesyan, Miroshnichenko, Vikhrieva, Lyashenko, & Leshkov, 2010). The zein based nanoparticles offered prolonged levels of resveratrol in plasma and increased oral bioavailability to around 50% (Penalva et al., 2015). In our study, the oral bioavailability of resveratrol was 72.4% when encapsulated in NP-100S, thus the newly developed NPs offer a sustained and prolonged resveratrol level in plasma.

6.3.6 Hepatoprotective effect

Oxidative stress and severe inflammatory response are major mechanisms of hepatotoxicity (Jaeschke, 2011). The beneficial effects and protective action of resveratrol in animal models of hepatic damage have been reported (Bishayee, Darvesh, Politis, & McGory, 2010; Sener et al., 2006). Based on the above results, it would be interesting to evaluate the capacity of resveratrol-loaded nanoparticles against hepatotoxicity. CCl₄ was used as a toxicant to induce hepatotoxicity in rats. High serum alanine aminotransferase (ALT) and aspartate aminotransferase (AST) levels are commonly found in hepatic disease. ALT and AST as indicators of hepatic functions were analyzed and the results are shown in Fig. 6-8a. The normal range of ALT and AST is 19-48 and 63-175 U/L, respectively, for rats (Giknis & Clifford, 2008). The ALT and AST levels in the control group (CCl₄-induced liver damage without treatment of resveratrol) significantly increased to around 400 U/L compared to the blank (animals without CCl₄ treatment) ($P < 0.05$), indicating a severe hepatotoxicity. The free-resveratrol group lowered

the ALT and AST levels, while the resveratrol encapsulated in NP-100S exhibited remarkable protective effect and reduced the ALT and AST levels in rats to the values similar to the blank.

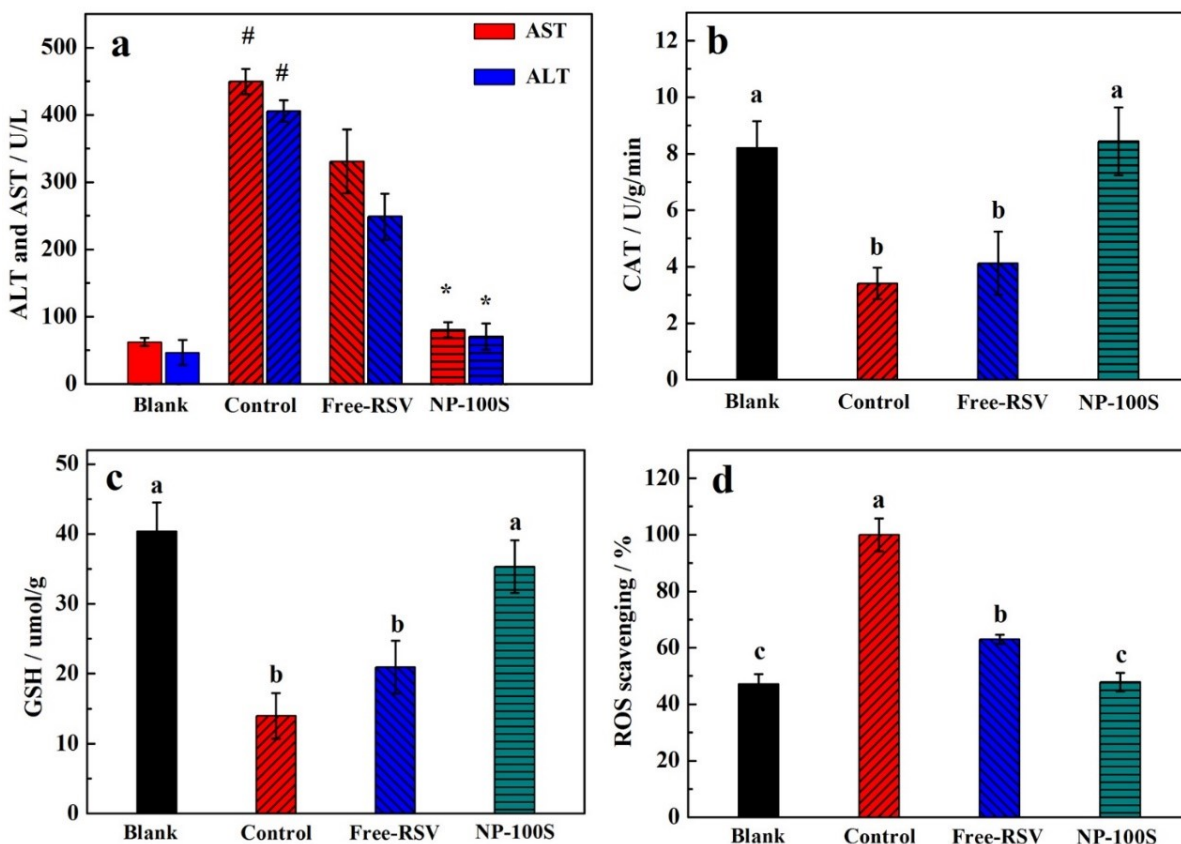


Fig. 6-8. (a) Effects of resveratrol treatment (20 mg/kg) on serum aspartate aminotransferase (AST) and alanine aminotransferase (ALT) levels in 20% CCl₄ (in olive oil 2.5 mL/kg) induced liver injury. Each column represents the mean of 6 animals, # significant difference from blank ($p < 0.01$), * significant difference from control ($p < 0.01$) and Free-resveratrol (Free-RSV). Effects of resveratrol treatment (20 mg/kg) on (b) catalase (CAT), (c) glutathione (GSH), and d) ROS levels in 20% CCl₄ (in olive oil 2.5 mL/kg) induced liver injury. Different letters indicated significant difference ($p < 0.05$) between each group.

The impacts of resveratrol on catalase (CAT), cellular glutathione (GSH), and ROS contents were also evaluated (Fig. 6-8b, 6-8c, and 6-8d). CAT and GSH had a protective effect against oxidative damage, which depleted in states of oxidative stress (Tung et al., 2009). ROS as indicator for oxidative stress were rapidly overproduced with CCl₄ induced hepatotoxicity. After CCl₄ administration, both CAT and GSH levels (3.4 ± 0.6 U/g/min and 13.9 ± 3.3 μ mol/g) in the liver significantly decreased compared to the blank (8.2 ± 0.9 U/g/min and 40.4 ± 4.2 μ mol/g) (Fig. 6-8b and 6-8c). Pretreatment of rats with resveratrol-loaded NP-100S significantly reversed the CCl₄-induced CAT activity reduction and GSH depletion (8.4 ± 1.2 μ mol/g and 35.3 ± 3.8 U/g/min), which were similar to the blank and higher than free-resveratrol group. At the same time, resveratrol-loaded NP-100S successfully prevented the CCl₄-induced increase of ROS content. Our studies demonstrated that pretreatment with resveratrol-loaded NP-100S could significantly reduce the leakage of AST and ALT from dying hepatocytes, decrease the amount of ROS, and maintain antioxidant enzyme activities (CAT and GSH) to prevent CCl₄-induced hepatotoxicity. The histopathological observation of the liver tissues after treatment with various formulations was also conducted and the results are shown in Fig. 6-9. Fatty accumulation was clearly observed in the livers of control sample (Fig. 6-9b, treated with CCl₄ only), but was rarely found in blank (Fig. 6-9a, without CCl₄ treatment). The pre-treatment with NP-0S was not sufficient to prevent the fatty accumulation, and microvesicular steatosis appeared in Fig. 6-9c. Importantly, NP-100S was able to stop the fatty accumulation and reduce the hepatic lesions (Fig.

6-9d). This observation further proves the protective efficiency of resveratrol-loaded NP-100S against the development of CCl₄-induced liver steatosis.

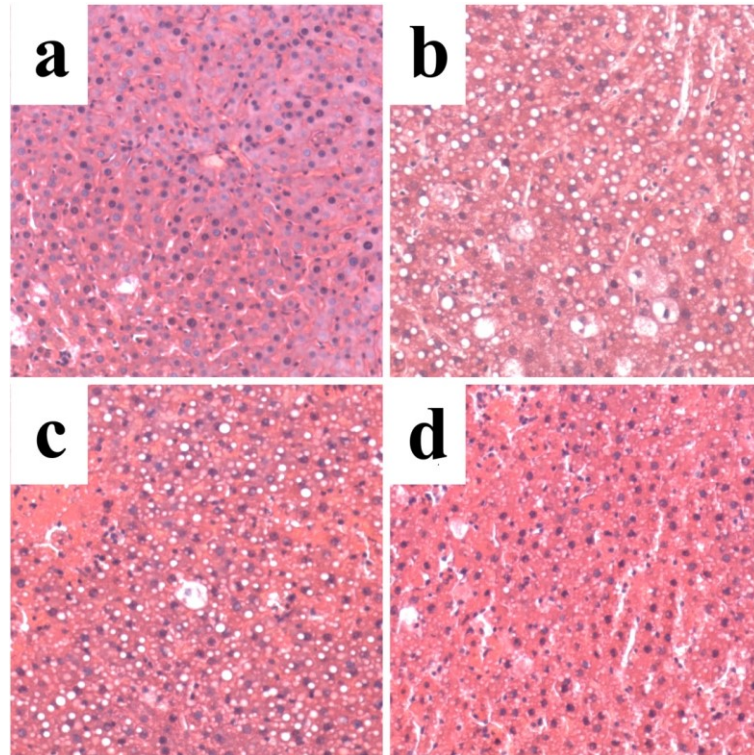


Fig. 6-9. Liver histological sections of rats from (a) blank; (b) control; (c) Free-resveratrol (Free-RSV); and (d) NP-100S groups.

Resveratrol has demonstrated beneficial effects for hepatic injury in animal models (Bishayee et al., 2010). The dosage of resveratrol used for hepatoprotective varied from 10mg/kg to 5g/kg (Bishayee et al., 2010). However, for the dosage with low resveratrol concentration, intraperitoneal or intravenous injection was required, and resveratrol was usually dissolved in

organic solvent (e.g. DMSO) that had negative effects on health. For oral administration, the concentration of resveratrol (100mg/kg – 5g/kg) used in previous studies was usually much higher than those for intraperitoneal or intravenous injections. The formulation of NP-100S improved the dissolution properties of resveratrol, which also significantly reduced the dosage resveratrol for health benefits by oral administration. Moreover, the resveratrol could be delivered by NPs into the bloodstream as demonstrated by pharmacokinetic studies to protect liver tissue. The hepatoprotective effect of resveratrol-loaded NP-100S were comparable with nanoparticle systems that prepared with synthetic polymers (e.g. PVA) in terms of reducing oxidative stress (Lee et al., 2012; Singh, Ahmad, Ahmad, Iqbal, & Ahmad, 2016).

6.4 Conclusions

Resveratrol-loaded OPI-shellac NPs were firstly prepared by cold-set gelation methods. The shellac and OPI together protected core materials under harsh stomach conditions and maintained slow release rate of resveratrol under small intestine conditions. The optimized sample NP-100S with a size of ~100 nm could be internalized by Caco-2 cells with high uptake efficiency mainly through CvME and CME pathway. It could also transport across Caco-2 cell monolayers that simulated the small intestine epithelium. The encapsulated resveratrol demonstrated excellent antioxidant activities in the cellular model as reflected by significantly reduced reactive oxygen species content and increased intracellular glutathione content. The *in vivo* study using the rat model indicates that the $t_{1/2}$ of resveratrol by oral administration was six times higher than that of

the injected free resveratrol, and the oral bioavailability was significantly improved from 26.2 to 72.4% for NP-100S. Resveratrol-loaded NP-100S also prevented the hepatotoxicity induced by CCl₄ by reducing the leakage of AST and ALT from dying hepatocytes, decreasing the amount of ROS, and maintaining antioxidant enzyme activities (CAT and GSH). The newly developed OPI-shellac NPs exhibit good protection and delivery properties, which have great potential to be used as a delivery system to improve bioavailability and health benefits of bioactive compounds as exemplified for resveratrol.

Chapter 7

Summary, conclusions and suggestions for future research

7.1 Summary and conclusions

Gelation plays an important role in food applications of proteins as it provides texture and mechanical support in foods. Gelatin, egg white and whey proteins are widely used as gelling agents in the food industry, particularly in meat and dairy-based products. Proteins from plant sources have attracted increasing interest by both academic and industry researchers due to health, religious and economic cost reasons. However, plant proteins are normally considered inferior to animal proteins in terms of gelling properties. The plant protein gel formation mechanisms were studied in this research, so that molecular strategies were developed to fabricate plant protein gels with improved mechanical properties for food applications. Protein from canola and oat are specifically focused on, as these are core crops in western Canada waiting for exploration of their full value.

Firstly, the gelling properties and formation mechanisms of thermally-induced canola protein gels were investigated over the broad range of pH (5 to 11) and processing temperatures (80 to 120 °C) involving two canola protein fractions, CP1 and CP2 with napin and cruciferin as major components, respectively (Chapter 3). CP1 and CP2 exhibited different thermal and gelling properties due to their distinct molecular weights and amino acid compositions. At a lower heating temperature and pH, protein denaturation without splitting of disulfide bonds produced a

randomly aggregated particulate fractal microstructure, which was mainly stabilized by hydrophobic interactions. At a high heating temperature and pH, new gels with a macro-porous dense wall structure and significantly improved mechanical properties were prepared due to the split of inter- and intra-chain disulfide bridges so as to facilitate the establishment of bridges between the interaction points on molecular chains. The results indicated that the mechanical properties of canola protein gels were closely related to the different types of gel network structures, which were induced by the degree of denatured canola protein structure and the development of molecular interactions through manipulating pH value and heating temperatures. Canola protein gels with various mechanical properties could be prepared through controlling the processing conditions, which were comparable to those of thermally-induced soy protein gels and legume protein gels.

Preliminary trials were conducted to develop canola protein gels via the cold-set method to explore new opportunities of food applications where heating is not preferred. However, cold-set gel of canola protein exhibits weak gelation properties and could only be formed at alkaline pH (e.g. pH higher than 9), which was not suitable for food applications. In contrast, cold-set oat protein gel prepared at neutral pH showed better mechanical properties than canola protein. Thus, the second study focused on oat protein cold-gelation using glucono- δ -lactone (GDL) as an acidification agent, which was new and worthy of investigation (Chapter 4). It was identified that cold-set oat protein isolate (OPI) gels possessed a percolating network structure and relatively

strong mechanical properties. Such structures were established by active OPI monomers as small building block units through abundant cross-linking points. At a low GDL concentration (3%), the pH reducing rate was low and the high electrostatic repulsive force controlled the association of the cold-set gelation method, offering promising opportunities to prepare the means to carry and protect sensitive nutraceutical compounds. The *in vitro* protection test demonstrated that these cold-set OPI gels could resist acidic conditions and pepsin digestion to a certain extent, enabling them to effectively protect both α -amylase enzyme activity and the viability of probiotics in harsh gastric conditions. The *in vitro* release experiment demonstrated that OPI gels had the capacity to prevent the premature release of riboflavin in simulated gastric fluids, but enabled the complete release of riboflavin in a simulated intestinal environment where they normally would be absorbed. A convenient and non-toxic method to prepare OPI gels with superior performance has been described. The results demonstrated that these gels had the potential to act as delivery vehicles for sensitive compounds in food applications.

In order to further improve the protection and delivery properties of oat protein gels, shellac was applied to combine with OPI in order to create oat protein-shellac based gels at near neutral pH and ambient temperature (Chapter 5). Moderate interactions between OPI and shellac happened with a binding constant (K_a) of $2.088 \times 10^3 \text{ M}^{-1}$ via hydrophobic interactions and hydrogen bonding, which allowed the formation of a mixed gel with good compatibility between OPI and shellac. The 18% (w/w) of shellac was critical to create solid beads with homogeneous

structure, smooth and integrated bead shells in a mainly OPI substrate. These structures could effectively restrict the swelling of the shell by the particular interaction between shellac and OPI and prevent premature diffusion of the contained riboflavin into the gastric buffer. Also, these structures could efficiently protect *L. acidophilus* and amylase against the harsh environment of simulated gastric fluid. When transferred to a simulated intestinal tract, riboflavin and *L. acidophilus* were released sustainably so as to promote their absorption and utilization in a living system. The OPI-shellac beads that were prepared using a simple extrusion method show good potential as a delivery system to improve the stability of sensitive bioactive compounds for food and biomedical applications.

The OPI-based nanoparticles (NPs) with size ranging from ~ 90 to 300 nm were subsequently designed in combination with shellac for the delivery of resveratrol (Chapter 6). The NPs exhibited regular spherical shapes and good encapsulation efficiency (60-90%). The optimized sample of NP-100S with a size of ~100 nm could be internalized by Caco-2 cells mainly through clathrin and caveolae-mediated endocytosis pathways, and the uptake and transport efficiency was 7.2 and 12.9 times higher than that of free-resveratrol. In addition, through decreasing reactive oxygen species content and increasing glutathione content, the encapsulated resveratrol demonstrated its excellent antioxidant activities in the cellular model. The further *in vivo* test in rat model demonstrated that the NP-100S significantly increased the oral bioavailability of resveratrol from 26.2 to 72.4%. Furthermore, pretreatment with

resveratrol-loaded NP-100S in rats also completely prevented the hepatotoxicity induced by CCl₄ by reducing oxidative stress and inhibition of liver steatosis. The well-designed OPI-shellac NPs can be used as potential delivery system of sensitive bioactive compounds to increase their bioavailability.

7.2 Significance of the research

This research has better elucidated the gel formation mechanisms of canola and oat proteins in controlling the gel mechanical properties. This was achieved by detailed characterizations of protein conformation and interactions during the gel formation process, and correlation of the generated information to gel microscopic structure and macroscopic properties. Such fundamental research has allowed development of strong oat and canola plant protein gels for food applications with the potential to replace gelling ingredients of animal resources.

Moreover, this research revealed a percolating network structure for cold-set oat protein gels, which was different from many other globular proteins but similar to gelatin. The polymer-like percolating structures were established by active OPI monomers as small building block units through abundant cross-linking points. This unique percolating structure could explain the superior mechanical properties of OPI gels compared to other plant protein gels.

In addition, novel OPI-shellac beads and nanoparticles were successfully prepared in this work. These systems were capable of protecting labile bioactive molecules (e.g. probiotics and enzymes) during storage and retard their release under harsh stomach condition (low pH and

pepsin), and then transferring and releasing them to the intestine for improved absorption or viability. The nanoparticle system significantly improved resveratrol bioavailability, demonstrated through *in vitro* and *in vivo* models. Thus, this research has laid a solid foundation for the development of new nutraceutical delivery systems using plant protein based gels.

Future collaboration with industry will lead to opportunities to develop novel functional foods to improve the health of Canadians and reduce health care costs. These applications can be transferred to pharmaceutical and cosmetic industries, because of the increasing consumer demand for natural gels of plant origin. Such vast potential will contribute significantly to the profitability and sustainability of the Canadian crop industry.

7.3 Recommendations for future work

Based on this research, canola and oat protein show good potential to be utilized as novel gelling agents for food applications. However, real food systems are complicated containing other food ingredients such as fat, polysaccharides, and small molecular ingredients (e.g. salt and sugar). All these may impact protein gelling properties. Thus, it is necessary to address how these factors impact canola and oat protein gelling properties in the next step, for food application development. Consequently, sensory evaluation should be conducted to assess consumers' acceptance to direct us in the rational incorporation of gelling agents (canola and oat protein) into foods to achieve desirable texture and flavor.

The extracted canola and oat proteins had around 80-88% protein purity. Other components included in the extracts could be soluble starch, lipid, phytic acid, among others. These components might impact the gelling properties of canola and oat protein. However, the influences of these factors were not addressed in the thesis. It would be beneficial to better understand the canola and oat protein gelling properties as impacted by such factors and their interactions, which not only contribute to the fundamental knowledge of the interactions of plant protein with other polymers, but also provide valuable information for food application development.

Oat protein-based micro- and nano-particles have been successfully prepared in this work. In order to develop new functional foods, it would be interesting to incorporate these oat protein-based particles into various real food systems, such as milk, juice, yogurt, etc to test their compatibility with real food products. In addition, the nutraceutical stability during food processing and storage should be evaluated, as well as the sensory quality.

Finally, it is interesting to explore the use of oat protein gels in non-food area such as pharmaceutical and biomedical applications due to its good biocompatibility and biodegradability. Gelatin with polymer-like percolating network structures is widely used for pharmaceutical applications. Analogue opportunity may exist for oat protein gels. This relies on a more fundamental understanding of oat protein network structure-function relationships.

References

- Acharya, D. P., Sanguansri, L., & Augustin, M. A. (2013). Binding of resveratrol with sodium caseinate in aqueous solutions. *Food Chemistry*, *141*, 1050-1054.
- Acosta, E. (2009). Bioavailability of nanoparticles in nutrient and nutraceutical delivery. *Current Opinion in Colloid and Interface Science*, *14*, 3-15.
- Aebi, H. (1984). Catalase *in vitro*. *Methods in Enzymology*, *105*, 121-126.
- Agriculture & Agri-Food Canada *Value-added soy protein*. [electronic resource]. Ottawa: Agriculture and Agri-Food Canada, c2009: 2009. <http://www.agr.gc.ca/eng/science-and-innovation/results-of-agricultural-research/technical-factsheets/archived-content-value-added-soy-protein/?id=1292966244688>. AAFC Publication No. 11018E.
- Aider, M., & Barbana, C. (2011). Canola proteins: composition, extraction, functional properties, bioactivity, applications as a food ingredient and allergenicity – A practical and critical review. *Trends in Food Science Technology*, *22*, 21–39.
- Almrhag, O., George, P., Bannikova, A., Katopo, L., Chaudhary, D., & Kasapis, S. (2013). Investigation on the phase behaviour of gelatin/agarose mixture in an environment of reduced solvent quality. *Food Chemistry*. *136*, 835-842.
- Aluko, R. E., & McIntosh, T. (2001). Polypeptide profile and functional properties of defatted meals and protein isolates of canola seeds. *Journal of the Science of Food and Agriculture*, *81*, 391–396.
- Allemann, E., Lerous, J. C., & Gurny, R. (1998). Polymeric nano- and microparticles for the oral delivery of peptides and peptidomimetics. *Advanced Drug Delivery Reviews*, *34*, 171-189.
- Ambalam, P., Raman, M., Purama, R. K., & Doble, M. (2016). Probiotics, prebiotics and colorectal cancer prevention. *Best Practice & Research Clinical Gastroenterology*, *30*, 119-131.
- Amri, A., Chaumeil, J. C., Sfar, S., & Charrueau, C. (2012). Administration of resveratrol: what formulation solutions to bioavailability limitations? *Journal of Controlled Release*, *158*, 182-193.
- Amsden, B. (1998). Solute diffusion within hydrogels. Mechanisms and models. *Macromolecules*, *31*, 8382-8395.

- Antonov, V. K. (1977). New data on pepsin mechanism and specificity. *Advances in Experimental and Medical Biology*, 95, 179-198.
- Augustin, M. A. (2003). The role of microencapsulation in the development of functional dairy foods. *Australian Journal of Dairy Technology*, 58, 1560160.
- Arbós, P., Arangoa, M. A., Campanero, M. A., & Irache, J. M. (2002). Quantification of the bioadhesive properties of protein-coated PVM/MA nanoparticles. *International Journal of Pharmaceutics*, 242, 129-136.
- Arifin, D. Y., Lee, L. Y., & Wang, C. H. (2006). Mathematical modeling and simulation of drug release from microspheres: implications to drug delivery systems. *Advanced Drug Delivery Review*, 58, 1274-325.
- Bandekar, J. (1992). Amide modes and protein conformation. *Biochimic et Biophysica Acta-Protein Structure and Molecular Enzymology*, 1120, 123-143.
- Banerjee, S., & Bhattacharya, S. (2012). Food gels: Gelling process and new applications. *Critical Reviews in Food Science and Nutrition*, 52, 334-346.
- Baranauskiene, R., Venskutonis, P. R., Dewettinck, K., & Verhe, R. (2006). Properties of oregano (*Origanum vulgare* L.), citronella (*Cymbopogon nardus* G.), and marjoram (*Majorana hortensis* L.) flavors encapsulated into milk protein-based matrices. *Food Research International*, 39, 413-425.
- Barbut, B., & Foegeding, E. A. (1993). Ca²⁺-induced gelation of pre-heated whey protein isolate. *Journal of Food Science*, 58, 867-871.
- Bareford, L. M., & Swaan, P. W. (2007). Endocytic mechanisms for targeted drug delivery. *Advanced Drug Delivery Reviews*, 59, 748-758.
- Beaulieu, L., Savoie, L., Paquin, P. & Subirade, M. (2002). Elaboration and characterization of whey protein beads by an emulsification/cold gelation process: application for the protection of retinol. *Biomacromolecules*, 3, 2239-2248.
- Bellan, L. M., Pearsall, M., Cropek, D. M., & Langer, R. (2012). A 3D interconnected microchannel network formed in gelatin by sacrificial shellac microfibers. *Advanced Materials*, 24, 5187-5191.
- Benseny-Cases, N., Klementieva, O., & Cladera, J. (2012). Chapter 3: In vitro oligomerization and fibrillogenesis of amyloid-beta peptides. *Subcellular Biochemistry*, 65, 53-74.

- Bell, L. N. (2001). In: R. E. C. Wildman (Eds.), *Handbook of Nutraceuticals and Functional Foods* (pp. 501-516). New York: CRC Press.
- Bernardos, A., Aznar, E., Coll, C., Martínez-Mañez, R., Barat, J. M., Marcos, M. D. et al. (2008). Controlled release of vitamin B2 using mesoporous materials functionalized with amine-bearing gate-like scaffoldings. *Journal of Controlled Release*, *121*, 181-189.
- Betz, M., Hörmansperger, J., Fuchs, T., & Kulozik, U. (2012). Swelling behavior, charge and mesh size of thermal protein hydrogels as influenced by pH during gelation. *Soft Matter*, *8*, 2477-2485.
- Bhatty, R. S., McKenzie, S. L., & Finlayson, A. J. (1968). The proteins of rapeseed (*Brassica napus* L.) soluble in salt solutions. *Biochemistry and Cell Biology*, *46*, 1191-1197.
- Bishayee, A., Darvesh, A. S., Politis, T., & McGory, R. (2010). Resveratrol and liver disease: from bench to bedside and community. *Liver International*, *30*, 1103-1114.
- Bouchemal, K., & Mazzaferro, S. (2012). How to conduct and interpret ITC experiments accurately for cyclodextrin-guest interactions. *Drug Discovery Today*, *17*, 623-629.
- Bourne, M. C. (2002). Food texture and viscosity: Concept and measurement. 2nd edition, New York: Academic Press.
- Brown, V. A., Patel, K. R., Viskaduraki, M., Crowell, J. A., Perloff, M., Booth, T. D., et al., (2010). Repeat dose study of the cancer chemopreventive agent resveratrol in healthy volunteers: safety, pharmacokinetics, and effect on the insulin-like growth factor axis. *Cancer Research*, *70*, 9003-9011.
- Brown, W. D., & Ball, R. C. (1985). Computer simulation of chemically limited aggregation. *Journal of Physics A: Mathematical and General*, *18*, L517-L521.
- Bruschi, M. L., Cardoso, M. L., Lucchesi, M. B., & Gremião, M. P. (2003). Gelatin microparticles containing propolis obtained by spray-drying technique: preparation and characterization. *International Journal of Pharmaceutics*, *264*, 45-55.
- Bryant, C. M., & McClement, D. J. (1998). Molecular basis of protein functionality with special consideration of cold-set gels derived from heat-denatured whey. *Trends in Food Science and Technology*, *9*, 143-151.
- Bryant, C. M., & McClements, D. J. (2000). Influence of NaCl and CaCl₂ on cold-set gelation of heat-denatured whey protein. *Journal of Food Science*, *65*, 801-804.

- Burgain, J., Gaiani, C., Linder, M., & Scher, J. (2011). Encapsulation of probiotics living cells: From laboratory scale to industrial applications. *Journal of Food Engineering*, *104*, 467-483.
- Burgess, S. R., Shewry, P. R., Matlashewski, G. J., Altosaar, I., & Mifflin, B. J. (1983). Characteristics of oat (*Avena sativa*) seed globulin. *Journal of Experimental Botany*, *34*, 1320-1332.
- Bushell, G. C., Yan, Y. D., Woodfield, D., Raper, J. & Amal, R. (2002). On techniques for the measurement of the mass fractal dimension of aggregates. *Advances in Colloid and Interface Science*, *95*, 1-50
- Byler, D. M., & Susi, H. (1986). Examination of the secondary structure of proteins by deconvolved FTIR spectra. *Biopolymers*, *25*, 469-487.
- Bysell, H., Månsson, R., Hansson, P., & Malmsten, M. (2011). Microgels and microcapsules in peptide and protein drug delivery. *Advanced Drug Delivery Reviews*, *63*, 1172-1185.
- Çakir, E., Daubert, C. R., Drake, M. A., Vinyard, C. J., Essick, G., & Foegeding, E. A. (2012a). The effect of microstructure on the sensory perception and textural characteristics of whey protein/ κ -carrageenan mixed gels. *Food Hydrocolloids*, *26*, 33-43.
- Çakir, E., & Foegeding, E. A. (2011). Combining protein micro-phase separation and protein-polysaccharide segregative phase separation to produce gel structure. *Food Hydrocolloids*, *25*, 1538-1546.
- Çakir, E., Khan, S. A., & Foegeding, E. A. (2012b). The effect of pH on gel structures produced using protein-polysaccharide phase separation and network inversion. *International Dairy Journal*, *27*, 99-102.
- Campbell, L. D., Eggum, B. Q., & Jacobsen, I. (1981). Biological value, amino acid availability and true metabolizable energy of low-glucosinolate rapeseed meal (canola) determined with rats and/or roosters. *Nutrition Reports International*, *24*, 791-797.
- Cavallieri, A. L. F., & da Cunha, R. L. (2008). The effects of acidification rate, pH, and ageing time on the acidic cold set gelation of whey proteins. *Food Hydrocolloids*, *22*, 439-448.
- Chabanon, G., Chevalot, I., Framboisier, X., Chenu, S., & Marc, I. (2007). Hydrolysis of rapeseed protein isolates: Kinetics, characterization and functional properties of hydrolysates. *Process Biochemistry*, *42*, 1419-1428.

- Chen, L., Du, Y., & Huang, R. (2003). Novel pH, ion sensitive polyampholyte gels based on carboxymethyl chitosan and gelatin. *Polymer International*, 52, 56-61.
- Chen, L. (2009). Protein micro/nanoparticles for controlled nutraceutical delivery in functional foods. In: D. J. McClements, & E. A. Decker (Eds), *Designing functional foods: Measuring and controlling food structure breakdown and nutrient absorption* (pp. 572-600). CRC Press, Woodhead Publishing Limited, New York, Washington, DC.
- Chen, L., Remondetto, G. E., & Subirade, M. (2006). Food protein-based materials as nutraceutical delivery systems. *Trends in Food Science and Technology*, 17, 272-283.
- Chen, L., Remondetto, G. E., Rouabhia, M., & Subirade, M. (2008). Kinetics of the breakdown of cross-linked soy protein films for drug delivery. *Biomaterials*, 29, 3750-3756.
- Chen, L., & Subirade, M. (2005). Chitosan/ β -lactoglobulin core-shell nanoparticles as nutraceutical carriers. *Biomaterials*, 26, 6041-6053.
- Chen, L., & Subirade, M. (2006). Alginate-whey protein granular microspheres as oral delivery vehicles for bioactive compounds. *Biomaterials*, 27, 4646-4654.
- Chen, L., & Subirade, M. (2009). Elaboration and Characterization of soy/zein protein microspheres for controlled nutraceutical delivery. *Biomacromolecules*, 10, 3327-3334.
- Cheow, W. S., & Hadinoto, K. (2013). Biofilm-like *Lactobacillus rhamnosus* probiotics encapsulated in alginate and carrageenan microcapsules exhibiting enhanced thermotolerance and freeze-drying resistance. *Biomacromolecules*, 14, 3214-3222.
- Cho, Y. H., Shim, H. K., & Park, J. (2003). Encapsulation of fish oil by an enzymatic gelation process using transglutaminase cross-linked protein. *Journal of Food Science*, 68, 2717-2723.
- Circu, M. L., & Aw, T. Y. (2010). Reactive oxygen species, cellular redox systems and apoptosis. *Free Radical Biology and Medicine*, 48, 749-762.
- Clark, A. H. (2006). Mixed biopolymer gelation: a route to versatile soft solids and complex gel microstructure, In: P. A. Williams, & G. O. Phillips (Eds.), *Gums and Stabilisers for the Food Industry 13* (pp. 170-184). Royal Society of Chemistry: Cambridge.
- Clark, A. H., Kavanagh, G. M., & Ross-Murphy, S. B. (2001). Globular protein gelation-theory and experiment. *Food Hydrocolloids*, 15, 383-400.

- Clark, A. H., Saunderson, D. H., & Suggett, A. (1981). Infrared and Laser-Raman spectroscopic studies of thermally-induced globular protein gels. *International Journal of Peptide Research and Therapeutics*, *17*, 353-64.
- Conner, S. D., & Schmid, S. L. (2003). Regulated portals of entry into the cell. *Nature*, *422*, 37-44.
- Cook, M. T., Tzortzis, G., Charalampopoulos, D., & Khutoryanskiy, V. V. (2012). Microencapsulation of probiotics for gastrointestinal delivery. *Journal of Controlled Release*, *162*, 56-67.
- Coppola, M., Djabourov, M., & Ferrand, M. (2012). Unified phase diagram of gelatin films plasticized by hydrogen bonded liquids. *Polymer*, *53*, 1483-1493.
- Coradini, K., Lima, F. O., Oliveira, C. M., Chaves, P. S., Athayde, M. L., Carvalho, L. M., et al. (2014). Co-encapsulation of resveratrol and curcumin in lipid-core nanoparticles improves their *in vitro* antioxidant effects. *European Journal of Pharmaceutics and Biopharmaceutics*, *88*, 178-185.
- Cordobes, F., Partal, P., & Guerrero, A. (2004). Rheology and microstructure of heat-induced egg yolk gels. *Rheologica Acta*, *43*, 184-195.
- Corona-Hernandez, R. I., Álvarez-Parrilla, E., Lizardi-Mendoza, J., Islas-Rubio, A. R., de la Rosa L. A., & Wall-Medrano, A. (2013). Structural stability and viability of microencapsulated probiotics bacteria: A review. *Comprehensive Reviews in Food Science and Food Safety*, *12*, 614-628.
- Croguennoc, P., Nicolai, T., Durand, D., & Clark, A. (2001). Phase separation and association of globular protein aggregates in the presence of polysaccharides: 2. Heated mixtures of native β -lactoglobulin and χ -carrageenan. *Langmuir*, *17*, 4380-4385.
- Cummings, C. L., Gawlitta, D., Nerem, R. M., & Stegermann, J. P. (2004). Properties of engineered vascular constructs made from collagen, fibrin, and collagen-fibrin mixtures. *Biomaterials*, *25*, 3699-3706.
- Czerner, M., Fasce, L. A., Martucci, J. F., Ruseckaite, R., & Frontini, P. M. (2016). Deformation and fracture behavior of physical gelatin gel systems. *Food Hydrocolloids*, *60*, 299-307.
- Czerner, M., Martucci, J., Fasce, L. A., Ruseckaite, R., & Frontini, P. M. (2013). Mechanical and fracture behavior of gelatin gels. 13th International Conference of Fracture. June 16-21.

- Dalgalarondo, M., Robin, J. M., & Azanza, J. L. (1986). Subunit composition of the globulin fraction of rapeseed (*Brassica napus L.*). *Plant Science*, *43*, 115–124.
- Davidov-Pardo, G., & McClements, D. J. (2014). Resveratrol encapsulation: Designing delivery systems to overcome solubility, stability and bioavailability issues. *Trends in Food Science and Technology*, *38*, 88-103.
- Dàvila, E., Parés, D., & Howell, N. (2007). Studies on plasma protein interactions in heat-induced gels by differential scanning calorimetry and FT-Raman spectroscopy. *Food Hydrocolloids*, *21*, 1144–1152.
- Desai, K. G. H., & Park, H. J. (2005). Recent developments in microencapsulation of food ingredients. *Drying technology*, *23*, 1361-1394.
- Derry, J. Investigating shellac: Documenting the process, defining the product. A study on the processing methods of shellac, and the analysis of selected physical and chemical characteristics. Master Thesis. 2012.
- Dickinson, E. (2003a). Hydrocolloids at interfaces and the influence on the properties of dispersed systems. *Food Hydrocolloids*. *17*, 25-39.
- Dickinson, E. (2003b). Colloidal aggregation: Mechanism and implications. In: E. Dickinson, & T. van Vlie (Eds.), *Food colloids, biopolymers and materials* (pp. 68–83). Cambridge: Royal Society of Chemistry.
- Dille, M. J., Draget, K. I., & Hattrem, M. N. (2015). The effect of filler particles on the texture of food gels. In: J. Chen, & A. Rosenthal (Eds.), *Modifying food texture, volume 1: Novel ingredients and processing techniques* (pp: 183-200). Elsevier Ltd.
- Dixon, S. J., & Stockwell, B. R. 2014. The role of iron and reactive oxygen species in cell death. *Nature Chemical Biology*, *10*, 9-17.
- Dobaczewski, M., Bujak, M., Zymek, P. Ren. G., Entman, M. L., & Frangogiannis, N. G. (2006). Extracellular matrix remodeling in canine and mouse myocardial infarcts. *Cell Tissue Research*, *324*, 475-488.
- Donato, L., Garnier, C., Novales, B., Durand, S., & Doublier, J. (2005). Heat-induced gelation of bovine serum albumin/low-methoxyl pectin systems and the effect of calcium ions. *Biomacromolecules*, *6*, 374-385.

- Dragicevic-Curic, N., Gräfe, S., Gitter, B., Winter, S., & Fahr, A. (2010). Surface charged temoprofin-loaded lexible vesicles: in vitro skin penetration studies and stability. *International Journal of Pharmaceutics*, 384, 100-108.
- Duconseille, A., Astruc, T., Quintana, N., Meersman, F., & Sante-Lhoutellier, V. (2015) Gelatin structure and composition linked to hard capsule dissolution: a review. *Food Hydrocolloids*, 43, 360-376.
- Elzoghby, A. O. (2013). Gelatin-based nanoparticles as drug and gene delivery systems: Reviewing three decades of research. *Journal of Controlled Release*, 172, 1075-1091.
- Escartin, C., Won, J. S., Malgorn, C., Auregan, G., Berman, A. E., Chen, P., et al. (2011). Nuclear factor erythroid 2-related factor 2 facilitates neuronal glutathione synthesis by upregulating neuronal excitatory amino acid transporter 3 expression. *The Journal of Neuroscience*, 31, 7392-7401.
- Ezhilarasi, P. N., Karthik, P., Chhanwal, N. & Anandharamakrishnan, C. (2013). Nanoencapsulation techniques for food bioactive components: A review. *Food and Bioprocess Technology*, 6, 628-647.
- Favaro-Trindade, C. S., & Grosso, C. R. (2002). Microencapsulation of *L. acidophilus* (La-05) and *B. lactis* (Bb-12) and evaluation of their survival at the pH values of the stomach and in bile. *Journal of Microencapsulation*, 19, 485-494.
- Figueroa-Gonzalez, I., Quijano, G., Ramirez, G., & Cruz-Guerrero, A. (2011). Probiotics and prebiotics: perspective and challenges, *Journal of the Science of Food and Agriculture*, 91, 1341-1348.
- Fizman, S. M., Pons, M., & Damásio, M. H. (1998). New parameters for instrumental texture profile analysis: Instantaneous and retarded recoverable springiness. *Journal of Texture Studies*, 29, 499-508.
- Forte, A. E., D'Amico, F., Charalambides, M. N., Dini, D., & Williams, J. G. (2015). Modelling and experimental characterization of the rate dependent fracture properties of gelatin gels. *Food Hydrocolloids*, 46, 180-190.
- Franz, J., Pokorova, D., Hampl, J., & Dittrich, M. (1998). Adjuvant efficacy of gelatin particles and microparticles. *International Journal of Pharmaceutics*, 168, 153-161.

- Funami, T. (2011). Next target for food hydrocolloid studies: Texture design of foods using hydrocolloid technology. *Food Hydrocolloids*, 25, 1904-1914.
- Furukawa, T., Ohta, S., & Yamamoto, A. (1980). Texture-structure relationship in heat-induced soy protein gels. *Journal of Texture Studies*, 10, 333-346.
- Galindo-Rodriguez, S., Allemann, E., Fessi, H., & Doelker, E. (2004). Physicochemical parameters associated with nanoparticle formation in the salting-out, emulsification-diffusion and nanoprecipitation methods. *Pharmaceutical Research*, 21, 1428-1439.
- Gan, C. Y., Cheng, L. H., & Easa, A. M. (2008). Evaluation of microbial transglutaminase and ribose cross-linked soy protein isolate-based microcapsules containing fish oil. *Innovative Food Science and Emerging Technologies*, 9, 563-569.
- Gan, Z., Zhang, T., Liu, Y., & Wu, D. (2012). Temperature-triggered enzyme immobilization and release based on cross-linked gelatin nanoparticles. *PloS One*, 7, e47154.
- Ganguly, K., Chaturvedi, K., More, U. A., Nadagouda, M. N., & Aminabhavi, T. M. (2014). Polysaccharide-based micro/nanohydrogels for delivery macromolecular therapeutics. *Journal of Controlled Release*, 193, 162-173.
- Gaowa, A., Horibe, T., Kohno, M., Sato, K., Harada, H., Hiraoka, M., Tabata, Y., & Kawakami, K. (2014). Combination of hybrid peptide with biodegradable gelatin hydrogel for controlled release and enhancement of anti-tumor activity in vivo. *Journal of Controlled Release*, 176C, 1-7.
- Garti, N. (2008). Delivery and controlled release of bioactives in food and nutraceuticals. Woodhead Publishing.
- de Geest, B. G., de Koker, S., Sukhorukov, G. B., Kreft, O., Parak, W. J., Skirtach, A. G. et al. (2009). Polyelectrolyte microcapsules for biomedical applications. *Soft Matter*, 5, 282-291.
- Gharsallaoui, A., Roudaut, G., Chambin, O., Voilley, A., & Saurel, R. (2007). Applications of spray-drying in microencapsulation of food ingredients: an overview. *Food Research International*, 40, 1107-1121.
- Ghodsvali, A., Khodaparast, M. H. H., Vosoughi, M., & Diosady, L. L. (2005). Preparation of canola protein materials using membrane technology and evaluation of meals functional properties. *Food Research International*, 38, 223-231.

- Gilbert, V., Rouabhia, M., Wang, H., Arnould, A., Remondetto, G., & Subirade, M. (2005). Characterization and evaluation of whey protein-based biofilms as substrates for *in vitro* cell cultures. *Biomaterials*, *26*, 7471–7480.
- Gill, T. A., & Tung, M. A. (1978). Thermally induced gelation of the 12S rapeseed glycoprotein. *Journal of Food Science*, *4*, 1481–1485.
- Giknis, M. L. A., & Clifford, C. B. (2008). Clinical laboratory parameters for CrI:WI (Han). Charles River laboratories.
- Gouin, S. (2004). Microencapsulation: industrial appraisal of existing technologies and trends. *Trends in Food Science and Technology*, *15*, 330-347.
- Gulvady, A. A., Brown, R. C., & Bell, J. A. (2013). Nutritional comparison of oats and other commonly consumed whole grains. *Oat Nutrition and Technology*, 71-93.
- Gunasekaran, S., Ko, S., & Xiao, L. (2007). Use of whey proteins for encapsulation and controlled delivery applications. *Journal of Food Engineering*, *83*, 31-40.
- Hagiwara, T., Kumagai, H., & Nakamura, K. (1998). Fractal analysis of aggregates in heat-induced BSA gels. *Food Hydrocolloids*, *12*, 29-36.
- Hamad, S. A., Stoyanov, S. D., Paunov, V. N. 2012. Triggered cell release from shellac-cell composite microcapsules. *Soft Matter*, *8*, 5069-5077.
- Hammershøj, M., & Larsen, L. B. (2001). Effect of hen egg production and protein composition on textural properties of egg albumen gels. *Journal of Texture Studies*, *32*, 105-129.
- Harper, J. D., & Lansbury, P. T. (1997). Models of amyloid seeding in Alzheimer's disease and scrapie: mechanistic truths and physiological consequences of the time-dependent solubility of amyloid proteins. *Annual Review of Biochemistry*, *66*, 385-407.
- Harley, V. S., Dance, D. A., Drasar, B. S., & Tovey, G. (1997). Effects of burkholderia pseudomallei and other burkholderia species on eukaryotic cells in tissue culture. *Microbios*. *96*, 71-93.
- He, C., Hu, Y., Yin, L., Tang, C., & Yin, C. (2010). Effects of particle size and surface charge on cellular uptake and biodistribution of polymeric nanoparticles. *Biomaterials*. *31*, 3657-3666.

- Hellio, D., & Djabourov, M. (2006). Physically and chemically crosslinked gelatin gels. *Macromolecular Symposia*, 241, 23-27.
- Hidalgo, I. J., Raub, T. J., & Borchardt, R. T. (1989). Characterization of the human colon carcinoma cell line (Caco-2) as a model system for intestinal epithelial permeability. *Gastroenterology*, 96, 736-49.
- Hillaireau, H., & Couvreur, P. (2009). Nanocarriers' entry into the cell: relevance to drug delivery. *Cellular and Molecular Life Science*, 66, 2873-2896.
- Hoglund, A. S., Rodin, J., Larsson, E., & Rask, L. (1992). Distribution of napin and cruciferin in developing rapeseed Embryos. *Plant Physiology*, 98, 509-515.
- Hu, H., Fan, X., Zhou, Z., Xu, X., Fan, G., Wang, L., et al. (2013). Acid-induced gelation behavior of soybean protein isolate with high intensity ultrasonic pre-treatments. *Ultrasonics Sonochemistry*, 20, 187-195.
- Huang, A. H. C. (1992). Oil bodies and oleosins in seed. *Annual Review of Plant Physiology and Plant Molecular Biology*, 43, 177-200.
- Huang, Q. R., Yu, H. L. & Ru, Q. M. (2010). Bioavailability and delivery of nutraceuticals using nanotechnology. *Journal of Food Science*, 75, R50-R57.
- Ikeda, H., Kume, Y., Arai, M., Arai, C., Omata, M., Fujiwara, K., et al. (2007). Rho-kinase inhibitor prevents hepatocyte damage in acute liver injury induced by carbon tetrachloride in rats. *American Journal of Physiology – Gastrointestinal and Liver Physiology*, 293, 911-917.
- Ikeda, S., Foegeding, E. A., & Hagiwara, T. (1999). Rheological study on the fractal nature of the protein gel structure. *Langmuir*, 15, 8584-8589.
- Inglett, G. E., Lee, S., & Stevenson, D. G. (2008). Converting oats to high-fiber products for use in functional foods. In: B. R. Hamaker (Eds.), *Technology of functional cereal products* (pp: 476-494). Cambridge: CRC, Woodhead.
- Ishizaka, T., & Koishi, M. (1981). Preparation of egg albumin microcapsules and microspheres. *Journal of Pharmaceutical Sciences*, 70, 358-361.
- Ismond, M. A. H., & Welsh, W. D. (1992). Application of new methodology to canola protein isolation. *Food Chemistry*, 45, 125-127.

- Jaeschke, H. (2011). Reactive oxygen and mechanisms of inflammatory liver injury: present concepts. *Journal of Gastroenterology and Hepatology*, 26, 173-179.
- Jiang, M., Gan, L., Zhu, C., Dong, Y., Liu, J., & Gan, Y. (2012). Cationic core-shell liponanoparticles for ocular gene delivery. *Biomaterials*, 33, 7621-7630.
- Jiang, X., Musyanovych, A., Röcker, C., Landfester, K., Mailänder, V., & Nienhaus, G. U. (2011). Specific effects of surface carboxyl groups on anionic polystyrene particles in their interactions with mesenchymal stem cells. *Nanoscale*, 3, 2028-2035.
- Jideani, V. A. (2011). Functional properties of soybean food ingredients in food systems. In: T. Ng (Eds.), *Soybean – biochemistry, chemistry and physiology* (pp: 345-366). InTech.
- Joly-Duhamel, C., Hellio, D., Ajdari, A., & Djabourov, M. (2006). All gelatin networks: 1. Biodiversity and physical chemistry. *Langmuir*, 18, 7208-7217.
- de Jongh, H. H. J. (2007). Protein in food microstructure formation, In: D. J. McClements (Eds.), *Understanding and controlling the microstructure of complex foods* (pp: 40-66), Boca Raton: CRC Press; Cambridge, England: Woodhead Pub.
- Jones, O, G., Adamcik, J., Handschin, S., Bolisetty, S., & Mezzenga, R. (2010). Fibrillation of β -lactoglobulin at low pH in the presence of a complexing anionic polysaccharide. *Langmuir*, 26, 17449-17458.
- Kagami, Y., Sugimura, S., Fujishima, N., Matsuda, K., Kometani, T., & Matsumura, Y. (2003). Oxidative stability, structure, and physical characteristics of microcapsules formed by spray ruing of fish oil with protein and dextrin wall materials. *Journal of Food Science*, 7, 2248-2255.
- Kamath, K. R., & Park, K. (1993). Biodegradable hydrogels in drug delivery. *Advanced Drug Delivery Reviews*, 11, 59-84.
- Kapetanovic, I. M., Muzzio, M., Huang, Z., Thompson, T. N., & McCormick, D. L. (2011). Pharmacokinetics, oral bioavailability, metabolic profile of resveratrol and its dimethylether analog, pterostilbene, in rats. *Cancer Chemotherapy and Pharmacology*, 68, 593-601.

- Kashyap, N., Kumar, N., & Ravi Kumar, M. N. V. (2005). Hydrogels for pharmaceutical and biomedical applications. *Critical Reviews in Therapeutic Drug Carrier Systems*, 22, 107-149.
- Keay, L., Edwards, K., & Stapleton, F. (2007). An early assessment of silicone hydrogel safety: Pearls and pitfalls, and current status. *Eye Contact Lenses*, 33, 358-361.
- Keim, S., & Hinrichs, J. (2004). Influence of stabilizing bonds on the texture properties of high-pressure-induced whey protein gel. *International Dairy Journal*, 14, 355-363.
- Keogh, M. K., O'Kennedy, B. T., Kelly, J., Auty, M. A., Kelly, P. M., Fureby, A., et al. (2001). Stability to oxidation of spray-dried fish oil powder microencapsulated using milk ingredients. *Journal of Food Science*, 66, 217-214.
- Kerman, V. M. Z. (2008). Studies on the gelation of gelatin solutions and on the use of resulting gels for medical scaffolds. Ph.D thesis.
- Khattab, R. Y., & Arntfield, S. D. (2009). Functional properties of raw and processed canola meal. *LWT – Food Science and Technology*, 42, 1119–1124.
- Kim, Y. H., Furuya, H., & Tabata, Y. (2014). Enhancement of bone regeneration by dual release of a macrophage recruitment agent and platelet-rich plasma from gelatin hydrogels. *Biomaterials*, 35, 214–224.
- Kinsella, J. E. (1981). Functional properties of proteins: Possible relationship between structure and function in foams. *Food Chemistry*, 7, 219-280.
- Klose, C., & Arendt, E. K. (2012). Proteins in oats: their synthesis and changes during germination: A review. *Critical Reviews in Food Science and Nutrition*, 52, 629-639.
- Kocher, P. N., & Foegeding, E. A. (1993). Microcentrifuge-based method for measuring water-holding of protein gels. *Journal of Food Science*, 58, 1040-1046.
- Kong, J., & Yu, S. (2007). Fourier transform infrared spectroscopic analysis of protein secondary structures. *Acta Biochimica Et Biophysica Sinica*, 39, 549-595.
- Korsmeyer, R. W., Gummy, R., Doelker, E., Buri, P., & Peppas, N. A. (1983). Mechanisms of solute release from porous hydrophilic polymers. *International Journal of Pharmaceutics*, 15, 25-35.
- de Kruif, C. G., Weinbrecka, F., & Vries, R. (2004). Complex coacervation of proteins and anionic polysaccharides. *Current Opinion of Colloid and Interface Science*, 9, 340-349.

- Krzyzaniak, A., Burova, T., & Barciszewski, J. (1998). The structure and properties of napin – seed storage protein from rape (*Brassica napus* L.). *Nahrung*, *42*, 201–204.
- Kuijpers, A. J., Engbers, G. H., Krijgsveld, J., Zaat, S. A., Dankert, J., & Feijen, J. (2000). Cross-linking and characterisation of gelatin matrices for biomedical applications. *Journal of Biomaterials Science Polymer Edition*, *11*, 225-243.
- Lai, L. F., & Guo, H. X. (2011). Preparation of new 5-fluorouracil-loaded zein nanoparticles for liver targeting. *International Journal of Pharmaceutics*, *404*, 317-323.
- Laneuville, S. I., Turgeon, S. L., Sanchez, C., & Paquin, P. (2006). Gelation of native β -lactoglobulin induced by electrostatic attractive interaction with xanthan gum. *Langmuir*, *22*, 7351-7357.
- Langer, R., & Peppas, N. A. (2003). Advances in biomaterials, drug delivery, and bionanotechnology. *AIChE Journal*, *49*, 2990–3006.
- Le, X. T., Rious, L., & Turgeon, S. L. (2016). Formation and functional properties of protein-polysaccharide electrostatic hydrogels in comparison to protein or polysaccharide hydrogels. *Advances in Colloid and Interface Science*, in press.
- Lee, J., Culyba, E. K., Powers, E. T., & Kelly, J. W. (2011). Amyloid- β forms fibrils by nucleated conformational conversion of oligomers. *Nature Chemical Biology*, *7*, 602-609.
- Lee, C., Yen, F., Huang, H., Wu, T., Ko, H., Tzeng, W., et al. (2012). Resveratrol nanoparticle system improves dissolution properties and enhances the hepatoprotective effect of resveratrol through antioxidant and anti-inflammatory pathways. *Journal of Agricultural and Food Chemistry*, *60*, 4662-4671.
- Lefèvre, T., & Subirade, M. (2000). Molecular differences in the formation and structure of fine-stranded and particulate beta-lactoglobulin gels. *Biopolymers*, *54*, 578–586.
- Léger, L. W., & Arntfield, S. D. (1993). Thermal gelation of the 12S canola globulin. *Journal of American Oil Chemists' Society*, *70*, 853–861.
- Limmatvapirat, S., Limmatvapirat, C., Puttipipatkachorn, S., Nuntanid, J., & Luangtana-anan, M., (2007). Enhanced enteric properties and stability of shellac films through composite salts formation. *European Journal of Pharmaceutics and Biopharmaceutics*, *67*, 690–698.
- Lin, C. C., & Metters, A. T. (2006). Hydrogels in controlled release formulations: network design and mathematical modeling. *Advanced Drug Delivery Review*, *58*, 1379-1408.

- Liu, K., Ding, H. J., Liu, J., Chen, Y., & Zhao, X. Z. (2006). Shape-controlled production of biodegradable calcium alginate gel microparticles using a novel microfluidic device. *Langmuir*, 22, 9453-9457.
- Liu, G., Li, J., Shi, K., Wang, S., Chen, J., Liu, Y. et al. (2009). Composition, secondary structure, and self-assembly of oat protein isolate. *Journal of Agricultural and Food Chemistry*, 57, 4552-4558.
- Llacuna, L., Mari, M., Lluís, J. M., Garcia-Ruiz, C., Fernandez-Checa, J. C., & Morales, A. (2009). Reactive oxygen species mediate liver injury through parenchymal nuclear factor-kappaB inactivation in prolonged ischemia/reperfusion. *American Journal of Pathology*, 174, 1776-1785.
- Luangtana-anan, M., Nunthanid, J., & Limmatvapirat, S. (2010). Effect of molecular weight and concentration of polyethylene glycol on physicochemical properties and stability of shellac film. *Journal of Agricultural and Food Chemistry*, 58, 12934-12940.
- Lukowski, G. Müller, R. H., Müller, B. W., & Dittgen, M. (1992). Acrylic acid copolymer nanoparticles for drug delivery: I. Characterization of the surface properties relevant for in vivo organ distribution. *International Journal of Pharmaceutics*, 84, 23-31.
- Luo, Y., Teng, Z., Wang, T. T., & Wang, Q. (2013). Cellular uptake and transport of zein nanoparticles: effect of sodium caseinate. *Journal of Agricultural and Food Chemistry*, 61, 7621-7629.
- Ma, C. Y., Khanzada, G., & Harwalkar, V. R. (1988). Thermal gelation of oat globulin. *Journal of Agricultural and Food Chemistry*, 36, 275-280.
- Ma, C. Y., & Harwalkar, V. R. (1984). Chemical characterization and functionality assessment of oat protein fractions. *Journal of Agriculture and Food Chemistry*, 32, 144-149.
- Ma, C. Y., & Wood, D. F. (1987). Functional properties of oat protein modified by acylation, trypsin hydrolysis or linoleate treatment. *Journal of the American Oil Chemists Society*, 64, 1726-1731.
- Makri, E. A., Papalamprou, E. M., & Doxastakis, G. (2006). Textural properties of legume protein isolate and polysaccharide gels. *Journal of the Science of Food and Agriculture*, 86, 1855-1862.

- Maltais, A., Remondetto, G. E., Gonzalez, R., & Subirade, M. (2005). Formation of soy protein isolate cold-set gels: protein and salt effects. *Journal of Food Science*, *70*, C67-C73.
- Maltais, A., Remondetto, G. E., & Subirade, M. (2008). Mechanisms involved in the formation and structure of soya protein cold-set gels: A molecular and supramolecular investigation. *Food Hydrocolloids*, *22*, 550-559.
- Maltais, A., Remondetto, G. E., & Subirade, M. (2009). Soy protein cold-set hydrogels as controlled delivery devices for nutraceutical compounds. *Food Hydrocolloids*, *23*, 1647–1653.
- Maltese, A., Borzacchiello, A., Mayol, L., Bucolo, C., Maugeri, F., Nicolais, L. et al. (2006). Novel polysaccharides-based viscoelastic formulations for ophthalmic surgery: Rheological characterization. *Biomaterials*, *27*, 5134-5142.
- Mandelbrot, B. B. (1982). *The fractal geometry of nature*. San Francisco, CA: Freeman.
- Mao, R., Tang, J., & Swanson, B. (2001). Water holding capacity and microstructure of gellan gels. *Carbohydrate Polymers*, *46*, 356-371.
- Marangoni, A. G., Barbut, S., McGauley, S. E., Marcone, M., & Narine, S. S. (2000). On the structure of particulate gels-the case of salt-induced cold gelation of heat-denatured whey protein isolate. *Food Hydrocolloids*, *14*, 61-74.
- Mason, M. N., Metters, A. T., Bowman, C. N., & Anseth, K. S. (2001). Predicting controlled release behavior of degradable PLA-b-PEG-b-PLA hydrogels. *Macromolecules*, *34*, 4630-4635.
- Massicotte, L. P., Baille, W. E., & Mateescu, M. A. (2008). Carboxylated high amylose starch as pharmaceutical excipients structural insights and formulation of pancreatic enzymes. *International Journal of Pharmaceutics*, *356*, 212-223.
- Matalanis, A., Jones, O. G., & McClements, D. J. (2011). Structured biopolymer-based delivery system for encapsulation, protection, and release of lipophilic compounds. *Food Hydrocolloids*, *25*, 1865-1880.
- Mauguet, M. C., Legrand, J., Brujes, L., Carnelle, G., Larré, C., & Popineau, Y., J. (2002). Gliadin matrices for microencapsulation processes by simple coacervation method. *Journal of Microencapsulation*, *19*, 377-384.

- Mellema, M., Heesakkers, J. W. M., van Opheusden, J. H. J., & van Vliet, T. (2000). Structure and scaling behavior of aging rennet-induced casein gels examined by confocal microscopy and permeametry. *Langmuir*, *16*, 6847-6854.
- McClements, D. J., Decker, E. A., Park, Y., & Weiss, J. (2009). Structural design principles for delivery of bioactive components in nutraceuticals and functional foods. *Critical Review in Food Science and Nutrition*, *49*, 577-606.
- McClements, D. J. (1999). *Food Emulsions: Principles, Practices and Techniques* (Vol. 5): CRC press.
- Mei, L., He, F., Zhou, R., Wu, C., Liang, R., Xie, R. et al. (2014). Novel intestinal-targeted Ca-alginate-based carrier for pH-responsive protection and release of lactic acid bacteria. *Applied Materials & Interface*, *6*, 5962-5970.
- Mitri, K., Shegokar, R., Gohla, S., Anselmi, C., & Müller, R. H. (2011). Lutein nanocrystals as antioxidant formulation for oral and dermal delivery. *International Journal of Pharmaceutics*, *420*, 141-146.
- Mohamed, A., Biresaw, G., Xu, J., Hojilla-Evangelista, M. P., & Rayas-Duarte, P. (2009). Oat protein isolate: Thermal, rheological, surface and functional properties. *Food Research International*, *42*, 107-114.
- Monsalve, R. I., Villalba, M., Lopez-Otin, C., & Rodriguez, R. (1991). Structural analysis of the small chain of the 2S albumin, napin nIII, from rapeseed. Chemical and spectroscopic evidence of an intramolecular bond formation. *Biochimica et Biophysica Acta*, *1078*, 265–272.
- Morris, V. (1986). Multicomponent gels, In: G. Phillips, D. Wedloc, & P. Williams (Eds.), *Gums and Stabilisers for the Food Industry 3* (pp. 87-99), Elsevier Applied Science: London.
- Morris, E. R. (2009). Functional interactions in gelling biopolymer mixtures. In: S. Kasapis, I. T. Norton, & J. B. Ubbink (Eds.), *Modern Biopolymer Science* (pp. 167-198), Academic press, London, UK.
- Muench, D. G., & Okita, T. W. (1997). The storage proteins of rice and oat, In: B. A. Larkins, & I. K. Vasil (Eds.), *Cellular and molecular biology of plant seed development* (pp. 289-330), Kluwer Academic Publisher, Netherlands.

- Müller, R. H., Mäder, K., & Gohla, S. (2000). Solid lipid nanoparticles (SLN) for controlled drug delivery – A review of the state of the art. *European Journal of Pharmaceutics and Biopharmaceutics*, *50*, 161-177.
- Nanjawade, B. K., Manvi, F. V., & Manjappa, A. S. (2007). In situ-forming hydrogels for sustained ophthalmic drug delivery. *Journal of Controlled Release*, *122*, 119-134.
- Nicolai, T., Britten, M., & Schmitt, C. (2011). β -lactoglobulin and WPI aggregates: Formation, structure and applications. *Food Hydrocolloids*, *25*, 1945–1962.
- Nieto-Nieto, T. V. (2015). Oat protein structure-function properties and value-added application. Ph.D Thesis.
- Nieto-Nieto, T. V., Wang, Y. X., Ozimek, L., & Chen, L. (2014). Effects of partial hydrolysis on structure and gelling properties of oat globular proteins. *Food Research International*, *55*, 418-425.
- Nieto-Nieto, T. V., Wang, Y. X., Ozimek, L., & Chen, L. (2015). Inulin at low concentrations significantly improves the gelling properties of oat protein – a molecular mechanism study. *Food Hydrocolloids*, *50*, 116-127.
- Nieto-Nieto, T. V., Wang, Y. X., Ozimek, L., & Chen, L. (2016). Improved thermal gelation of oat protein with the formation of controlled phase-separated networks using dextrin and carrageenan polysaccharides. *Food Research International*, *82*, 95-103.
- Nishinari, K., Fang, Y., Guo, S., & Philips, G. O. (2014). Soy proteins: A review on composition, aggregation and emulsification. *Food Hydrocolloids*, *39*, 301-318.
- Nordgård, C. T., & Draget, K. I. (2011). Oligosacchrides as modulators of rheology in complex mucous systems. *Biomacromolecules*, *12*, 3084-3090.
- Nunes, M. C., Raymundo, A., & Sousa, I. (2006). Rheological behavior and microstructure of pea protein/ κ -carrageenan/starch gel with different setting condition. *Food Hydrocolloids*, *20*, 106-114.
- Oakenfull, D., Pearce, J., & Burley, R. W. (1997). Protein gelation. In: S. Damodaran, & A. Paraf (Eds.), *Food proteins and their applications* (pp. 111-142), Marcel Dekker Inc., New York.
- Oakenfull, D., & Scott, A. (2003). Gelatin gels in deuterium oxide. *Food Hydrocolloids*, *17*, 207-210.

- Oganesyan, E., Miroshnichenko, L., Vikhrieva, N., Lyashenko, A., & Leshkov, S. Y. (2010). Use of nanoparticles to increase the systemic bioavailability of trans-resveratrol. *Pharmaceutical Chemistry Journal*, *44*, 74-76.
- Ould Eleya, M. M., & Gunasekaran, S. Ko, S. (2004). Scaling and fractal analysis of viscoelastic properties of heat-induced protein gels. *Food Hydrocolloids*, *18*, 315-323.
- Pandey, H., Parashar, V., Parashar, R., Prakash, R., Ramteke, P. W., & Pandey, A. C. (2011). Controlled Drug Release Characteristics and Enhanced Antibacterial Effect of Graphene Nanosheets Containing Gentamicin Sulfate. *Nanoscale*, *3*, 4104 – 4108.
- Park, H., & Park, K. (1996). Hydrogels in bioapplications. In: R. M. Ottenbrite, S. J. Huang, & K. Park (Eds.), *Hydrogels and biodegradable polymers for bioapplications* (pp. 2-10). American Chemical Society.
- Pastuszewska, B., Ochtabinska, A., & Morawski, A. (2000). A note on the nutritional adequacy of stock diets for laboratory rats and mice. *Journal of Animal and Feed Science*, *9*, 533–42.
- Patel, A. R., Drost, E., den Adel, R., Hazekamp, J., & Velikov, K. P. (2012). Temperature responsive colloidal particles from non-covalently interacting small molecular weight natural bioactive molecules. *Soft matter*, *8*, 3515-3517.
- Patel, A., Heussen, P., Hazekamp, J., & Velikov, K. P. (2011). Stabilisation and controlled release of silibinin from pH responsive shellac colloidal particles. *Soft Matter*, *7*, 8549-8555.
- Patel, A. R., Remijn, C., Cabero, A. M., Heussen, P. C. M., Seijen ten Hoorn, J. W. M., & Velikov, K. P. (2013). Novel all-natural microcapsules from gelatin and shellac for biorelated applications. *Advanced Functional Materials*, *23*, 4710-4718.
- Patel, K. R., Scott, E., Brown, V. A., Gescher, A. J., Steward, W. P., & Brown, K. (2011). Clinical trials of resveratrol. *Annals of the New York Academy of Sciences*, *1215*, 161-169.
- Penalva, R., Esparza, I, Agüeros, M., Gonzalez-Navarro, C. J., Ganzalez-Ferrero, C., & Irache, J. M. (2015). Casein nanoparticles as carriers for the oral delivery of folic acid. *Food hydrocolloids*, *44*, 399-406.
- Peppas, N. A., Bures, P., Leobandung, W., & Ichikawa, H. (2000). Hydrogels in pharmaceutical formulations. *European Journal of Pharmaceutics and Biopharmaceutics*, *50*, 27-46.
- Peterson, D. M. (1978). Subunit structure and composition of oat seed globulin. *Plant Physiology*, *62*, 506-509.

- Phillips, L G., Whitehead, D. M., & Kinsella, J. (1994). Chapter 9- protein gelation, In: L. G. P. M. W. Kinsella (Eds.), *Structure-Functional Properties of Food Proteins* (pp. 179-204), Academic Press: Boston.
- Pinterits, A., & Arntfield, S. D. (2008). Improvement of canola protein gelation properties through enzymatic modification with transglutaminase. *LWT – Food Science and Technology*, *41*, 128–138.
- Pothakamury, U. R., & Barbosa-Cánovas, G. V. (1995). Fundamental aspects of controlled release in foods. *Trends in Food Science and Technology*, *6*, 397-406.
- Pouzot, M., Benyahia, L., & Nicolai, T. (2004). Dynamic mechanical characterization of the heat-induced formation of fractal globular protein gels. *Journal of Rheology*, *48*, 1123-1134.
- Qiu, Y., & Park, K. (2001). Environment-sensitive hydrogels for drug delivery. *Advanced Drug Delivery Reviews*, *53*, 321-339.
- Quincozes-Santos, A., Bobermin, L. D., Latini, A., Wajner, M., Souza, D. O., Gonçalves, G., et al. (2013). Resveratrol protects C6 astrocyte cell line against hydrogen peroxide-induced oxidative stress through heme oxygenase 1. *PLOS ONE*, *8*, 1-10
- Reis, C. P., Neufeld, R. J., Ribeiro, A. J., & Veiga, F. (2006). Nanoencapsulation I. methods for preparation of drug-loaded polymeric nanoparticles. *Nanomedicine: Nanotechnology, Biology and Medicine*, *2*, 8-21.
- Remondetto, G. E., Beyssac, E., & Subirade, M. (2004). Iron availability from whey protein hydrogels: An *in vitro* study. *Journal of Agricultural and Food Chemistry*, *52*, 8137–8143.
- Remondetto, G. E., Paquin, P., & Subirade, M. (2002). Cold gelation of β -lactoglobulin in the presence of Iron. *Journal of Food Science*, *67*, 586–595.
- Remondetto, G. E., & Subirade, M. (2003). Molecular mechanisms of Fe^{2+} -induced β -lactoglobulin cold gelation. *Biopolymer*, *69*, 461–469.
- Renkema, J. M. S., & van Vliet, T. (2004). Concentration dependence of dynamic moduli of heat-induced soy protein gels. *Food Hydrocolloids*, *18*, 483-487.
- des Rieux, A., Fievez, V., Garinot, M., Schneider, Y. J., & Pr at, V. (2006). Nanoparticles as potential oral delivery systems of proteins and vaccines: a mechanistic approach. *Journal of Controlled Release*, *116*, 1-27.
- Renkema, J. M. S., & van Vliet, T. (2002). Heat-induced gel formation by soy proteins at neutral pH. *Journal of Agricultural and Food Chemistry*, *50*, 1569-1573.

- Robert, L. S., Adeli, K., & Altosaar, I. (1985). Characterisation of oat (*Avena sativa L.*) residual proteins. *Cereal Chemistry*, 78, 812-816.
- Robert, L. S., Nozzolillo, C., Cudjoe, A., & Altosaar, I. (1983). Total solubilization of groat proteins in high protein oat (*Avena sativa L.* cv. Hinoat): Evidence that glutelins are a minor component. *Canadian Institute of Food Science and Technology Journal*, 16, 196-200.
- Roff, C. F., & Foegeding, E. A. (1996). Dicationic-induced gelation of pre-denatured whey protein isolate. *Food Hydrocolloids*, 10, 193-198.
- Roger, E., Lagarce, F., Garcion, E., & Benoit, J. (2009). Lipid nanocarriers improve paclitaxel transport throughout human intestinal epithelial cells by using vesicle-mediated transcytosis. *Journal of Controlled Release*, 140, 174-181.
- Saguer, E., Alvarez, P. A., Sedman, J., & Ismail, A. A. (2013). Study of the denaturation / aggregation behavior of whole porcine plasma and its protein fractions during heating under acidic pH by variable-temperature FTIR spectroscopy. *Food Hydrocolloids*, 33, 402-414.
- Saier, M. H., & Mansour, N. M. (2005). Probiotics and prebiotics in human health. *Journal of Molecular Microbiology and Biotechnology*, 10, 22-25.
- Sakai, S., Moriyama, K., & Kawakami, K. (2011). Controlling thermos-reversibility of gelatin gels through a peroxidase-catalyzed reaction under mild conditions for mammalian cells. *Journal of Biomaterials Science Polymer Edition*, 22, 1147-1156.
- Salunkhe, D. K., Chavan, J. K., Adsule, R. N., & Kadam, S. S. World oilseeds: chemistry, technology, and utilization. New York: Van Nostrand Reinhold. 1992.
- Sanguansri, P., & Augustin, M. A. (2006). Nanoscale materials development – a food industry perspective. *Trends in Food Science and Technology*, 17, 547-556.
- Sanjukta, S., & Rai, A. K. (2016). Production of bioactive peptides during soybean fermentation and their potential health benefits. *Trends in Food Science & Technology*, 50, 1-10.
- Santoro, M., Tatara, A. M., & Mikos, A. G. (2014). Gelatin carriers for drug and cell delivery in tissue engineering. *Journal of Controlled Release*, 190, 210-218.
- Sathe, S. K. (2002). Dry bean protein functionality. *Critical Reviews in Biothechnology*, 22, 173-223.
- Savadkoohi, S., & Farahnaky, A. (2012). Dynamic rheological and thermal study of the heat-induced gelation of tomato-seed proteins. *Journal of Food Engineering*, 113, 479-485.

- Sener, G., Toklu, H. Z., Sehirli, A. O., Velioglu-Ogünç, A., Cetinel, S., & Gedik, N. (2006). Protective effects of resveratrol against acetaminophen-induced toxicity in mice. *Hepatology Research*, 35, 62-68.
- Senevirathne, M., Jeon, Y. J., Kim, Y. T., Park, P. J., Jung, W. K., Ahn, C. B., et al. (2012). Prevention of oxidative stress in Chang liver cells by gallic acid-grafted-chitosans. *Carbohydrate Polymers*, 87, 876-880.
- Schmitt, C., Sanchez, C., Desobry-Banon, S., & Hardy, J. (1998). Structure and technofunctional properties of protein-polysaccharide complexes: a review. *Critical Reviews in Food Science and Nutrition*, 38, 689-735.
- Schrieber, R., & Gareis, H. (2007). Gelatin handbook: Theory and industrial practice. Wiley-VCH Verlag GmbH & Co. KGaA, Weinheim.
- Schwenke, K. D. (1994). Rapeseed protein. In: B. J. F. Hudson (Eds.), *New and developing sources of food proteins* (pp 281–306). London: Chapman and Hall. U.K.
- Schwenke, K. D., Drescher, B., Zirwer, D., & Raab, B. (1988). Structural studies on the native and chemically modified low-molecular mass basic storage protein (napin) from rapeseed (*Brassica napus* L.). *Biochemie und Physiologie der Pflanzen*, 183, 219–224.
- Schwenke, K. D., Dahme, A., & Wolter, T. (1998). Heat-induced gelation of rapeseed proteins: effect of protein interaction and acetylation. *Journal of American Oil Chemists' and Society*, 75, 83–87.
- Semenova, M G., & Dickinson, E. B. (2010). Biopolymers in food colloids: thermodynamics and molecular interactions. Taylor & Francis Group, Leiden; Boston.
- Shang, L., Nienhaus, K., Jiang, X., Yang, L., Landfester, K., Mailänder, V., et al. (2014). Nanoparticle interactions with live cells: Quantitative fluorescence microscopy of nanoparticle size effects. *Beilstein Journal of Nanotechnology*, 5, 2388-2397.
- Shih, W. H., Shih, W. Y., Kim, S.I, Liu, J., & Aksay, I. A. (1990). Scaling behavior of the elastic properties of colloidal gels. *Physical Review A*, 42, 4772-4779.
- Shim, J., Kim, M., Kim, H., Ahn, J., Yun, Y., & Song, J. (2010). Protective action of immunomodulatory ginsan against carbon tetrachloride-induced liver injury via control of

- oxidative stress and the inflammatory response. *Toxicology and Applied Pharmacology*, *242*, 318-325.
- Shotwell, M. A., Boyer, S. K., Chesnut, R. S., & Larkins, B. A. (1990). Analysis of seed storage protein genes of oats. *Journal of Biological Chemistry*, *265*, 9652-9658.
- Simpson, D. J. (2001) Proteolytic degradation of cereal prolamins-the problem with proline. *Plant Science*, *161*, 825-838.
- Singh, A., Ahmad, I., Ahmad, S., Iqbal, Z., & Ahmad, F, J. (2016). A novel monolithic controlled delivery system of resveratrol for enhanced hepatoprotection: nanoformulaion development, pharmacokinetics and pharmacodynamics. *Drug Development and Industrial Pharmacy*, *42*, 1524-1536.
- Singh, G., & Pai, R. S. (2014). Optimized PLGS nanoparticles platform for orally dosed trans-resveratrol with enhance bioavailability potential. *Expert Opinion on Drug Delivery*, *11*, 647-659.
- Solans, C., Izquierdo, P., Nolla, J., Azemar, N., & Garcia-Celma, M. J. (2005). Nano-emulsions. *Current Opinion in Colloid and Interface Science*, *10*, 102-110.
- Stabenfeldt, S. E., Garcia, A. J., Laplaca, M. C. (2006). Thermoreversible laminin-functionalized hydrogel for neural tissue engineering. *Journal of Biomedical Materials Research A*, *77*, 718-725.
- Stein, R. W., Place, A. R., Lacourse, T., Guglielmo, C. G., & Williams. T. D., (2015). Digestive organ sizes and enzyme activities of refueling western sandpipers (*Calidris mauri*): Contrasting Effects of season and age. *Physiological and Biochemical Zoology*, *78*, 434-446.
- Sun, X, D., & Arntfield, S. D. (2010). Gelation properties of salt-extracted pea protein induced by heat treatment. *Food Research International*, *43*, 509-515.
- Tan, S. H., Mailer, R. J., Blanchard, C. L., & Agboola, S. O. (2011). Canola proteins for human consumption: extraction, profile, and functional properties. *Journal of Food Science*, *76*, R16–R28.
- Tay, S. L., Xu, G. Q., & Perera, C. O. (2005). Aggregation profile of 11S, 7S, and 2S coagulated with GDL. *Food Chemistry*, *91*, 457-462.

- Tessmar, J. K., & Gopferich, A. M. (2007). Customized PEG-derived copolymers for tissue engineering applications. *Macromolecular Bioscience*, 7, 23-39.
- Titova, E. F., Belavtseva, E. M., Braudo, E. E., & Tolstoguzov, V. B. (1974). Electron microscopic investigation of gelatin gelation. *Colloid and Polymer Science*, 252, 497–503.
- Tolstoguzov, V. B. (2007). Ingredient interactions in complex foods: aggregation and phase separation. In: D. J. McClements (Eds.), *Understanding and controlling the microstructure of complex foods* (pp: 185-206). Woodhead Publishing, Cambridge.
- Tseng, Y. C., Xiong, Y., & Boatright, W. (2008). Effects of inulin/oligofructose on the thermal stability and acid-induced gelation of soy protein. *Journal of Food Science*, 73, E44-E50.
- Tung, Y. T., Wu, J. H., Huang, C. C., Peng, H. C., Chen, Y. L., Yang, S. C., et al., (2009). Protective effect of Acacia confuse bark extract and its active compound gallic acid against carbon tetrachloride-induced chronic liver injury in rats. *Food and Chemical Toxicology*, 47, 1385-1392.
- Tunick, M. H. (2010). Small-strain dynamic rheology of food protein networks, *Journal of Agricultural and Food Chemistry*, 59, 1481–1486.
- Turgeon, S. L., & Beaulieu, M. (2001). Improvement of whey protein gel texture using polysaccharides. *Food Hydrocolloids*, 15, 583-591.
- Turgeon, S. L., & Beaulieu, M. (2004). Effect of thermal treatment on large and small deformation properties of whey protein/pectin mixed gels. In: P. A. Williams, & G. O. Phillips (Eds.), *Gums and stabilizers for the food industry 12* (pp. 211-226), RSC, Cambridge.
- Turgeon, S. L., & Laneuville, S. I. (2009). Chapter 11: Protein + Polysaccharide Coacervates and Complexes: From Scientific Background to their Application as Functional Ingredients in Food Products. In: S. Kasapis, I. T. Norton, & J. B. Ubbink (Eds.), *Modern Biopolymer Science* (pp:327-363). Academic Press.
- Twomey, M. Keogh, M. K., Mehra, R., & O’Kennedy, T. (1997). Gel characteristics of β -lactoglobulin, whey protein concentrate and whey protein isolate. *Journal of Texture Studies*, 28, 387-403.

- Urbonaite, V., van der Kaaij, S., de Jongh, H. H. J., Scholten, E., Ako, K., van der Linden, E., et al. (2016). Relation between gel stiffness and water holding for coarse and fine-stranded protein gels. *Food Hydrocolloids*, *56*, 334-343.
- Uruakpa, F. O., & Arntfield, S. D. (2004). Rheological characteristics of commercial canola protein isolate – κ -carrageenan systems. *Food Hydrocolloids*, *18*, 419–427.
- Vang, O., Ahmad, N., Baile, C. A., Baur, J. A., Brown, K., Csiszar, A., et al., (2011). What is new for an old molecule? Systematic review and recommendation on the use of resveratrol. *PLOS ONE*, *6*, e19881.
- Vasanthan, T., & Temelli, F. (2008). Grain fractionation technologies for cereal beta-glucan concentration. *Food Research International*, *41*, 876-881.
- Vermonden, T., Censi, R., & Hennink, W. E. (2012). Hydrogels for protein delivery. *Chemical Reviews*, *112*, 2853-2888.
- Vilela, J. A. P., Cavallieri, Â. L. F., & da Cunha, R. L. (2011). The influence of gelation rate on the physical properties/structure of salt-induced gels of soy protein isolate-gellan gum. *Food Hydrocolloids*, *25*, 1710-1718.
- van Vliet, T., & Walstra, P. (1995). Large deformation and fracture behaviour of gels. *Faraday Discuss*, *101*, 359-370.
- Vreeker, P., Hoekstra, L. L., den Boer, D. C., & Agterof, W. G. (1992). Fractal aggregation of whey proteins. *Food Hydrocolloids*, *6*, 423-435.
- Wallace, D. G., & Rosenblatt, J. (2003). Collagen gel systems for sustained delivery and tissue engineering. *Advanced Drug Delivery Reviews*, *55*, 1631-1649.
- Walle, T., Hsieh, F., Delegge, M, H., Oatis, J. E. Jr., & Walle, U. K. (2004). High absorption but very low bioavailability of oral resveratrol in humans. *Drug Metabolism and Disposition*, *32*, 1377-1382.
- Walstra, P. (2003). Studying food colloids: Past, present and future. In: E. Dickinson, & T. van Vlie (Eds.), *Food colloids, biopolymers and materials* (pp: 391-400). Cambridge: Royal Society of Chemistry.
- Wang, Y., Bamdad, F., Song, Y., Chen, L. (2012). Chapter 14: Hydrogel particles and other novel protein-based methods food ingredient and nutraceutical delivery systems. In: N. Garti,

- & D. J. McClements (Eds.), *Encapsulation technologies and delivery systems for food ingredients and nutraceuticals* (pp. 412-450). Woodhead Publishing Limited. UK.
- Wang, Y., & Chen, L. (2011). Impacts of nanowhisker on formation kinetics and properties of all-cellulose composite gel. *Carbohydrate Polymers*, *83*, 1937–1946.
- Wang, Y., & Chen, L. (2012). Fabrication and characterization of novel assembled prolamin protein nanofabrics with improved stability, mechanical property and release profiles. *Journal of Materials Chemistry*, *22*, 21592-21601.
- Wang, Y., & Chen, L. (2014). Cellulose nanowhiskers and fiber alignment greatly improve mechanical properties of electrospun prolamin protein fibers. *Applied Materials and Interfaces*, *6*, 1709-1718.
- Wang, K., Luo, S., Zhong, X., Cai, J., Jiang, S., & Zheng, Z. (2017). Changes in chemical interactions and protein conformation during heat-induced wheat gluten gel formation. *Food Chemistry*, *214*, 393-399.
- Weber, C., Coester, C., Kreuter, J., & Langer, K. (2000). Desolvation process and surface characterisation of protein nanoparticles. *International Journal of Pharmaceutics*, *194*, 91-102.
- Weitz, D. A., Huang, J. S., Lin, M. Y., & Sung, J. (1985). Limits of the fractal dimension for irreversible kinetic aggregation of gold colloids. *Physical Review Letters*, *54*, 1416-1419.
- Wenzel, E., & Somoza, V. (2005). Metabolism and bioavailability of trans-resveratrol. *Molecular Nutrition & Food Research*, *49*, 472-481.
- Weyermann, J., Lochmanna, D., Georgensa, C., & Zimmer, A. (2005). Albumin-protamine-oligonucleotide-nanoparticles as a new antisense delivery system. Part 2: Cellular uptake and effect. *European Journal of Pharmaceutics and Biopharmaceutics*, *59*, 431-438.
- Win, K. Y., & Feng, S. (2005). Effects of particle size and surface coating on cellular uptake of polymeric nanoparticles for oral delivery of anticancer drugs. *Biomaterials*, *26*, 2713-2722.
- Wu, H., & Morbidelli, M. (2001). A model relating structure of colloidal gels to their elastic properties. *Langmuir*, *17*, 1030-1036.
- Wu, J., & Muir, A. D. (2008). Comparative structural, Emulsifying, and biological properties of 2 major canola proteins, cruciferin and napin. *Journal of Food Science*, *73*, C210–C216.

- Xia, Y., Wang, Y., & Chen, L. (2011). Molecular structure, physicochemical characterization, and in vitro degradation of barley protein films. *Journal of Agricultural and Food Chemistry*, *59*, 13221–13229.
- Xue, J., & Zhang, Z. (2008). Preparation and characterization of calcium-shellac spheres as a carrier of carbamide peroxide, *J. Microencapsulation*, *25*, 523-530.
- Yan, C., & Pochan, D. J. (2010). Rheological properties of peptide-based hydrogels for biomedical and other applications. *Chemical Society Reviews*, *39*, 3528-3540.
- Yang, J., Zhou, Y., & Chen, L. (2014). Elaboration and characterization of barley protein nanoparticles as an oral delivery system for lipophilic bioactive compounds. *Food and Function*, *5*, 92-101.
- Young, S., Wong, M., Tabata, Y., & Mikos, A. G. (2005). Gelatin as delivery vehicle for the controlled release of bioactive molecules. *Journal of Controlled Release*, *109*, 256-274.
- Zhang, J. (2014). Soy protein nanoparticles as an oral delivery vehicle for nutraceuticals. Ph. D thesis.
- Zhang, J., Field, C. J., Vine, D., & Chen, L. (2015). Intestinal uptake and transport of vitamin B₁₂-loaded soy protein nanoparticles. *Pharmaceutical Research*, *32*, 1288-1303.
- Zhang, J., Liang, L., Tian, Z., Chen, L., & Subirade, M. (2012). Preparation and in vitro evaluation of calcium-induced soy protein isolate nanoparticles and their formation mechanism study. *Food Chemistry*, *133*, 390–399.
- Zhang, T., Jiang, B., & Wang, Z. (2007). Gelation properties of chickpea protein isolates. *Food Hydrocolloids*, *21*, 280-286.
- Zhao Y, Mine Y, & Ma C. Y. (2004) Study of thermal aggregation of oat globulin by laser light scattering. *Journal of Agricultural and Food Chemistry*, *52*, 3089–3096.
- Zhou, Y. Intestinal uptake of barley protein nanoparticles as delivery vehicles for bioactive compounds. Master thesis. 2013.
- Ziegler, G. R., & Foegeding, E. A. (1990). The gelation of proteins. *Advances in Food Nutrition Research*, *34*, 203-298.
- Zimet, P., & Livney, Y. D. (2009). Beta-lactoglobulin and its nano-complexes with pectin as vehicles for ω -3 polyunsaturated fatty acids. *Food Hydrocolloids*, *23(4)*, 1120-1126.

- Zirwer, D., Gast, K., Welfle, H., Schlesier, B., & Schwenke, K. D. (1985). Secondary structure of globulins from plant seeds: a re-evaluation from circular dichroism measurements. *International Journal of Biological Macromolecules*, 7, 105–108.
- Zhu, F., Du, B., & Xu, B. (2016). A critical review on production and industrial applications of beta-glucans. *Food Hydrocolloids*, 52, 275-288.